

VNIVERSITAT^Ŏ DE VALÈNCIA

Facultat de Física

Departamento de Óptica y Optometría y Ciencias de la Visión



TESIS DOCTORAL

SPATIO-TEMPORAL DYNAMICS OF LASERS AND PHOTOREFRACTIVE OSCILLATORS UNDER ROCKING: PHASE-BISTABLE PATTERNS AND LOCALIZED STRUCTURES

por

Manuel Francisco Martínez Quesada

Bajo la dirección de
Germán José de Valcárcel Gonzalvo

Programa de doctorado 3126 Física

València, octubre 2018

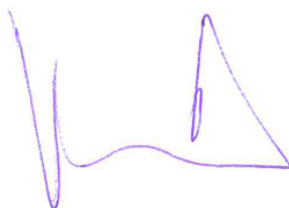
Germán de Valcárcel Gonzalvo, catedrático del departamento de Óptica y Optometría y Ciencias de la Visión de la Universitat de València,

CERTIFICA

Que la presente memoria. “Spatio-temporal dynamics of lasers and photorefractive oscillators under rocking: phase-bistable patterns and localized structures”, ha sido realizada bajo su dirección en el departamento de Óptica y Optometría y Ciencias de la Visión de la Universitat de València por D. Manuel Francisco Martínez Quesada y constituye su tesis para optar al grado de doctor.

Y para que conste, firma el presente certificado en Valencia, a 25 de octubre de 2018

Germán J. de Valcárcel Gonzalvo



The dream goes over time,
floating like a sailboat
no one can crack open the seeds
in the heart of the dream

...

And if the dream pretends to be walls
in the plain of time
then time makes it (the dream) believe
that it is born at that moment

Legend of time (Camaron de la Isla, Federico Garcia Lorca)

El sueño va sobre el tiempo
flotando como un velero
nadie puede abrir semillas
en el corazón del sueño

...

Y si el sueño finge muros
en la llanura del tiempo
el tiempo le hace creer
que nace en aquel momento

La leyenda del tiempo (Camaron de la Isla, Federico Garcia Lorca)

El trabajo de una tesis doctoral, y más una tan dilatada en el tiempo, nunca es el fruto de una única persona. En primer lugar, quisiera agradecer a mi director Germán por el apoyo y comprensión (y paciencia) que me ha brindado, sin las cuales todo esto no sería posible. Asimismo, me gustaría agradecer a Eugenio y Fernando toda la ayuda que me han ofrecido sin ni siquiera pedirla muchas veces. Esta tesis es, en gran parte, también suya.

Después, claro está, debo agradecer al clan Murcia, Moisés, Pablo y Pascual, su amistad, su solidaridad y su compañía, a veces desde la distancia. Al resto de compañeros colegiales del Colegio Mayor San Juan de Ribera, en especial José Carlos y Javi Resta, les mando un fuerte abrazo y les doy las gracias por el cariño que se siempre me han mostrado siempre que nos reunimos. Espero que sigamos haciéndolo en el futuro.

A los compañeros de comidas, cenas y concursongs varios les debo el no haberme sentido demasiado solo y hacer que me olvidara de mí mismo (en el buen sentido). Son muchos para nombrarlos a todos: desde Alberto y Antonio pasando por Jonathan, Cuesta y Erica hasta los novísimos: Matteo, Aurora, Leo, Silvia, Pablo, Fei, Isabel, Roberto... Os deseo lo mejor allá donde estéis o vayáis. A Óscar le perdono por adentrarme en los caminos de la heterodoxia intelectual.

A Franco y a Lorenzo les agradezco su hospitalidad y su apoyo en esos momentos lejos de casa. También a Isabel, Adolfo, Rubén, Rafa, Joaquín y César y el resto de colegas del departamento de Óptica por los buenos momentos, científicos y no tan científicos, que compartimos en aquellas tardes ahora lejanas.

Por último, quisiera agradecer de corazón a mis padres, Paco y Gloria, y a mi hermano, Jesús Luis, por su ayuda incondicional en todo momento.

Contents

Overview	xi
Versió en valencià	xv
Versión en castellano	xix
1 Introduction	1
1.1 Dissipative structures in Optics	1
1.2 Universal dynamics	10
1.3 Rocking mechanism	13
1.4 Mathematical techniques	17
2 Main results	23
2.1 Rocking in class C lasers	25
2.2 Rocking in class B lasers	35
2.3 Universal description of optical oscillators under rocking	39
2.4 Bidirectional rocked lasers	47
3 Conclusions	53
Versió en valencià	56
Versión en castellano	59
Appended Papers	
<i>Bistable Phase Locking of a Nonlinear Optical Cavity via Rocking: Transmuting Vortices into Phase Patterns</i>	65
<i>Bistable phase locking in rocked lasers</i>	71
<i>Rocking bidirectional lasers</i>	83
<i>Phase-bistable pattern formation in oscillatory systems via rocking: application to nonlinear optical systems</i>	91
<i>Universal description of pattern formation in optical oscillators under bichromatic injection.</i>	113
Bibliography	127

Overview

This thesis is presented as a collection of articles [1–5]. From now on they will be cited as Paper I, Paper II, Paper III, Paper IV and Paper V respectively.

The formation of patterns in spatially extended systems is a recurring phenomenon in nature which is usually related to situations in which there is a nonlinear response of a system under an external forcing which drives it far away from its (thermodynamic) equilibrium. This leads to the generation of spatially inhomogeneous structures which are known as dissipative as in these forced systems there is a balance between the external source of energy and the losses of the system.

In particular, this kind of structures are very common in Nonlinear Optics, specially in those configurations in which a medium interacts nonlinearly with light surrounded by two mirrors (optical cavity). In this situation, the patterns appear in the plane perpendicular to the propagation direction and this is the reason why they are called "transverse patterns". One specially interesting example are the localized structures or cavity solitons (they exist in a confined region of the transverse plane and are stable); these structures are of great interest as they can be written or erased with coherent beams, so potentially they could be useful for information storage and processing through purely optical methods only. As an example, a set of $N \times N$ solitons constitutes an optical memory of $2^{N \times N}$ different states.

The objective of this thesis is the theoretical, analytical and numerical, study of the spatio-temporal dynamics of optical oscillators under bichromatic forcing (rocking). This kind of injection, introduced in [6], possesses the feature of breaking the phase invariance (any phase of the complex field is possible)

of the free-running system and generates a phase-bistable system in which two only phases (separated by π) are allowed for the homogeneous stationary solutions.

This change in the nature of the system enables a new dynamics characterized by the presence of a new kind of spatial structures in the bidimensional transverse plane: bistable phase patterns in which both phases coexist separated by domain walls (Ising if they have null intensity or Bloch if it is different from zero). These domains can evolve either to homogeneous patterns (in which only one phase is present) or to more complex ones, in which curvature effects lead to the emergence of labyrinthic patterns depending on the value of the parameters of the system. Moreover, localized structures (stable minimum-size domains) as dark-ring cavity solitons can exist.

Other phase symmetry breaking methods have been used to control the dynamics of many systems. One of the most popular is the parametric resonance, i.e. injecting a field whose frequency is twice the natural frequency of the system. However these methods are less versatile than rocking, which can be applied to a broad range of systems like lasers, which are insensitive to parametric resonance. In fact, many theoretical and experimental proposals involving rocking in different (optical and non-optical) systems have been made. In the scope of this thesis, we have focused on the influence of rocking in two systems which have been studied profusely in the literature, as they are very interesting both from a fundamental and a practical point of views:

Laser. The Laser (acronym for light amplification by stimulated emission of radiation) is probably the most relevant nonlinear optical system, both for its intrinsically nonlinear nature and the singular properties of laser emission (extreme monochromaticity and high focusability), which allow to study many nonlinear processes requiring high power density. A laser consists essentially in a medium with population inversion (more electrons in an excited state than in the fundamental one) due to interaction with a pump, being able to generate electromagnetic radiation by stimulated emission which is amplified after passing a large number of times through the amplifier, as given by the bouncing back and forth between the cavity mirrors. The most studied laser model is the two-level laser (an abstraction as population inversion requires at least three levels) as an affordable analytical treatment is possible, being the Maxwell-Bloch (MB) equations the ones which describe this model. Any phase is allowed in lasing emission as it is a self-oscillatory system in which the phase is not fixed, which determines the nature of the patterns in the system. Pattern formation in those systems have been analyzed in small

aperture configurations (low Fresnel number), in which the small transverse modes allowed by the system and their nonlinear interaction are responsible for the spatial structures (Gaussian modes), as well as in situations, when the Fresnel number is large, in which the number of modes is enormous and the presence of vortices and traveling waves is common. Due to its interest, many theoretical and experimental proposals have been made to generate localized structures (solitons) in lasers, specifically in semiconductor lasers, which are very interesting for creating a compact system for information processing (*soliton laser*). In our case, we will focus on the application of rocking to: (i) unidirectional lasers and (ii) bidirectional lasers, in which two counterpropagating fields coexist in a ring cavity.

Photorefractive oscillator (PRO). This system is an optical cavity in which the nonlinear medium is a photorefractive crystal, which has a refractive index which depends on the spatial modulation of light intensity. The interference of two beams in the crystal creates a periodic pattern in the electric field which is responsible for an index spatial modulation. This nonlinear effect, combined with two-wave mixing in a ring cavity, gives rise to a radiation emission which, like lasers, possesses continuous phase symmetry. The main difference is that, in this case, the dynamics in the transverse plane can be much slower (of the order of seconds, several orders of magnitude larger than in the laser) due to the special features of photorefractive media (specifically their gain curve). This produces enormous advantages when experimental setups for studying pattern formation are considered as sophisticated recording devices are no longer needed to analyze them. Because of this, photorefractive oscillators are regarded as perfect laboratories to study transverse patterns in optical cavities and they have generated a large numbers of experimental results. In our case, we will study theoretically the influence of rocking in two-wave mixing photorefractive oscillators in a ring cavity configuration.

Along this thesis, we will study the influence of rocking in those systems in detail. As it is usual in nonlinear science, is convenient to derive equations describing the behaviour of those systems close to (critical) points where the stationary solutions emerge. These equations (called order parameter equations) are relatively simple and are able to describe a large number of nonlinear systems: physical, chemical, biological.. (the meaning of the parameters being the only difference, but the mathematical structure is the same). Moreover, we will analyze the stability of the solutions and we will perform numerical simulations of the theoretical models.

The structure of this manuscript is as follows. The first chapter will be

devoted to an introduction, containing:

- A discussion about the pattern formation phenomenon in nature.
- A general introduction to some of the main contributions in the field of pattern formation in nonlinear optics.
- A formal introduction to the rocking mechanism and a review of the systems where it has been already applied.
- A short discussion about the order-parameter equations, specifically the (real and complex) Ginzburg-Landau and Swift-Hohenberg equations, which have been derived so far for optical cavities.
- A summary of the mathematical, analytical and numerical tools we have used to carry out our study like: the multiple scales expansion to derive order parameter equations, the linear stability analysis to analyze instabilities against spatio-temporal perturbations, and the method of numerical integration split-step, conveniently modified to incorporate time-dependent external forcing like rocking.

In the second chapter, I will summarize my main contributions to the published articles, organized by topic. Also unpublished results will be presented:

- Starting from the MB equations under rocking injection, an order parameter equation will be derived for class C lasers with positive cavity detuning and the patterns of the system will be studied numerically.
- A reduced model of two equations will be obtained for class B lasers and its temporal dynamics and the influence of the detuning of rocking injection will be studied. We will also show spatial patterns obtained from simulations of the MB equations.
- A unified model (valid for positive and negative cavity detunings) for two-level lasers (class C and A) and photorefractive oscillators will be developed, providing the stability domains of the phase bistable states and studying numerically the spatial patterns that arise from the system.
- The temporal dynamics of a bidirectional laser under rocking injection will be analyzed and some preliminary results regarding spatial patterns will be given.

Lastly, I will review our main conclusions in chapter three. A copy of the five published articles that support this thesis is presented as an addendum.

Versió en valencià

Aquesta tesi es presenta en la modalitat de compendi de publicacions [1–5]. A partir d'ara se citaran com Paper I, Paper II, Paper III, Paper IV i Paper V respectivament.

En la natura, la formació de patrons en sistemes espacialment extensos és un fenomen recurrent que sol estar associat a situacions en les quals hi ha una resposta no lineal d'un sistema sotmès a un forçament extern que ho situa lluny del seu estat d'equilibri (termodinàmic). Això condueix a la generació d'estructures inhomogènies espacialment que són conegudes com *dissipatives*, atès que en aquests sistemes forçats hi ha un balanç entre l'aportació externa d'energia i les pèrdues pròpies del sistema dissipatiu.

En particular, aquest tipus d'estructures són molt comunes en el camp de l'Òptica no lineal, especialment aquelles configuracions en les quals un medi interacciona no linealment amb la llum envoltat de dos espills (cavitat òptica). En aquesta situació, els patrons apareixen en el pla perpendicular a la direcció de propagació i aquesta és la raó per la qual es denominen "patrons transversals". Un exemple especialment rellevant són les anomenades estructures localitzades o solitons de cavitat (existeixen en una regió limitada del pla transversal i són estables), aquestes estructures posseeixen un gran interès ja que poden ser escrites o esborrades independentment mitjançant feixos de llum coherents, per la qual cosa potencialment podrien ser usades per a emmagatzematge i processament d'informació mitjançant mètodes purament òptics. Per exemple, un conjunt d' $N \times N$ solitons constitueix una memòria òptica de $2^{N \times N}$ estats diferents.

Aquesta tesi té com a objectiu l'estudi teòric, analític i numèric, de la dinàmica espaciotemporal d'oscil·ladors òptics no lineals sotmesos a un forçament bicromàtic (rocking). Aquest tipus d'injecció, introduïda en [6], té la característica principal de trencar la invariància de fase (qualsevol fase del camp complex) del sistema lliure (sense forçament) i genera un sistema que és biestable en fase, ja que únicament dues fases (separades per π) són permeses per a les solucions estacionàries homogènies.

Aquest canvi en la naturalesa del sistema provoca l'aparició d'una nova dinàmica caracteritzada per la presència d'un nou tipus d'estructures espacials en el pla transversal bidimensional: patrons biestables de fase en els quals dominis d'ambdues fases conviuen separades per parets de domini (Ising si la intensitat s'anul·la en elles o Bloch, en cas contrari). Aquests dominis poden evolucionar a patrons homogenis (d'una de les dues fases) o uns altres, més

complexos, que els efectes de curvatura condueixen a la creació de patrons laberíntics segons els valors dels paràmetres del sistema. A més, poden existir estructures localitzades (dominis de grandària mínima estables) en la forma de solitons de cavitat d'anell fosc.

Altres mètodes de trencament de la simetria de fase han sigut usats per a controlar la dinàmica de molts sistemes. Un dels més populars és la ressonància paramètrica, i.e. injectar un camp la freqüència del qual és aproximadament el doble de la freqüència natural de oscil·lació del sistema. No obstant això, aquests mètodes són menys versàtils que el rocking, el qual pot aplicar-se a una àmplia gamma de sistemes com el làser, que són insensibles a la ressonància paramètrica. De fet, s'han fet múltiples propostes teòriques i experimentals d'aplicació del rocking a diferents sistemes (òptics i no òptics). En el domini d'aquesta tesi, ens centrarem en la influència del rocking en dos sistemes que han sigut estudiats profusament en la literatura, donat el seu gran interès tant des del punt de vista fonamental com pràctic:

Làser. El làser (acrònim d'amplificació de llum per emissió estimulada de radiació) és possiblement el sistema òptic no lineal més rellevant, tant per la seua naturalesa, intrínsecament no lineal, com perquè gràcies a les propietats singulars de l'emissió làser (profundament monocromàtics i altament focalitzables), es poden estudiar multitud d'efectes no lineals que requereixen altes concentracions d'energia per a manifestar-se. Un làser consisteix essencialment en un mitjà que presenta inversió de població (més electrons en un estat excitat que en el fonamental) per la interacció amb un bombeig i és capaç de generar radiació electromagnètica per emissió estimulada que es veu amplificada després de passar un gran nombre de vegades a través de l'ampli

ficador que ve dau pel pas de la llum una vegada i una altra entre els espills de la cavitat. El model de làser més estudiat és el làser de dos nivells (una abstracció, ja que es necessiten almenys tres nivells per a aconseguir inversió de població) ja que permet un tractament analític assumible, sent les equacions de Maxwell-Bloch (MB) les que descriuen aquest model. En l'emissió làser qualsevol fase és possible ja que és un sistema autooscilant en el qual la fase no està fixada, la qual cosa determina el tipus de patrons que apareixen. La formació de patrons transversals en làsers (en absència d'injecció) ha sigut estudiada tant en configuracions de cavitat amb xicoteta obertura (sota número de Fresnel), en els quals el xicotet nombre de modes transversals admeses pel sistema i la seua interacció no lineal són els responsables de les estructures espacials (modes gaussianes), com en

casos on el número de Fresnel és gran, en els quals el nombre de modes és gran i la presència de vòrtexs i ones viatgeres és usual. A causa del seu interès, s'han realitzat nombroses propostes teòriques i experimentals per a la generació d'estructures localitzades (solitons) en làsers, especialment en làsers de semiconductor, que són interessants per a possibles aplicacions, en el sentit de ser capaços de crear un sistema compacte per al processament de la informació (textitlàser de solitones). En el nostre cas, ens centrarem en l'aplicació del rocking a làsers: (i) unidireccionals i (ii) bidireccionals, en els quals dos camps contrapropagants conviuen dins d'una cavitat en anell.

Oscil·lador fotorrefractiu. Aquest sistema és una cavitat òptica en la qual el mitjà no lineal és un cristall fotorrefractiu, el qual posseeix un índex de refracció que depèn de la modulació espacial de la intensitat de la llum. La interferència de dos feixos en el cristall crea un patró periòdic en el camp elèctric sent responsable una modulació espacial en l'índex. Aquest efecte no lineal, combinat amb una mescla de dues ones en cavitat d'anell, dóna lloc a l'emissió de radiació que, com el làser, presenta invariància de fase. La principal diferència és que, en aquest cas, la dinàmica en el pla transversal és molt més lenta (de l'ordre de segons, diversos ordres de magnitud major que la del làser) a causa de les especials característiques del mitjà fotorrefractiu (especialment de la seua corba de guany). Això presenta indubtables avantatges a l'hora d'estudiar experimentalment la formació de patrons, ja que no calen equips sofisticats d'enregistrament per a analitzar-los. És per això que els oscil·ladors fotorrefractius s'han convertit en perfectes *laboratoris* per a l'estudi de patrons transversals en cavitats òptiques i el nombre de resultats experimentals obtinguts en ells és enorme. En el nostre cas, estudiarem teòricament la influència del rocking en oscil·ladors fotorrefractius en configuració de mescla de dues ones, en cavitat d'anell.

Al llarg d'aquesta tesi, estudiarem detalladament la influència del rocking en aquests sistemes. Com és usual en el camp de la ciència no lineal, és convenient deduir equacions que descriguen el comportament d'aquests sistemes prop dels punts (punts crítics) on emergeixen les solucions estacionàries del sistema. Aquestes equacions (anomenades de paràmetre d'ordre) tenen una forma aparentment simple i són capaces de descriure multitud de sistemes no lineals, físics, químics, biològics.. (l'única diferència és el significat dels diferents paràmetres, però l'estructura matemàtica és la mateixa), per la qual cosa posseeixen un caràcter universal. Així mateix, analitzarem l'estabilitat de les solucions trobades i realitzarem simulacions numèriques dels diferents models teòrics.

L'estructura del manuscrit de la tesi és la següent. El primer capítol es dedicarà a una introducció que contindrà:

- Una discussió sobre el fenomen de la formació de patrons en la naturalesa.
- Una introducció general d'algunes de les principals contribucions fetes fins ara en el camp de la formació de patrons en el camp de l'òptica no lineal.
- Una introducció formal al mecanisme del rocking i una revisió dels sistemes on ha sigut aplicat.
- Una xicoteta discussió sobre les equacions de paràmetre d'ordre, en concret les equacions (reals i complexes) de Ginzburg-Landau i Swift-Hohenberg, que han sigut deduïdes fins ara per a cavitats òptiques.
- Un resum de les eines matemàtiques, analítiques i numèriques que hem emprat per a dur a terme el nostre estudi, com són: l'anàlisi d'escala múltiple per a l'obtenció d'equacions de paràmetre d'ordre, l'anàlisi d'estabilitat lineal per a analitzar les inestabilitats de les solucions estacionàries del sistema enfront de pertorbacions espaciotemporals, i el mètode d'integració numèrica split-step, convenientment modificat per a incorporar forçaments externs dependents del temps com el rocking.

En el segon capítol resumiré les meues principals contribucions als articles presentats organitzats per temàtica. Així mateix, es presentaran alguns resultats que no han sigut publicats encara:

- A partir de les equacions de MB amb injecció rocking, es deduirà una equació de paràmetre d'ordre per a làsers de classe C amb desintonia positiva de la cavitat i s'estudiaran numèricament els patrons del sistema.
- Per a làsers de classe B, s'obté un model reduït de dues equacions i s'analitzarà la seua dinàmica temporal i la influència de la desintonia de la injecció rocking. També es mostraran patrons espacials obtinguts a partir de la simulació de les equacions de MB.
- Es desenvoluparà un model unificat (vàlid per a desintonies de la cavitat positives i negatives) per a làsers de dos nivells (classe C i A) i oscil·ladors fotrorefractius, proporcionant els dominis d'estabilitat dels estats biestables en fase i estudiant numèricament els patrons espacials que apareixen.
- S'analitzarà la dinàmica temporal d'un làser bidireccional amb injecció rocking i es presentaran alguns resultats preliminars de patrons espacials.

Finalment, en el tercer capítol exposaré les nostres principals conclusions del treball realitzat. Com a annex inclourem una còpia dels cinc articles publicats que donen suport a aquesta tesi.

Versión en castellano

Esta tesis se presenta como compendio de publicaciones [1–5]. A partir de ahora se citarán como Paper I, Paper II, Paper III, Paper IV y Paper V respectivamente.

En la naturaleza, la formación de patrones en sistemas espacialmente extensos es un fenómeno recurrente que suele estar asociado a situaciones en los que hay una respuesta no lineal de un sistema sometido a un forzamiento externo que lo sitúa lejos de su estado de equilibrio (termodinámico). Esto conduce a la generación de estructuras inhomogéneas espacialmente que son conocidas como *disipativas*, dado que en estos sistemas forzados hay un balance entre el aporte externo de energía y las pérdidas propias del sistema disipativo.

En particular, este tipo de estructuras son muy comunes en el campo de la Óptica no lineal, especialmente en aquellas configuraciones en las que un medio interactúa no linealmente con la luz rodeado de dos espejos (cavidad óptica). En esta situación, los patrones aparecen en el plano perpendicular a la dirección de propagación y esta es la razón por la que se denominan "patrones transversales". Un ejemplo especialmente relevante son las llamadas estructuras localizadas o solitones de cavidad (existen en una región limitada del plano transversal y son estables), las cuales poseen un gran interés ya que pueden ser escritas o borradas independientemente mediante haces de luz coherentes, por lo que potencialmente podrían ser usadas para almacenamiento y procesamiento de información mediante métodos puramente ópticos. Por ejemplo, un conjunto de $N \times N$ solitones constituye una memoria óptica de $2^{N \times N}$ estados diferentes.

Esta tesis tiene como objetivo el estudio teórico, analítico y numérico, de la dinámica espaciotemporal de osciladores ópticos no lineales sometidos a un forzamiento bicromático (rocking). Este tipo de inyección, introducida en [6], tiene la característica principal de romper la invariancia de fase (cualquier fase del campo complejo) del sistema libre (sin forzamiento) y genera un sistema que es biestable en fase en el que únicamente dos fases (separadas por π) son permitidas para las soluciones estacionarias homogéneas.

Este cambio en la naturaleza del sistema provoca la aparición de una nueva dinámica caracterizada por la presencia de un nuevo tipo de estructuras espaciales en el plano transversal bidimensional: patrones biestables de fase en los que dominios de ambas fases conviven separadas por paredes de dominio (Ising si la intensidad se anula en ellas o Bloch, en caso contrario). Estos

dominios pueden evolucionar a patrones homogéneos (de una de las dos fases) u otros, más complejos, en que los efectos de curvatura conducen a la creación de patrones laberínticos según los valores de los parámetros del sistema. Además, pueden existir estructuras localizadas (dominios de tamaño mínimo estables) en la forma de solitones de cavidad de anillo oscuro.

Otros métodos de rotura de la simetría de fase han sido usados para controlar la dinámica de muchos sistemas. Uno de los más populares es la resonancia paramétrica, i.e. forzar periódicamente un sistema a una frecuencia que es aproximadamente el doble de su frecuencia natural de oscilación. Sin embargo, estos métodos son menos versátiles que el rocking, el cual puede aplicarse a una amplia gama de sistemas como el láser, que son insensibles a la resonancia paramétrica. De hecho, se han hecho múltiples propuestas teóricas y experimentales de aplicación del rocking a diferentes sistemas (ópticos y no ópticos). En el dominio de esta tesis, nos centraremos en la influencia del rocking en dos sistemas que han sido estudiados profusamente en la literatura, dado su gran interés tanto desde el punto de vista fundamental como práctico:

Láser. El láser (acrónimo de amplificación de luz por emisión estimulada de radiación) es posiblemente el sistema óptico no lineal más relevante, tanto por su naturaleza, intrínsecamente no lineal, como porque gracias a las propiedades singulares de la emisión láser (profundamente monocromáticos y altamente focalizables), se pueden estudiar multitud de efectos no lineales que requieren altas concentraciones de energía para manifestarse. Un láser consiste esencialmente en un medio que presenta inversión de población (más electrones en un estado excitado que en el fundamental) por la interacción con un bombeo y es capaz de generar radiación electromagnética por emisión estimulada que se ve amplificada tras pasar un gran número de veces a través del amplificador que viene dado por el paso de la luz una y otra vez entre los espejos de la cavidad. El modelo de láser más estudiado es el láser de dos niveles (una abstracción, ya que se necesitan al menos tres niveles para conseguir inversión de población) ya que permite un tratamiento analítico asumible, siendo las ecuaciones de Maxwell-Bloch (MB) las que describen este modelo. En la emisión láser cualquier fase es posible ya que es un sistema autooscilante en el que la fase no está fijada, lo que determina el tipo de patrones que aparecen. La formación de patrones transversales en láseres (en ausencia de inyección) ha sido estudiada tanto en configuraciones de cavidad con pequeña apertura (bajo número de Fresnel), en los que el pequeño número de modos transversales admitidos por el sistema y su interacción no lineal son

los responsables de las estructuras espaciales (modos gaussianos), como en casos donde el número de Fresnel es grande, en los que el número de modos es grande y la presencia de vórtices y ondas viajeras es usual. Debido a su interés, se han realizado numerosas propuestas teóricas y experimentales para la generación de estructuras localizadas (solitones) en láseres, especialmente en láseres de semiconductor, que son interesantes para posibles aplicaciones, en el sentido de ser capaces de crear un sistema compacto para el procesado de la información (*láser de solitones*). En nuestro caso, nos centraremos en la aplicación del rocking a láseres: (i) unidireccionales y (ii) bidireccionales, en los que dos campos contrapropagantes conviven dentro de una cavidad en anillo.

Oscilador fotorrefractivo. Este sistema es una cavidad óptica en la que el medio no lineal es un cristal fotorrefractivo, el cual posee un índice de refracción que depende de la modulación espacial de la intensidad de la luz. La interferencia de dos haces en el cristal crea un patrón periódico en el campo eléctrico siendo responsable una modulación espacial en el índice. Este efecto no lineal, combinado con una mezcla de dos ondas en cavidad de anillo, da lugar a la emisión de radiación que, como el láser, presenta invariancia de fase. La principal diferencia es que, en este caso, la dinámica en el plano transversal es mucho más lenta (del orden de segundos, varios órdenes de magnitud mayor que la del láser) debido a las especiales características del medio fotorrefractivo (en especial de su curva de ganancia). Esto presenta indudables ventajas a la hora de estudiar experimentalmente la formación de patrones, ya que no hacen falta equipos sofisticados de grabación para analizarlos. Es por ello que los osciladores fotorrefractivos se han convertido en perfectos *laboratorios* para el estudio de patrones transversales en cavidades ópticas y el número de resultados experimentales obtenidos en ellos es enorme. En nuestro caso, estudiaremos teóricamente la influencia del rocking en osciladores fotorrefractivos en configuración de mezcla de dos ondas, en cavidad de anillo.

A lo largo de esta tesis, estudiaremos detalladamente la influencia del rocking en dichos sistemas. Cómo es usual en el campo de la ciencia no lineal, es conveniente deducir ecuaciones que describan el comportamiento de dichos sistemas cerca de los puntos (puntos críticos) donde emergen las soluciones estacionarias del sistema. Estas ecuaciones (llamadas de parámetro de orden) tienen una forma aparentemente simple y son capaces de describir multitud de sistemas no lineales, físicos, químicos, biológicos.. (la única diferencia es el significado de los diferentes parámetros, pero la estructura matemática es la misma), por lo que poseen un carácter universal. Asimismo,

analizaremos la estabilidad de las soluciones encontradas y realizaremos simulaciones numéricas de los diferentes modelos teóricos.

La estructura de este manuscrito es la siguiente. El primer capítulo se dedicará a una introducción que contendrá:

- Una discusión sobre el fenómeno de la formación de patrones en la naturaleza.
- Una introducción general de algunas de las principales contribuciones hechas hasta ahora en el campo de la formación de patrones en el campo de la óptica no lineal.
- Una introducción formal al mecanismo del rocking y una revisión de los sistemas donde ha sido aplicado.
- Una pequeña discusión sobre las ecuaciones de parámetro de orden, en concreto las ecuaciones (reales y complejas) de Ginzburg-Landau y Swift-Hohenberg, que han sido deducidas hasta ahora para cavidades ópticas.
- Un resumen de las herramientas matemáticas, analíticas y numéricas que hemos empleado para llevar a cabo nuestro estudio, como son: el análisis de escalas múltiples para la obtención de ecuaciones de parámetro de orden, el análisis de estabilidad lineal para analizar las inestabilidades de las soluciones estacionarias del sistema frente a perturbaciones espacio-temporales, y el método de integración numérica split-step, convenientemente modificado para incorporar forzamientos externos dependientes del tiempo como el rocking.

En el segundo capítulo resumiré mis principales contribuciones a los artículos presentados organizados por temática. Asimismo, se presentarán algunos resultados que no han sido publicados todavía:

- A partir de las ecuaciones de MB con inyección rocking, se deducirá una ecuación de parámetro de orden para láseres de clase C con desintonía positiva de la cavidad y se estudiarán numéricamente los patrones del sistema.
- Para láseres de clase B, se obtendrá un modelo reducido de dos ecuaciones y se analizará su dinámica temporal y la influencia de la desintonía de la inyección rocking. También se mostrarán patrones espaciales obtenidos a partir de la simulación de las ecuaciones de MB.
- Se desarrollará un modelo unificado (válido para desintonías de la cavidad positivas y negativas) para láseres de dos niveles (clase C y A) y osciladores fotrorefractivos, proporcionando los dominios de estabilidad de los estados biestables en fase y estudiando numéricamente los patrones espaciales que aparecen.
- Se analizará la dinámica temporal de un láser bidireccional con

inyección rocking y se presentarán algunos resultados preliminares de patrones espaciales.

Por último, en el tercer capítulo expondré nuestras principales conclusiones del trabajo realizado. Como anexo incluiremos una copia de los cinco artículos publicados que apoyan esta tesis.

1.1 Dissipative structures in Optics

Dissipative structures in nature

Spatio-temporal pattern formation occurs everywhere and everytime in nature [7, 8]. Complex non-trivial structures can be found in systems [9] apparently so different like the sand of a beach, the interior of a cell or a galaxy (Fig. 1.1). The dynamics of these systems have very different typical (spatial and temporal) evolution scales (from milimeters to light-years) but the mechanisms that lead to pattern formation are similar in all of them. Those have been studied since a long time ago, in hydrodynamics [10], biology [11] or chemical reactions [12]. In nonlinear optics (the invention of the lasers in 1960s allowed to study experimentally nonlinear phenomena in optics), the seminal paper by Lugiato and Lefever [13] was one of the first ones to address this question.

If we look closer to these systems displaying pattern formation, we see that, in many cases, they are far from thermodynamic equilibrium [14] in the sense that they are permanently forced by an external force which interacts nonlinearly with the system. This externality, combined with the natural losses of any real system, produces the appearance of patterns (stationary or dynamical) which are called dissipative [15] due to this balance of energy (which prevents the system from having merely decaying solutions as it is usual in systems with losses). Nonlinear systems [16] possess features, like the non-superposition principle, which helps to explain the appearance of patterns in extended systems. Specifically, the Turing mechanism for reaction-diffusion models [11] arises from a competition between diffusion (diffraction in optics),



Figure 1.1: Extended spatial patterns found in nature: (left) sand ripples (from pixabay.com) and (right) spiral Pinwheel Galaxy M101 (from Hubble telescope, ESA/NASA).

which tends to preserve spatial uniformity and nonlinearity, which encourages inhomogeneity in the system. The balance between the two is responsible for the stability of these structures. Extended patterns like traveling waves, labyrinths or hexagons have been predicted in chemical reactions of Belousov-Zhabotinsky-type [17].

Similar explanations for pattern formation have been also proposed in nonlinear optics [13], where there has been much progress since 1990s (section 1.1). This proves that the particular microscopical physical mechanism is not essential for understanding these systems (at least in certain limits like critical points where solutions of the systems are born or cease to exist). Moreover, they can be studied from a more general approach which involves (relatively simple) nonlinear equations which describe a wide range of nonlinear systems close to critical points. These equations are called order parameter equations and they have a universal character. So the derivation of one of these equations for a nonlinear system happens to be the best way to understand, qualitatively and also quantitatively, its basic behaviour and making predictions of its spatio-temporal dynamics which can be confirmed experimentally. In section 1.2 we will study these equations more deeply.

Dissipative solitons (stable localized structures) constitute one of the most interesting patterns we may find in these nonlinear systems. Such structures are a generalization, in dissipative systems, of the "conventional" solitons [18], which were observed for the first time (*solitary wave*) in [19] although the concept was introduced in [20] when studying the numerical solutions of the Korteweg de Vries equation. These solitons (also solitary pulses) can be regarded as (a family of) nonlinear modes of a conservative system and have

a different nature than the dissipative ones. Dissipative solitons have been experimentally found in fluid, granulates and chemical systems [21–23].

In the following subsections, I will describe some of the spatial structures which appear in Nonlinear Optics, starting with a short discussion about under which conditions those patterns are observable.

Extended patterns in Optics

Patterns in nonlinear optics are ubiquitous and are present in a large variety of systems [24, 25] like lasers, optical fibers, planar waveguides or liquid crystals among others. For the sake of concreteness, we will restrict ourselves to pattern formation in optical cavities (nonlinear medium placed between two mirrors of high reflectance) with large Fresnel number¹ (aspect ratio) in the transverse (to the direction of propagation) dimensions [26, 27]. In this case the nonlinearity comes for the interaction between the material and the electromagnetic field. The cavity can be active if the medium provides energy to the field (i.e. laser) or passive (Kerr-type cavity in the Lugiato-Lefever model) [28, 29].

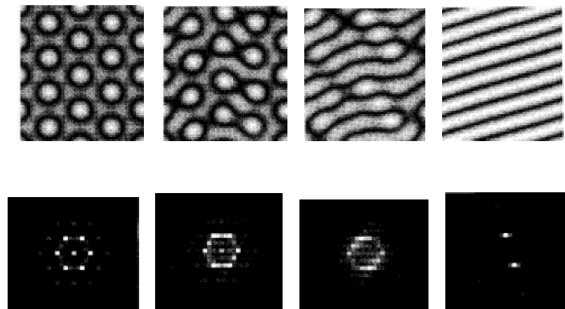


Figure 1.2: Transitions from hexagons (left) to rolls (right) in a degenerate optical parametric oscillator (DOPO). Spatial spectrum is shown in the second row. From [32].

For large aspect ratio systems a practical separation between transverse and longitudinal modes (as it is usual in optical cavities like lasers [30]) can be made. The longitudinal dimension usually admits a single-mode (uniform) emission whereas for the transverse directions a large number of modes are

¹If L_x is one transverse length and L_z the longitudinal length, L_x/L_z is the angle of view of an object of linear size L_x from a distance L_z . As wavelength λ/L_x is the minimal angular resolution due to diffraction, then $F = L_x^2/\lambda L_z$ can be seen as the number of independent resolution elements along L_x detectable at a distance L_z .

allowed. If the number of these transverse modes is small (low Fresnel number) the resulting transverse patterns are determined essentially by the geometry of the cavity and its boundary conditions and they are the result of the competition between a finite number of modes and the nonlinear interaction. However, if a large number of transverse modes is present, the emerging patterns only depend on dynamical variables and its formation can be modelled using universal order parameter equations similar to the ones employed in other (not only physical) systems. Additionally, this large Fresnel number condition allows us to establish analogies between different nonlinear optical systems as they can be described, in certain limits, by the same equation despite the different nature of the nonlinear processes involved (section 2.4).

If we consider nonlinear optical cavities with flat mirrors, the inherent translational symmetry simplifies the theoretical analysis as we don't have to deal with the set of cavity modes as it happens when curved mirrors are considered [31]. The stationary homogeneous solutions of the systems can become unstable against small perturbations of wavevector \mathbf{k} with modulus k_c^2 which maximizes the (positive) real part of the associated eigenvalue. All these modes initially experiences linear growth but the nonlinear competition between them leads to the survival of only a finite number of them. This produces traveling waves (one surviving mode), rolls (two), squares (four) or hexagons (six). The resulting patterns are not always stable and can suffer secondary instabilities (Fig. 1.2).

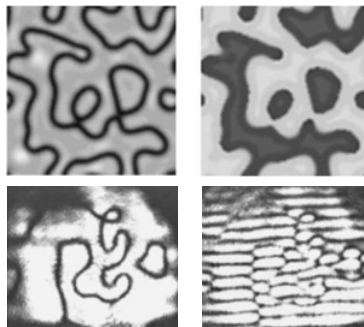


Figure 1.3: (Upper Row) Intensity (left) and Phase (right) distributions of phase domains obtained numerically in a DOPO [29]. (Lower row) Intensity (left) and interferogram showing the π -phase jumps in the boundaries (right) of phase domains obtained experimentally in a PRO [33].

In phase bistable systems a different kind of spatial patterns appear. They are characterized (in 2D) by phase domains (Fig. 1.3) of one phase embedded in a background of the opposite phase. These are transient structures which may suffer modulational instabilities [34] leading to labyrinthic patterns.

Localized structures in Optics

The presence of solitons in nonlinear cavities (cavity solitons [35]) was first studied by Moloney and collaborators [36] and by Rosanov in [37, 38], where solitons ("diffractive autosolitons") came from the interaction of switching waves with two homogeneous stationary states.

Other localized structures arise when two or more transverse patterns are stable for the same range of parameters and the resulting multistability generates more complex structures. Specifically, if a homogeneous stationary solution and a spatially modulated stationary solution coexist, localized structures (for instance, a *piece* of the modulated solution surrounded by the homogenous one) can appear. The existence of such structures was predicted in [39]. The location, shape and size of the localized states can be very diverse depending on the system and the value of the parameters governing its dynamics. Their movement (they can spontaneously move due to thermal noise) can be controlled using phase or amplitude gradients in the holding beam [40]. Moreover, control and steering of domain walls in phase-sensitive systems has been explored (theoretically) in a DOPO [41] and (experimentally) in a four-wave mixing PRO [42].



Figure 1.4: Bright amplitude (left) and dark-ring (right) cavity solitons in a DOPO. From [29].

A basic classification of CS can be made, according to their relative intensity to the background, between bright (Fig. 1.4) solitons (intensity peak) and dark/grey (a minimum of intensity) solitons. In both cases they are amplitude solitons and they appear in subcritical bifurcations (Fig. 1.5) where bistability between homogeneous solutions is present.

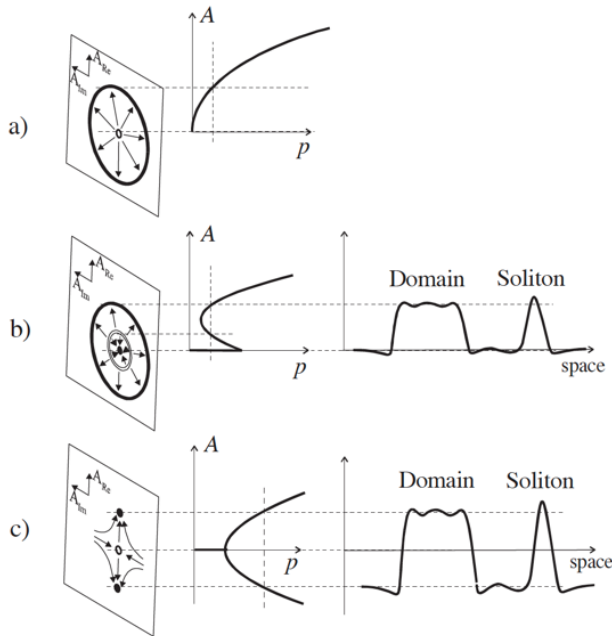


Figure 1.5: Different types of bifurcation in nonlinear systems. (a) Supercritical Hopf bifurcation (like free-running laser), (b) subcritical Hopf bifurcation, (c) supercritical pitchfork bifurcation. A is the amplitude of the solution, and p is the pump (criticality) parameter. From [29].

Another kind of CS are the phase solitons, these are formed in phase bistable systems experiencing pitchfork bifurcations (Fig. 1.5) and can be interpreted as minimum size phase domains. They are characterized by domain walls (black or grey) which separate the two phases of the system leading to straight lines (quasi 1D systems) or rings (2D) (Fig. 1.4). These CS are the ones we usually find in optical cavities under rocking injection although amplitude solitons are also found in these systems [43].

As it was mentioned earlier, these CS should not be confused with other kind of solitons, which appear in (integrable or not) Hamiltonian systems and have a different nature (Fig. 1.6). In dissipative systems, apart from the balance between diffraction/dispersion and nonlinearity, there is an energy balance between gain and loss.

Other mechanisms for cavity soliton formation include intra-cavity materials (for passive Kerr cavities) with modulated refractive index (photonic

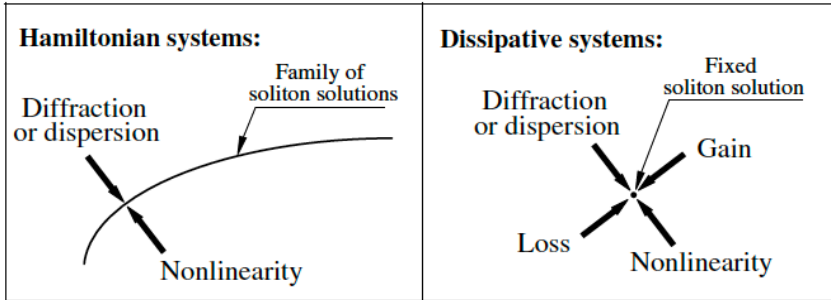


Figure 1.6: Qualitative difference between the soliton solutions in Hamiltonian and dissipative systems. In Hamiltonian systems, soliton solutions are the result of a single balance, and comprise one- or few-parameter families, whereas, in dissipative systems, the soliton solutions are the result of a double balance and, in general, are isolated. From [44].

crystal) which inhibits the formation of periodic transverse patterns, extending the bistability region where CS appear [45] and discrete models [46] for dissipative systems [47] giving rise to discrete CS. Additionally, not restricting ourselves to 2D spatial structures, 3D spatial CS (cavity light bullets) have been considered in [48].

Recently, much theoretical and experimental effort have been made regarding temporal cavity solitons (persisting light pulses) [49] although they are beyond the scope of this introduction and are cited only for completeness.

Patterns in Lasers and Photorefractive Oscillators

Transverse patterns in broad area free-running lasers have been studied since the late 1980s [50–54]. Universality of pattern formation in lasers was considered in [55, 56], where an analogy with hydrodynamics was found and the existence of optical vortices was predicted for class A lasers for the zero detuning case [56]. For finite positive detuning [57], vortex sheets and vortex lattices appear. When a monochromatic off-axis injected signal is included [58], patterns due to superposition of traveling waves are found.

The bifurcation which originates emission in a free-running laser is supercritical so amplitude cavity soliton are not possible (their existence requires subcritical bifurcation as we saw before) in this configuration. Many mechanisms for generating (creating subcritical bifurcations) cavity solitons

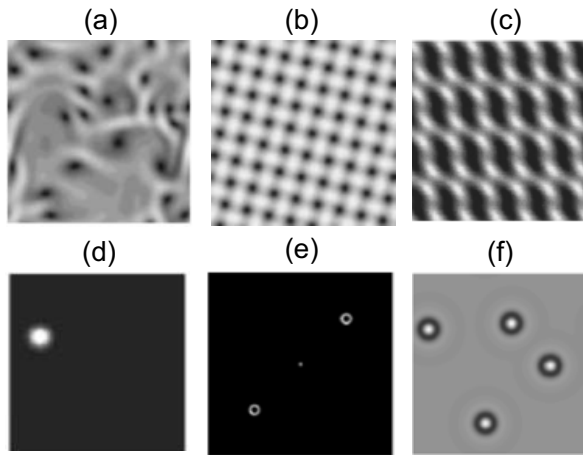


Figure 1.7: Transverse patterns predicted in lasers under different conditions: (a) vortices in free-running resonant laser [56], (b) vortex square in lasers with finite detuning [57], (c) laser with injected signal [58], (d) laser with saturable absorber [60], (e) dense media [63] and (f) laser pumped by squeezed light [64].

in lasers have been proposed since 2000s: if a saturable absorber is placed intracavity [59], a subcritical bifurcation is achieved and amplitude solitons are predicted to exist [60] and further investigation taking into account the nonlocal and noninstantaneous nature of nonlinearity has been made [18, 61]. Amplitude solitons are also predicted for two photon emission in cascade lasers [62] and when local field effects in dense media are considered [63]. On the other hand, sources of squeezed light lead to the formation of phase solitons and other phase structures in lasers [64]. (Fig. 1.7)

Experimental investigations regarding CS were made in semiconductor microcavities below the lasing emission threshold [65], where writing and erasing of CS was demonstrated (Fig. 1.8). Temporal phase² cavity solitons in multimode semiconductor lasers have been explored theoretically and experimentally in [66]. Excitability associated to topological phase solitons in semiconductor lasers with delayed feedback is shown in [67].

In bidirectional lasers [68] 1D CS were predicted several years ago [69]. Further analysis and investigation of the influence of coherent external injection was given in [70] and the impact of diffusion for stabilizing CS was analyzed

²In this case, an injected signal allows a single phase in the system and the phase structure displays a 2π rotation.

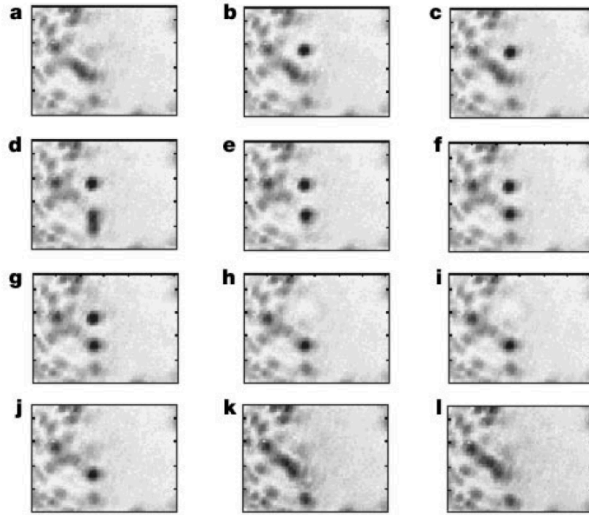


Figure 1.8: Writing/erasing process of cavity solitons in semiconductor microcavities. From [65].

in [71, 72]. Lastly, In photorefractive oscillators (PRO), experiments involving a large Fresnel number [73, 74] led to the appearance of vortices in the transverse plane (Fig. 1.9).

Some practical applications of CS in nonlinear optics were discussed in [75], including optical memories, through writing/erasing CS (although their size and mobility are a problem against other alternatives), all-optic delay line, in which CS can be considered "stopped light" which can be moved at controllable velocity, and *soliton-force* microscopy (SFM), exploiting the (spontaneous or defects-driven) movement of CS to design a SFM in the few-micrometers (size of a CS) range.

A cavity soliton laser (CSL), in which the lasing emission consists of cavity solitons and can be regarded as a set of microlasers in a background of pure spontaneous emission, is an active device which would allow to generate CS without the need of a driven external beam which besides determines (in a CSL the CS would have the freedom to choose its phase leading to interesting fundamental and application-focused studies) the characteristics of CS in passive systems. Experimental realizations of a CSL using a semiconductor laser (VCSELs: vertical-cavity surface-emitting lasers) were made in [76] by means of frequency-selective feedback VCSELs, [77] where two coupled VCSELs in a face-to-face configuration are used and [78] in which a monolithic

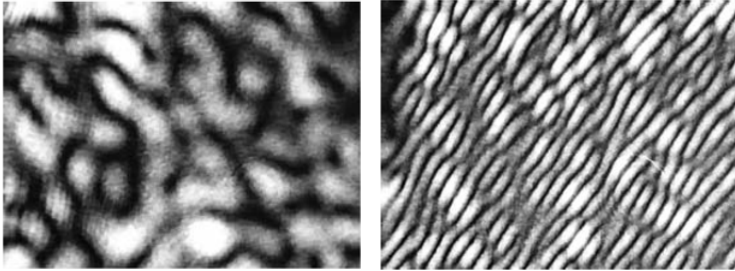


Figure 1.9: Transverse pattern of a PRO with large Fresnel number where vortices of different charges can be observed: intensity distribution (left) and interferogram (right). From [74].

VCSEL with saturable absorber is considered. In these systems the motion of CS can't be controlled through an external beam but it is possible to introduce gradients in the pump parameter. This has been analyzed theoretically for CSL with saturable absorber lasers in which (self-propelled) movement of CS (in absence of defects in the material) with constant velocity was predicted [79] and a cavity-soliton billiard (using a square pump profile) was proposed [80].

1.2

Universal dynamics

As it was mentioned in section 1.1, it is possible to describe the spatio-temporal dynamics of many nonlinear systems close to critical points by means of a series of so-called order parameter equations (OPE). These equations have a relatively simple mathematical structure and are valid for a large number of physical and no-physical systems, being the only difference the meaning of the parameters. This is why the dynamics described by OPE is known also as universal dynamics.

OPE can be classified between real and complex according to the nature of the variables used. In nonlinear optics it is usual to describe the electric field in its complex form³ so the complex OPE are widely used, although in context where phase locking is present (like in phase bistable system) it is possible to describe the dynamics by means of real OPE [29]. Two equations have been widely used in nonlinear optics: Ginzburg-Landau and Swift-Hohenberg models:

³The actual electric field is the real part of its complex description

Complex Ginzburg-Landau equation

The standard Complex Ginzburg-Landau equation (CGLE), which was originally developed for a phenomenological approach to superconductivity [81], reads:

$$\partial_t A = (1 + i\theta)A + (\alpha_1 + i\alpha_2)\nabla^2 A - (\beta_1 + i\beta_2)f(|A|^2)A \quad (1.1)$$

where $f(x) = x$ usually in cavity nonlinear optics (although the version with an extra quintic term [18] is also commonly used when studying fiber solitons). In the equation, the distance to threshold has been normalized to 1, α_1 (α_2) stands for diffusion (diffraction), β_1 (β_2) stands for saturation (nonlinear dispersion) and θ is the detuning parameter. In cavity nonlinear optics $\alpha_1 \ll \alpha_2$ and $\beta_2 \ll \beta_1$ in most cases. This equation has been analyzed in many contexts [82] and possesses a continuous phase symmetry: If A is a solution, then $Ae^{i\phi}$ is also a solution for any ϕ . This leads to the appearance of vortices in spatially extended systems [29].

The previous equation is a prototypical model for describing self-oscillatory systems close to threshold of emission and CGLEs have been derived for doubly resonant DOPO [84] and lasers [83] among other nonlinear optical systems. A real version of this equation was obtained in [85] where optics bistability was analyzed and in [32] for the DOPO with positive detuning. If the laplacian is removed we obtain a, temporal only, evolution equation (Stuart-Landau) which will be used to analyze bidirectional lasers in section 2.4.

A CGLE describes the dynamics of a (class C or class A) laser for (large) positive cavity detuning. In the treshold the trivial solution is destabilized through a Hopf bifurcation to a solution showin homogeneous oscillations. However the expected traveling wave emission [86] for negative detuning is not captured by this model. This led to the derivation of a more complex model also valid for negative detuning: A Swift-Hohenberg equation (CSHE).

Complex Swift-Hohenberg equation

The CSHE is the complex version of the, most usual, real SHE [87] used first in hydrodynamics:

$$\partial_t A = (1 + i\theta)A + i\alpha\nabla^2 A - (\Delta + \nabla^2)^2 A - (\beta_1 + i\beta_2)|A|^2 A \quad (1.2)$$

The parameters have the same meaning as the CGLE except for Δ (usually related to the cavity detuning in nonlinear optics) which controls the kind of structures which emerges in the system when the trivial solution loses its

stability. The natural solution of the system are traveling waves for negative Δ and homogeneous oscillations or positive Δ .

In 1990s a CSHE was derived [88, 89] for a laser with (small) positive and negative detuning which captured the predicted behaviour for every case and, additionally, a reduced model of two coupled equations for (mathematically stiff) class B lasers was provided. We will comment on that in the next subsection.

The real SHE appears in DOPO [32] and other phase-bistable systems [85]:

$$\partial_t A = A - A^3 - (\Delta + \nabla^2)^2 A \quad (1.3)$$

It has only one parameter, and it has been studied analytically and numerically in many contexts, eg in [90], in which the stability of localized structures was analyzed.

Class B lasers

It is possible to derive reduced models based on CGLE or CSHE for class A and class C lasers (section 2.1) starting from MB equations for two-level lasers. But class B lasers, which are characterized by a very small damping rate of the population dynamics ($b \ll 1$ in (2.1)), can't be described by these equations. Semiconductor lasers (like VCSELs), belong to this class so it is important to have reduced models for them. These usually require two equations (three variables: one complex and one real) as the fact that b is so small (stiffness of the equation) implies that in the linear stability analysis of stationary solutions of MB equations [89] three eigenvalues remain close to zero and can't be eliminated. So typical SHE-based reduced models for class B lasers read⁴:

$$\partial_t A = (1 + i\theta)A + i\alpha\nabla^2 A - (\Delta + \nabla^2)^2 A - (\beta_1 + i\beta_2)NA \quad (1.4a)$$

$$\partial_t N = -bN + |A|^2 \quad (1.4b)$$

where the additional equation for the population inversion N acts like a mean-flow.

A linear stability analysis of class B lasers reveals [25] that above the emission threshold the nontrivial stationary solution is always stable, but the very small b makes the laser exhibit a very long transient to the stationary state when moved (significantly) above the threshold. This behaviour is

⁴Similar equations using a Ginzburg-Landau model can be obtained

characterized, in an initial state, by pulsing regime and in the final state by damped oscillations (relaxation oscillations). The frequency of these oscillations frequency is crucial for the efficiency of rocking as we will see in section 2.2.

The presence of stiffness in the model possesses undesired effects as very slow dynamics, which prevents the possibility of making exhaustive numerical simulations in these system. One alternative, using center manifold techniques, was provided in [91] for deriving reduced model for class B lasers in which stiffness is removed and computational times are strongly reduced .

1.3 Rocking mechanism

As it has been said before, along this thesis I will apply the rocking technique [6] to several nonlinear optical systems (lasers and photorefractive oscillators). In this section I will provide a general introduction to the rocking mechanism, including its motivation and main features.

Periodic forcing of nonlinear systems

The phase symmetries on nonlinear oscillators determines the nature of the patterns that are formed in the system. The continuous phase symmetry is responsible for spiral waves or vortices. A more structured behaviour arises when some kind of external forcing is considered, being the periodic temporal forcing [92, 93] the most usual one. This kind of injection acts an external clock, breaking the continuous phase symmetry of the system, which now becomes discrete. It is possible to show [92] that when the ratio between the external frequency and the natural frequency of the system ω_f/ω_0 is a rational number, the so called $n : m$ resonance, then n equivalent phases given by $\phi_k = \phi_1 + 2\pi(k-1)/n, k = 1, \dots, n$ are present in the (now) n -phase multi-stable. If the oscillator is well described, close to the onset of a Hopf bifurcation, by a complex Ginzburg-Landau equation with saturation and diffusion, then the effect of the external forcing close to a $n : m$ resonance can be expressed as:

$$\partial_t A = (\mu + i\nu)A + (1 + i\alpha)\nabla^2 A - (1 + i\beta)|A|^2 A + F^m (A^*)^{n-1} \quad (1.5)$$

where A is the amplitude, F is proportional to the amplitude of the external, forcing, α is the diffraction parameter and β is the nonlinear dispersion. Finally ν measures the (small) detuning respect to perfect tuned forcing: $\omega_f = (n/m)(\omega_0 + \nu)$

The (widely studied) 2 : 1 resonance (also called parametric forcing) gives rise to the appearance of phase bistable patterns, like phase domains, domain walls (Ising-type or Bloch-type [94]), labyrinths and localized structures like dissipative spatial (cavity) solitons (like the ones in section 1.1). However, this parametric forcing is not always useful as it requires the system to be sensitive (highly nonlinear) to a frequency which is far away from his natural frequency. This is not the case for many optical systems like lasers. So the idea is to obtain a similar behaviour we observe with parametric forcing using a 1 : 1 (frequency of the injection close to the one of the system) resonance which could work in those systems.

Intuition behind rocking

The rocking [6, 95] can be defined like a generalized 1 : 1 resonance in which the *amplitude* of the external forcing is modulated (in space and/or time) in a way that the sign (π separation between phases) is alternating from positive to negative in a periodic way. If this modulation is high enough (fast time scale or short spatial scale), then *on average* the system will see the same amount of every phase to it will tend to be phase bistable.

We can think of a mechanical analogy for rocking in which a massless particle in a bidimensional world, with coordinates q_1 and q_2 , evolves under the action of damping and a potential V which has a Mexican sombrero shape (Fig. 1.10). The maximum of V corresponds to an unstable off state and its degenerate minimum to the self oscillations state of finite amplitude (Fig. 1.10). If we start to *rock* the potential periodically very fast around one axis (say q_1), then the particle will tend to rest in the areas where the perturbation is minimal and this happens in two points of the perpendicular axis q_2 which are also in the minimum of the potential. (Fig. 1.10). The simplest candidate for V would be:

$$V(\mathbf{q}) = -\frac{\mu}{2}q^2 + \frac{1}{4}q^4 - q_1 F_0 \cos \Omega t, \quad (1.6)$$

where $q = \sqrt{q_1^2 + q_2^2}$ is the radial coordinate. If μ is positive then there is a maximum in the origin and a circle of radius $q = \sqrt{\mu}$ in which there is a minimum. The dynamical equations obey $dq_i/dt = -\partial V/\partial q_i$ as $m = 0$. Defining $A = q_1 + i q_2$ we can write:

$$\frac{dA}{dt} = \mu A - |A|^2 A + F_0 \cos(\Omega t) \quad (1.7)$$

which is the normal form of a Hopf bifurcation with a time-modulated forcing,

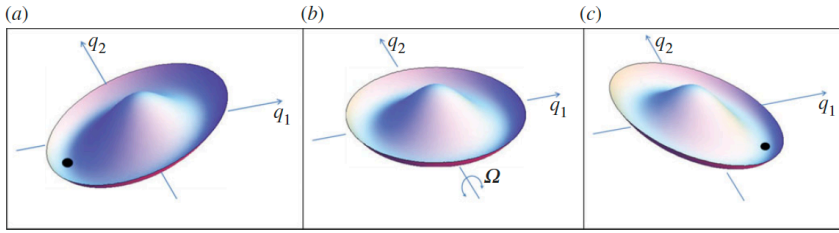


Figure 1.10: Qualitative three-dimensional plot of the potential V (1.6) which describes a rocked system. (From Paper IV).

so rocking an oscillator is equivalent to a periodic 1 : 1 forcing in which the amplitude oscillates periodically in time.

Following the previous analogy, in Fig (1.10)(b) without injection ($F = 0$), the potential is radially symmetric in agreement with the phase invariance of the free-running laser. In Fig (1.10)(a,c), with constant injection ($\Omega = 0$), the potential tilts along the direction $Re(A)$ proportionally to the forcing amplitude F and a single isolated minimum (marked with a black dot) appears, corresponding to the usual phase-locked state of the usual laser with injected signal. Under rocking ($\Omega \neq 0$) the potential oscillates back and forth between the two cases (a) and (c), through (b). Under such forcing, a particle would tend to remain close to the imaginary axis $Re(A) = 0$ around either of the two regions separated by the local maximum around the origin. The phase bistability occurs in phases in quadrature respect to the injection. If this is real (as in Fig. 1.10), phase locking occurs at $\pm\pi/2$.

Formal description of rocking

We will consider a complex Ginzburg-Landau (CGL), as the one in section 1.2, in which rocking injection is present:

$$\partial_t A = (\mu + i\theta)A + \alpha \nabla^2 A - \beta |A|^2 A + F(r, t), \quad (1.8)$$

where A , space and time have been normalized ⁵ so that $|\alpha| = |\beta| = 1$ without loss of generality. Moreover we can take $\mu = 1$. The real (imaginary) part of parameters α and β represents diffusion (diffraction) and saturation (nonlinear

⁵The details can be found in Paper IV

dispersion) respectively. The expression for $F(r, t)$ is:

$$\text{temporal case } F(r, t) = F_0 \cos \Omega t \quad (1.9)$$

$$\text{spatial case } F(r, t) = F_0 \cos Kx \quad (1.10)$$

where F_0 can be taken real without loss of generality, if the spatial (K) or temporal (Ω) frequencies are large then the dynamics of A can be decoupled [6] in a fast and slow component:

$$A(\mathbf{r}, t) = A_f(\mathbf{r}, t) + A_s(\mathbf{r}, t) \quad (1.11)$$

where the evolution equations for the fast components are:

$$\partial_t A_f = F_0 \cos \Omega t \text{ and } \nabla^2 A_f = -\frac{F_0}{\alpha} \cos Kx \quad (1.12)$$

whose solutions are:

$$A_f = \frac{F_0}{\Omega} \sin \Omega t \text{ and } A_f = \frac{F_0}{\alpha K^2} \cos Kx \quad (1.13)$$

so the fast part merely follows the injection whereas the slow part verifies:

$$\begin{aligned} \partial_t A_s = (1 + i\theta) A_s + \alpha \nabla^2 A_s - \beta \left[\langle A_f^2 \rangle A_s^* + 2 \langle |A_f|^2 \rangle A_s + \right. \\ \left. |A_s|^2 A_s + \langle |A_f|^2 A_f \rangle + 2 |A_s|^2 \langle A_f \rangle \right] \end{aligned} \quad (1.14)$$

where the angular brackets stand for averaging (time or space). Then we can write:

$$\partial_t A_s = (1 + i\theta - 2\gamma\beta) A_s - \gamma A_s^* + \alpha \nabla^2 A_s - \beta |A_s|^2 A_s, \quad (1.15)$$

where $\gamma = 1/2(F_0/\Omega)^2$ and $\gamma = 1/2(F_0/K^2)^2$ for the temporal and spatial case. Although we have considered the simplest harmonic case, the previous equation is valid in general and the only change is the definition of γ which depends on the functional form of the rocking. Equation (1.15) is a parametric CGL equation which has a term A_s^* that breaks the phase invariance of the free-running system ($\gamma = 0$) generating a discrete symmetry where only two phases (separated by π) are possible for the homogeneous solution. In order for the rocking to be efficient, as we can check from (1.14) that the average of the fast part $\langle A_f \rangle$ must be null, which implies that the injected rocking must have zero average. Additionally, it is also necessary that $\langle |A_f|^2 \rangle \neq 0$.

Apart from the systems studied in the articles which constitute this thesis, rocking (temporal and spatial) has been investigated (theoretically and experimentally) in a large variety of nonlinear systems. These include

nonlinear (0-dimensional) electronic circuits for both periodic [96] and random temporal rocking [97], passive Kerr cavities [43], small aspect ratio two-level lasers [98] and PRO [99] and semiconductor lasers [100]. More recently, spatial rocking in a large aspect ratio PRO was demonstrated experimentally [101]. Application of rocking to an already phase bistable system, generating phase tetrastability is analyzed in [102].

1.4 Mathematical techniques

In this section I will briefly describe the mathematical tools I have used to carry out the research presented in this thesis. First, we calculate the stationary solutions of the full model and perform a linear stability analysis. We can use this information to derive a reduced model (OPE) using the multiple scale expansion technique. Once this simplified model is obtained we can calculate its solutions and their stability region (by means of, again, a linear stability analysis). Lastly, we perform numerical simulations of the full or the reduced model to check the analytical results we have obtained and exploring the space of parameters looking for spatial patterns which can't be calculated analytically.

Linear stability analysis

A linear stability analysis [14] of a model provides information about the behaviour of the system close (in the parameter space) to its stationary solutions and allows us to study their stability/instability regions. In this analysis, the stationary (fixed point) homogeneous solution is perturbed with a small periodic perturbation of wavevector k . After linearizing the system, dropping out the nonlinear terms of the perturbation, these perturbations either are exponentially damped (stable solution) or grow exponentially (unstable solution). Thus, the parameter space can be divided into stable and unstable regions, with a threshold curve that is the marginal-stability curve, where the growth rate of the perturbations changes sign. In these curves the qualitative structures of the solutions change. These changes are called bifurcations and can be local or global (cannot be studied locally). In this kind of analysis only the local ones can be considered.

The simplest bifurcations of fixed-point solutions depending on one control parameter are saddle node, transcritical and pitchfork bifurcations [14]. In a Hopf bifurcation (Fig. 1.5), a complex pair of eigenvalues crosses from the stable to the unstable regime. Thus, a stable fixed point loses stability to

a stable limit cycle (as in the threshold of emission of a laser). A saddle-node bifurcation can connect (finite amplitude) stationary solutions with oscillatory regimes [5]. The pitchfork bifurcation (Fig 1.5) appears in systems with broken phase symmetry for complex variables (or when only non-even power terms are present for real variables).

Specifically, for a system of variables A_i modelled by first order equations \mathbf{G} for a set of parameters \mathbf{R} :

$$\partial_t A_i = G_i(A_j; \mathbf{R}) \quad (1.16)$$

The stationary solutions A_{0i} are slightly perturbed with a Fourier mode:

$$A_i = A_{0i} + \delta A_i(\mathbf{r}, t), \quad (1.17)$$

where $\delta A_i(\mathbf{r}, t) = \delta A_{0i} e^{\lambda_i t + \mathbf{k} \cdot \mathbf{r}}$.

We plug (1.17) into (1.16) and solve the system for λ_i (they will be the eigenvalues of the linearized G around A_{0i}). The solution in general will be complex and the eigenvalue with largest positive real part (growth rate) will be analyzed. The wavevector \mathbf{k}_c which maximizes the growth rate will inform us about the Fourier mode which will grow the fastest, and the value of the parameters \mathbf{R} which makes the growth rate equal to zero will define the stability region as we commented before. The imaginary part of the eigenvalue will tell us the nature of the instability: If $\text{Im}(\lambda) = 0$, it will be static and if $\text{Im}(\lambda) \neq 0$ we will have an oscillatory one. According to [14] we can have three types of pattern-forming systems (defining $\omega = \text{Im}(\lambda(\mathbf{k}_c))$):

- Type I_s ($\omega = 0, k_c \neq 0$), stationary periodic.
- Type I₀ ($\omega \neq 0, k_c \neq 0$), oscillatory periodic.
- Type III₀ ($\omega \neq 0, k_c = 0$), oscillatory uniform.

The case III_s ($\omega = 0, k_c = 0$) does not lead to pattern formation (only a switch between stationary homogeneous solutions)

How the real and imaginary parts of the eigenvalue depend on the parameters is essential for performing a multiple scale expansion as it will be commented in the next subsection.

In the case of nonlinear optics it is usual that the equations contain a (transverse) laplacian term ∇^2 for diffraction/diffusion (this is not true when an advective term, for instance, is present), so the eigenvalue depends only on the modulus of the wavevector. This rotational symmetry implies that a ring of critical wavevectors (Fig. 1.11) in the transverse Fourier plane which experience growth.

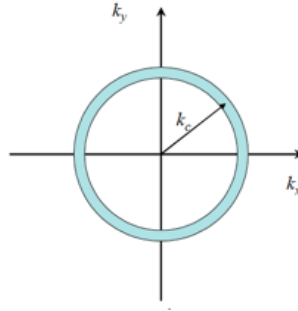


Figure 1.11: Critical ring of unstable modes of modulus k_c in transverse Fourier plane. (From [103]).

However, a nonlinear competition (as it was commented in section 1.1) between modes breaks this symmetry and only a finite number modes survive after the initial stages of evolution. The number of this modes determines the spatial pattern shown by the system (Fig. 1.12).

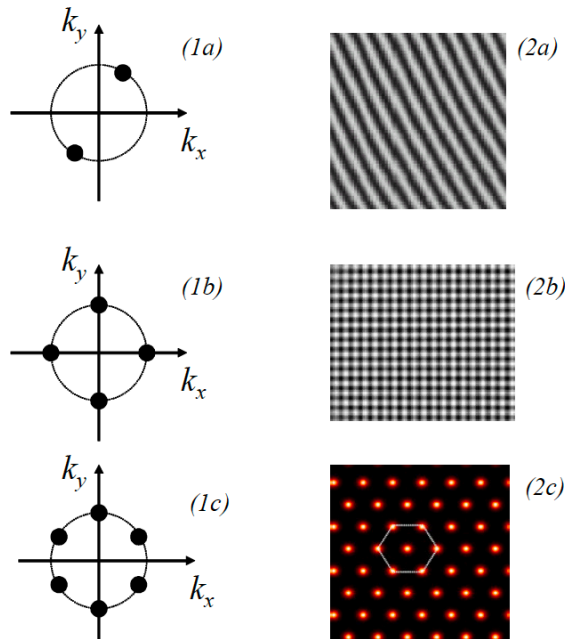


Figure 1.12: Rotational symmetry breaking. Examples of the simplest patterns: rolls (a), squares (b) and hexagons (c) in the far-field (1) and near-field (2). (From [103]).

Multiple scale expansion

A method commonly used in Nonlinear Physics for deriving OPEs is the multiple-scale expansion technique [29], The starting point a linear stability analysis, but the evolution equation of the order parameter is found as a solvability condition. This technique consists of the following steps:

1. The relevant variables and parameters of the system are expressed in terms of a smallness parameter ϵ . This allows one to write the fields as an asymptotic expansion,

$$\mathbf{v} = \sum_{n=1}^{\infty} \epsilon^n \mathbf{v}_n \quad (1.18)$$

The appropriate scales for every variable are obtained from a linear stability analysis of the stationary solution, which tells us how those variables grow close to the critical point where that solution loses its stability and how the growth rate depends on the parameters.

2. In the case of rocking, as it has been commented in section 1.3, it is useful to define two time scales: $T_1 = \epsilon t$ (fast), which is the time scale of rocking, and $T_2 = \epsilon^2 t$ (slow), being t the usual time. Under these conditions: $\partial_t \rightarrow \epsilon \partial_{T_1} + \epsilon^2 \partial_{T_2}$.

3. The original equations are expanded, and the coefficients of powers of ϵ are gathered. At order n , the equation has the form $L v_n = g_n$, which is linear in v_n , where g_n contains the nonlinear interactions and variations of the fields at lower orders, and L is a linear operator.

4. A solvability condition is applied at some order n , to require the existence of solutions.

5. Finally, at a given order, a closed equation is obtained for the evolution of the variables. In the case of rocking, the dynamics of the system under rocking can be divided into two parts: $A(T_1, T_2) = A_1(T_1) + A_2(T_2)$, in which A_1 which merely follows the fast injection and A_2 has a slow dynamics governed by an OPE with broken phase symmetry.

Examples of the application of this technique can be found in section 2.1 and in the appendices of Paper V.

Numerical simulations

We will use a modified version of the usual split-step method [104] for simulations of nonlinear partial differential equations. We will consider first the system:

$$\frac{\partial}{\partial t} \mathbf{X}(\mathbf{r}, t) = M(\mathbf{X}) \mathbf{X}, \quad (1.19)$$

where $M(\mathbf{X}) = L + N(\mathbf{X})$ being L independent from $\mathbf{X}(\mathbf{r}, t)$. A formal solution of this equation reads:

$$\mathbf{X}(\mathbf{r}, t + \Delta t) = \exp\left(\int_t^{t+\Delta t} M(\mathbf{X}(\mathbf{r}, t)) dt\right) \mathbf{X}(\mathbf{r}, t) \quad (1.20)$$

The linear part L usually contains laplacian and other non-local terms so we separate the linear part from the nonlinear part. Up to second order in t , we can write:

$$\mathbf{X}(\mathbf{r}, t + \Delta t) = \mathcal{L} \mathcal{N} \mathcal{L} \mathbf{X}(\mathbf{r}, t) + \mathcal{O}(\Delta t^3) \quad (1.21)$$

where

$$\begin{aligned} \mathcal{L} &= \exp\left(L \frac{\Delta t}{2}\right) \\ \mathcal{N} &= \exp\left(\int_t^{t+\Delta t} dt' N(\mathbf{X}(\mathbf{r}, t'))\right) \end{aligned}$$

where we have used:

$$e^{(A+B)\Delta t} \approx e^{\Delta t A/2} e^{\Delta t B} e^{\Delta t A/2} + [[A, B], A] \Delta t^3 + \dots, \quad (1.22)$$

In order to calculate (1.21) we will use the following algorithm, where \mathcal{F} is the spatial Fourier transform:

$$\mathbf{X}(\mathbf{r}, t + \Delta t) = \mathcal{F}^{-1} \widetilde{\mathcal{L}}(\mathbf{k}) \mathcal{F} \mathcal{N} \mathcal{F}^{-1} \widetilde{\mathcal{L}}(\mathbf{k}) \mathcal{F} \mathbf{X}(\mathbf{r}, t) \quad (1.23)$$

where $\widetilde{\mathcal{L}}(\mathbf{k})$ is the linear operator in Fourier space. In the usual case where $\mathcal{L} = \mathcal{L}(\nabla^2)$, then $\widetilde{\mathcal{L}}(\mathbf{k}) = \widetilde{\mathcal{L}}(-k^2)$.

Regarding the nonlinear part, we have to solve the next integral

$$\begin{aligned} \int_t^{t+\Delta t} dt' N(\mathbf{X}(\mathbf{r}, t')) &\approx \int_t^{t+\Delta t} dt' \left[N(\mathbf{X}(\mathbf{r}, t)) + \frac{\partial}{\partial t} N(\mathbf{X}(\mathbf{r}, t))(t' - t) \right] = \\ &N(\mathbf{X}(\mathbf{r}, t)) \Delta t + \frac{1}{2} \frac{\partial}{\partial t} N(\mathbf{X}(\mathbf{r}, t)) \Delta t^2 = \\ &N(\mathbf{X}(\mathbf{r}, t)) \Delta t + \frac{1}{2} \frac{\partial N}{\partial X_i} \frac{\partial}{\partial t} X_i(\mathbf{r}, t) \Delta t^2 = \\ &N(\mathbf{X}(\mathbf{r}, t)) \Delta t + \frac{1}{2} \frac{\partial N}{\partial X_i} (L X_i(\mathbf{r}, t) + N(X_i(\mathbf{r}, t)) X_i(\mathbf{r}, t)) \Delta t^2 \end{aligned} \quad (1.24)$$

this is equivalent (up to second order) to replace, in the integral above, X with the result obtained after completing the first iteration (the first half of the linear part) and then, in the second part (nonlinear term), using only the nonlinear

part of the evolution equation. So first we evolve only with half of the linear part, then only with the nonlinear section and finally only with the another half of the linear part.

Now, we will consider the case where there is a time dependent term, as it happens when rocking is present:

$$\frac{\partial}{\partial t} \mathbf{X}(\mathbf{r}, t) = \mathbf{M}(\mathbf{X})\mathbf{X} + \Theta(t) \quad (1.25)$$

A formal solution is given by

$$\begin{aligned} \mathbf{X}(\mathbf{r}, t + \Delta t) = & \exp\left(\int_t^{t+\Delta t} M(\mathbf{X}(\mathbf{r}, t')) dt'\right) \mathbf{X}(\mathbf{r}, t) + \\ & \int_t^{t+\Delta t} dt' \exp\left[\int_{t'}^{t+\Delta t} dt'' M(\mathbf{X}(\mathbf{r}, t''))\right] \Theta(t') \end{aligned} \quad (1.26)$$

This expression and its justification is given in [105]. An approximation to the previous solution is:

$$\begin{aligned} \mathbf{X}(\mathbf{r}, t + \Delta t) \approx & \exp\left[\int_t^{t+\Delta t/2} M(\mathbf{X}(\mathbf{r}, t')) dt\right] \\ & \times \left(\exp\left[\int_t^{t+\Delta t/2} M(\mathbf{X}(\mathbf{r}, t)) dt\right] \mathbf{X}(\mathbf{r}, t) + \int_t^{t+\Delta t} dt' \Theta(t')\right) \end{aligned} \quad (1.27)$$

So first we apply the split-step method (for the homogeneous part M) for the half of the interval, then we add the extra time integral and then we apply again the standard split-step to the rest of the interval.

In this chapter, I will present a summary of all my contributions to the five research articles which appear appended to this thesis. For the sake of simplicity and readability, I will group all the obtained results in four sections, each of them not corresponding necessarily to one of the published articles.

Paper I

Bistable phase Locking of a Nonlinear Optical Cavity via Rocking: Transmuting Vortices into Phase Patterns.

A. Esteban-Martín, **M. Martínez-Quesada**, V. B. Taranenko, E. Roldán and G. J. de Valcárcel.

Physical Review Letters, **97**, 093903 (2006).

Paper II

Bistable phase locking in rocked lasers.

K. Staliunas, G. J. de Valcárcel, **M. Martínez-Quesada**, S. Gilliland, A. González-Segura, G. Muñoz-Matutano, J. Cascante-Vindas, J. Marqués-Hueso and S. Torres-Peiró.

Optics Communications, **268**, 160-168 (2006).

Paper III

Rocking bidirectional lasers.

M. Martínez-Quesada, E. Roldán and G. J. de Valcárcel.

Optics Communications, **284**, 2554-2559 (2011).

Paper IV

Phase-bistable pattern formation in oscillatory systems via rocking: application to nonlinear optical systems.

G. J. de Valcárcel, **M. Martínez-Quesada** and K. Staliunas.

Philosophical Transactions of the Royal Society A, **372**, 20140008 (2014).

Paper V

Universal description of pattern formation in optical oscillators under bichromatic injection.

M. Martínez-Quesada and G. J. de Valcárcel.

Journal of the Optical Society of America B, **35**, 1379-1389 (2018).

2.1 Rocking in class C lasers[†]

As it has been mentioned before in this thesis (section 1.3), the rocking injection has been successfully applied to a wide range of nonlinear systems. One of the paradigmatical nonlinear optical systems where rocking could be very useful is the two level laser as it is insensitive to the common 2:1 resonance (feature which is shared by many other optical systems). Our primary goal is to derive a order parameter equation for class C laser under rocking to provide some analytical insight about the nonlinear dynamics (close to threshold) of the resulting phase bistable system after rocking injection.

We start with the set of Maxwell-Bloch equations [51] that model pattern formation in a single longitudinal mode, two-level laser with injected signal, inside a plane mirrors resonator,

$$\partial_t E(x, y, t) = \sigma [-(1 + i\Delta) E + P] + i\nabla^2 E + E_{in}, \quad (2.1a)$$

$$\partial_t P(x, y, t) = -(1 - i\Delta) P + (r - N) E, \quad (2.1b)$$

$$\partial_t N(x, y, t) = b \left[-N + \frac{1}{2} (E^* P + P^* E) \right]. \quad (2.1c)$$

The complex fields E and P are the scaled envelopes of the electric field and polarization, $-N$ is proportional to the difference between the population inversion and its steady value in the absence of lasing, and E_{in} is the scaled complex envelope of the injected signal. $\sigma = \kappa/\gamma_{\perp}$ and $b = \gamma_{\parallel}/\gamma_{\perp}$, where κ , γ_{\perp} , and γ_{\parallel} are, respectively, the decay rates of E , P , and N . The transverse Laplacian $\nabla^2 = \partial_x^2 + \partial_y^2$, where the spatial coordinates (x, y) have been normalized so as to make unity the diffraction coefficient, and $t = \gamma_{\perp} T$ where T is the physical time. r is the pump parameter and the detuning $\Delta = (\omega_C - \omega_A) / (\gamma_{\perp} + \kappa)$, being ω_C (ω_A) the cavity (atomic) frequency. For class C lasers $\sigma \sim b \sim 1$.

Equations (2.1) have been written in the frequency frame $\omega_0 = (\gamma_{\perp} \omega_C + \kappa \omega_A) / (\gamma_{\perp} + \kappa)$ of the on-axis, or plane-wave ($\nabla^2 E = 0$), lasing solution in the absence of injected signal. In particular, this means that the actual light electric field and the injected field at the entrance face of the amplifying medium are proportional to $E e^{-i\omega_0 \gamma_{\perp} t} + c.c.$ and $E_{in} e^{-i\omega_0 \gamma_{\perp} t} + c.c.$ Lastly, we consider an injected signal of the form:

$$E_{in} = F \cos(\omega t) e^{-i\delta t}, \quad (2.2)$$

[†]This section will focus mainly on Paper IV as well as some unpublished material.

which represents an amplitude-modulated field of carrier frequency $\omega_0 + \gamma_\perp \delta$ and modulation frequency $\gamma_\perp \omega$ or, equivalently, the superposition of two coherent fields of equal amplitudes, and frequencies $\omega_0 + \gamma_\perp \delta \pm \gamma_\perp \omega$.

A weakly nonlinear analysis of the laser equations, based on the technique of multiple scales (section 1.4), will eventually give rise to the searched reduced model. Up to second order, the solution of (2.1) can be written as:

$$E = (A_f + A_s)e^{-i\delta t}, \quad P = (1 + i\Delta)E, \quad N = |E|^2 \quad (2.3)$$

where $A_f = D(F/\omega)\sin(\omega t)$ and A_s verifies (a detailed derivation, not present in Paper IV, of the equation is provided in the next section):

$$\partial_t A_s = \frac{\sigma D}{1 - i\Delta} [(r - r_0 - 2\gamma)A_s - \gamma A_s^* - |A_s|^2 A_s] + i\delta A_s + iD\nabla^2 A_s \quad (2.4)$$

where $D = (1 + \sigma \frac{1+i\Delta}{1-i\Delta})^{-1}$ and $\gamma = \frac{1}{2} (\frac{F}{\omega})^2$ is the rocking parameter. This equation is a PCGLE equation formally equivalent to the one which was studied in [6]. The diffusion coefficient $Re(iD)$ needs to be positive (section 1.2) and this only happens iff detuning Δ is also positive¹ so we have imposed this condition in the derivation of the equation (see next section). The result is not surprising as we know that a free-running class C laser is well described close to threshold by a CGLE for positive and large values of detuning [83]. The introduction of rocking has changed, as expected, the phase symmetry of the system and a parametric term (the one multiplied by γ) shows up. The PCGLE has been studied previously in a variety of contexts (optical and non-optical). For a simple optical case (there is diffraction but not diffusion and saturation but not nonlinear dispersion) the bifurcation diagram is shown in Fig. 2.1.

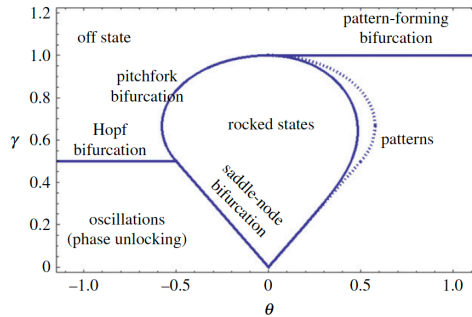


Figure 2.1: Bifurcation diagram of a PCGLE (eq. (3.8) in Paper IV) with $\alpha = i$ and $\beta = 1$. (From Paper IV)

¹A complex Swift-Hohenberg equation for rocked lasers, valid for small positive and negative Δ , will be studied in section 2.3.

Numerical simulations of Eqs. (2.1) using a Split-Step method (section 1.4) were performed, for class C lasers, for a variety of situations. In Fig. 2.2 a comparison between free-running laser transverse patterns, including vortices in the absence of rocking, and the phase domains of the phase bistable laser, when temporal rocking is considered, is shown.

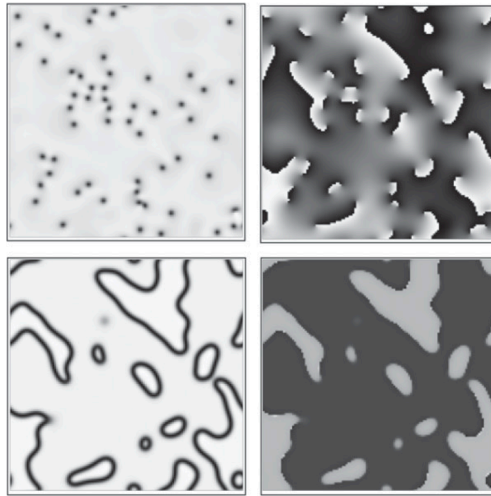


Figure 2.2: Intensity (left) and phase(right) distributions in the transverse pattern of a two-level laser without (first row) and with (second row)temporal rocking injection obtained from the simulation of Eqs. (2.1) starting from noisy initial condition. Rocking is injected in $t = 40$ and first row corresponds to $t = 0$ and second row is $t = 80$. Parameters are $\sigma = b = 1$, $r = 6$, $\Delta = 2$, $\delta = 0$, $F = 20$ and $\omega = 2\pi$. (From Paper IV).

Additionally, phase domains existence are proved for two-level lasers in Paper IV². Plots of Bloch (gray) and Ising(black) domain walls are given in Fig. 2.3. These phase domains exist for zero and small values of the detuning of rocking δ whereas for large detuning, curvature instabilities appear and labyrinthic patterns (Fig. 6 of Paper IV) show up. An important result is the confirmation the existence of localized phase structures (dark-ring cavity solitons) for intermediate values of δ . (Fig. 2.4).

²The results regarding lasers with temporal rocking presented in this paper are original and constitute my main contribution to it.

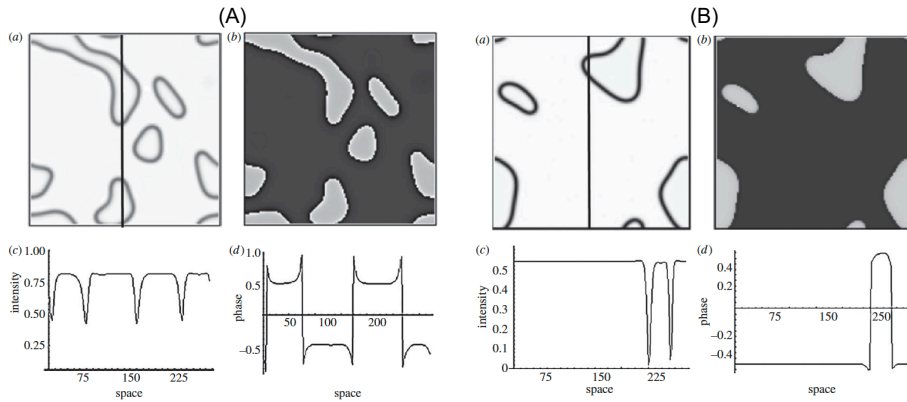


Figure 2.3: (a) Intensity, (b) Phase, (c) Intensity profile and (d) Phase profile of: (A) Bloch-type domain walls for $F = 13$ and (B) Ising-type domain walls for $F = 20$ for class C lasers. Rest of parameters are as in Fig. 2.2. (From Paper IV).

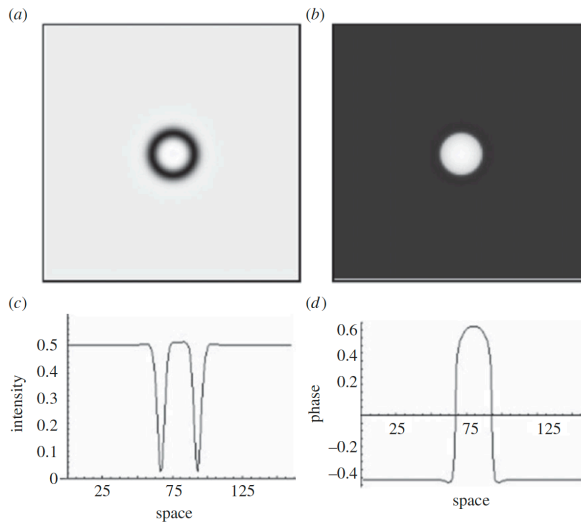


Figure 2.4: Dark-ring cavity soliton for class C lasers. $\delta = 0.055$. (a) Intensity, (b) Phase, (c) Intensity profile and (d) Phase profile. Rest of parameters are as in Fig. 2.2. (From Paper IV).

Formal derivation of the PCGLE (2.4)

In order for the chosen form (2.2) for the injected signal to be consistent with the uniform field and single mode approximations that lead to Eqs. (2.1), both the carrier frequency offset $\gamma_{\perp}\delta$ and the modulation frequency $\gamma_{\perp}\omega$ must be much smaller than the free spectral range of the cavity $\alpha = 2\pi c/L$ (c is the velocity of light and L the cavity length), *i.e.*,

$$|\delta|, |\omega| \ll \alpha/\gamma_{\perp}. \quad (2.5)$$

Taking into account that the cavity loss rate in the uniform field limit reads $\kappa = c\mathcal{T}/2L$, being \mathcal{T} the cavity mirrors transmissivity, α can be written as $\alpha = (4\pi/\mathcal{T})\kappa$. Thus, condition (2.5) reads $|\delta|, |\omega| \ll (4\pi\mathcal{T}^{-1})\sigma$ (remind that $\sigma = \kappa/\gamma_{\perp}$). Since $\mathcal{T} \ll 1$ is assumed in the uniform field limit, δ and ω can be much larger than the normalized cavity linewidth σ without violating the assumptions that lead to the single-mode and mean field approximations.

We concentrate on the case $\Delta > 0$ for which, in the absence of injected signal, the nonlasing solution ($E = 0$) is destabilized towards the on-axis lasing solution at $r = r_0$ [83],

$$r_0 \equiv 1 + \Delta^2. \quad (2.6)$$

The reduction of the laser dynamics to simpler equations will be done in the close to threshold regime:

$$r = r_0 + \varepsilon^2 r_2, \quad (2.7)$$

being $0 < \varepsilon \ll 1$ a smallness parameter. In order to deal with a problem as simple as possible we consider that $\Delta = \mathcal{O}(\varepsilon^0)$, where a complex Ginzburg–Landau (CGL) equation describes the laser in the absence of injection [83]. For smaller detunings, $\Delta = \mathcal{O}(\varepsilon)$, the nature of the bifurcation changes and a complex Swift–Hohenberg equation, and not a CGL equation, is obtained as we will show in section 2.3.

Together with the close to threshold condition, appropriate scalings for time and space are needed. In the absence of injected signal ($F = 0$) these scales would be uniquely dictated by the linear stability analysis of the nonlasing solution. In our case, we need also to take into account the driving field. We will proceed as follows: first we will determine the relevant scales associated with the autonomous problem ($F = 0$), and then we will set right scalings for the injection that are compatible with the former. Anyway we will only consider weak injected signals.

In the absence of injected signal and close to threshold [Eq. (2.7)] the linear stability analysis of the trivial state ($E = P = N = 0$) against perturbations of the

form $\exp(\lambda t + i\mathbf{k} \cdot \mathbf{r})$ yields that only modes verifying $|\mathbf{k}| = \varepsilon k_1$ can experience growth (section 1.4). This result sets the relevant spatial scales of the problem:

$$X = \varepsilon x, \quad Y = \varepsilon y, \quad (2.8)$$

associated to which we define a slow Laplacian operator

$$\nabla_1^2 \equiv \partial_X^2 + \partial_Y^2. \quad (2.9)$$

For these small wavenumber modes ($|\mathbf{k}| = \varepsilon k_1$) the three Lyapunov exponents λ read

$$\lambda_1 = \varepsilon^2 D^{-1} \lambda_{12} + \mathcal{O}(\varepsilon^4), \quad (2.10)$$

$$\lambda_2 = -(1 + \sigma) + i\Delta(1 - \sigma) + \mathcal{O}(\varepsilon^2), \quad (2.11)$$

$$\lambda_3 = -b, \quad (2.12)$$

where $D = (1 + \sigma)^2 + \Delta^2(1 - \sigma)^2$, and

$$\begin{aligned} \lambda_{12} = & \sigma \left[(1 + \sigma) r_2 - 2\Delta k_1^2 + i\Delta(1 - \sigma) r_2 \right] \\ & - i \left[1 + \sigma + \Delta^2(1 - \sigma) \right] k_1^2. \end{aligned} \quad (2.13)$$

Since no eigenvalue has an order 1 *positive* real part the asymptotic dynamics of the system involves long times $t \sim \varepsilon^{-1}, \varepsilon^{-2}, \dots$. Accordingly we define slow time scales:

$$T_1 = \varepsilon t, T_2 = \varepsilon^2 t, \dots \quad (2.14)$$

and search solutions to the laser equations in the form:

$$E(x, y, t) = \varepsilon E_1(X, Y, T_1, T_2, \dots) + \varepsilon^2 E_2(X, Y, T_1, T_2, \dots) + \dots, \quad (2.15)$$

with corresponding expressions for P and N . In principle scale T_1 is damped out since the eigenvalue with largest real part is λ_1 and $\text{Re} \lambda_1 \sim \varepsilon^2$. We keep however the scale T_1 as we will allow the injected field amplitude to excite it. Making use of the chain rule for differentiation, the action of the operators ∂_t and ∇^2 on functions of the form (2.15) becomes

$$\partial_t \rightarrow \varepsilon \partial_{T_1} + \varepsilon^2 \partial_{T_2} + \dots, \quad \nabla^2 \rightarrow \varepsilon^2 \nabla_1^2. \quad (2.16)$$

Clearly, expansion (2.15) will be valid only as far as the injected signal amplitude and frequencies have right scalings. As stated, we will assume that Eq. (2.15) holds and look for injected signals compatible with it. In particular,

two types of scalings, one corresponding to a very slowly modulated, weak injected signal almost resonant with the lasing line,

$$\text{Slow modulation: } F = \sigma F_3 \varepsilon^3, \quad \omega = \sigma \omega_2 \varepsilon^2, \quad \delta = \sigma \delta_2 \varepsilon^2, \quad (2.17)$$

and a second choice corresponding to a "fast" injected signal modulation,

$$\text{Fast modulation: } F = F_2 \varepsilon^2, \quad \omega = \omega_1 \varepsilon, \quad \delta = \sigma \delta_2 \varepsilon^2. \quad (2.18)$$

can be considered. In the following we will deal with the "fast" case. (the another case leads to the same final equation). In the fast modulation case we try to decouple the natural time scales of the system from those of injection. At a first sight a good choice could be $\omega = \sigma \omega_1 \varepsilon$ (2.18). The choice $F \sim \varepsilon$ is needed if the injected signal is to play a role to the leading order dynamics of the system, as will be evidenced below (smaller F 's have no effect in the system dynamics, whilst larger ones forbid the asymptotic expansion).

We are considering class C ($\sigma \sim b \sim 1$) lasers, so σ and b are $\mathcal{O}(\varepsilon^0)$. We substitute Eqs. (2.7), (2.15), (2.16), and (2.18) into to the laser equations (2.1) and (2.2), and solve at increasing orders in ε .

$\mathcal{O}(\varepsilon)$

This is the first nontrivial order and reads

$$N_1 = 0, \quad (2.19)$$

$$\mathcal{L}_0 |v_1\rangle = 0, \quad (2.20)$$

where

$$\mathcal{L}_0 = \begin{pmatrix} -\sigma(1+i\Delta) & \sigma \\ r_0 & -(1-i\Delta) \end{pmatrix}, \quad (2.21)$$

and we have introduced the notation

$$|v_i\rangle = \begin{pmatrix} E_i \\ P_i \end{pmatrix}, \quad i = 1, 2, 3, \dots \quad (2.22)$$

Eq. (2.20) can be easily solved:

$$P_1 = (1+i\Delta) E_1, \quad (2.23)$$

hence

$$|v_1\rangle = E_1 \begin{pmatrix} 1 \\ 1+i\Delta \end{pmatrix}. \quad (2.24)$$

$\mathcal{O}(\varepsilon^2)$

Making use of Eqs. (2.19) and (2.23), we obtain

$$N_2 = |E_1|^2, \quad (2.25)$$

$$\frac{\partial}{\partial T_1} |v_1\rangle = \mathcal{L}_0 |v_2\rangle + |g_2\rangle, \quad (2.26)$$

$$|g_2\rangle = F_2 \cos(\omega_1 T_1) \exp(-i\sigma\delta_2 T_2) \begin{pmatrix} 1 \\ 0 \end{pmatrix}. \quad (2.27)$$

Projecting Eq. (2.26) onto $\langle\zeta_1|$ and making use of Eq. (2.24) we obtain

$$\left(1 + \sigma \frac{1 + i\Delta}{1 - i\Delta}\right) \frac{\partial E_1}{\partial T_1} = F_2 \cos(\omega_1 T_1) \exp(-i\sigma\delta_2 T_2), \quad (2.28)$$

whose solution reads

$$E_1(X, Y, T_1, T_2) = \left(1 + \sigma \frac{1 + i\Delta}{1 - i\Delta}\right)^{-1} \frac{F_2}{\omega_1} \sin(\omega_1 T_1) \exp(-i\sigma\delta_2 T_2) + A_1(X, Y, T_2), \quad (2.29)$$

being A_1 a function not depending on T_1 . Projecting Eq. (2.26) onto $\langle\zeta_2|$ and making use of Eq. (2.24) we obtain

$$P_2 = (1 + i\Delta) E_2 + (1 + i\Delta) \frac{F_2}{\mu} \cos(\omega_1 T_1) \exp(-i\sigma\delta_2 T_2), \quad (2.30)$$

hence

$$|v_2\rangle = E_2 \begin{pmatrix} 1 \\ 1 + i\Delta \end{pmatrix} + (1 + i\Delta) \frac{F_2}{\mu} \cos(\omega_1 T_1) \exp(-i\sigma\delta_2 T_2) \begin{pmatrix} 0 \\ 1 \end{pmatrix}. \quad (2.31)$$

$\mathcal{O}(\varepsilon^3)$

Making use of Eq. (2.25) we obtain

$$\frac{\partial}{\partial T_1} |v_2\rangle = \mathcal{L}_0 |v_3\rangle - \frac{\partial}{\partial T_2} |v_1\rangle + |g_3\rangle, \quad (2.32)$$

$$|g_3\rangle = \begin{pmatrix} i\nabla_1^2 E_1 \\ (r_2 - |E_1|^2) E_1 \end{pmatrix}, \quad (2.33)$$

and an equation for N_3 which is not relevant for our purposes.

Projecting Eq. (2.32) onto $\langle\zeta_2|$ and equation for $|v_3\rangle$ is obtained (not relevant for our purposes), and projecting onto $\langle\zeta_1|$ and making use of Eqs.

(2.24) and (2.31) we obtain

$$\begin{aligned} \left(1 + \sigma \frac{1+i\Delta}{1-i\Delta}\right) \frac{\partial E_2}{\partial T_1} = & - \left(1 + \sigma \frac{1+i\Delta}{1-i\Delta}\right) \frac{\partial E_1}{\partial T_2} + \frac{\sigma}{1-i\Delta} (r_2 - |E_1|^2) E_1 \\ & + i\nabla_1^2 E_1 + \sigma \frac{1+i\Delta}{1-i\Delta} \frac{F_2 \omega_1}{\mu} \sin(\omega_1 T_1) \exp(-i\sigma\delta_2 T_2) \end{aligned} \quad (2.34)$$

On the other hand, from Eq. (2.29) we obtain

$$\frac{\partial E_1}{\partial T_2} = -i\sigma\delta_2 \left(1 + \sigma \frac{1+i\Delta}{1-i\Delta}\right)^{-1} \frac{F_2}{\omega_1} \sin(\omega_1 T_1) \exp(-i\sigma\delta_2 T_2) + \frac{\partial A_1}{\partial T_2}, \quad (2.35)$$

which substituted into Eq. (2.34) yields

$$\left(1 + \sigma \frac{1+i\Delta}{1-i\Delta}\right) \frac{\partial E_2}{\partial T_1} = g(T_1, T_2), \quad (2.36)$$

where

$$\begin{aligned} g(T_1, T_2) = & F_2 \left(\sigma \frac{1+i\Delta}{1-i\Delta} \frac{\omega_1}{\mu} + i \frac{\delta_2}{\omega_1} \right) \sin(\omega_1 T_1) \exp(-i\delta_2 T_2) \\ & - \left(1 + \sigma \frac{1+i\Delta}{1-i\Delta}\right) \frac{\partial A_1}{\partial T_2} + \frac{\sigma}{1-i\Delta} (r_2 - |E_1|^2) E_1 + i\nabla_1^2 E_1. \end{aligned} \quad (2.37)$$

Since g does not depend on E_2 , the solution to Eq. (2.36) reads $E_2(T_1, T_2) = \int_0^{T_1} dT'_1 g(T'_1, T_2) + A_2(T_2)$, whose boundedness requires

$$\lim_{T_1 \rightarrow \infty} \frac{1}{T_1} \int_0^{T_1} dT'_1 g(T'_1, T_2) = 0. \quad (2.38)$$

Substitution of Eq. (2.37) into condition (2.38), making use of Eq. (2.29) yields

$$\begin{aligned} \left(1 + \sigma \frac{1+i\Delta}{1-i\Delta}\right) \frac{\partial A_1}{\partial T_2} = & \frac{\sigma}{1-i\Delta} \left(r_2 - \left(\frac{F_2}{\omega_1}\right)^2 - |A_1|^2 \right) A_1 + i\nabla_1^2 A_1 \\ & - \frac{1}{2} \frac{\sigma}{1-i\Delta} \left(\frac{F_2}{\omega_1}\right)^2 \exp(-i2\delta_2 T_2) A_1^*. \end{aligned} \quad (2.39)$$

The final solution to the problem, to the leading order, reads [Eqs. (2.23), (2.19)]:

$$E = \varepsilon E_1 + \mathcal{O}(\varepsilon^2), \quad P = \varepsilon (1+i\Delta) E_1 + \mathcal{O}(\varepsilon^2), \quad N = \varepsilon^2 |E_1|^2 + \mathcal{O}(\varepsilon^3), \quad (2.40)$$

with Eq. (2.29)

$$E_1(X, Y, T_1, T_2) = \left(1 + \sigma \frac{1+i\Delta}{1-i\Delta}\right)^{-1} \frac{F_2}{\omega_1} \sin(\omega_1 T_1) \exp(-i\delta_2 T_2) + A_1(X, Y, T_2). \quad (2.41)$$

We thus see that the laser field is the superposition of a rapidly varying term (proportional to $\sin(\omega_1 T_1)$) and a slow part represented by A_1 , whose evolution is governed by Eq. (2.39).

Defining $D = \left(1 + \sigma \frac{1+i\Delta}{1-i\Delta}\right)^{-1}$, $\gamma = \frac{1}{2} \left(\frac{F}{\omega}\right)^2$ and making the change $A_s = e^{i\delta t} \varepsilon A_1$, we get (after recovering the original variables):

$$\partial_t A_s = \frac{\sigma D}{1-i\Delta} \left[(r - r_0 - 2\gamma) A_s - \gamma A_s^* - |A_s|^2 A_s \right] + i\delta A_s + iD\nabla^2 A_s. \quad (2.42)$$

Another way to look at A_1 in Eq. (2.41) is the following. We define the average $\langle E(r, t) \rangle = \frac{2\pi}{\omega} \int_t^{t+2\pi/\omega} dt' E(r, t')$ which is the one-modulation-period average of the field amplitude. Using (2.40) and (2.41), and $T_n = \varepsilon^n t$ we obtain $\langle E(r, t) \rangle = \varepsilon A_1 + \mathcal{O}(\varepsilon^2)$, since $A_1(\varepsilon^2 t')$ remains almost constant within the integration interval (which has a length $\sim \varepsilon^{-1}$), as well as $\exp(-i\varepsilon^2 \delta_2 t')$. Thus εA_1 is the average of the field amplitude along a modulation period of the injected signal, to the leading order. We can write an equation for this average as $\partial_t \langle E \rangle = \varepsilon^3 \partial_{T_2} A_1$, returning to the original scales via Eqs. (2.7), (2.14), (2.16), (2.18), and (2.39) obtaining the same equation as (2.39) for $\langle E(r, t) \rangle$.

2.2 Rocking in class B lasers[†]

In the previous section, class C lasers were considered and a PCGLE was obtained. This equation also describes well class A lasers under rocking injection as it is shown in Paper II. However this is not the case for class B lasers, in which the population inversion has a very slow dynamics compared to electric field and polarization ($b \ll \sigma \ll 1$ in Eqs (2.1)). These lasers, as we saw in section 1.2, possess relaxation oscillations which strongly influence the dynamics of the system. For the free-running case (without rocking), a single order parameter equation is not able to capture its behaviour close to threshold and a set of two equations is needed.

Consequently, we need to derive an equation for class B rocked lasers in order to understand better the influence of rocking in these systems as well as making some analytical predictions we can confirm in the numerical simulations of the full model. Due to the complexity of the system, we first consider only the temporal dynamics so we start from Eqs (2.1) in which we remove the laplacian term and we take $E_{in} = E_0 \cos(\sigma t) \exp(-i\nu\sigma t)$. If we eliminate adiabatically the equation of the polarization and define a new time scale $\tau = \sigma t$, we can write in the limit of $\mu \ll 1$ (close to threshold) and $F \ll 1$ (which implies $N, |A|^2 \ll 1$):

$$\frac{dA}{d\tau} = i\nu A + (1 + i\Delta)NA + F \cos(\Omega\tau), \quad (2.43a)$$

$$\frac{dN}{d\tau} = -b[N - \mu + |A|^2], \quad (2.43b)$$

where $A = E \exp(i\nu t) / \sqrt{1 + \Delta^2}$, $F = E_0 / \sqrt{1 + \Delta^2}$ and $\mu = r / \sqrt{1 + \Delta^2} - 1$. We have also defined a new variable $N' = (r - N) / \sqrt{1 + \Delta^2} - 1$ and renormalized $b' = b / \sigma$ (we have removed the primes for simplicity).

As we have done before, we can perform a multiple scale analysis. Consistently with the previous approximations, we choose $\mu, F, N \sim \mathcal{O}(\varepsilon^2)$ and $b, \Omega, A \sim \mathcal{O}(\varepsilon)$. We get up to second order:

$$A = a + \frac{F}{\Omega} \sin(\Omega\tau), \quad N = n + \frac{i}{2} \frac{F}{\Omega} (a + a^*) \left(\frac{b}{b + i\Omega} e^{i\Omega\tau} - \frac{b}{b - i\Omega} e^{-i\Omega\tau} \right), \quad (2.44)$$

[†]This section contains contributions from Paper II and part of Paper IV.

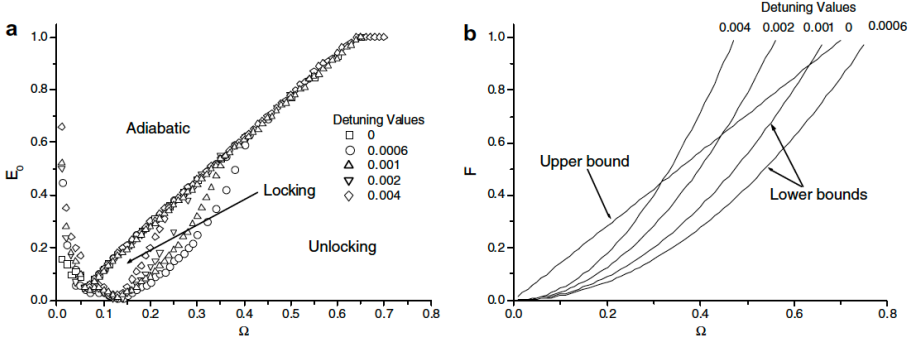


Figure 2.5: Locking regions of class B lasers for cavity resonance ($\Delta = 0$). (a) is obtained from numerical integration of Eqs. (2.1) with $\sigma = 0.1$, $b = 0.001$ and $r = 2$ and (b) comes from Eqs. (2.46) with (equivalent parameters to (a)) $\mu = 1$ and $b = 0.01$. (From Paper II).

where the equations for a and n are:

$$\frac{da}{d\tau} = i\nu a + (1 + i\Delta) \left[\left(n - \gamma_B \frac{b^2}{\Omega^2 + b^2} \right) a - \gamma_B \frac{b^2}{\Omega^2 + b^2} a^* \right] \quad (2.45a)$$

$$\frac{dn}{d\tau} = -b(n - \mu + \gamma_B + |a|^2), \quad (2.45b)$$

where $\gamma_B = 1/2(F/\Omega)^2$.

As we can see in (2.44), we can write the variables of the system like the sum of a "slow" part (a and n) and a "fast" oscillatory part which follows the external injection and has zero time average (averaging time equals to one period of rocking). This is similar to the case of the PCGLE equation and it is a common feature when dealing with rocking (section 1.3).

An analysis of the steady state of (2.45) reveals that we can express $a = u_{\pm} \exp(i\phi_{\pm})$ (the expressions can be found in Paper II) where the solutions for ϕ_{+} , as the solutions with "−" are unstable, are two values separated by π . The range of existence of these rocked states without cavity detuning can be written ($E_0 = F$ for $\Delta = 0$) for small values of ν as:

$$\sqrt{2|\nu|} \frac{\Omega^2}{b} < E_0 < \sqrt{(2\mu)\Omega} \quad (2.46)$$

In the space $E_0 - \Omega$ the locking area is bounded by a straight line (upper limit) and a parabola (lower limit). This is shown in Fig. 2.5b for different values of the detuning of rocking ν . Numerical simulations of Eqs (2.1) confirm approximately this behaviour (Fig. 2.5a). The main difference between both

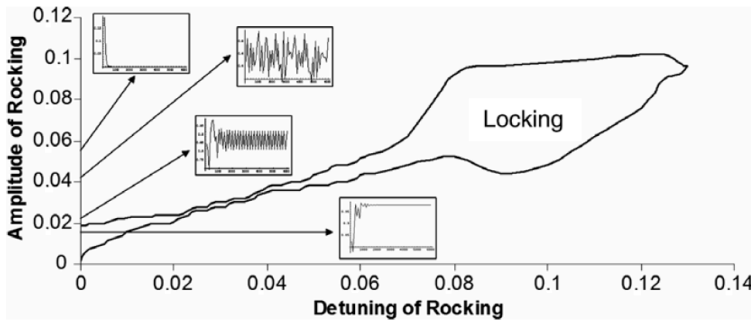


Figure 2.6: Locking regime for class B laser obtained after numerical integration of Eqs (2.1) with $\Delta = 2$, $r = 5(\mu = 1)$, $\Omega = 0.0628$, $\sigma = 0.01$ and $b = 0.0001$. Snapshots of time evolution of the one-rocking period average modulus of the electric field are shown for $\nu = 0$ for different amplitudes of rocking. (From Paper II).

approaches is the area close to the relaxation oscillations frequency, which in this case is (for small b) $\sqrt{2b\mu}$ (its value for the parameters in Fig. 2.5 is 0.14). As we will see later, this is important when spatial effects are considered.

The results presented so far have been obtained for perfect cavity resonance ($\Delta = 0$). We have studied numerically the case $\Delta = 2$ (Fig. 2.6), where we observe that for lower values of the detuning of rocking (ν), the locking area decreases as ν increases, which is the same behavior observed in Fig. 2.6 for zero cavity detuning. However, for larger values of ν the locking area becomes bigger until it eventually disappears (Fig. 2.6). From this we infer that the detuning of rocking is an important parameter which strongly determines the efficiency of the injection, this may be very useful in experimental realizations of rocking.

When dealing with the behavior of the system, out of cavity resonance, outside the locking region we see that there is a dynamical transition between the locking regime, where the average field has constant modulus, and the adiabatic regime (corresponding to the trivial solution of Eqs. (2.45) and appears for very large values of the amplitude of rocking), where the average field is zero (it merely follows the injection). Between the two regimes we observe, close to the locking region, oscillations of the modulus of the average field at a frequency which is half of the frequency of rocking and, as long we are moving away of the locked regime, more complicated temporal dynamics is found. Lastly, we can incorporate the spatial dimensions by considering

the laplacian term in Eqs. (2.1). From the previous analysis we know that the relaxation oscillations frequency³ $\omega_{RO} = \sqrt{2(r - r_0)\sigma b}$ plays an important role, as the frequency of the rocking ω must be of its same order for an effective injection (more details in Paper II). So we choose a frequency of rocking which is close to ω_{RO} . In Figs. 2.7 and 2.8 patterns obtained from the numerical integration of Eqs (2.1) with the injected field defined above are shown. Phase domains, for small values of detuning of rocking, and labyrinths patterns (for large detuning) forming from a modulational instability, are obtained (Fig. 2.7). Moreover, phase cavity solitons are found (Fig. 2.8) for intermediate values of the detuning of rocking. The main differences between those and the ones we presented in Fig. 2.4 are that in this case the width of the dark ring is larger and a higher central intensity peak.

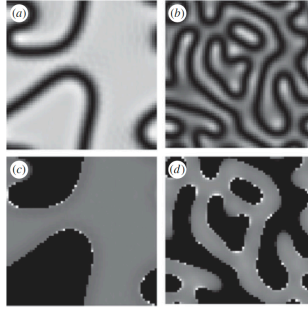


Figure 2.7: Intensity (a,b) and phase (c,d) obtained in class B lasers. Phase domains ($\nu = 0$) and labyrinths ($\nu = 0.04$). Parameters are $\sigma = 0.1$, $b = 0.01$, $r = 1.5$, $\Delta = 0$, $E_0 = 0.4$ and $\omega = 0.42$. (From Paper IV).

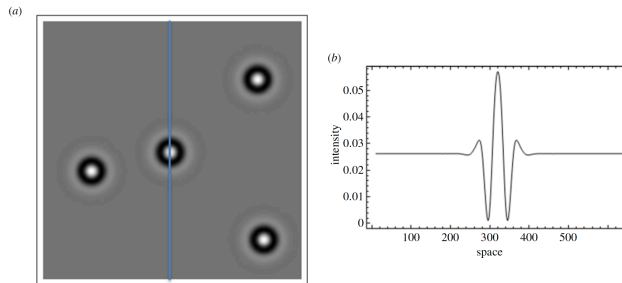


Figure 2.8: Dark-ring cavity solitons for class B lasers for $\nu = 0.026$. (a) Intensity and (b) Intensity profile are shown. Rest of parameters are as in Fig 2.7. (From Paper IV).

³The expression for ω_{RO} is the same as the one used before as $\mu = r - r_0$ and $t = \tau/\sigma$.

2.3

Universal description of optical oscillators under rocking[†]

In section 2.1 a PCGLE equation was derived for a class C laser with rocking injection. The validity of such an equation is restricted to positive (and large) values of the cavity detuning between the atomic resonance frequency and the closest longitudinal cavity mode frequency. The derivation of an order parameter equation for that system which remains valid for positive and negative values of the detuning is an open question.

On the other hand, the first experimental observation of rocking, concerning transformation of vortices into phase domains patterns, in a Photorefractive oscillator (PRO), is reported in Paper I. For this optical system, PCGLE is again not valid to describe its dynamics (we are close to cavity resonance) so a new model needs to be developed.

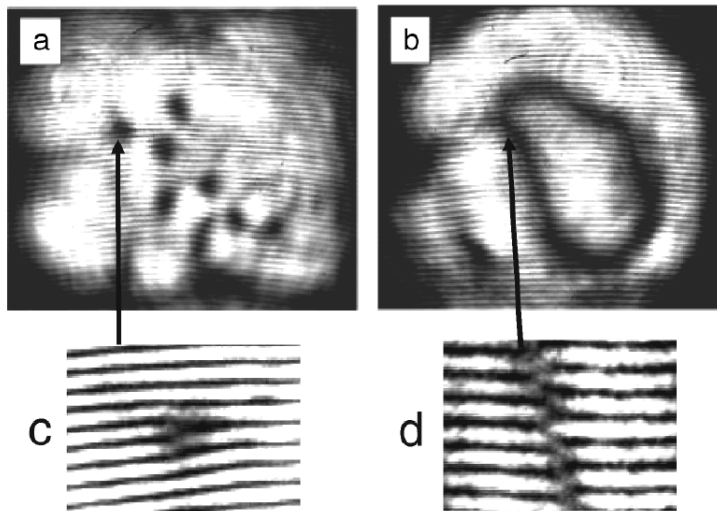


Figure 2.9: Interferometric snapshots of spontaneously formed patterns. (a) Vortices for free running PRO and (b) Phase domains under rocking. (c) and (d) are magnification at a vortex (c) and π phase jump for a domain wall (d). (From Paper I)

[†]This is made of contributions which were published in Paper V (mainly) and Paper I.

For the sake of completeness, although I was not involved in the experiment, I will comment briefly on the experimental setup employed in Paper I. The PRO consists of a photorefractive BaTiO₃ crystal inside a nearly (self)-imaging ring resonator of cavity length 1.2 m (free-spectral range is 250 MHz). The effective cavity length is 2 cm. The crystal is pumped by a single mode 514 nm Ar⁺ laser with power around 100 mW and the chosen cavity length makes the system be close to resonance. When there is no rocking injection, vortices are spontaneously formed in the transverse pattern of the output field whereas when rocking is present, two-dimensional phase domains are formed (Fig. 2.9) due to the generated phase bistability. This behavior is in good qualitative agreement with numerical simulations of rocking in lasers presented in the previous chapter. These bidimensional structures are unstable due to curvature effect leading to single-phase patterns.

Now we will try to obtain an order parameter equation for a two-level laser and a two wave mixing PRO⁴ under rocking. Details of the derivations can be found in the appendices of Paper V.

For the two level laser, our starting point is the standard set of Maxwell-Bloch Equations for a two-level laser with injected signal as we did previously:

$$\partial_t E = \sigma [-(1 + i\Delta)E + P] + i\nabla^2 E + E_{in} \quad (2.47a)$$

$$\partial_t P = -(1 - i\Delta)P + (r - N)E \quad (2.47b)$$

$$\partial_t N = b \left[-N + \frac{1}{2} (E^* P + P^* E) \right] \quad (2.47c)$$

where the injected field is

$$E_{in} = F \cos(\omega t) e^{i\theta t} \quad (2.48)$$

The parameters are like in Eqs (2.1) so we will only remark the differences. Like in the previous chapter, a linear stability analysis of the trivial solution[89] will give insight about the necessary scales: the main change is how the detuning Δ is chosen, in this case it will be (note that we are dealing with small detuning) $\mathcal{O}(\varepsilon)$ so the laplacian ∇^2 is also $\mathcal{O}(\varepsilon)$. We use two different scales for the parameters of the rocking, "fast" and "slow" but, as it is shown in the appendix A of Paper V (where all the details about the scales we use can be found), both choices lead to the same final equation. The results, up to second order, for

⁴The CSHE model for a PRO was first presented in Paper I but the detailed derivation was provided in Paper V

the slow case (expressions for the fast case can be found in the aforementioned appendix A) are:

$$E = \frac{F e^{i\theta t}}{(1 + \sigma)\omega} \sin(\omega t) + i e^{i\theta t} \psi(\mathbf{r}, t) \quad (2.49)$$

$$P = E - \frac{i}{(1 + \sigma)} (\nabla^2 E - (1 + \sigma) \Delta E) \quad , \quad N = |E|^2$$

After renormalization⁵, the equation for ψ reads:

$$\partial_t \psi = (\mu - 2\gamma - i\theta)\psi - |\psi|^2 \psi - (\Delta - \nabla^2)^2 \psi + i\alpha \nabla^2 \psi + \gamma \psi^* \quad (2.50)$$

where $\alpha \equiv \frac{\sigma+1}{\sigma}$ and the rocking parameter is:

$$\gamma = \frac{1}{2} \frac{F^2}{(1 + \sigma)^2 \omega^2} \quad (2.51)$$

Now we will deal with the two-mixing Photorefractive Oscillator. Our starting point is the set of equations⁶ as in Paper I

$$\sigma^{-1} \partial_t E = -(1 + i\Delta)E + i\nabla^2 E + N + E_{in} \quad (2.52a)$$

$$\partial_t N = -(1 - i\Delta)N + g \frac{E}{1 + |E|^2} \quad (2.52b)$$

where the injected field is as in the previous section $E(\mathbf{r}, t)$ is the slowly varying envelope of the intracavity field, $N(\mathbf{r}, t)$ is the complex amplitude of the photorefractive nonlinear grating, $\Delta = (\omega_C - \omega_P)/\kappa$ (ω_P and ω_C are the frequencies of the pump and its nearest longitudinal mode, respectively, whereas κ is the cavity linewidth) $\sigma = \kappa\tau$, where τ is the photorefractive response time ($\sigma \gtrsim 10^8$ under typical conditions, and $\tau \sim 1$ s), t is time measured in units of τ , the detuning, g is the (real) gain parameter that depends of the crystal parameters and the geometry of the interaction.

A linear stability analysis of the trivial solution [106] provides us the scales for the parameters (in Appendix B of Paper V we can find all the details of the derivation). Solving up to second order, we get:

$$E = E^\omega(t) - i e^{-i\theta t} \psi(\mathbf{r}, t) \quad (2.53)$$

$$N = (1 + (-i\Delta + i\nabla^2))E - F \cos(\omega t) e^{i\theta t}$$

⁵We set $\frac{\nabla^2}{1+\sigma} \equiv \nabla'^2$, $t' \equiv \frac{\sigma}{\sigma+1} t$, $\theta' \equiv \frac{\sigma+1}{\sigma} \theta$, define $\mu = r - 1$ and remove the primed notation for simplicity.

⁶We are considering $\frac{\sigma+1}{\sigma} \simeq 1$ as $\sigma \gg 1$ as it is explained in the text. We apply this approximation throughout the analysis.

where E^ω is a periodic function (see appendix B in Paper V).

We finally obtain (details are provided in the aforementioned appendix B), as in the case of the laser, a Swift-Hohenberg equation with parametric gain. Defining $\mu = g - 1$ we can write:

$$\partial_t \psi = (\mu - 2\gamma - i\theta)\psi - |\psi|^2 \psi + i\nabla^2 \psi - (\nabla^2 - \Delta)^2 \psi + \gamma \psi^* \quad (2.54)$$

where the rocking parameter is:

$$\gamma = \frac{1}{2} \frac{F^2}{\omega^2} (\omega^2 + 1) \quad (2.55)$$

The only difference between (2.50) and (2.54) is the parameter α . As we will see later, the specific value of this parameter does not change the essential dynamics of the system. This allows us to state that this CSHE can be regarded as an universal description of pattern formation of nonlinear optical oscillations under bichromatic injection close to threshold, as it is applicable to a wide range of systems with different sources of nonlinearity. Consequently, the model we are going to analyze is:

$$\partial_t \psi = (\mu - 2\gamma - i\theta)\psi - |\psi|^2 \psi - (\Delta - \nabla^2)^2 \psi + i\alpha \nabla^2 \psi + \gamma \psi^* \quad (2.56)$$

where $\alpha = 1$ in the PRO while $\alpha > 1$ for the laser. Setting $\gamma = 0$ we recover the usual Swift-Hohenberg equation for lasers [88]. The extra term $\gamma \psi^*$ breaks the phase invariance of the system, which becomes phase bistable as the equation only has the discrete symmetry $\psi \rightarrow -\psi$. Additionally, Δ is the detuning of the cavity from the natural frequency of the unforced system in the optical case and θ is the detuning of the forcing from the natural frequency of the system. Finally the "rocking parameter" γ is proportional to the squared amplitude of rocking F^2 and also depends on its frequency ω being the exact form different for each system as it has been shown before.

The spatially homogeneous stationary solutions (rocked states) of (2.56) are $\psi_\pm = |\psi_\pm| e^{i\phi_\pm}$ where the expression for ψ_\pm and ϕ_\pm (only the solutions with subscript '+' are stable) are given in Paper V. These states are phase bistable as only two values for the phase, separated by π are allowed. In Fig. 2.10 the intensity of these states as a function of γ is given.

We make a linear stability analysis of the trivial and rocked solutions against spatial instabilities of wavenumber k (section 1.4). Expressions for the stability regions boundaries and wavevectors that maximise the eigenvalue with the largest real part as a function of the parameters of the system are given in Paper V (section 4). Here (Fig. 2.11), we show bifurcation diagrams for both positive

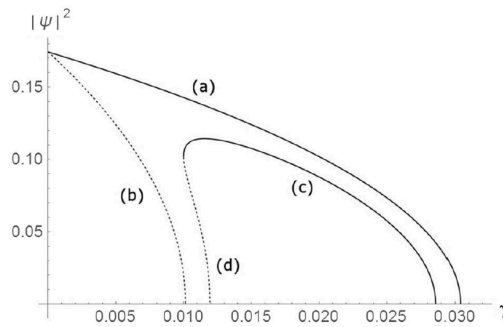


Figure 2.10: Intensity of the rocking states versus γ for $\theta = 0$, (a) ψ_+ , (b) ψ_- and $\theta = 0.01$, (c) ψ_+ , (d) ψ_- . (From Paper V)

and negative cavity detuning (unlike the PCGLE). If we compare them with Fig. 2.1 we see that we have more complexity, especially for negative detuning Δ . In both diagrams we check that for $\gamma = 0$ (free-running case) the solutions we find reproduce the known behaviour of the laser without injection (homogeneous solutions for positive detuning and traveling waves for negative detuning)

Numerical simulations of Eqs. (2.47) are performed in Paper I to reproduce the experimental behavior observed when, after narrowing the intracavity split in order to work in a quasi 1D geometry (to avoid the curvature effects), domain walls (section 1.1) are injected into the system. It is verified that under rocking injection these structures remain stable (unlike the free-running case in which they eventually disappear). The results, both experimental and numerical, are shown in Fig. 2.12 showing a good agreement between the model and the experiment.

The rest of numerical results are obtained from simulations of (2.56). The specific value of the parameter α (we use $\alpha = 2$ all over the numerical analysis) is not important, as it just controls the temporal and spatial scale of the dynamics, being the relevant parameter the ratio between that scale and the detuning Δ . In Paper V, a variety of simulations showing transient dynamics and stationary states and all the patterns which appear in Fig. 2.11 are provided. The existence of phase domains and labyrinthic patterns is shown in Fig. 2.13. Writable/erasable cavity solitons (Fig. 2.14) are found in narrow region (Fig. 2.11) of the space of parameters for both positive and negative detuning.

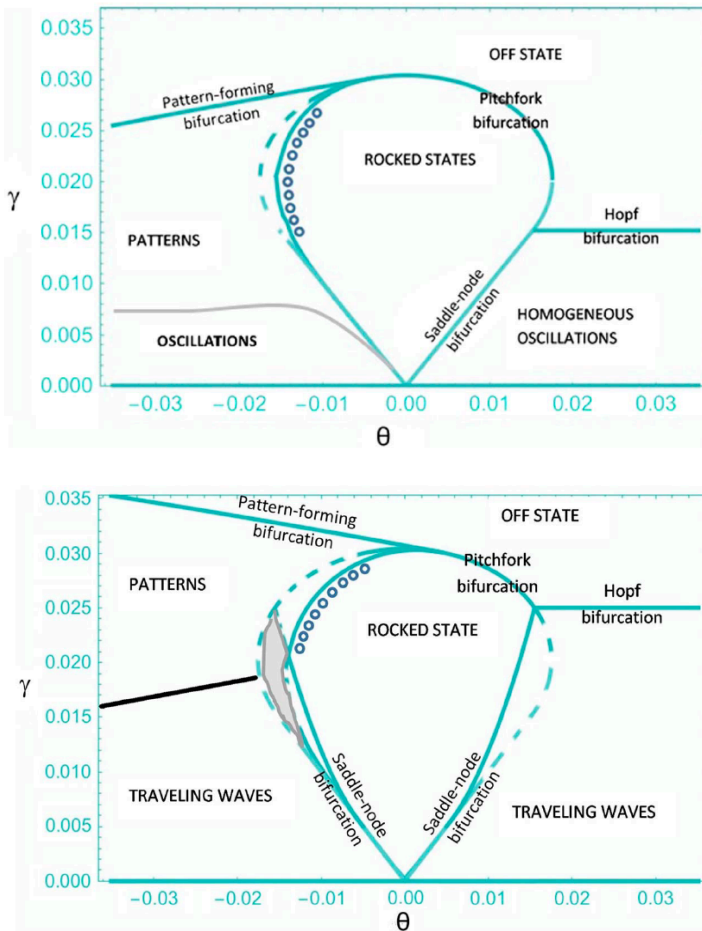


Figure 2.11: Bifurcation diagrams of the CSHE model (2.56) for $\Delta = 0.14$ (**Top**) and $\Delta = -0.14$ (**Bottom**). Dashed line represents the boundary of existence of rocked state and continuous line is the boundary of stability. Circles stand for dark-ring cavity solitons. Rest of parameters are $\alpha = 2$ and $\mu = 0.05$. (From Paper V).

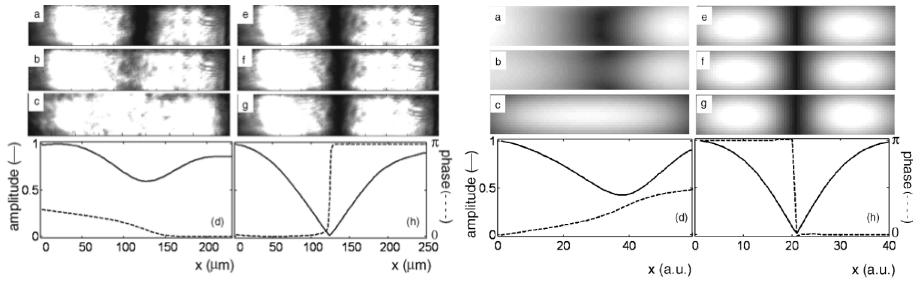


Figure 2.12: (Left) Experimental snapshots of injected 1D domain walls without (a-c time sequence) and with rocking (e-f time sequence). Lowest row is the intensity and phase profile for b (left) and f (right) snapshots. (Right) Simulations of Eqs (2.47) reproducing injection of 1D domain walls without (time sequence a-c) and with rocking injection (time sequence e-g). Intensity and phase profile are given for b (left) and f(right). Parameters are $\sigma = 10^2$, $\Delta = 0$, $g = 2$, $\omega = 2\pi$ and $F = 0.5$. (From Paper I).

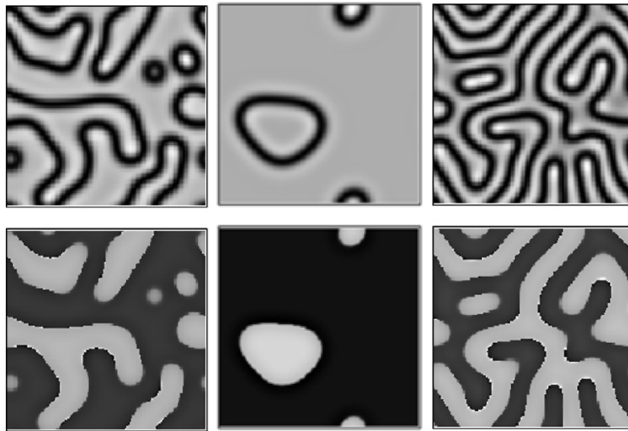


Figure 2.13: Contracting phase domains (middle column) for $\theta = -0.005$ and labyrinths formation (right column) for $\theta = -0.012$ starting from initial condition (left column). Intensity (upper row) and phase (lower row) distributions are shown. The final evolution time is 3000 and the rest of parameters are $\mu = 0.05$, $\Delta = 0.14$, $\alpha = 2$ and $\gamma = 0.02$. (From Paper V).

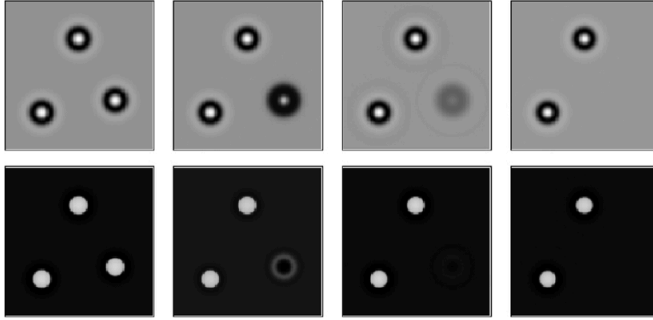


Figure 2.14: Time sequence of writing/erasing a dark-ring cavity soliton for $\theta = -0.011$, Times (left to right) are $t=0, t=150, t=300$ and $t=450$. Intensity (upper row) and phase (lower row) distributions are shown. Rest of parameters like in Fig. 2.13. (From Paper V).

2.4 Bidirectional rocked lasers[†]

In the previous sections we have studied how the rocking modifies the dynamics of single field models, in which the external forcing produces a phase locking where a (phase) bistability is achieved giving rise to the appearance of a different spatio-temporal dynamics and new kind of patterns in the transverse plane. Now, we will consider a system of two coupled fields (class A bidirectional laser) where rocking is applied independently to each of them. This system is very interesting because localized structures were predicted to exist [69, 70]. Due to the complexity of the system (as we will see below), we will restrict ourselves to the single transverse mode in which spatial effects are not considered.

Our starting point is the following pair of complex Stuart-Landau equations, which model a homogeneously broadened bidirectional class A laser (section 1.2), where we add the effect of the rocking in both equations:

$$\frac{1}{\kappa} \frac{dE_n}{dt} = (1 + i\Delta) (\mu - |E_n|^2 - 2|E_m|^2) E_n + F_n \cos(\omega t + \sigma_n \phi/2) e^{-i\delta t} \quad (2.57)$$

with $n, m = 1, 2$ ($n \neq m$) and $\sigma_n = \pm$. The parameters are $\mu = \frac{r}{1+\Delta^2} - 1$ and $\Delta = \frac{\omega_c - \omega_a}{\kappa + \gamma_\perp}$, being r the pumping rate and ω_c and ω_a are frequencies of the cavity mode closest to resonance and of the atomic cavity respectively. Parameters of rocking are F_n , which is proportional to the amplitude of forcing, ω is the modulation frequency, ϕ is the dephase between the two injections and δ is the detuning between the central frequency of rocking and the lasing frequency.

Defining $E_n = \sqrt{\mu} A_n e^{-i\delta t}$ (change of frequency frame to that of the rocking) and $F_n = \mu^{3/2} \sqrt{2\gamma_n} \Omega$, where $\Omega = \frac{\omega}{\mu\kappa}$ is considered to be large, we can write the solution up to first order in Ω^{-1} (using standard multiple scale analysis) as:

$$A_n(t) = \sqrt{2\gamma_n} \sin(\Omega t + \sigma_n \phi/2) + U_n(t) \quad (2.58)$$

where ($n = 1, 2$)

$$(1 + i\Delta)^{-1} \partial_t U_n = \frac{\lambda + i\nu}{1 + i\Delta} U_n - (|U_n|^2 + 2|U_m|^2) U_n - \gamma_n U_n^* - 4\eta \sqrt{\gamma_1 \gamma_2} \text{Re}(U_m) \quad (2.59)$$

being

$$\lambda = 1 - 2(\gamma_1 + \gamma_2), \nu = \frac{\delta}{\mu\kappa} + \lambda\Delta, \eta = \cos(\phi) \quad (2.60)$$

[†]This section reflects the work done for Paper III and some extensions.

As in the previous systems under rocking injection, we can express the emission (2.58) of the system like the addition of a part that merely follows the injection and a "slow" part that verifies a certain order parameter equation. As expected, the equations for U_n possess a broken invariance phase because of the terms proportional to U_n^* and $Re(U_m)$. We will consider two cases⁷, resonant ($\delta = 0$) and non-resonant ($\delta \neq 0$) injection.

Resonant injection. In this case the frequency of the rocking is the same as the lasing frequency (this means $\nu = \lambda\Delta$). We will study the steady state solutions for two cases⁸: unidirectional rocking ($\gamma_1 \equiv \gamma, \gamma_2 = 0$) and symmetric rocking ($\gamma_1 = \gamma_2 \equiv \gamma$).

The unidirectional rocking case has six steady state solutions: the trivial solution, three unidirectional solutions (U_1, U_2 and U_3) and two bidirectional solutions. U_1 and U_3 consist of a phase bistable emission in the rocked field and U_2 implies emission only in the unrocked field, in this case the phase symmetry is preserved as the phase-breaking terms are neglected (see equation (2.59) for U_2 when $\gamma_2 = 0$). A linear stability analysis (details can be found in Paper III) that bidirectional solutions and U_1 are always unstable. Additionally, the trivial solution is stable for $\gamma > 1$, U_2 is stable for $\gamma < 1/3$ and U_3 is stable for $\gamma < 1$. So there is bistability between the two counterpropagating solutions for $\gamma < 1/3$ and for $1/3 < \gamma < 1$ only rocked field U_1 is activated.

The symmetric case is more complex: there are seven different solutions (as now both fields are rocked, phase bistability is present in all the cases): the trivial solution, two equivalent unidirectional solutions and five bidirectional solutions, three of which are symmetric as the intensity of both field is the same and two are asymmetric for the intensities (the expressions for all the solutions are provided in Paper III (section 4)). As before, a linear stability analysis shows that all the solutions are always unstable except the trivial one, one unidirectional (U), one bidirectional symmetric (S) and one bidirectional asymmetric (A). The crucial parameter is $\eta = \cos(\phi)$. For $\eta < 1/2$ there is only a transition between the trivial solution and U as shown in Fig. 2.15. If $\eta > 1/2$ we have five stability regions, where two of them show bistability (whose boundary is $\gamma_U > \gamma > \gamma_A$), one between U and S and another between U and A (Fig. 2.15). Connections between the different stable and unstable solutions are illustrated in Fig. 2.15 being subcritical pitchfork bifurcations the ones which give rise to bistability ($B2$ and $B3$ in Fig. 2.15).

⁷The equations are symmetric under the transformation $[U_n, U_m, \eta] \rightarrow [U_n, -U_m, -\eta]$ so we only need to consider $\eta > 0$.

⁸Expressions for the solutions can be found in Paper III (section 4)

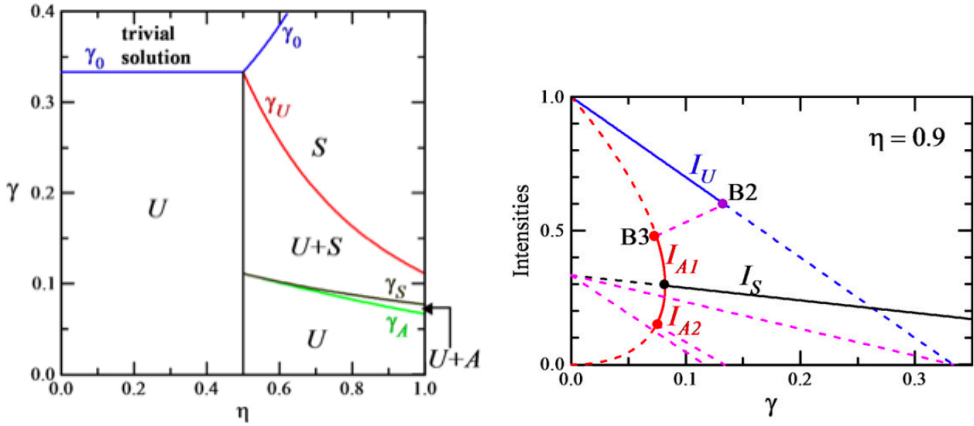


Figure 2.15: (Left) Domains of stability of solutions of Eqs (2.59) for the resonant symmetric rocking case in the $\eta - \gamma$ plane. Only the solution(s) marked is (are) stable in each region. Expressions for γ_0 , γ_U , γ_S and γ_A are given in Paper III. (Right) Intensities of all the solutions of Eqs (2.59) for $\eta = 0.9$. only those with some domain of stability are marked with I_k (I_{A1} and I_{A2} are the intensities of the asymmetric solution A for both fields). Continuous (dashed) line indicates (un)stability of the solutions. $B2$ and $B3$ stand for bifurcation points. (From Paper III).

Non-resonant injection. In this case, a non-null detuning ($\delta \neq 0$) prevents the system from having purely unidirectional solutions (these are replaced by bidirectional solutions in which one of the field is much weaker than the other one). Analytical expressions for the solutions are not possible in this case so a numerical approach is mandatory. Therefore, as we will set $\Delta = 0$ (resonant cavity laser), we will study the cases where $\nu \neq 0$ in Eqs. (2.60). Additionally, $\eta = 0.9$ and the symmetric rocking case is considered.

If rocking is not present ($\gamma = 0$), a non-null detuning ν implies oscillations in the amplitude of the emission due to the chosen frequency frame (the one of the rocking). As soon as γ becomes non-zero, a self-pulsing regime appear, in which the intensity of the fields oscillates between two values, in the quasi-unidirectional solution (Fig. 2.16). When γ reaches a certain value γ_{B1} this regime is replaced by a stationary solution through a saddle-node bifurcation ($B1$ in Fig. 2.16). For $\nu < 0.0225$, the qualitative behaviour is similar to the resonant case (except for $B1$), in which we observe again the bifurcations $B2$ and $B3$ (appearing at γ_{B2} and γ_{B3} respectively, being $\gamma_{B2} > \gamma_{B3}$) connecting quasi-unidirectional and bidirectional solutions (symmetric for $B2$

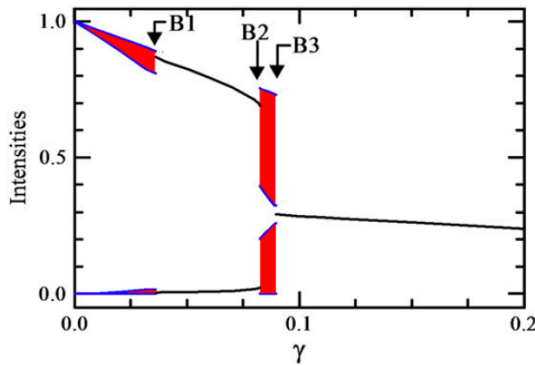


Figure 2.16: Intensities of the different solutions obtained by numerical integration of Eqs (2.59) for $\eta = 0.9$, $\Delta = 0$ and $\nu = 0.025$. Shaded regions correspond to oscillatory regimes between the upper and lower limits of the shadow. (From Paper III).

and asymmetric for $B3$). As ν increases, the distance between $B2$ and $B3$ becomes smaller and at $\nu = 0.0225$ both bifurcations coincide. From this point onwards $\gamma_{B2} < \gamma_{B3}$ and a new self-pulsing regime (again due to a saddle-node bifurcation) appears between γ_{B2} and γ_{B3} (Fig. 2.16). For $\gamma > \gamma_{B3}$ we recover the symmetric stationary solution.

In Fig. 2.17 we can see an illustration of the oscillating regime we have previously described. Oscillations of phase (Fig. 2.17 (a)) and intensity (Fig. 2.17 (b)) of both fields are shown and we can see how they connect two unstable steady states: the symmetric bidirectional (long dash) and the antisymmetric quasi-unidirectional (short dash) solutions. A phase portrait showing the trajectory followed by one of the field compare to the position of the unstable steady states is given in Fig. 2.17 (c).

Lastly, for larger values of η (> 0.0313 for our parameters) the bifurcations $B1$ and $B2$ eventually collide and the two dynamical regimes we have seen before merge. In this case, the quasi-unidirectional solution is no longer stable in any region and the bidirectional emission is the only stable stationary state.

As we can see, the presence of detuning affects largely the domains of existence of phase-locked steady states of the systems. Nevertheless, even for non-zero detuning, the symmetric bidirectional solution exists and remains always stable for values of γ large enough, so perfect resonance should not be necessary to observe phase-locking due to rocking injection.

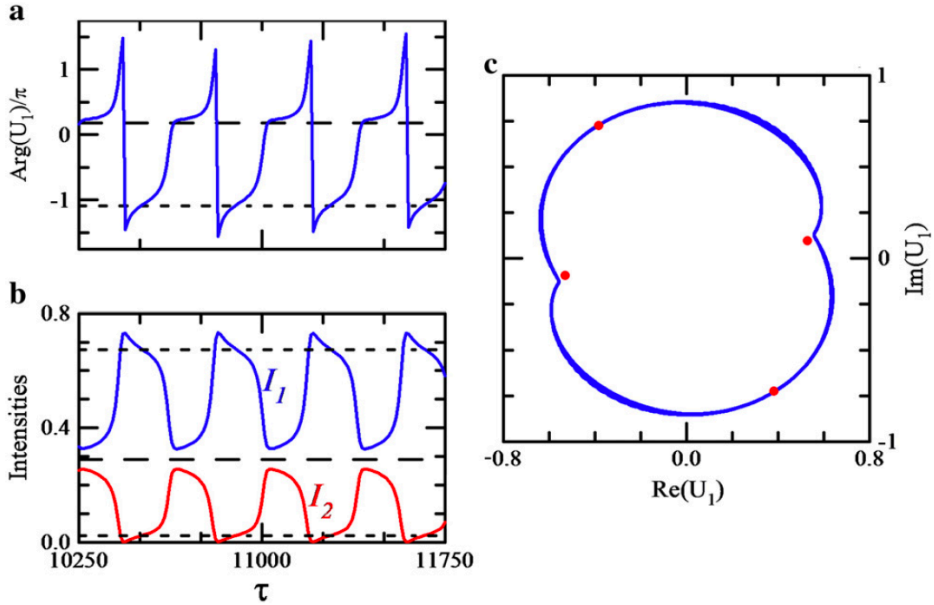


Figure 2.17: Temporal evolution of (a) Phase of U_1 and (b) Intensity of both fields (b) obtained by numerical integration of Eqs (2.59) for $\eta = 0.9$, $\Delta = 0$, $\nu = 0.025$ and $\gamma = 0.089$. Long (short) dash corresponds to unstable symmetric bidirectional (antisymmetric quasi-unidirectional) solutions. These states are portrayed as dots in the phase portrait of field U_1 in (c). (From Paper III).

Spatial patterns. In Fig. 2.18 we show numerical simulations of (2.59) for the resonant case (symmetric rocking) just to illustrate the different solutions found for the temporal case when spatial dimensions are considered. We can see that in the symmetric case (A), the phase distributions of both field are inverted due to the antiphase condition of the symmetric solution S (Paper III). In the unidirectional case (B) the transverse pattern is divided in areas when only one field is present. Phase distributions confirm phase bistability (colors correspond to two phases separated by π) in the regions with non-zero intensity (right part of (B)).

This a preliminary unpublished work that has to be extended by: (i) performing a stability analysis of the solutions for spatial perturbations, (ii): studying the influence of bistability of solutions (like S+U or S+A) in phase bistable patterns and (iii) investigating the existence of localized structures. We are currently working on it.

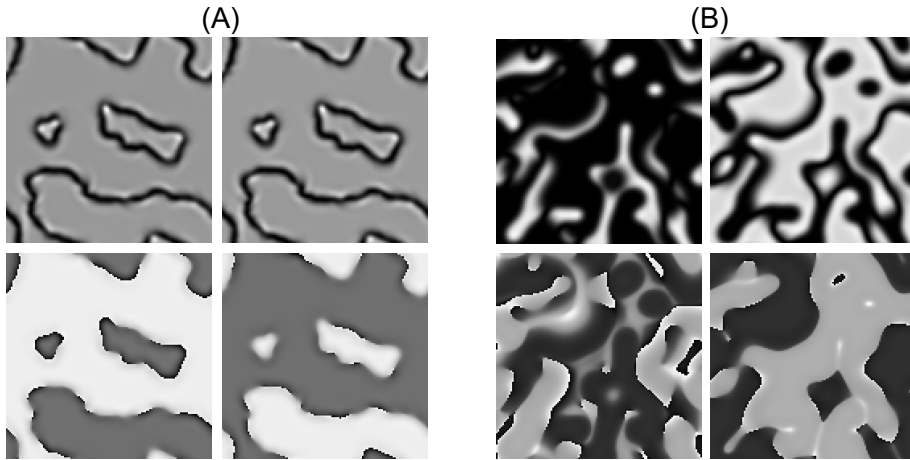


Figure 2.18: Resonant case ($\Delta = \theta = 0$). Intensity (upper row) and phase (lower row) distributions of U_1 (left) and U_2 (right) for symmetric emission corresponding to numerical simulations of (2.59) for **(A)** (symmetric emission): $\eta = 0.7$, $\gamma_1 = \gamma_2 = 0.3$ and **(B)** (unidirectional emission): $\eta = 0.4$, $\gamma_1 = \gamma_2 = 0.2$.

Conclusions

Along this thesis we have studied analytically and numerically the effect of a bichromatic injection (rocking) in several nonlinear optical oscillators: class C and class B two-level lasers, a photorefractive oscillator and a bidirectional laser.

In all the cases we have derived order parameter equations, which capture the dynamics of the systems close to critical points. We have solved (when possible) those equations, obtaining the stationary solutions of the different systems and we have performed a linear stability analysis of these solutions in order to study how the instabilities that can arise from the system may depend on the physical variables. Additionally we have performed numerical experiments, making simulations of the behaviour of the oscillators under different conditions and values of the parameters, trying to observe all the predicted analytical solutions and nonlinear patterns admitted by the system. Specifically, as under rocking injection a system with continuous phase symmetry becomes a phase bistable one, we were interested in phase bistable pattern formation, as phase domains, domain walls, labyrinths as well localized structures which take the form of dark-ring cavity solitons. First, I will provide some general conclusions before analyzing the results we obtained in detail.

A first straight general conclusion is that, although the theoretical conditions for derivation of order parameter equations for oscillators under rocking injection can be restrictive (and they are if we want to obtain relatively simple equations which helps us to gain analytical insight and physical intuition about the phenomenon of rocking), the numerical range of efficiency of rocking is much larger than the analytical expected one (from the assumed approximations). Simulations of the full models, as opposed to the

reduced model represented by the order parameter equations, reveal that the persistence of rocking in the space of parameters of the system is much larger than expected for instance in class C two-level lasers (Paper IV). These are good news from the experimental point of view as it increases the possibility of observing the predicted phenomena in real-world systems.

Another interesting conclusion we obtained is the strong influence of the detunings in rocking phenomenology. Both the cavity detuning (the longitudinal mode selected by the system is different from one of the modes allowed by the optical cavity) and the injection detuning (respect to the natural frequency of the system) have a strong influence in the regions of appearance of the phase-locked structures and their stability. One example is the bidirectional laser (Paper III), in which a small detuning changes radically the nature of the temporal (the only one we analyzed) dynamics of the system (non-resonant case). In class B lasers (Paper II) we also observed a (less important) influence of the detuning.

One last general conclusion is that the kind of nonlinearity present in the system does not play a crucial role when rocking is involved. In certain limits, it is possible to derive universal equations which model pattern formation in oscillator under rocking injection for different systems like lasers or photorefractive oscillator (Paper V). When the full models are considered, the quantitative aspects may be lost but the general behaviour remains and our numerical simulations were able to reproduce qualitatively an observed experimental behaviour (Paper I).

Lasers

We derived an order parameter equation for class C two-level lasers, for positive cavity detuning, under rocking which corresponds to a CGLE with broken invariance (PCGLE) (Paper IV). An analytical study of this equation revealed the existence of homogeneous phase bistable solutions which destabilized to homogeneous oscillations or spatial static patterns depending of the sign of the detuning of the rocking respect to the frequency of the lasing emission. The existence of both Ising and Bloch type (depending on the intensity of rocking) domain walls separating (transient) phase domains was numerically confirmed. These domain walls experiences modulational instability (in 2D) giving rise to the appearance of labyrinthic patterns. Close to this region, (dark-ring) phase cavity solitons were found.

The obtention of a reduced equation for studying the temporal dynamics

class B lasers with rocking injection (Paper II) led to a model of two equations with broken phase invariance which described relatively well the domains of existence (calculated numerically from the MB equations) of the locked phase of the lasing emission to any of two values separated by π (phase bistability). These regions are affected by the detuning of rocking (they are smaller for higher detunings) but the main conclusion we extracted is that the rocking is effective only if its frequency is close to relaxation oscillation frequency. This is relevant if we want to study (theoretically and experimentally) the influence of rocking in realistic models of class B (like semiconductor) lasers.

A Swift-Hohenberg equation with broken phase invariance was obtained for (class C and class A) rocked lasers for positive or negative (provided it is small) values of the cavity detuning (Paper V). This turned out to be the same model (except for one parameter which is not relevant for the dynamics as it only changes one of the the spatial scales of the equation) as we obtained for PRO (Paper I) so we will comment our results in the next section.

Regarding bidirectional lasers (Paper III), we have seen how the presence of rocking was able to stabilize bidirectional solutions which were unstable without external injection. Moreover, domains of bistability between unidirectional and bidirectional solutions appeared in the parameter space. The case for nonzero detuning become very complex as dynamical solutions coming from newly formed bifurcations not present in the purely resonant case show up. Lastly, spatial patterns showing phase domains both for bidirectional and unidirectional lasing emission were encountered.

Photorefractive oscillator

A model of two equations for PRO under rocking injection was simulated numerically and 1D domain walls were found. These results were in good agreement with experimental results (Paper I), showing how the vortices that appear in the transverse plane in absence of injection become phase domains when rocking is present.

A Swift-Hohenberg (SHE) equation with broken phase invariance is found to describe PRO close to the emission threshold for any sign of (small) cavity detuning (Paper I) and was analyzed in detail (Paper V). Its stationary homogeneous solutions were calculated and the linear stability analysis of them revealed a complex dynamics outside the phase-locked stability region. As the SHE possesses two non-local terms, the analysis of the instabilities became more complicated, giving rise to coexistence (in transients states)

of different solutions. Both positive and negative cavity detuning situations were studied numerically and a transition (not possible in the PCGLE model) between phase-locked states and traveling waves for the negative case through a saddle-node bifurcation was encountered. Phase domains, labyrinthic patterns and localized structures were numerically found in both cases.

Future lines of research would include analysis of (temporal) rocking in realistic models of semiconductor lasers (as VCSELs in [100]) and the study of spatial patterns in bidirectional lasers under rocking.

Versió en valencià

Al llarg d'aquesta tesi hem estudiat analíticament i numèricament l'efecte d'una injecció bicromàtica (rocking) en diversos oscil·ladors òptics no lineals: làsers de dos nivells de classe B i C, un oscil·lador fotorefractiu i un làser bidireccional.

En tots els casos hem deduït equacions de paràmetre d'ordre, que capturen la dinàmica dels sistemes prop de punts crítics. Hem resolt (quan era possible) aqueixes equacions, obtenint les solucions estacionàries dels diferents sistemes i hem realitzat una anàlisi d'estabilitat lineal d'aquestes solucions per a estudiar com les inestabilitats que emergeixen en el sistema depenen de les variables físiques. Així mateix, hem dut a terme simulacions numèriques del comportament dels oscil·ladors sota diferents condicions i valors dels paràmetres, intentant observar totes la solucions analítiques predites i els patrons no lineals admesos pel sistema. Específicament, ja que la injecció rocking converteix un sistema amb simetria continua de fase en un sistema biestable en fase, vam estar interessats en la formació de patrons biestables, com a dominis de fase, parets de domini, laberints així com estructures localitzades que prenen la forma de solitons de cavitat d'anell fosc. Primer, exposaré unes conclusions generals abans d'analitzar els resultats obtinguts detalladament.

Una primera conclusió directa és que, encara que les condicions teòriques per a la deducció de les equacions de paràmetre d'ordre per a oscil·ladors amb injecció rocking puguen ser restrictives (i ho són si volem obtindre equacions relativament simples que ens ajuden a tindre una visió analítica i intuïció física sobre el fenomen del rocking), el rang d'eficiència del rocking és molt més gran que que l'esperat analíticament (tenint en compte les aproximacions realitzades). Simulacions numèriques dels models complets, en oposició als models reduïts representats per les equacions de paràmetre d'ordre, revelen

que la persistència del rocking en l'espai de paràmetres del sistema és molt major en, per exemple, els làsers de dos nivells de classe C (Paper IV). Això són bones notícies des d'un punt de vista experimental ja que incrementa la possibilitat d'observar els fenòmens predits en sistemes del món real.

Una altra conclusió interessant que vam obtenir, és l'enorme influència de la desintonia en relació al fenomen del rocking. Tant la desintonia de la cavitat (el mode longitudinal seleccionada pel sistema no coincideix amb un dels modes permeses per la cavitat òptica) com la desintonia de la injecció (respecte a la freqüència natural del sistema) tenen una gran influència a les regions d'aparició de les estructures phase-locked i la seua estabilitat. Un exemple és el làser bidireccional (Paper III), en el qual una xicoteta desintonia canvia radicalment la naturalesa de la dinàmica temporal (única estudiada) del sistema. En làsers de classe B també observem una influència de la desintonia encara que no tan important.

Una última conclusió és que el tipus de no-linealitat present en el sistema no juga un paper crucial quan estem en presència de rocking. En certs límits, és possible deduir equacions universals que modelen la formació de patrons en oscil·ladors amb rocking per a sistemes diferents com a làsers i oscil·ladors fotorefractius (Paper V). Quan es consideren els models complets, els aspectes quantitius poden perdre's però el comportament general roman i les nostres simulacions numèriques van ser capaces de reproduir qualitativament un comportament experimental observat (Paper I).

Làsers

Vam obtenir una equació de paràmetre d'ordre per a làsers de dos nivells de classe C, per a desintonia de cavitat positiva, amb injecció rocking que correspon a una CGLE amb invariància de fase trencada (PCGLE) (Paper IV). Un estudi analític d'aquesta equació va revelar l'existència de solucions homogènies biestables en fase que es desestabilitzen a oscil·lacions homogènies o patrons espacials estàtics depenent del signe de la desintonia del rocking respecte a la freqüència de l'emissió làser. L'existència de parets de domini, tant Ising com Bloch (depenent de la intensitat del rocking) separant (transitoris) dominis de fase va ser confirmada numèricament. Aquestes parets de domini experimenten inestabilitats modulacionals (en 2D) donant lloc a l'aparició de patrons laberíntics. Prop d'aquesta regió, es van trobar solitons de cavitat de fase (d'anell fosc).

L'obtenció d'una equació reduïda per a l'estudi de la dinàmica temporal

de làsers de classe B amb rocking (Paper II) va conduir a un model de dues equacions amb invariància de fase trencada que va descriure relativament bé les regions d'existència (calculades numèricament a partir de les equacions de MB) de l'emissió làser amb la fase restringida a dos valors separats per π (biestabilitat de fase). Aquestes regions estan afectades per la desintonia del rocking (són més xicotetes per a valors alts d'aquesta) però la principal conclusió que vam obtenir va ser que el rocking només és efectiu si la seua freqüència està propera a la de les oscil·lacions de relaxació. Això és rellevant si volem estudiar la influència del rocking en models realistes de làsers de classe B (com els de semiconductor).

Es va deduir una equació Swift-Hohenberg amb invariància de fase trencada per a làsers (de classe A i C) amb rocking per a valors (xicotets) positius i negatius de la desintonia de cavitat (Paper V). Aquesta equació va resultar ser la mateixa (excepte per un paràmetre que no és rellevant per a la dinàmica ja que només canvia una de les escales espacials de l'equació) que vam obtenir per al PRO (Paper I) pel que comentarem els nostres resultats en la següent secció.

En relació als làsers bidireccionals (Paper III), hem vist que la presència del rocking va ser capaç d'estabilitzar solucions bidireccionals que eren inestables en absència d'injecció. Així mateix, es van trobar regions de biestabilitat, en l'espai de paràmetres, entre solucions unidireccionals i bidireccionals. El cas de desintonia no nul·la va resultar ser molt complex ja que sorgeixen solucions dinàmiques provinents de bifurcacions no presents en el cas purament ressonants. Finalment, es van trobar patrons espacials mostrant dominis de fase tant per a emissió làser unidireccional i bidireccional.

Oscil·lador fotorrefractiu

Simulem numèricament un model de dues equacions per a PRO amb rocking, trobant-se parets de domini 1D. Aquests resultats estan en concordança amb els resultats experimentals (Paper I), mostrant com els vòrtexs que apareixen en el pla transversal en absència d'injecció es converteixen en dominis de fase quan el rocking està present.

Vam deduir una equació de Swift-Hohenberg (SHE) amb invariància de fase trencada per a descriure PRO amb rocking prop del llindar d'emissió per a qualsevol signe de la (xicoteta) desintonia de cavitat (Paper I) i va ser analitzada detalladament (Paper V). Es van calcular les seues solucions estacionàries homogènies i la seua anàlisi lineal d'estabilitat va revelar una

dinàmica complexa fóra de la regió d'estabilitat phase-locked. Com la SHE té dos termes no locals, l'anàlisi de les inestabilitats va ser més complex, donant lloc a la coexistència (en transitoris) de solucions diferents. Les situacions de desintonia de cavitat positiva i negativa es van estudiar numèricament i es va trobar una transició (que no és possible en models PCGLE) entre estats phase-locked i ones viatgeres a través d'una bifurcació cadira-node. Dominis de fase, patrons laberíntics i estructures localitzades es van trobar numèricament en tots dos casos.

Com a futures línies d'investigació, inclouríem anàlisi de rocking temporal en models realistes de làsers de semiconductor (com VCSELS en [100]) i l'estudi de patrons espacials en làsers bidireccionals amb rocking.

Versión en castellano

A lo largo de esta tesis hemos estudiado analíticamente y numéricamente el efecto de una inyección bicromática (rocking) en varios osciladores ópticos no lineales: láseres de dos niveles de clase B y C, un oscilador fotorefractivo y un laser bidireccional.

En todos los casos hemos deducido ecuaciones de parámetro de orden, que capturan la dinámica de los sistemas cerca de puntos críticos. Hemos resuelto (cuando era posible) esas ecuaciones, obteniendo las soluciones estacionarias de los diferentes sistemas y hemos realizado un análisis de estabilidad lineal de estas soluciones para estudiar como las inestabilidades que emergen en el sistema dependen de las variables físicas. Asimismo, hemos llevado a cabo simulaciones numéricas del comportamiento de los osciladores bajo diferentes condiciones y valores de los parámetros, intentando observar todas la soluciones analíticas predichas y los patrones no lineales admitidos por el sistema, Específicamente, ya que la inyección rocking convierte un sistema con simetría continua de fase en uno biestable en fase, estuvimos interesados en la formación de patrones biestables, como dominios de fase, paredes de dominio, laberintos así como estructuras localizadas que toman la forma de solitones de cavidad de anillo oscuro. Primero, expondré unas conclusiones generales antes de analizar los resultados obtenidos en detalle.

Una primera conclusión directa es que, aunque las condiciones teóricas para la deducción de las ecuaciones de parámetro de orden para osciladores con inyección rocking puedan ser restrictivas (y lo son si queremos obtener ecuaciones relativamente simples que nos ayuden a tener una visión analítica e intuición física sobre el fenómeno del rocking), el rango de eficiencia del

rocking es mucho más grande que el esperado analíticamente (teniendo en cuenta las aproximaciones realizadas). Simulaciones numéricas de los modelos completos, en oposición a los modelos reducidos representados por las ecuaciones de parámetro de orden, revelan que la persistencia del rocking en el espacio de parámetros del sistema es mucho mayor en , por ejemplo, los láseres de dos niveles de clase C (Paper IV). Esto son buenas noticias desde un punto de vista experimental ya que incrementa la posibilidad de observar los fenómenos predichos en sistemas del mundo real.

Otra conclusión interesante que obtuvimos, es la enorme influencia de la desintonía en relación al fenómeno del rocking. Tanto la desintonía de la cavidad (el modo longitudinal seleccionado por el sistema no coincide con uno de los modos permitidos por la cavidad óptica) como la desintonía de la inyección (respecto a la frecuencia natural del sistema) tienen una gran influencia en las regiones de aparición de las estructuras phase-locked y su estabilidad. Un ejemplo es el láser bidireccional (Paper III), en el que una pequeña desintonía cambia radicalmente la naturaleza de la dinámica temporal (única estudiada) del sistema. En láseres de clase B también observamos una influencia de la desintonía aunque no tan importante.

Una última conclusión es que el tipo de no-linealidad presente en el sistema no juega un papel crucial cuando estamos en presencia de rocking. En ciertos límites, es posible deducir ecuaciones universales que modelen la formación de patrones en osciladores con rocking para sistemas diferentes como láseres y osciladores fotorefractivos (Paper V). Cuando se consideran los modelos completos, los aspectos cuantitativos pueden perderse pero el comportamiento general permanece y nuestras simulaciones numéricas fueron capaces de reproducir cualitativamente un comportamiento experimental observado (Paper I).

Láseres

Obtuvimos una ecuación de parámetro de orden para láseres de dos niveles de clase C, para desintonía de cavidad positiva, con inyección rocking que corresponde a una CGLE con invariancia de fase rota (PCGLE) (Paper IV). Un estudio analítico de esta ecuación reveló la existencia de soluciones homogéneas biestables en fase que se desestabilizan a oscilaciones homogéneas o patrones espaciales estáticos dependiendo del signo de la desintonía del rocking respecto a la frecuencia de la emisión láser. La existencia de paredes de dominio, tanto Ising como Bloch (dependiendo

de la intensidad del rocking) separando (transitorios) dominios de fase fue confirmada numéricamente. Estas paredes de dominio experimentan inestabilidades modulacionales (en 2D) dando lugar a la aparición de patrones laberínticos. Cerca de esta región, se encontraron solitones de cavidad de fase (de anillo oscuro).

La obtención de una ecuación reducida para el estudio de la dinámica temporal de láseres de clase B con rocking (Paper II) condujo a un modelo de dos ecuaciones con invariancia de fase rota que describió relativamente bien las regiones de existencia (calculadas numéricamente a partir de las ecuaciones de MB) de la emisión laser con la fase restringida a dos valores separados por π (biestabilidad de fase). Estas reguines esán afectadas por la desintonía del rocking (son más pequeñas para valores altos de esta) pero la principal conclusión que extraímos fue que el rocking sólo es efectivo si su frecuencia está cercana a la de las oscilaciones de relajación. Esto es relevante si queremos estudiar la influencia del rocking en modelos realistas de láseres de clase B (como los de semiconductor).

Se dedujo una ecuación Swift-Hohenberg con invariancia de fase rota para láseres (de clase A y C) con rocking para valores (pequeños) positivos y negativos de la desintonía de cavidad (Paper V). Esta ecuación resultó ser la misma (excepto por un parámetro que no es relevante para la dinámica ya que sólo cambia una de las escalas espaciales de la ecuación) que obtuvimos para el PRO (Paper I) por lo que comentaremos nuestros resultados en la siguiente sección.

En relación a los láseres bidireccionales (Paper III), hemos visto que la presencia del rocking fue capaz de estabilizar soluciones bidireccionales que eran inestables en ausencia de inyección. Asimismo, se encontraron regiones de biestabilidad, en el espacio de parámetros, entre soluciones unidireccionales y bidireccionales. El caso de desintonía no nula resultó ser muy complejo ya que surgen soluciones dinámicas provenientes de bifurcaciones no presentes en el caso puramente resonantes. Por último, se encontraron patrones espaciales mostrando dominios de fase tanto para emisión láser unidireccional y bidireccional.

Oscilador fotorrefractivo

Simulamos numéricamente un modelo de dos ecuaciones para PRO con rocking, encontrándose paredes de dominio 1D. Estos resultados están en concordancia con los resultados experimentales (Paper I), mostrando como los

vórtices que aparecen en el plano transversal en ausencia de inyección se convierten en dominios de fase cuando el rocking está presente.

Dedujimos una ecuación de Swift-Hohenberg (SHE) con invariancia de fase rota para describir PRO con rocking cerca del umbral de emisión para cualquier signo de la (pequeña) desintonía de cavidad (Paper I) y fue analizada en detalle (Paper V). Se calcularon sus soluciones estacionarias homogéneas y su análisis lineal de estabilidad reveló una dinámica compleja fuera de la región de estabilidad phase-locked. Como la SHE tiene dos términos no locales, el análisis de las inestabilidades fue más complejo, dando lugar a la coexistencia (en transitorios) de soluciones diferentes. Las situaciones de desintonía de cavidad positiva y negativa se estudiaron numéricamente y se encontró una transición (que no es posible en modelos PCGLE) entre estados phase-locks y ondas viajeras a través de una bifurcación silla-nodo. Dominios de fase, patrones laberínticos y estructuras localizadas se encontraron numéricamente en ambos casos.

Como futuras líneas de investigación, incluiríamos análisis de rocking temporal en modelos realistas de láseres de semiconductor (como VCSELS en [100]) y el estudio de patrones espaciales en láseres bidireccionales con rocking.

Appended Papers

Bistable Phase Locking of a Nonlinear Optical Cavity via Rocking: Transmuting Vortices into Phase Patterns.

Adolfo Esteban-Martín, Manuel Martínez-Quesada, Victor B. Taranenko, Eugenio Roldán and Germán J. de Valcárcel.

Physical Review Letters **97** 093903 (2006).

Bistable Phase Locking of a Nonlinear Optical Cavity via Rocking: Transmuting Vortices into Phase Patterns

Adolfo Esteban-Martín, Manuel Martínez-Quesada, Victor B. Taranenko, Eugenio Roldán, and Germán J. de Valcárcel*

Departament d'Òptica, Universitat de València, Dr. Moliner 50, 46100-Burjassot, Spain

(Received 9 February 2006; published 1 September 2006)

We report the experimental observation of the conversion of a phase-invariant nonlinear system into a bistable phase-locked one via rocking [G. J. de Valcárcel and K. Staliunas, Phys. Rev. E **67**, 026604 (2003)]. This conversion results in vortices of the phase-invariant system being replaced by phase patterns such as domain walls. A model for the experimental device, a photorefractive oscillator, is given that reproduces the observed behavior.

DOI: [10.1103/PhysRevLett.97.093903](https://doi.org/10.1103/PhysRevLett.97.093903)

PACS numbers: 42.65.Sf, 05.45.-a, 42.65.Hw, 89.75.Kd

Introduction.—The symmetry properties of the order parameter phase in extended nonlinear systems determine the type of localized structures supported by these systems. On one hand, phase-invariant systems display vortices, which are phase defects of the order parameter, around which the phase changes in 2π , forcing the order parameter to be null at the vortex center. Self-oscillatory systems represent a paradigm of such behavior as the oscillating state reached after a homogeneous Hopf bifurcation can have any phase (the system is autonomous) [1]. Examples of such systems are certain chemical reactions (like the Belousov-Zhabotinsky reaction) and several optical systems [like lasers, nondegenerate optical parametric oscillators (OPOs), and nondegenerate wave mixing photorefractive oscillators]. On the other hand, there are nonlinear systems with broken phase invariance that, obviously, cannot support vortices. Among them, especially interesting systems are those displaying phase bistability. Such systems support a different type of localized structure, the domain wall, which connects spatial regions where the order parameter passes from one homogeneous state, F_0 , to the equivalent, symmetric state, $-F_0$, so that the phase changes by π from one side of the wall to the other one [1]. A paradigm of such type of phase-bistable system is the degenerate OPO.

The question we address here is whether it is possible to convert a phase-invariant system into a phase-bistable one by some simple external action. In other words, can a system displaying vortices be forced to display domain walls? An old and well-known answer to these questions consists in the periodic forcing of a self-oscillatory system at a frequency around 2 times its natural oscillation frequency ω_0 (resonance 2:1). Under that type of (so-called) parametric driving the originally phase-invariant system is predicted [2] and experimentally observed [3,4] to transform into a phase-bistable system, exhibiting domain walls. But while parametric driving is useful in many contexts it is not so in general in nonlinear optics. For instance, a laser emitting at frequency ω_0 is insensitive to a forcing at $2\omega_0$ because the gain line is extremely narrow as compared with the magnitude of the optical frequency ω_0 .

Yet, a new mechanism coined *rocking* [5] has been recently proposed to overcome such limitation of the usual parametric driving. Rocking consists in forcing a self-oscillatory system around its natural oscillation frequency (resonance 1:1) so that the forcing amplitude is periodically modulated in time at a frequency $\omega \ll \omega_0$. Thus rocking is a multifrequency forcing (in its simplest case, a sinusoidal modulation of the forcing amplitude, it is a bichromatic forcing) around the resonance 1:1 of a self-oscillatory system. We want to remark that, unlike the parametric driving, any self-oscillatory system (including lasers and any nonlinear optical system) should be sensitive to rocking as this forcing acts on the main resonance of the system.

In order to gain insight into the rocking idea, consider a particle in a 2D space with coordinates (x, y) under the action of a potential with the shape of a sombrero—having a maximum at the origin $(0, 0)$ and a degenerated minimum at $x^2 + y^2 = r_{\min}^2$. This is a phase-invariant system, which means that the equilibrium position is phase (angle) degenerated. Suppose now that this potential is rocked along the x direction (e.g., by adding a term $x \sin \omega t$ to the original potential). In this case the phase degeneracy is obviously broken and now the system tends to be around $(x = 0, y = \pm r_{\min})$: The system is now phase bistable. This pictorial image illustrates the physical rationale behind the rocking idea: The coordinates of the fictitious particle correspond to the real and imaginary parts of the complex amplitude of oscillations of the self-oscillatory system, whose evolution derives from a sombrero-like potential in the simplest case, as originally introduced in [5] through an analysis of a complex Ginzburg-Landau equation, which is the simplest model for spatially extended self-oscillatory systems [1]. As shown in [5], under the action of rocking the order parameter of the system $F(\mathbf{r}, t)$ (e.g., the laser electric field complex amplitude) develops two components, $F(\mathbf{r}, t) = F_\omega(t) + i\psi(\mathbf{r}, t)$, where F_ω is a $\frac{2\pi}{\omega}$ -periodic function of time that follows the modulation at frequency ω of the forcing amplitude and ψ is a phase-bistable, reduced order parameter that can display domain walls, phase domains, and phase domain solitons [5]. Even if the original pre-

diction is based on a complex Ginzburg-Landau model, rocking is expected to be of wide applicability as the phase-bistability mechanism introduced above seems to be quite model independent.

In this Letter we give the first experimental evidence of rocking induced phase bistability and the associated formation of phase domains and domain walls. Our system is a (nondegenerate) two-wave mixing photorefractive oscillator (PRO), which highly resembles a laser from the nonlinear dynamics viewpoint. Rocking is done by injecting an amplitude modulated laser beam into the resonator. We show that in the absence of rocking (free running configuration) the PRO exhibits vortices, which are converted into phase domains under the action of rocking. Experiments performed under a quasi-1D transverse geometry (in order to avoid curvature effects) show that the system displays domain walls in a window of rocking modulation frequencies, in agreement with [5]. A model for the experimental device is presented that reproduces the experimental findings. In a limit, such a model reduces to a parametrically driven complex Swift-Hohenberg equation, which represents an extension of [5] to other types of order parameter equations and hence enlarges the range of the applicability of rocking.

Experimental setup.—The PRO (Fig. 1) consists of a photorefractive BaTiO₃ crystal placed inside a (near) self-imaging ring resonator [6] of cavity length 1.2 m (the resonator free-spectral range is 250 MHz), similar to that used in [7]. The effective cavity length is approximately 2 cm, which is actively stabilized by means of piezomirror PZT1 in order to have precise control of cavity detuning (the difference between the frequencies of the pump field and that of the closest cavity mode). The crystal is pumped by a single mode 514 nm Ar⁺ laser with a power around 100 mW · cm⁻². An amplitude modulated beam (the rocking beam) coherent to the pump field is injected into the cavity. The intracavity slit D is placed in a Fourier plane in order to make the system quasi-1D in the transverse dimension [8]. Finally, there is the possibility of injecting a tilted coherent beam in order to “write” domain walls [9,10].

The rocking beam must be spatially uniform and amplitude modulated in time with zero mean [5]: We choose to

use a field of constant amplitude, whose phase changes exactly by π in every half period. We do this by injecting into the cavity a beam coming from the pumping laser, after being reflected on piezomirror PZT2 (Fig. 1), which is moved periodically back and forth by half a wavelength (the modulation frequency is on the order of 1 Hz). This way the rocking has a pure amplitude modulation (only the sign of the field amplitude changes). This operation must be very precise as phase jumps different than π do not produce the desired result.

Experimental results.—The cavity length is chosen for the system to be in (almost) exact cavity resonance. This is not mandatory but is the simplest way for the rocking field to be resonant with the intracavity field (see the model section below). When the rocking beam is off and the intracavity slit is open, the system spontaneously forms vortices in the output field, as expected [11]. Under these conditions, the application of a rocking beam is able to transform vortices into phase domains, as shown in Fig. 2. This result is a direct demonstration of the rocking induced phase bistability.

Two-dimensional phase domains are transient structures due to curvature [5]. Hence we performed a series of experiments under quasi-1D conditions (by narrowing the intracavity slit), which allows stable domain walls in phase-bistable systems [9]. These domain walls are, however, unstable in 1D phase-invariant systems: When a domain wall is injected into the free running PRO [Fig. 3(a)], we observe that it vanishes with time [Fig. 3(b)] and is replaced by a spatially uniform state [Fig. 3(c)]. On the contrary, when the PRO is rocked, dramatically different results are obtained. Now an injected domain wall [Fig. 3(e)] remains stable and fixed [Figs. 3(f) and 3(g)]. (The amplitude modulation frequency of the rocking beam was 1.5 Hz, and its intensity was of the same order as that of the output field in the absence of rocking.) Figure 3(h)

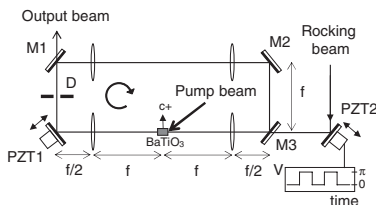


FIG. 1. Scheme of the experimental setup. BaTiO₃, photorefractive crystal; M1, M2, and M3, mirrors; PZT1 and PZT2, piezomirrors; f , focal length of corresponding lenses; D, rectangular slit. PZT2 is driven by a square-wave voltage V .

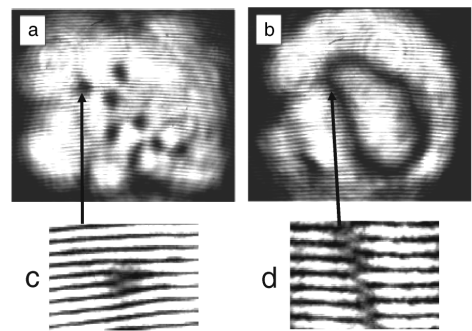


FIG. 2. Interferometric snapshots of spontaneously formed patterns. Vortices (a) existing in the free running PRO are substituted by phase domains (b) under the action of rocking. Lower panels are magnifications showing the annihilation of the interference fringes at a vortex (c) and a π phase jump at a domain wall (d).

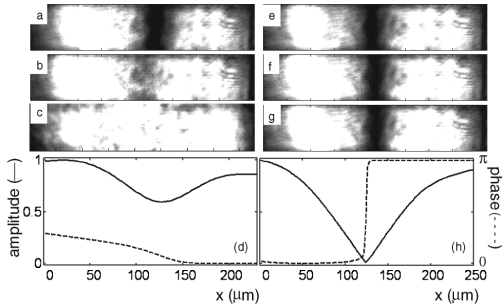


FIG. 3. Experimental snapshots of injected domain walls (DWs). (a)–(c) DWs are unstable in the free running PRO (the time interval between snapshots is 5 s). (e)–(g) Stabilization of the DW in the rocked PRO (the rocking frequency is 1.5 Hz and the time interval between snapshots is 15 s). (d),(h) Horizontal cuts showing the field amplitude (a.u.) and phase corresponding to snapshots (b) and (f), respectively. The snapshots' transverse dimension is 1.2 mm.

evidences that we are in the presence of an Ising wall [2,9]. The structure is robust, and this proves that the system is now phase bistable. The ability of rocking to sustain domain walls is thus confirmed.

There remains to assess the influence of the amplitude and the modulation frequency of rocking on its effectivity. We have observed that the frequency of modulation cannot be too small or too large: For modulation frequencies of 0.1 Hz or below, rocking cannot sustain the injected domain wall. The same happens for modulation frequencies greater than 10 Hz. It seems that modulations from 1 to 3 Hz are optimal, which are on the order of the inverse of the photorefractive grating decay time. While we do not have definite measurements, we can say that rocking is effective in a window of rocking intensities as well.

All previous features are in agreement with the predictions of Ref. [5]. The theory is, however, based on a Ginzburg-Landau model, which should not be valid near cavity resonance [12–14], the case considered here. In order to justify theoretically the results on a more firm basis we thus proceed to model the PRO.

Theory.—We adopt the two-wave mixing PRO model for a purely diffusive photorefractive crystal [15], such as BaTiO₃, generalized to account for the injection of the rocking beam. The model equations, suitably normalized, can be written as

$$\sigma^{-1} \partial_t F = -(1 + i\Delta)F + ia\nabla^2 F + N + F_R(t), \quad (1)$$

$$\partial_t N = -N + g \frac{F}{1 + |F|^2}, \quad (2)$$

where $F(\mathbf{r}, t)$ is the slowly varying envelope of the intracavity field, $N(\mathbf{r}, t)$ is the complex amplitude of the photorefractive nonlinear grating, $\mathbf{r} = (x, y)$ are the transverse coordinates, $\nabla^2 = \partial_x^2 + \partial_y^2$, $\sigma = \kappa\tau$ is the product of the cavity linewidth κ with the photorefractive response time τ

($\sigma \geq 10^8$ under typical conditions, and $\tau \sim 1$ s), t is time measured in units of τ , the detuning $\Delta = (\omega_C - \omega_P)/\kappa$ (ω_P and ω_C are the frequencies of the pump and its nearest cavity longitudinal mode, respectively), a is the diffraction coefficient (which depends upon geometry [8] and can take either sign), F_R is the complex envelope of the rocking (injected) field, and g is the (real) gain parameter that depends on crystal parameters and on the geometry of the interaction. The actual intracavity field \mathcal{E} , and rocking field \mathcal{E}_R read $\mathcal{E} = \text{Re}(FE_P e^{-i\omega_P \tau t})$ and $\mathcal{E}_R = \text{Re}(F_R E_P e^{-i\omega_P \tau t})$, respectively, where E_P and ω_P are the complex amplitude and the angular frequency of the pumping laser field. Note that E_P acts just as a scaling factor (it is unrelated with the gain parameter g) [15,16].

For $F_R = 0$ the model is equivalent to that in [15], which holds the continuous symmetry $(F, N) \rightarrow (F e^{i\phi}, N e^{i\phi})$. Hence the system is phase invariant in the absence of forcing. This free running PRO model has two main solutions [15]: the trivial solution $F = N = 0$, and the family of traveling-wave solutions (parametrized by the wave vector \mathbf{k}) $F = \sqrt{g/g_0 - 1} e^{i(\mathbf{k} \cdot \mathbf{r} - \Omega t)}$ and $N = (1 + i\Omega)F$, with $g_0 = 1 + \Omega^2$, and $\Omega = \frac{\sigma}{\sigma+1}(\Delta + ak^2) \rightarrow \Delta + ak^2$ as $\sigma \gg 1$. One easily sees that (i) for $\Delta/a > 0$ the oscillation threshold is minimum for $k = 0$ (on-axis emission), occurs at $g = 1 + \Delta^2$, and the frequency of the generated field is shifted by $\Omega = \Delta$ from that of the pump beam, and (ii) for $\Delta/a < 0$ the threshold is minimum for $k = \sqrt{-\Delta/a}$ (off-axis emission), occurs at $g = 1$, and there is no frequency shift ($\Omega = 0$). We checked these features in our experiment. In particular, cavity resonance was determined by interfering the emitted field with a reference coming from the pumping laser: The cavity length at which the beating frequency (Ω) passes from zero to a nonnull value (or vice versa) corresponds to exact cavity resonance [15]. These facts, together with the phase invariance of the model, make the PRO in the two-wave mixing configuration a system largely equivalent to a large aspect ratio laser [15,17].

In the following we use $F_R = R \cos \omega t$ (R real without loss of generality), which is the simplest form of amplitude modulation and corresponds to a bichromatic injected signal. In order to give analytical evidence of the rocking induced phase bistability in the PRO model we perform an asymptotic expansion of Eqs. (1) and (2) based on the of multiple scales technique [18]. In order to approach the experimental conditions, we assume small detuning and large cavity linewidth: We take $\Delta = O(\varepsilon)$, $\sigma = O(\varepsilon^{-4})$ with ε a smallness parameter ($0 < \varepsilon \ll 1$) (the final result does not depend on the precise scaling for σ whenever $\sigma \gg 1$ is assumed). We further assume that gain is close to threshold, $g = 1 + O(\varepsilon^2)$, and that the rocking parameters verify $R = O(\varepsilon)$, $\omega = O(1)$. The analysis, similar to that performed in laser [12] and nondegenerate OPO [13,14] models, yields $N = [1 + i(\Delta - a\nabla^2)]F - R \cos \omega t$,

$$F(\mathbf{r}, t) = F_\omega(t) + i\psi(\mathbf{r}, t) + O(\varepsilon^3), \quad (3)$$

$$F_\omega(t) = \frac{R}{\omega} [(1 - 2i\Delta) \sin \omega t + (1 - i\Delta \frac{\omega^2 - 1}{\omega^2}) \omega \cos \omega t], \quad \text{the}$$

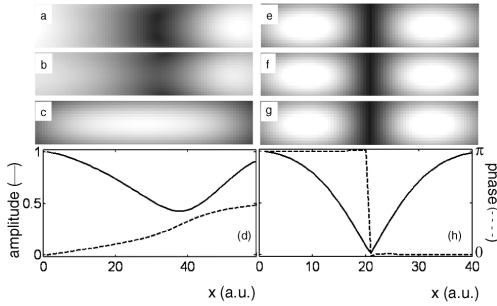


FIG. 4. As Fig. 3 but from the numerical simulations of Eqs. (1) and (2). Parameters: $\sigma = 10^2$, $\Delta = 0$, $g = 2$, $\omega = 2\pi$, and $R = 0.5$. The length of the horizontal dimension is $21\sqrt{a}$ in (a)–(c) and (e)–(g), $14\sqrt{a}$ in (d), and $9.3\sqrt{a}$ in (h).

order parameter ψ verifying a complex Swift-Hohenberg equation with parametric gain:

$$\partial_t \psi = \gamma \psi^* + (g - 1 - 2\gamma)\psi - |\psi|^2 \psi + i(a\nabla^2 - \Delta)\psi - (a\nabla^2 - \Delta)^2 \psi, \quad (4)$$

where $\gamma = \frac{R^2}{2} \frac{1+\omega^2}{\omega^2}$ is the rocking parameter (note that $\gamma \geq \frac{R^2}{2}$). In the absence of rocking ($\gamma = 0$), Eq. (4) is phase invariant and is isomorphic to those describing lasers [12] and nondegenerate OPOs [13,14], as well as highly resembling that for drift-type PROs [17]. The role of rocking is clearly appreciated in Eq. (4): It introduces a phase-sensitive gain (first term in the right-hand side) that breaks the original phase invariance of the undriven system down to the discrete one $\psi \rightarrow -\psi$. Thus the PRO becomes phase bistable. The spatially uniform steady states of Eq. (4) are given by $\psi = \pm |\psi| e^{i\varphi}$, $|\psi|^2 = \mu - 2\gamma + \sqrt{\gamma^2 - \Delta^2}$, $\mu = g - 1 - \Delta^2$, and $e^{2i\varphi} = \frac{\sqrt{\gamma^2 - \Delta^2} - i\Delta}{\gamma}$ (another two, intrinsically unstable states exist as well, which we do not consider). These phase-locked states exist if $|\Delta| \leq \gamma \leq \gamma_{\max}$ ($\gamma_{\max} = \frac{2\mu}{3} + \frac{1}{3}\sqrt{\mu^2 - 3\Delta^2}$) as far as $\mu \geq \sqrt{3}|\Delta|$. These inequalities imply analogous ones for the rocking intensity R^2 or the rocking modulation frequency ω depending on which parameter (ω or R) is kept fixed. This prediction supports the experimental findings described above. Finally, note that as $\gamma \geq \frac{R^2}{2}$ the rocked states will exist only if $R^2 \leq 2\gamma_{\max}$ and $\mu \geq \sqrt{3}|\Delta|$, for any ω .

In a series of numerical experiments we have checked the above predictions and have found that they remain valid even far from the asymptotic limit described by Eq. (4), as it happens in the original proposal [5]. In order to have additional comparison between theory and experiment, we present in Fig. 4 some numerical simulations of Eqs. (1) and (2) for $\sigma = 10^2$ (large, but not extremely large in order to avoid stiffness problems), $\Delta = 0$, $g = 2$ (we estimate that the gain in the experiment is about 100% above threshold), $\omega = 2\pi$, and $R = 0.5$. Comparison with

Fig. 3 shows that the results are very similar to the experimental ones. A message from this theoretical treatment arises: Phase-invariant systems described by order parameter equations of different nature (like the Ginzburg-Landau and the Swift-Hohenberg complex models) behave similarly under the influence of rocking.

In conclusion, we have experimentally demonstrated, and theoretically justified, the ability of the rocking mechanism introduced in [5] to generate phase-bistable states in otherwise phase-invariant systems. The studied system, a PRO in a two-wave mixing configuration, highly resembles laser systems from the nonlinear dynamics viewpoint. Hence the results put forth in this Letter should motivate similar experiments in laser systems, which could have potential applications in the field of information technologies.

This work was supported by the Spanish Ministerio de Educación y Ciencia and European Union FEDER (Project No. FIS2005-07931-C03-01). We gratefully acknowledge fruitful discussions with Javier García Monreal and Kestutis Staliunas.

*Electronic address: german.valcarcel@uv.es

- [1] M. C. Cross and P. C. Hohenberg, *Rev. Mod. Phys.* **65**, 851 (1993).
- [2] P. Coulet, J. Lega, B. Houchmanzadeh, and J. Lajzerowicz, *Phys. Rev. Lett.* **65**, 1352 (1990).
- [3] V. Petrov, C. Ouyang, and H. L. Swinney, *Nature (London)* **388**, 655 (1997).
- [4] A. L. Lin, M. Bertram, K. Martínez, H. L. Swinney, A. Ardelea, and G. F. Carey, *Phys. Rev. Lett.* **84**, 4240 (2000).
- [5] G. J. de Valcárcel and K. Staliunas, *Phys. Rev. E* **67**, 026604 (2003).
- [6] J. A. Arnaud, *Appl. Opt.* **8**, 189 (1969).
- [7] M. Vaupel and C. O. Weiss, *Phys. Rev. A* **51**, 4078 (1995).
- [8] A. Esteban-Martín, J. García, E. Roldán, V. B. Taranenko, G. J. de Valcárcel, and C. O. Weiss, *Phys. Rev. A* **69**, 033816 (2004).
- [9] A. Esteban-Martín, V. B. Taranenko, J. García, G. J. de Valcárcel, and E. Roldán, *Phys. Rev. Lett.* **94**, 223903 (2005).
- [10] A. Esteban-Martín, V. B. Taranenko, E. Roldán, and G. J. de Valcárcel, *Opt. Express* **13**, 3631 (2005).
- [11] K. Staliunas, G. Sleky, and C. O. Weiss, *Phys. Rev. Lett.* **79**, 2658 (1997).
- [12] J. Lega, J. V. Moloney, and A. C. Newell, *Phys. Rev. Lett.* **73**, 2978 (1994).
- [13] S. Longhi and A. Geraci, *Phys. Rev. A* **54**, 4581 (1996).
- [14] V. J. Sánchez-Morcillo, E. Roldán, G. J. de Valcárcel, and K. Staliunas, *Phys. Rev. A* **56**, 3237 (1997).
- [15] U. Bortolozzo, P. Villoresi, and P. L. Ramazza, *Phys. Rev. Lett.* **87**, 274102 (2001).
- [16] P. Yeh, *Introduction to Photorefractive Nonlinear Optics* (John Wiley & Sons, New York, 1993).
- [17] K. Staliunas, M. F. H. Tarroja, G. Sleky, C. O. Weiss, and L. Dambly, *Phys. Rev. A* **51**, 4140 (1995).
- [18] A. H. Nayfeh, *Perturbation Methods* (John Wiley & Sons, New York, 2000).

Bistable phase locking in rocked lasers.

Kestutis Staliunas, Germán J. de Valcárcel, Manuel Martínez-Quesada, Samuel Gilliland, Ángeles González-Segura, Guillermo Muñoz-Matutano, Jaime Cascante-Vindas, José Marqués-Hueso and Salvador Torres-Peiró.

Optics Communications **268** 160-168 (2006).

Bistable phase locking in rocked lasers

K. Staliunas^{a,*}, G.J. de Valcárcel^b, M. Martínez-Quesada^b, S. Gilliland^c,
A. González-Segura^c, G. Muñoz-Matutano^c, J. Cascante-Vindas^c,
J. Marqués-Hueso^c, S. Torres-Peiró^c

^a ICREA, Departament de Física i Enginyeria Nuclear, Universitat Politècnica de Catalunya, Colom 11, 08222 Terrassa, Spain

^b Departament d'Òptica, Universitat de València, Dr. Moliner 50, 46100 Burjassot, Spain

^c Institut de Ciència dels Materials, Universitat de València, Dr. Moliner 50, 46100 Burjassot, Spain

Received 13 April 2006; received in revised form 12 June 2006; accepted 5 July 2006

Abstract

We investigate analytically and numerically the dynamics of single mode lasers with periodic ac injection (rocked lasers). Such lasers show phase bistability as the phase of the light emitted by such lasers can lock to either of two values shifted by π . Locking regimes for different lasers are studied showing that the system response is strongly modified in class B lasers due to the influence of relaxation oscillations.

© 2006 Published by Elsevier B.V.

1. Introduction

Lasers driven by ac periodic injected signals, so-called rocked lasers, have been predicted to display phase bistability between two π -shifted values [1]. Such phenomenon is interesting as bistability is at the root of possible applications in information technologies. Phase bistability is also a prerequisite for the existence of interesting phase patterns, including cavity solitons, in very large Fresnel number optical cavities [1,2]. This rocking induced phase bistability has just been demonstrated for the first time in a laser-like system [2]. Here, we consider the single mode case as our main purpose is to gain insight into the phase locking bistability mechanism. Such knowledge will be obviously useful for single mode laser applications, but also for multi-transverse mode lasers.

In the simplest case when the laser cavity is exactly tuned to the atomic transition frequency and when the injection occurs at two sidebands, oppositely and symmetrically detuned from the resonance, these two phase values

are $\pi/2$ and $-\pi/2$ relative to that of injection. This somewhat counterintuitive phase-locking to two symmetric values can be qualitatively interpreted by analyzing the periodically forced complex Landau (CL) equation [3],

$$\frac{dA}{d\tau} = \mu A - |A|^2 A + F \cos(\Omega\tau), \quad (1)$$

which serves as an order parameter equation for single-mode two-level lasers with bichromatic injection, close to the free running laser threshold. In this context A is proportional to the laser electric field slowly varying complex amplitude (the carrier frequency is that of the free running laser; see below), τ is a dimensionless time, μ is proportional to the amount of pumping over threshold (threshold is at $\mu = 0$), and the ac term $F \cos(\Omega\tau)$ is proportional to the amplitude of the external injection, being F a real number without loss of generality. As the injected field envelope is harmonic the actual injected electric field consists of the superposition of two monochromatic waves of equal amplitudes. When $\Omega = 0$ the ac term transforms into a constant term and the forced CL Eq. (1) becomes that describing usual two-level lasers with (monochromatic) injected signal (LIS) [4]. Eq. (1) is variational as it can be written as $dA/d\tau = -\delta V/\delta A^*$ ($dA^*/d\tau = -\delta V/\delta A$) with potential

* Corresponding author. Tel.: +34 9373 98739; fax: +34 9373 98000.
E-mail address: kestutis.staliunas@icrea.es (K. Staliunas).

$V = -\mu|A|^2 + \frac{1}{2}|A|^4 - 2F \cos(\Omega t) \text{Re}(A)$. In the absence of injection ($F = 0$) and for positive μ , the potential has the shape of a sombrero and displays a degenerated minimum along the circumference $|A|^2 = \mu$ in the complex plane $\text{Re } A - \text{Im } A$, see Fig. 1a. The phase of the complex field, $\varphi = \arg(A)$, is thus arbitrary. (Alternatively, one says that Eq. (1) displays phase invariance.) In the presence of a constant injection ($\Omega = 0$) the potential is tilted along the axis $\text{Re } A$, where it exhibits an isolated minimum, see Fig. 1b and c. Phase invariance is thus broken and the phase of the emitted radiation is locked to that of injection ($\varphi = 0, \pi$). Finally, for a periodically modulated injection ($F \neq 0 \neq \Omega$), the case we consider here, the potential is periodically tilted, or “rocked”, around the axis $\text{Im } A$ (hence the name “rocking” [1]). Under this rocking the system state in the phase space $\text{Re } A - \text{Im } A$ avoids “noisy” areas (located on the axis $\text{Re } A$ in this case) and drifts to the quiet areas (located on the axis $\text{Im } A$) [1] in the phase space, according to the general principles of physics [3]. The phase symmetry is again broken, however, unlike the usual case of constant injection (LIS), the laser phase can lock to two symmetric values with respect that of injection, differing by π . In other words, the radially symmetric Hopf bifurcation describing the free-running laser (of which Eq. (1) with $F = 0$ represents its normal form) deforms into a pitchfork bifurcation due to the rocking of the potential. When the laser is below threshold ($\mu < 0$) the potential displays no more a local maximum at the origin and the phase locking mechanism does not work [1].

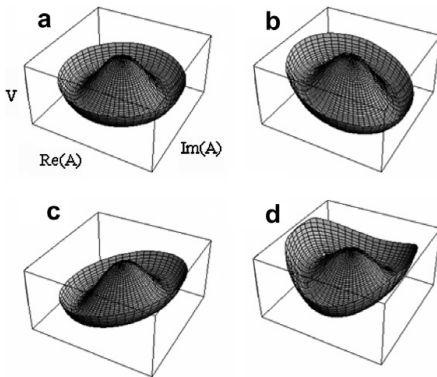


Fig. 1. Qualitative 3D plot of the potential V associated with Eq. (1), which describes a rocked laser (arbitrary units are used). (a) Without injection ($F = 0$) the potential is radially symmetric in agreement with the phase invariance of the free running laser. (b) With constant injection ($\Omega = 0$) the potential tilts along the direction $\text{Re}(A)$ proportionally to the forcing amplitude F and a single isolated minimum appears, corresponding to the phase-locked state of the usual laser with injected signal; here $F < 0$. (c) as the (b), but with $F > 0$. Under rocking ($\Omega \neq 0$) the potential oscillates back and forth between the two cases (b) and (c) through (a). Under such forcing a particle would tend to remain close to the imaginary axis $\text{Re}(A) = 0$, around either of the two regions separated by the local maximum around the origin. (d) Effective potential describing the rocking induced phase-locking; it is the potential associated with Eq. (9), for, which is the initial potential (a) deformed due to fast rocking.

The precise mechanisms of this phase locking have not been explored so far for the different types of lasers. In fact Eq. (1) represents a good description of the so-called class A and class C lasers (where the relaxation rate of the laser field is much smaller than those of the medium polarization and population inversion or all relaxation rates are comparable, respectively; see below) close to threshold, but it cannot describe the dynamics of class B lasers (where the population inversion is slow as compared with field and polarization) or, in general, the response of lasers well above threshold. Substantial peculiarities can be expected for class B lasers, especially because such lasers show relaxation oscillations: hence for rocking frequencies close to that of its relaxation oscillation frequency, or its harmonics and subharmonics, specific resonant phenomena can be expected that could affect the phase locking.

This article is devoted to the detailed analysis of the rocking-induced phase locking in class A and class B lasers, based on the numerical solution of the corresponding Maxwell–Bloch equations and on the analytical solutions of the models. We have checked that class C rocked lasers behave essentially as class A rocked lasers hence our presentation will not consider class C lasers.

2. Model

We consider the standard Maxwell–Bloch (MB) equations for the single longitudinal, single transverse mode, two-level ring laser with injected signal [4], which can be written as:

$$\frac{dE}{dt} = \kappa[P - (1 + iA)E + E_{\text{in}}], \quad (2a)$$

$$\frac{dP}{dt} = \gamma_{\perp}[ED - (1 - iA)P], \quad (2b)$$

$$\frac{dD}{dt} = \gamma_{\parallel} \left[D_0 - D - \frac{1}{2}(E^*P + EP^*) \right]. \quad (2c)$$

The complex functions $E(t)$ and $P(t)$ are the scaled envelopes of the electric field and the medium polarization, respectively, $D(t)$ is the (real) scaled population inversion, D_0 is the scaled population inversion in the absence of lasing (pumping parameter), and $E_{\text{in}}(t)$ is the scaled complex envelope of the injected signal. All these quantities are dimensionless. Eq. (2) have been written in the frequency frame of the corresponding free running laser, ω_L , which is given by the pulling formula $\omega_L = (\gamma_{\perp}\omega_C + \kappa\omega_A)/(\gamma_{\perp} + \kappa)$, with ω_C (ω_A) being the cavity (atomic) frequency, and κ (γ_{\perp}) being the decay rate of $E(P)$. Hence the actual laser field is proportional to $\text{Re}[E(t)\exp(-i\omega_L t)]$. Finally γ_{\parallel} is the decay rate of the population inversion and $\Delta = (\omega_C - \omega_A)/(\kappa + \gamma_{\perp})$ is the scaled atom-cavity detuning.

We consider a periodically modulated injection of the form

$$E_{\text{in}}(t) = E_0 \cos(\Omega t) \exp(-iv\kappa t), \quad (3)$$

which alternatively represents a bichromatic injection formed by the superposition of two coherent light beams

of frequencies $\omega_R \pm \Omega\kappa$ ($\omega_R = \omega_L + \nu\kappa$) and of amplitudes $E_0/2$, which we choose to be real without loss of generality. Thus $\nu\kappa$ represents the detuning of the rocking field mid-frequency ω_R from the free running laser frequency ω_L .

In order that Eqs. (2) and (3) be consistent with the (assumed) uniform field and single longitudinal mode approximations, the modulation frequency $\Omega\kappa$, and the rocking detuning $\nu\kappa$ must be smaller than the cavity free spectral range ($\delta\omega_{\text{FSR}}$), which relates to the cavity linewidth as $\kappa = (4\pi)^{-1}T\delta\omega_{\text{FSR}}$, T being the cavity mirrors transmissivity ($0 < T \ll 1$ is assumed). Additionally the cavity detuning $\omega_C - \omega_A = (\kappa + \gamma_{\perp})A$ must be less (in absolute value) than half the free spectral range. These inequalities are equivalent to $|\Omega|, |\nu| \ll 4\pi/T$, and to $|A| < (2\pi/T)/(1 + \gamma_{\perp}/\kappa)$. The restrictions imposed by the latter depend on the type of laser:

$$\text{Class A lasers : } \gamma_{\perp}, \gamma_{\parallel} \gg \kappa, \quad (4a)$$

$$\text{Class B lasers : } \gamma_{\perp} \gg \kappa \gg \gamma_{\parallel}, \quad (4b)$$

$$\text{Class C lasers : } \gamma_{\perp} \approx \gamma_{\parallel} \approx \kappa. \quad (4c)$$

In class C lasers the last inequality becomes $|A| < 2\pi/T$, which is a nonrestrictive condition. In class A and class B lasers the inequality becomes $|A| < (2\pi/T)(\kappa/\gamma_{\perp})$, which can be restrictive as (κ/γ_{\perp}) is a small quantity. In our simulations we chose parameter values compatible with these restrictions.

In the following sections, we describe the phase locking properties of class A and class B rocked lasers, both analytically and numerically. Class C lasers were also investigated, which, however, did not add much to the dynamics obtained for class A lasers, as already commented.

3. Class A lasers

In order to gain insight into the basic mechanisms of rocking we undergo a reduction of Eq. (2) to a compact form that allows a simplified treatment of the problem. The reduction can be done, following [5], through the adiabatic elimination of the fast material variables, polarization and population inversion, characterizing class A lasers. In addition to the main assumption used in [5] ($\gamma_{\perp}, \gamma_{\parallel} \gg \kappa$) we additionally assume that the different coefficients and frequencies in the field Eq. (2a) are much smaller than $\min(\gamma_{\perp}, \gamma_{\parallel})$. Then the adiabatic elimination of the fast material variables results straightforwardly in

$$\frac{dA}{d\tau} = ivA + (1 + iA)\frac{\mu - |A|^2}{1 + |A|^2}A + F\cos(\Omega\tau), \quad (5)$$

where $A = E \exp(i\nu\tau)/\sqrt{1 + A^2}$ (Eq. (5) is written in the frequency frame of the rocking field mid-frequency ω_R), $F = E_0/\sqrt{1 + A^2}$ is proportional to the forcing amplitude, $\mu = D_0/(1 + A^2) - 1$ plays now the role of pump parameter, and $\tau = \kappa t$ is time measured in units of the inverse of the cavity linewidth.

In the absence of forcing the lasing state $A = a_L(\tau) = \sqrt{\mu} \exp(i\nu\tau)$ exists for $\mu > 0$, and the free running lasing threshold occurs at $\mu = 0$. Eq. (5) can be simplified for a

laser operated below or slightly above threshold ($-\infty < \mu \ll 1$) and for $0 \leq F \ll 1$. In this case $|A| \ll 1$, which allows a cubic approximation:

$$\frac{dA}{d\tau} = ivA + (1 + iA)(\mu - |A|^2)A + F\cos(\Omega\tau) \quad (6)$$

to the leading order. In the special case of complete resonance, $A = v = 0$, Eq. (6) reduces to Eq. (1). We note that both Eqs. (5) and (6), as well as the original MB equations, hold the discrete, nontrivial symmetry $A(\tau) \rightarrow -A(\tau + \pi/\Omega)$. This symmetry is at the origin of the phase bistability discussed below. (Another, trivial symmetry hold by Eqs. (5) and (6) is $A(\tau) \rightarrow A(\tau + 2\pi/\Omega)$, which merely reflects the periodic nature of forcing.)

The analytical study of the locking regimes of Eq. (1) was performed in [1], which we adapt here to Eq. (6). The limit of “strong and fast” rocking is considered ($F, \Omega \gg \mu, A, v$) that is mathematically equivalent to $F = \varepsilon^{-1}f$, $\Omega = \varepsilon^{-1}\omega$, $0 < \varepsilon \ll 1$, and the rest of parameters as $O(1)$ quantities. This allows the separation of the slow time scale τ of the unforced system from the fast time scale $T = \varepsilon^{-1}\tau$ of rocking, and a multiple time scale analysis [6,7] is possible: the electric field A is expanded as $A(\tau) = A_0(T, \tau) + \varepsilon A_1(T, \tau) + O(\varepsilon^2)$, and the time derivative is transformed according to the chain rule: $\partial/\partial\tau \rightarrow \varepsilon^{-1}\partial/\partial T + \partial/\partial\tau$. A hierarchy of equations at increasing orders in ε is obtained, which at the lowest order (ε^{-1}) reads $\partial A_0/\partial T = f\cos(\omega T)$, with the trivial solution:

$$A_0(T, \tau) = (f/\omega) \sin(\omega T) + a(\tau), \quad (7)$$

where $a(\tau)$ depends on the slow time scale only. The evolution equation for $a(\tau)$ is found as a solvability condition at the next order (ε^0) of the asymptotic expansion:

$$\frac{\partial A_1}{\partial T} = -\frac{\partial A_0}{\partial\tau} + ivA_0 + (1 + iA)(\mu - |A_0|^2)A_0. \quad (8)$$

The r.h.s. of this equation, viewed as a function of the fast time T , can be written, in virtue of Eq. (7), as $c_0(\tau) + c_1(\tau)\sin(\omega T) + c_2(\tau)\cos(2\omega T) + c_3(\tau)\sin(3\omega T)$. As that side does not depend on A_1 the term $c_0(\tau)$ must be null: otherwise A_1 would diverge. This is the solvability condition for Eq. (8), $c_0(\tau) = 0$, that reads explicitly:

$$\frac{da}{d\tau} = iva + (1 + iA)[(\mu - 2\gamma)a - \gamma a^* - |a|^2 a], \quad (9)$$

where

$$\gamma = \frac{1}{2}(f/\omega)^2 = \frac{1}{2}(F/\Omega)^2 \quad (10)$$

is the rocking parameter [1]. The laser electric field reads

$$A(\tau) = \sqrt{2\gamma} \sin(\Omega\tau) + a(\tau) \quad (11)$$

to the leading order, see Eq. (7). When $a = 0$ the rocked laser just follows the injection and we say that the laser is in the “adiabatic following” regime.

In the nonrocked limit $\gamma = 0$ (free running laser) the laser electric field $A = a$ and Eq. (9) reduces to Eq. (6). In that limit the nontrivial solution to Eq. (9) reads $a(\tau) = a_L(\tau) \equiv \sqrt{\mu} \exp(i\nu\tau)$, which is the free running lasing state in the frequency frame of the rocking field.

Eq. (9) is a CL equation with broken phase symmetry due to the term proportional to a^* . i.e. posses the symmetry group $a \rightarrow -a$. We can anticipate that Eq. (9) will support bistable phase locked states corresponding to the two equivalent signs of a . We note that Eq. (9) is also the order parameter equation derived for parametrically driven systems close to Hopf bifurcations [8] (where the self-oscillatory system is periodically forced at a frequency that is close to twice the natural frequency of oscillations). Eq. (9) shows that rocking is the mechanism for making a laser to behave as a parametrically driven system, thus exhibiting phase bistability.

Eq. (9) in the resonant limit $\Delta = \nu = 0$ is variational, like Eq. (1), and its potential reads $V = -(\mu - 2\gamma)|a|^2 + \frac{1}{2}|a|^4 + \gamma\frac{1}{2}(a^2 + a^{*2})$. Comparison with the potential of Eq. (1) reveals that the effect of rocking consists in deforming the rotationally symmetric potential of the undriven system so that now local minima appear at $a = \pm i\sqrt{\mu - \gamma}$ (two symmetric points located at the axis $\text{Im } a$) as a straightforward analysis of the potential reveals. These minima correspond to the steady solutions of Eq. (9) in the resonant case. The deformation of the potential is compatible with the general theory of motion in quickly oscillating fields [3], and is illustrated in Fig. 1d.

In the general, nonresonant case Eq. (9) has four steady solutions (apart from the trivial one $a = 0$):

$$a = u_{\pm} \exp(i\phi_{\pm}), \tag{12a}$$

$$u_{\pm}^2 = \mu - 2\gamma + \frac{\Delta v \pm \sqrt{\gamma^2(1 + \Delta^2)^2 - \nu^2}}{1 + \Delta^2},$$

$$\exp(2i\phi_{\pm}) = \mp \frac{\sqrt{\gamma^2(1 + \Delta^2)^2 - \nu^2 + i\nu}}{\gamma(1 + \Delta^2)}. \tag{12b}$$

The existence of four solutions comes from the fact that the phase equation has two solutions (differing by π) both for ϕ_+ and ϕ_- . Solutions with subscript “-” are always unstable, as is easy to be checked. Hence there are two relevant “rocked” solutions, those with subscript “+”, that differ just in their sign. We note that the two rocked solutions are related by the symmetry $A(\tau) \rightarrow -A(\tau + \pi/\Omega)$, according to (11).

The existence range of the “rocked states”,

$$\frac{|v|}{1 + \Delta^2} \equiv \gamma_{\min} < \gamma < \gamma_{\max}$$

$$\equiv \frac{2\mu(1 + \Delta^2) + 2\Delta v + \sqrt{[\mu(1 + \Delta^2) + \Delta v]^2 - 3\nu^2}}{3(1 + \Delta^2)}, \tag{13}$$

follows from the analysis of Eq. (12a), which in its turn requires that $[\mu(1 + \Delta^2) + \Delta v]^2 > 3\nu^2$. The latter sets a minimum pumping μ in order that these “rocked states” exist. Two cases are particularly simple to be analyzed: (i) when the cavity is tuned to the atomic line ($\Delta = 0$) the existence range of rocked states reads $|v| \equiv \gamma_{\min} < \gamma < \gamma_{\max}$

$\equiv [2\mu + \sqrt{\mu^2 - 3\nu^2}]/3$, and the minimum pumping level reduces to $\mu > \sqrt{3}|v|$ and (ii) when the rocking mid-frequency is tuned to the free running laser frequency ($\nu = 0$) the existence range of rocked states reads $0 \equiv \gamma_{\min} < \gamma < \gamma_{\max} \equiv \mu$, and the minimum pumping level reduces to $\mu > 0$, independently of the value of Δ . The dependence of the intensity $|a|^2 = u^2$ of these states on the rocking parameter γ is depicted in Fig. 2.

The double inequality (13) is an estimation of the area of locking regimes of class A lasers. In order to have a complete picture the stability of the rocked states must be explored. A linear stability analysis of those states readily shows that they are destabilized by a Hopf bifurcation at

$$\gamma = \gamma_{\text{HB}} \equiv \frac{1}{4} \frac{\mu^2 + (\Delta\mu + 2\nu)^2}{\mu(1 + \Delta^2) + 2\Delta v}, \tag{14}$$

whenever the quantity $H \equiv z(z + 2\nu)(z - 2\nu) < 0$ where $z = \mu(1 + \Delta^2) + 2\Delta v$. (Note that this condition is never fulfilled if either $\Delta = 0$ or $\nu = 0$ as in this case the condition $H < 0$ reduces to $\mu < 0$ that forbids the existence of rocked states.) Under the condition $H < 0$ the rocked states are Hopf unstable for $\gamma < \gamma_{\text{HB}}$. For $H > 0$ the rocked states are stable along their whole existence range ($\gamma_{\min} < \gamma < \gamma_{\max}$) and the branch of large amplitude periodic orbits terminates at the turning point existing at $\gamma = \gamma_{\min}$ (see Fig. 2) in a periodic orbit of infinite period. All this largely resembles the behavior of the usual LIS [9] as well as that of the two-photon LIS [10]. We note that the appearance of these periodic orbits (either at the Hopf bifurcation or a the turning point) that extend towards smaller values of the rocking parameter γ is due to a lack of the phase sensitive gain provided by the rocking, which is not able to overcome the normal (phase insensitive) gain existing in the laser above threshold, which is controlled by the pumping parameter μ . In any case these oscillations entail the loss of phase locking and their existence limits the phase locking range of the rocked laser at low values of the rocking parameter γ .

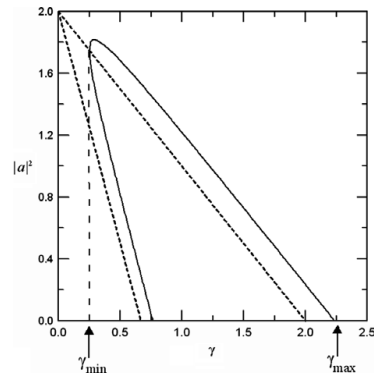


Fig. 2. Intensity of the “rocked states” for $\mu = 2$, $\Delta = 1$, and $\nu = 0.25$ (solid lines), $\nu = 0$ (dotted lines). In both cases the lower branch (given by solution (12) with the minus sign) is unstable. γ_{\min} and γ_{\max} , see (13), are marked for the case $\nu = 0.25$.

All these predictions are based on Eq. (9) that corresponds to a limiting case of the original Eq. (6), which in its turn is an approximation to the original MB Eq. (2) for class A lasers. Hence we must consider the numerical integration of Eq. (2) in order to have a more precise picture of the behavior of class A rocked lasers. We make the presentation of different dynamical regimes in the plane $\Omega - E_0$, i.e., we use the quantities defining the amplitude and modulation of the rocking field, Eq. (3), as our control parameters. Keeping fixed the rest of parameters, the phase locking area on this plane is bounded by two straight lines: (i) from above $\gamma = \gamma_{\max}$ or, equivalently, $E_0 = E_0^{\max} \equiv \sqrt{1 + \Delta^2} \sqrt{2\gamma_{\max}} \Omega$ and (ii) from below $\gamma = \gamma_{\min}$ or equivalently $E_0 = E_0^{\min} \equiv \sqrt{1 + \Delta^2} \sqrt{2\gamma_{\min}} \Omega$. In the numerics we considered the resonant cavity case $\Delta = 0$, fixed pump $\mu = 1$, what means that the laser is twice above its generation threshold (note that in the case of Eqs. (6) and (9) one can take always this value after rescaling) and let the rocking detuning ν vary, keeping it always small. In such case the upper boundary reads $E_0 = E_0^{\max} \equiv [(2\mu + \sqrt{\mu^2 - 3\nu^2})/3]^{1/2} \sqrt{2}\Omega \approx \sqrt{2\mu}\Omega$, thus weakly depends on the detuning. On the contrary the lower boundary depends strongly on the rocking detuning and reads $E_0 = E_0^{\min} \equiv \sqrt{2|\nu|}\Omega$ in this case.

For relatively large amplitudes of rocking, $E_0 > E_0^{\max}$, the homogeneous component of the oscillations $a(\tau)$ decays to zero, Fig. 2, therefore the field of the locked laser follows adiabatically the injection of the master laser. For small values of the rocking amplitude, $E_0 < E_0^{\min}$, the phase of the laser is unlocked from that of the master laser, and evolves freely, as commented. The adiabatic and unlocked regimes are separated one from another in the frame of analysis (9)–(13). For real lasers these regimes are connected, leading to nontrivial dynamics regimes, as investigated numerically in the following.

We integrated numerically (second order Runge–Kutta scheme) the MB Eq. (2) with the following parameters with the following values of the decay rates: $\gamma_{\perp} = \gamma_{\parallel} = 10\kappa$, which means relatively fast material variables, P and D , with respect to the electric field E . As a check we increased the above ratio, however the locking regimes did not vary

significantly from the used values. The results are summarized in Fig. 3a, where the locking areas are numerically calculated for different rocking detunings. The locking area decreases with increasing detuning, in qualitative agreement with the analytical evaluation given by (12) and depicted by the lines in Fig. 3b. Note that the resonance condition $\Delta = 0$ used in the numerics precludes the existence of a Hopf bifurcation limiting the locking area as discussed above.

Small quantitative difference between the analytical calculations and numerical is explained by noting that the calculations have been performed for the pump-above-threshold ratio of the order of two, whereas the CL model, and the analytical expressions are strictly valid close the generation threshold. We note also that the area of small F and Ω , where the discrepancies a largest, are outside of smallness assumptions.

The different dynamical regimes observed in our numerical calculations are summarized in Fig. 4, where the phase trajectories on the complex plane of the electric field are depicted. Locking corresponds to the closed trajectories, which are placed symmetrically with respect to the axis $\text{Re } E$ in the case of zero detuning, Fig. 4a, or shifted correspondingly for nonzero detuning, Fig. 4b. The maximum rotation angle is $\varphi = \pi/4$, corresponding to the lower boundary of the locking regime, in a good agreement with (12).

To conclude the analysis of the class A rocked laser we note that a related model was previously studied by Yamada and Graham [11] that in our notation reads

$$\frac{dA}{d\tau} = ivA + \frac{\mu - |A|^2}{1 + |A|^2} A + F_0 + F \cos(\Omega\tau). \quad (15)$$

This model is thus a perturbation of the usual LIS model. It is apparently quite similar to our Eq. (5), with $\Delta = 0$, but has a main, and deep, difference with respect to that equation: the presence of the constant, bias, term F_0 , which corresponds to a resonant injection. Thus Eq. (15) describes a resonant class A laser driven by an external field composed by the superposition of three frequencies: the resonant one, of amplitude F_0 , and two symmetric sidebands. We note that in our study the central frequency is absent from the injection. (That frequency does appear however in the response of the laser

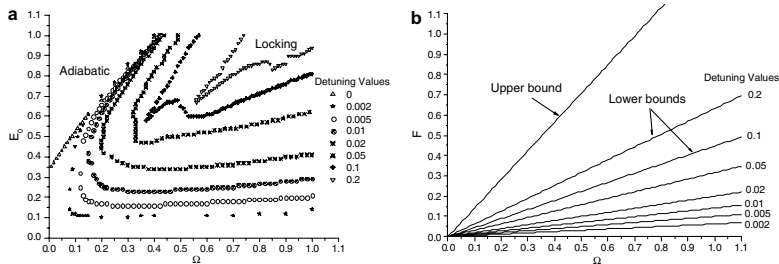


Fig. 3. Locking areas of class A lasers. (a) Results of the numerical integration of the MB Eqs. (2) and (3). (b) Analytical evaluations given by Eq. (13). The parameters are $\gamma_{\perp} = \gamma_{\parallel} = 10\kappa$, $\Delta = 0$, $D_0 = 2$ (equivalently, $\mu = 1$), and the value of the rocking detuning ν is indicated in the figures. In (a) the top-right areas correspond to locking, the top-left areas correspond to adiabatic regime, and the bottom-right areas corresponds to unlocking.

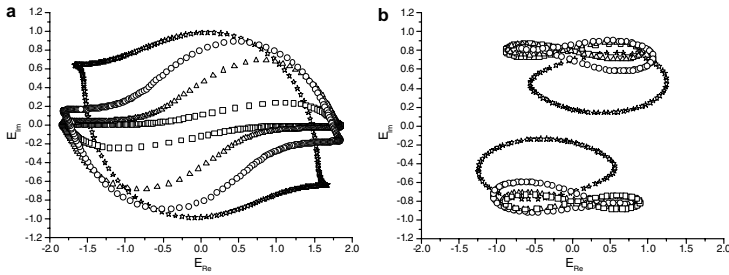


Fig. 4. Trajectories for class A lasers shown in phase space for $E_0 = 1$ and $\Omega = 0.1$ (a) and $\Omega = 1$ (b). In both cases the rocking detuning values are $\nu = 0.002$ (squares), 0.01 (triangles), 0.05 (circles) and 0.2 (stars) at injection parameters of (a) $E_0 = 1, \Omega = 0.1$ and (b) $E_0 = 1, \Omega = 1$. Adiabatic (a), and locked (b) regimes areas of class A lasers are given. The rest of parameters as in Fig. 3.

due to resonant four-wave mixing.) A main effect of the bias term F_0 in Eq. (15) is to break the nontrivial symmetry $A(\tau) \rightarrow -A(\tau + \pi/\Omega)$ of the rocked laser, see discussion after Eq. (6). Thus the phase bistability of the rocked laser is forbidden in the case of Eq. (15) and, consequently, was not described in [11]. Zehnle and Zeghlache [12] also studied a similar situation but only considered the case $F \ll F_0$, very far from the case studied by us. (Incidentally we note that they considered the low excitation regime in which the cubic approximation for the nonlinearity is in order, as in our Eq. (6).) Again these authors did not describe any phase-locking bistability but phenomena unrelated with the ones we discuss here.

4. Class B lasers

In class B lasers, characterized by the decay rates inequalities $\gamma_{\parallel} \ll \kappa \ll \gamma_{\perp}$, the polarization can be adiabatically eliminated from the Maxwell–Bloch Eqs. (2) and (3), yielding:

$$\frac{dA}{d\tau} = ivA + (1 + iA)NA + F \cos(\Omega\tau), \tag{16a}$$

$$\frac{dN}{d\tau} = -b[N - \mu + (1 + N)|A|^2], \tag{16b}$$

where, as in the class A laser model analyzed in the previous section, $A = E \exp(iv\tau)/\sqrt{1 + \Delta^2}$, $F = E_0/\sqrt{1 + \Delta^2}$, $\mu = D_0/(1 + \Delta^2) - 1$, and $\tau = \kappa t$. Additionally we have defined a new scaled inversion $N = D/(1 + \Delta^2) - 1$ and a scaled inversion decay rate $b = \gamma_{\parallel}/\kappa \ll 1$. [Note that in the class A laser limit $b \gg 1$, the inversion variable N can be adiabatically eliminated from Eq. (16) and (16a) becomes Eq. (5).]

We integrated numerically the MB Eqs. (2) and (3) with the following parameters: $\Delta = 0, \mu = 1$ (which, like in previous section, means that the laser is twice above the generation threshold), $\gamma_{\perp} = 10\kappa, \gamma_{\parallel} = 0.01\kappa$ (equivalently, $b = 0.01$) which means relatively fast polarization P , and slow population inversion D , with respect to the electric field. Apart from the spectral width of the mode (κ), class B laser have two more characteristic frequencies: the pop-

ulation relaxation decay rate, γ_{\parallel} , and the relaxation oscillation frequency already introduced. We chose the value $b = 0.01$ in order to separate clearly these three characteristic frequencies. The obtained results can, however, be applied for class B lasers with different values of b (γ_{\parallel}), since the character of phase locking of rocked class B laser is essentially the same.

The calculation results are summarized in Fig. 5. The locking area decreases with increasing detuning, similarly to class A lasers, however much more rapidly. Another two essential differences have been found from class A lasers:

- (1) Both the upper and the bottom boundaries of the locking area are strongly deformed at the frequencies of relaxation oscillation and of subharmonics of relaxation oscillation – most strongly at the half of the relaxation oscillation frequency (Figs. 5 and 6). In particular the strongest resonance in resonant case is at the half of relaxation oscillation frequency and, in the detuned case, at the relaxation oscillation frequency. This deformation is interpreted by the fact that the rocking at the half of relaxation oscillation frequency meets a strong resonance, and the oscillations of the field are strongly enhanced.
- (2) The locking area at nonzero detuning is no more unbounded as in case of class A laser, but represents now a closed balloon. In the other words, the locking area is no more located between two straight lines at different slopes: the bottom area is deformed into a curve (parabola).

Again, for an analytic treatment, we consider the low excitation regime, defined by $-\infty < \mu \ll 1$ and $0 \leq F \ll 1$, in which case $N, |A|^2 \ll 1$ as well and Eq. (16b) can be approximated by

$$\frac{dN}{d\tau} = -b(N - \mu + |A|^2). \tag{16c}$$

An approximate analysis of the effect of rocking on class B lasers can be done making use of a multiple time scale technique, similar to that used in the class A laser case. Now appropriate scalings are $\mu, F, N = O(\epsilon^2)$ and $b, \Omega, A = O(\epsilon)$. The result of the analysis is the following:

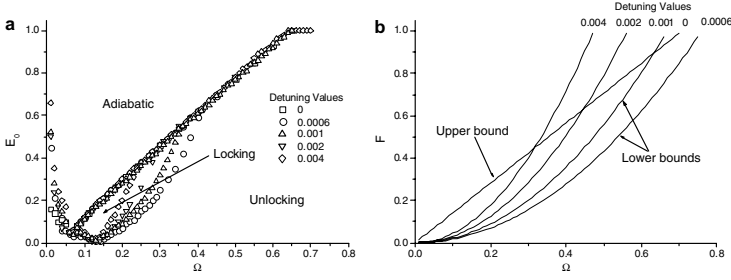


Fig. 5. Locking–unlocking regimes of class B lasers as obtained: (a) from numerical simulation of the MB Eqs. (2) and (3) and (b) from Eq. (22). Parameters are: $A = 0$, $\mu = 1$, $\gamma_{\perp} = 10\kappa$, $\gamma_{\parallel} = 0.01\kappa$ (equivalently, $b = 0.01$). The values of the rocking detuning ν are marked in the legends.

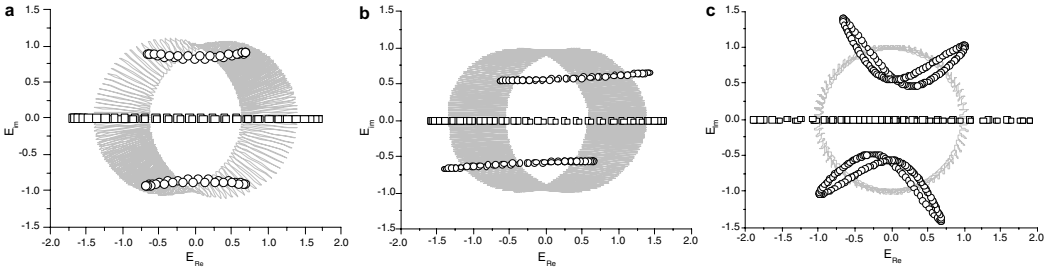


Fig. 6. Trajectories for class B lasers shown in phase space for a rocking detuning value $\nu = 0.001$. Circles correspond to the locking regime, squares to the adiabatic and the gray line indicates the unlocking trajectory: (a) is close to the relaxation frequency, $\Omega = 0.14$ ($E_0 = 0.01, 0.1$ and 0.3 for unlocking, locking and adiabatic respectively), (b) is close to twice the relaxation frequency, $\Omega = 0.28$ ($E_0 = 0.1, 0.3$, and 0.5) and (c) is close to half the relaxation frequency, $\Omega = 0.07$ ($E_0 = 0.01, 0.04$, and 0.1). Rest of parameters as in Fig. 5.

$$A = a + \frac{F}{\Omega} \sin(\Omega\tau) + O(\varepsilon^2), \quad (17a)$$

$$N = n + \frac{i}{2} \frac{F}{\Omega} (a + a^*) \left(\frac{b}{b + i\Omega} e^{i\Omega\tau} - \frac{b}{b - i\Omega} e^{-i\Omega\tau} \right) + O(\varepsilon^3), \quad (17b)$$

$$\frac{da}{d\tau} = i\nu a + (1 + i\Delta) \left[\left(n - \gamma_B \frac{b^2}{\Omega^2 + b^2} \right) a - \gamma_B \frac{b^2}{\Omega^2 + b^2} a^* \right], \quad (17c)$$

$$\frac{dn}{d\tau} = -b(n - \mu + \gamma_B + |a|^2), \quad (17d)$$

where γ_B coincides with the rocking parameter γ of the class A laser, Eq. (10). Derivation of (17) assumes a kind of slowly varying envelope approximation with respect to the rocking modulation frequency Ω .

The peculiarities of rocking in class B lasers described above can be interpreted by separately inspecting the deformations of the upper and lower boundaries forming the locking area. Similarly as in the class A laser case analyzed in the previous section, these can be determined analytically from the steady state of Eqs. (17c) and (17d), which in this case is given by the equation

$$0 = i\nu a + (1 + i\Delta) \left[(\mu - \gamma_B(1 + L) - |a|^2) a - \gamma_B L a^* \right], \quad (18)$$

where $L = b^2/(\Omega^2 + b^2)$. Another, alternative way of analysis considers the derivation of an equation for the steady state. The advantage of this straightforward derivation is that no scaling assumptions on rocking are done. The derivation leads to basically the same Eq. (18) but with γ_B given by

$$\gamma_B = \frac{1}{2} \frac{F^2}{\Omega^2} \frac{\Omega^2(b^2 + \Omega^2)}{(\Omega^2 - \omega_{RO}^2)^2 + b^2\Omega^2}, \quad (19)$$

where $\omega_{RO} = \sqrt{2b\mu}$ is the angular frequency (in units of κ) of the relaxation oscillations of the class B laser in the considered limit. (The actual value of the relaxation oscillations frequency is $\omega_{RO} = \sqrt{2b\mu - b^2(1 + \mu)/4}$.) Note that when $b \gg \Omega$ the rocking coefficient γ_B (19) reduces to coefficient γ in Eq. (10), in agreement with the scalings used in the derivation of Eqs. (17a–d). Eq. (19) shows that for class B lasers the rocking parameter (γ_B in this case) experiences a strong increase at the relaxation oscillation frequency.

Expressing a as in Eq. (12a) one easily finds:

$$u_{\pm}^2 = \mu - \gamma_B(1 + L) + \frac{\Delta\nu \pm \sqrt{\gamma_B^2 L^2 (1 + \Delta^2)^2 - \nu^2}}{1 + \Delta^2}, \quad (20a)$$

$$\exp(2i\phi_{\pm}) = \mp \frac{\sqrt{\gamma_B^2 L^2 (1 + \Delta^2)^2 - \nu^2} + i\nu}{\gamma_B L (1 + \Delta^2)}. \quad (20b)$$

The existence range of these rocked states reads now

$$\frac{|v|}{L(1+\Delta^2)} \equiv \gamma_{B,\min} < \gamma_B < \gamma_{B,\max}$$

$$\equiv \frac{(1+L)\mu(1+\Delta^2) + 2\Delta v + \sqrt{[\mu(1+\Delta^2) + \Delta v]^2 L^2 - (1+2L)v^2}}{(1+2L)(1+\Delta^2)}, \quad (21)$$

which is very similar to the class A laser result given by Eq. (13). In order to make contact with the simulations we consider Eq. (21) in the limit $\Delta = 0$. In this case $\gamma_{B,\min} = |v|/L$ and, further assuming small v as in the numerics, $\gamma_{B,\max} = \mu$. Thus the upper and lower boundaries of the phase locking regime in class B lasers are given by (in the case $\Delta = 0$ and $v \rightarrow 0$):

$$(E_0^{\min})^2 = 2|v| \frac{(\Omega^2 - \omega_{R0}^2)^2 + b^2 \Omega^2}{b^2} \quad (22)$$

$$(E_0^{\max})^2 = 2\mu \frac{(\Omega^2 - \omega_{R0}^2)^2 + b^2 \Omega^2}{b^2 + \Omega^2}$$

phase locking existing for rocking amplitudes in the range $E_0^{\min} \leq E_0 \leq E_0^{\max}$ (note that $E_0 = F$ when $\Delta = 0$). This means that the upper boundary is strongly modified at rocking frequencies close to resonance frequency, but not for large rocking frequencies, where it coincides with that of class A laser: $E_0^{\max} \approx \sqrt{2\mu}\Omega$. Also the lower boundary is strongly modified (compared with the class A laser) around the resonance frequency, and also has different asymptotes for large rocking frequencies. In the limit of large rocking frequencies one finds:

$$\sqrt{2|v|} \frac{\Omega^2}{b} < E_0 < \sqrt{2\mu}\Omega, \quad (23)$$

which is now bounded by a straight line from above and by a parabola from below, in a good agreement with the numerical results (in the limit of large frequencies). Condition (23) predicts that rocking will be efficient as far as $\Omega < b\sqrt{\mu}/|v|$. This condition indicates that the rocking region shrinks rapidly with increasing rocking detuning (v) or decreasing the inversion relaxation rate. Finally note that the area of the locking region on the parameter

space (Ω, F) can be estimated, in the case $\Delta = 0$, as $\sqrt{2}b^2\mu^{3/2}/(6|v|)$.

All the previous results have been obtained assuming that the atomic (ω_A) and cavity frequency (ω_C) coincide: $\Delta = 0$. This means that the emission frequency of the laser without forcing coincides with both frequencies. We also have considered the case in which $\omega_A \neq \omega_C$ in order to get a more complete view. For the case $\Delta = 2$ (emission frequency is much closer to ω_C than to ω_A), we have obtained interesting results which are summarized in Fig. 7. We have found that the range of existence of locking is increased for large values of the detuning of rocking (v). We also show that the transition locking-unlocking is not abrupt. As we increase the amplitude of forcing we pass through several dynamical regimes until we reach the adiabatic state (in which the signal merely follows the injection). We observe that the modulus of average field (that is constant in locking regime and zero in adiabatic regime) oscillates with half of rocking frequency close to the locking regime whereas for moderate amplitudes its behavior is more complicated (Fig. 7).

To conclude the analysis of the rocked class B laser, a comment on apparently related models is in order, as we did in the class A laser section. Braza [13] studied the same problem as Yamada and Graham [11] but in the class B limit. In our notation the model studied by Braza is represented by Eqs. (16a) and (16b), but with an injection term of the form $F_0 + F\cos(\Omega\tau)$, with $F \ll F_0$ as Zehnlé and Zeghlache [12]. Again, this perturbed LIS model does not hold the nontrivial symmetry $A(\tau) \rightarrow -A(\tau + \pi/\Omega)$ already discussed, hence no phase bistability as that discussed along our paper was identified in [13]. For the sake of completeness we note that Braza studied laser dynamics in a parameter region where phase entrainment is observed and the field phase exhibits a periodic dynamics characterized by π -jumps, as was already observed by Braza [14] and by Yamada and Graham [11] in the usual LIS case (without periodic injection). We note that this periodic alternation between two π -shifted phase values has nothing to do with the bistability between two π -shifted phase values discussed here.

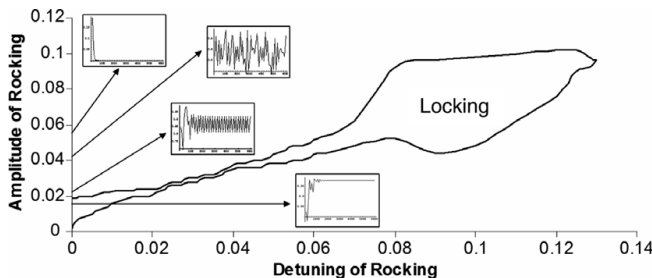


Fig. 7. Locking regime for class B lasers out of cavity resonance as obtained numerically from Eqs. (2) and (3) for $\Delta = 2$, $D_0 = 5$ (equivalently, $\mu = 1$), $\Omega = 2\pi \times 0.01\kappa$, $\gamma_{\perp} = 100\kappa$, and $\gamma_{\parallel} = 0.01\kappa$. The two variables are the amplitude of forcing (E_0) and its detuning (v) from the emission frequency of the free running laser. For the zero rocking-detuning case ($v = 0$) some time traces corresponding to different dynamical regimes are plotted. (The modulus of the one-rocking-period average of the field is plotted as a function of time.) The values of the rocking amplitude E_0 are 0.019, 0.021, 0.041, and 0.055.

5. Conclusions

The aim of this study was to theoretically and numerically investigate the dynamics of single mode lasers with ac periodically modulated injection. This was done by analyzing both reduced equations (complex Landau type) for class A and class B lasers, and by numerically simulating corresponding Maxwell–Bloch equations. The theory correctly predicts that in certain ranges of injection amplitude and frequency, the laser phase locks to any of two values shifted by π . In the class A laser the locking area was found to decrease with increasing detuning, in qualitative agreement with the numerically obtained results. In the class B lasers a locking area consisting of a parabola bound by a straight line was predicted, in good agreement with the numerical results, in the limit of large rocking frequencies. Strong phase modulation was found for injection frequencies close to the relaxation oscillation frequency.

Acknowledgement

We are grateful to the anonymous referees for bringing Refs. [11,13,14] to our attention. This work was financially

supported by Ministerio de Educación y Ciencia (Spain) and FEDER (European Union) through projects FIS2004-02587, FIS2005-07931-C03-01, and -03.

References

- [1] G.J. de Valcárcel, K. Staliunas, *Phys. Rev. E* 67 (2003) 026604.
- [2] A. Esteban-Martín, M. Martínez-Quesada, V.B. Taranenko, E. Roldán, G.J. de Valcárcel, arXiv.org:nlin/0602023.
- [3] See, e.g. L.D. Landau, E.M. Lifschitz, *Course of Theoretical Physics*, vol. 1, Pergamon, London, 1959.
- [4] L.A. Lugiato, M. Brambilla, A. Gatti, *Adv. At. Mol. Opt. Phys.* 40 (1998) 229.
- [5] H. Haken, *Synergetics, an Introduction*, Springer, Berlin, 1977.
- [6] A.H. Nayfeh, *Perturbation Methods*, Wiley Classics Library edition., Wiley, New York, 2000.
- [7] A.C. Newell, J.V. Moloney, *Nonlinear Optics*, Addison-Wesley, Redwood City, 1992.
- [8] P. Coulet, J. Lega, B. Houchmanzadeh, J. Lajzerowicz, *Phys. Rev. Lett.* 65 (1990) 1352.
- [9] H. Zeghlache, V. Zehnlé, *Phys. Rev. A* 46 (1992) 6015.
- [10] J.F. Urchueguía, V. Espinosa, E. Roldán, G.J. de Valcárcel, *J. Mod. Opt.* 46 (1996) 2311.
- [11] T. Yamada, R. Graham, *Phys. Rev. Lett.* 45 (1980) 1322.
- [12] V. Zehnlé, H. Zeghlache, *Phys. Rev. A* 46 (1992) 6028.
- [13] P.A. Braza, *Physica D* 134 (1999) 394.
- [14] P.A. Braza, *Opt. Commun.* 103 (1993) 95.

Rocking bidirectional lasers.

Manuel Martínez-Quesada, Eugenio Roldán and Germán J. de Valcárcel.

Optics communications **284** 2554-2559 (2011).



Rocking bidirectional lasers

Manuel Martínez–Quesada, Eugenio Roldán*, Germán J. de Valcárcel

Departament d'Òptica, Universitat de València, Dr. Moliner 50, 46100 Burjassot, Spain

ARTICLE INFO

Article history:

Received 12 October 2010

Received in revised form 28 December 2010

Accepted 10 January 2011

Available online 26 January 2011

ABSTRACT

We study the emission properties of a class A bidirectional laser under the action of an amplitude modulated injected signal, i.e. a rocked bidirectional laser. We derive two coupled autonomous amplitude equations valid close to the emission threshold and study their solutions. The most relevant result is that while in the absence of rocking the laser can only emit in either of the two unidirectional solutions, under suitable rocking conditions cw bidirectional emission appears and, moreover, it coexists bistably with unidirectional emission.

© 2011 Elsevier B.V. All rights reserved.

1. Introduction

Rocking is a modulation technique consisting in the forcing of a self-oscillatory system with two coherent signals of different frequencies but both close to the system's natural oscillation frequency. In other words, rocking consists in forcing the system with an *amplitude modulated* field whose carrier is close to the system's resonance. This technique was originally introduced as a means for transmuting phase-invariant systems into phase-bistable ones [1,2] in self-oscillatory systems for which parametric driving [3] cannot be applied. Parametric driving consists in forcing periodically of a self-oscillatory system at a frequency around *twice* its natural oscillation frequency, hence it is not well suited for optical systems given the small width of the response function of these systems compared to the optical frequency. Then the rocking technique is particularly well suited for optical systems as the forcing (the amplitude modulated field) is close to their natural oscillation frequency. Let us remark that while forcing with a monochromatic signal (as in usual lasers with injected signal) induces a phase locking of the system's response to that of the driving, rocking induces a different type of phase locking, namely a *bistable phase-locking*, i.e., under rocking the system's response is phase bistable. Rocking has been experimentally demonstrated in a photorefractive oscillator [4], analyzed in single-mode lasers [5], demonstrated with noisy injected fields [6], and applied to electronic oscillators [7]. In the present article, we study the effect of rocking in homogeneously-broadened bidirectional class A lasers.

Our motivation for this study comes from the fact that in a bidirectional laser there are two coupled fields that can be rocked independently and we expect new effects when the two fields are simultaneously rocked. Moreover, cavity solitons and related localized

structures have been theoretically predicted for bidirectional lasers quite recently [8–11]. Although in the present article we shall limit ourselves to the study of the plane wave model (i.e., single-transverse mode), it is worth mentioning that rocking can open new ways for stabilizing or manipulating these localized structures, even more, could lead to the prediction of new types of them for these systems.

As stated, we consider the single-transverse mode case in this article. Moreover, we treat the simplest configuration possible, i.e., we assume a homogeneously-broadened class A laser (for which all atomic variables can be adiabatically eliminated) in which the two fields have equal detunings and losses and further assume that the laser works close to the emission threshold. Then we add the rocking signal and derive a simplified autonomous model consisting of two complex Stuart–Landau equations with broken phase invariance. This simplified model contains the most relevant result of the present article namely that the rocked bidirectional laser can exhibit stable cw bidirectional emission, something impossible in a homogeneously broadened bidirectional laser [12,13]. Another relevant result is the existence of bistability between unidirectional and bidirectional solutions for a wide enough range of rocking strengths amplitudes.

2. Model

It can be shown [8,13] that a homogeneously-broadened bidirectional class A laser (i.e., a laser verifying $\gamma_{\perp} \gg \gamma_{\parallel} \gg \kappa$ with $\gamma_{\perp}, \gamma_{\parallel}$, and κ the decay rates of the atomic coherence, atomic inversion and field amplitude, respectively) can be described, sufficiently close to the emission threshold, by a pair of complex Stuart–Landau equations. These equations can be put in the form

$$\frac{1}{\kappa} \frac{d}{dt} E_n = (1 + i\Delta) (\mu - |E_n|^2 - 2|E_m|^2) E_n, \quad (1)$$

with $n, m = 1, 2$ and $n \neq m$. In the above equations E_n are proportional to the fields intracavity amplitudes (say running clockwise or anti-

* Corresponding author.

E-mail address: eugenio.roldan@uv.es (E. Roldán).

clockwise), and the normalized pump and cavity detuning parameters read

$$\mu = \frac{r}{1 + \Delta^2} - 1, \tag{2a}$$

$$\Delta = \frac{\omega_c - \omega_a}{\kappa + \gamma_{\perp}}, \tag{2b}$$

with r the incoherent pumping rate, and ω_c and ω_a the frequencies of the cavity mode closest to resonance and of the atomic transition, respectively. Eq. (1) is written in the frequency frame of the unidirectional lasing state frequency, which is given by the well known pulling-formula $\omega_L = (\kappa\omega_a + \gamma_{\perp}\omega_c)/(\kappa + \gamma_{\perp})$.

Let us briefly review the solutions and stability properties of Eq. (1) [12]. It contains up to four possible stationary solutions: the laser-off solution, $E_1 = E_2 = 0$; two equivalent unidirectional (or single-mode) solutions, $\{|E_m|^2 = \mu, E_m = 0, n \neq m\}$; and the bidirectional (or bimode) solution, $|E_1|^2 = |E_2|^2 = \mu/3$. The linear stability analyses of these solutions reveal that: (i) the laser-off solution loses its stability at $\mu = 1$ giving rise to any of the equivalent unidirectional solution, which is always linearly stable for $\mu \geq 1$; and (ii) the bidirectional solution is always unstable. Thus bidirectional cw emission is impossible in a homogeneously broadened bidirectional laser [12–14] and the only bistability exhibited by the system is that between the two equivalent unidirectional solutions.

Now we consider the effect of rocking, i.e., we add two *amplitude modulated* injected signals, each of them acting on one of the two counterpropagating fields. Hence, we write

$$\frac{1}{\kappa} \frac{d}{dt} E_n = (1 + i\Delta) (\mu - |E_n|^2 - 2|E_m|^2) E_n + F_n \cos(\omega t + \sigma_n \phi / 2) e^{-i\omega t}, \tag{3}$$

with $\sigma_{1,2} = \pm$. In this equation F_n are proportional to the driving amplitudes, which are taken to be real and positive without loss of generality. These are modulated at a frequency ω and are dephased by ϕ among them. As the above equations are written in the unidirectional lasing frequency frame, δ is the detuning between the carrier of the injections, ω_R , and the lasing frequency, i.e. $\delta = \omega_R - \omega_L$.

It is convenient to define new field amplitudes as

$$E_{1,2} = \sqrt{\mu} A_{1,2} e^{-i\omega t}, \tag{4}$$

that, apart from a rescaling, implies a change in the frequency frame to that of the rocking fields ($\omega_R = \omega_L + \delta$). We also define a new dimensionless time $\tau = \mu\kappa t$ and obtain

$$\frac{d}{d\tau} A_n = \left[(1 + i\theta) - (1 + i\Delta) (|A_n|^2 + 2|A_m|^2) \right] A_n + B_n \cos(\Omega\tau + \sigma_n \phi / 2), \tag{5}$$

where we have introduced

$$B_n = \frac{1}{\mu\sqrt{\mu}} F_n, \quad \Omega = \frac{\omega}{\mu\kappa}, \quad \theta = \frac{\delta}{\mu\kappa} + \Delta. \tag{6}$$

3. Derivation of a reduced model

In order to better understand the effect of rocking, we consider the formal limit $B_n \sim \Omega \gg 1$ [1], i.e., large amplitude and also large frequency of the rocking fields as compared to $\mu\kappa$. Then we write $B_n = \sqrt{2\gamma_n} \Omega$, which introduces the new rocking strength γ_n , define a fast time through $T = \Omega t$ and search multiple-scale solutions of the form

$$A_n(\tau) = A_n^{(0)}(\tau, T) + \Omega^{-1} A_n^{(1)}(\tau, T) + \mathcal{O}(\Omega^{-2}). \tag{7}$$

Substituting this expansion and the scalings into Eq. (5), and making use of the chain rule for differentiation, an infinite hierarchy of problems at decreasing order in Ω is obtained. To the leading, Ω^0 order one obtains

$$\partial_T A_n^{(0)}(\tau, T) = \sqrt{2\gamma_n} \cos(T + \sigma_n \phi / 2), \tag{8}$$

whose solution is

$$A_n^{(0)}(\tau, T) = \sqrt{2\gamma_n} \sin(T + \sigma_n \phi / 2) + U_n(\tau), \tag{9}$$

with $U_n(\tau)$ a yet undetermined function not depending on the fast time scale T . The next, Ω^1 order reads

$$\partial_T U_n(\tau) + f(\tau) = -\partial_T A_n^{(1)}(\tau, T) + \sum_{k=1}^3 g_k(\tau) \sin kT. \tag{10}$$

As the left hand side of this equation does not depend on T , its solvability requires $\partial_T U_n(\tau) + f(\tau) = 0$, which reads explicitly as

$$(1 + i\Delta)^{-1} \partial_T U_n = \frac{\lambda + i\nu}{1 + i\Delta} U_n - (|U_n|^2 + 2|U_m|^2) U_n, \\ -\gamma_n U_n^* - 4\eta \sqrt{\gamma_1 \gamma_2} \text{Re} U_m, \tag{11a}$$

where

$$\lambda = 1 - 2(\gamma_1 + \gamma_2), \tag{11b}$$

$$\nu = \theta - 2(\gamma_1 + \gamma_2)\Delta = \frac{\delta}{\mu\kappa} + \lambda\Delta, \tag{11c}$$

$$\eta = \cos\phi. \tag{11d}$$

Eq. (11a) ($n=1,2$) forms a set of two coupled complex Stuart–Landau equations with broken phase invariance because of the extra terms proportional to U_n and $\text{Re}U_m$. The term proportional to U_n introduces a parametric coupling that breaks the original system's phase invariance, while the term $\text{Re}U_m$ also does but its existence depends on the simultaneous rocking of both fields ($\gamma_1 \gamma_2 \neq 0$) as well as on the rockings' relative phase through η . Notice finally that the above equations are symmetric under the transformation $\{U_n, U_m, \eta\} \leftrightarrow \{U_m, -U_m, -\eta\}$ hence we only need to consider $\eta > 0$, which is what we do below.

Before analyzing the solutions of Eq. (11a) let us remark that the actual (approximated) physical solutions describing the emission of the rocked bidirectional laser are given by Eq. (9). They consist of a trivial part that follows the injection oscillating with frequency Ω , first term in Eq. (9), plus the nontrivial part governed by Eq. (11a) that evolves on the much slower temporal scale τ , second term in Eq. (9). In the following we shall refer only to the nontrivial part of the solutions, but one must keep in mind the existence of the first trivial term. Notice that the trivial part of the solutions could be easily removed from the laser output by using a low-pass frequency filter as Ω is large as compared to the frequencies governing the evolution of amplitudes U_n . Next we split our study into two cases: resonant injection with the lasing frequency (cases for which $\delta = \omega_R - \omega_L = 0$) and non-resonant injection.

4. Resonant injection

Once the reduced model (11a) has been derived, we pass to obtain its cw solutions and study their linear stability. Within the present section we take $\delta = 0$, that is, we assume that the injected signal has the same frequency as the lasing solution. This implies taking $\nu = \lambda\Delta$ or, equivalently, $\Delta = \theta \neq 0$, see Eqs. (6) and (11c).

Next we consider two special cases regarding the amplitudes of the rocking fields: (i) unidirectional rocking ($\gamma_2 = 0$ and $\gamma_1 \neq 0$, i.e., rocking acting only on one field); and symmetric rocking ($\gamma_1 = \gamma_2 = \gamma$, i.e., rocking acting symmetrically on both counterpropagating fields).

4.1. Unidirectional rocking

We define $\gamma \equiv \gamma_1$ in this case. Eq. (11a) has up to six different steady state solutions. These solutions are: (i), the trivial solution $U_1 = U_2 = 0$ (which is not the laser-off solution as there is the trivial part of the solution in Eq.(9), but plays the same role, hence we call it laser-“off” solution); (ii), the three unidirectional emission solutions (five indeed, but we shall count the number of solutions attending only the field modulus)

$$U_1^{(U_1)} = \pm \sqrt{1-3\gamma}, \quad U_2^{(U_1)} = 0, \tag{12a}$$

$$U_1^{(U_2)} = 0, \quad U_2^{(U_2)} = \sqrt{1-2\gamma}e^{i\phi_2}, \tag{12b}$$

$$U_1^{(U_3)} = \pm \sqrt{1-\gamma}e^{\pm i\pi/2}, U_2^{(U_3)} = 0; \tag{12c}$$

and (iii), the two bidirectional emission solutions

$$U_1^{(B_1)} = \pm \sqrt{\frac{1}{3}-\gamma}e^{\pm i\pi/2}, U_2^{(B_1)} = \pm \frac{1}{\sqrt{3}}e^{i\phi_2}, \tag{13a}$$

$$U_1^{(B_2)} = \pm \sqrt{\frac{1-\gamma}{3}}, \quad U_2^{(B_2)} = \pm \sqrt{\frac{1-4\gamma}{3}}e^{i\phi_2}. \tag{13b}$$

In the above expressions ϕ_2 is an arbitrary phase and the superscripts in the above solutions refer to their unidirectional or bidirectional character.

The above list of solutions shows that rocking is effective in removing the phase invariance of the field U_1 , the field in which the rocking signal acts, converting it into a phase bistable field (only the phases $\phi_1 = 0, \pi$ appear in the solutions), but leaving the counter-propagating field U_2 phase invariant (ϕ_2 is arbitrary). This is not surprising as for $\gamma_2 = 0$, the only way that U_1 influences U_2 is through its modulus in the saturating nonlinearity, see Eq. (11a), and U_2 does not feel U_1 phase in any way. Hence the phase invariance in U_2 in spite of the phase bistability in U_1 .

The linear stability of the above solutions is governed by the eigenvalues of the stability matrix M that reads

$$\mathcal{M} = \begin{pmatrix} \mathcal{Y} & A_1 & B_0 & C_0 \\ A_1^* & \mathcal{Y}^* & C_0^* & B_0^* \\ B_0^* & C_0 & \mathcal{Y} & -U_2^2 \\ C_0^* & B_0 & -U_2^{*2} & \mathcal{Y}^* \end{pmatrix}, \tag{14a}$$

with

$$A_1 = -(1 + i\Delta)(\gamma + U_1^2), \tag{14b}$$

$$B_0 = -2(1 + i\Delta)U_1U_2^*, \tag{14c}$$

$$C_0 = -2(1 + i\Delta)U_1U_2, \tag{14d}$$

$$\mathcal{Y} = (1 + i\Delta)[1 - 2(\gamma + |U_1|^2 + |U_2|^2)]. \tag{14e}$$

Substitution of the steady state solutions on \mathcal{M} allows the fixing of their stability properties. It is easy to demonstrate that the two bidirectional emission solutions (Eqs. (13)) are always unstable, as it is the unidirectional solution (Eq. (12a)). The stability of the other three solutions is not sensitive to Δ and summarizes as follows: The

trivial solution is stable for $\gamma > 1$, solution (Eq. (12b)) is stable for $\gamma < 1/3$, and solution (Eq. (12c)) is stable for $\gamma < 1$.

We see that asymmetric rocking ($\gamma_2 = 0$) breaks the original equivalence between the two unidirectional solutions: the two counterpropagating fields have different intensities, different phase properties (U_1 is phase bistable whilst U_2 is not), and different domains of existence: bistability between counterpropagating solutions is limited to $\gamma < 1/3$, and for $1/3 < \gamma < 1$ only field U_1 is on. We remark that rocking one of the two fields does not stabilize any bidirectional solution in the system.

4.2. Symmetric rocking

We define $\gamma \equiv \gamma_1 = \gamma_2$ in this case. Eq. (11a) has now up to seven different steady state solutions. They are: (i), the trivial solution $U_1 = U_2 = 0$; (ii), the two equivalent unidirectional emission solutions

$$U_n^{(U)} = \pm \sqrt{1-3\gamma}e^{i\pi/2}, U_m^{(U)} = 0, n \neq m; \tag{15}$$

and (iii), up to five different bidirectional solutions. Of these, the following three solutions are symmetric with respect to the intensities of the two modes (i.e., they verify $|U_1| = |U_2|$)

$$U_n^{(S1)} = \pm \sqrt{\frac{1-3\gamma}{3}}e^{i\pi/2}, U_m^{(S1)} = \pm U_n^{(S1)}, \tag{16a}$$

$$U_n^{(S2)} = U_m^{(S2)} = \pm \sqrt{\frac{1-5\gamma-4\eta}{3}}, \tag{16b}$$

$$U_n^{(S)} = -U_m^{(S)} = \pm \sqrt{\frac{1-5\gamma+4\eta}{3}}, \tag{16c}$$

($n, m = 1, 2$ and $n \neq m$); and there are two other bidirectional solutions that are asymmetric with respect to the intensities, reading

$$U_{1,2}^{(A)} = \pm \sqrt{\frac{1-5\gamma \mp \sqrt{(1-5\gamma)^2 - (8\eta)^2}}{2}}, \tag{17}$$

and

$$U_n^{(A')} = \frac{\mathcal{F}_n}{\sqrt{3}}e^{i\phi_n}, \tag{18a}$$

$$\cos\phi_1 = -2\eta \frac{\mathcal{F}_2}{\mathcal{F}_1}, \phi_2 = 0, \tag{18b}$$

with

$$\mathcal{F}_1 = \pm \sqrt{1-\gamma(7-16\eta^2)}, \tag{18c}$$

$$\mathcal{F}_2 = \pm \sqrt{1-\gamma(1+8\eta^2)}. \tag{18d}$$

The superindexes in the bidirectional solutions refer to their symmetric or asymmetric character with respect to intensities. Notice that in this symmetric rocking case, both fields have lost their original phase invariance, becoming phase bistable.

The linear stability of these solutions is governed by the eigenvalues of the stability matrix \mathcal{L} that reads

$$\mathcal{L} = \begin{pmatrix} \mathcal{Z} & A_1 & B & C \\ A_1^* & \mathcal{Z}^* & C^* & B^* \\ B^* & C & \mathcal{Z} & A_2 \\ C^* & B & A_2^* & \mathcal{Z}^* \end{pmatrix}, \tag{19a}$$

where

$$A_n = -(1 + i\Delta)(\gamma + U_n^2), \quad n = 1, 2, \tag{19b}$$

$$B = -2(1 + i\Delta)(\eta\gamma + U_1U_2), \tag{19c}$$

$$C = -2(1 + i\Delta)(\eta\gamma + U_1U_2), \tag{19d}$$

$$Z = (1 + i\Delta)[1 - 2(2\gamma + |U_1|^2 + |U_2|^2)]. \tag{19e}$$

The linear stability analysis shows that all bifurcations occurring in the system are pitchfork bifurcations and, as before, are insensitive to Δ . The results can be put in short as follows: (i) the trivial solution is stable for $\gamma > \gamma_0$ with

$$\gamma_0 = \max\{1/3, (5-4\eta)^{-1}\}; \tag{20}$$

(ii) the unidirectional solution Eq. (15) is linearly stable for $\gamma < \min\{1/3, \gamma_U\}$ with

$$\gamma_U = (1 + 8\eta^2)^{-1}; \tag{21}$$

(iii) the bidirectional solutions Eq. (18) are always unstable; (iv) the bidirectional solution (Eq. (16c)) is stable for $\gamma_0 > \gamma > \gamma_S$ with

$$\gamma_S = (5 + 8\eta)^{-1}, \tag{22}$$

provided $\eta > 1/2$; and (v), the bidirectional solution (Eq. (17)) is stable whenever $\gamma_S > \gamma > \gamma_A$, with

$$\gamma_A = (7 + 8\eta^2)^{-1}, \tag{23}$$

which again requires $\eta > 1/2$. These results are shown in Fig. 1 where the domain of stability of the different solutions are represented on the parameter plane (η, γ) .

Clearly $\eta = 1/2$ is a crucial value for the dephasing between the two rocking signals as only for $\eta > 1/2$ the bidirectional solutions can be stabilized (the stability domain being quite large for the symmetrical solution (Eq. (16c)) and quite reduced for the asymmetrical solution (Eq. (17))). Thanks to this stabilization, apart from the phase-bistability exhibited by all the solutions, for $\eta > 1/2$ there are two domains of bistability between the unidirectional emission solution (Eq. (15)) and the bidirectional solutions, as marked in the figure. Notice that one of these bistable domains (that denoted by $U+A$ in Fig.1) is larger for larger η , while the other domain ($U+S$) becomes smaller.

In order to better understand the above results, Fig. 2 illustrates how the different bifurcations affect the different solutions by representing their intensities as a function of the rocking strength γ for a special value of the dephasing between the two rocking signals (we choose $\eta = 0.9$). This case illustrates well the behaviour of the system for $\eta > 1/2$ (for $\eta < 1/2$ only the unidirectional emission solution is stable, hence no plot is needed for these cases). All the steady state solution intensities have been represented in Fig. 2, the dashed lines corresponding to the unstable solutions. Notice that the bifurcations affecting the unidirectional and asymmetric bidirectional solutions (whose intensities are denoted by I_U , I_{A1} , and I_{A2} in the figure) are subcritical pitchfork bifurcations (denoted as B2 and B3 in the figure). We shall come back to them in the following section.

In passing we would like to note the similarity between the results shown and those found in [15]: the competition between the bidirectional and unidirectional solutions (which are connected via the unstable bidirectional solution that appears at their corresponding subcritical pitchfork bifurcations B2 and B3) reminds that occurring in

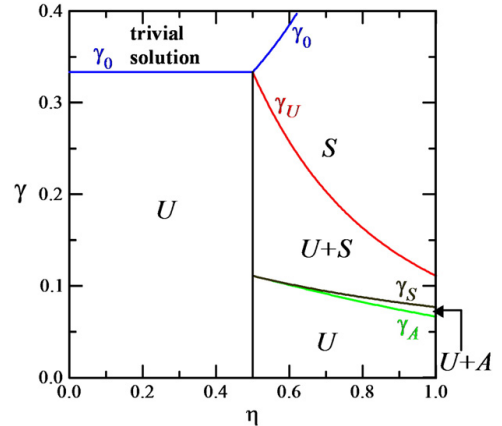


Fig. 1. Domains of stability of the different solutions in the parameter plane (η, γ) . For $\gamma < \gamma_0$ the nontrivial part of the laser solution, see Eq. (9), is on: Within the domain marked by S only the symmetric bidirectional solution (Eq. (16c)) is stable, within the domain $U+S$ both the symmetric bidirectional solution and the unidirectional one coexist stably, within the domain $U+A$ both the asymmetric bidirectional solution (Eq. (17)) and the unidirectional one coexist stably, and in the domain U only the unidirectional solution exists. See text for the analytical expressions of the different boundaries.

the extended optical parametric oscillator model of Ref. [15] (consisting of two coupled generalized complex Swift-Hohenberg equations) between traveling-wave and standing-wave patterns.

In resume, the properties of the bidirectional laser under symmetric rocking conditions notably differ from those of unidirectional rocking as far as $\eta > 0.5$ (that is, when the two rocking fields are dephased among them by less than $\pi/4$): now there are two stable bidirectional solutions, each of them with two possible phase values for each of the two fields, that coexist bistably with the unidirectional solutions for rocking strengths $\gamma_U > \gamma > \gamma_A$.

Now we recall the comments made in the introduction on localized structures in bidirectional lasers [8–11]. It has been shown that for large Fresnel number lasers localized structures consisting of walls separating adjacent spatial domains in which different unidirectional solutions exist. Rocking adds phase bistability as well as bistability between unidirectional and bidirectional solutions, which notably increases the types of localized structures that these lasers could exhibit. We are currently investigating these possibilities.

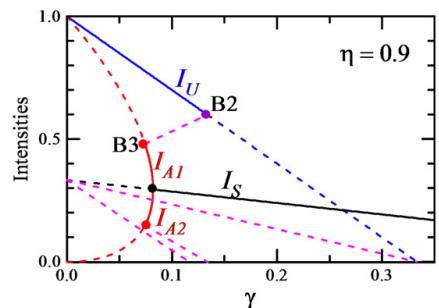


Fig. 2. Intensities of all possible stationary solutions for $\delta = 0$ and $\eta = 0.9$. Only those having some domain of stability are marked with $I_k = |U^{(k)}|^2$. Continuous (dashed) lines indicate stable (unstable) solutions, and the bifurcations are marked with a filled circle. Solution I_S extends till $\gamma \approx 0.7143$. The (unstable) solution connecting the bifurcations affecting I_A and I_U is that given by Eq. (18). B2 and B3 mark two of the bifurcations for discussion convenience, see text.

5. Non-resonant injection

We have seen that cavity detuning effects can be compensated by properly choosing injection detuning as stability turns out to be insensitive to detuning as far as $\delta = \omega_R - \omega_L$ remains null. But if not compensated in this way, detuning is detrimental for the effectivity of rocking as it reduces the domain of phase locking [5].

It is easy to see that unidirectional solutions cease to exist when $\delta \neq 0$, being replaced by bidirectional solutions in which one of the fields is much weaker than the other. However cases involving a non null detuning δ are more difficult to handle as the steady states are not analytical in this case. As a general analytical treatment is not possible, we choose to make a numerical study in order to gain some insight into the system's behaviour. In particular, we choose the special case $\Delta = 0$ (resonant laser cavity) and study the influence of a non-null θ .

Numerics reveal the appearance of oscillations for small γ values as soon as $\theta \neq 0$. These oscillations have their origin in the limit cycle that exists for $\gamma = 0$ and $\theta \neq 0$: as Eq. (11a) is written in the frequency frame of the rocking field, in the absence of rocking ($\gamma = 0$) the unidirectional solutions have a (trivial) oscillation with frequency θ . We say that this oscillation is trivial because it manifests in the field amplitudes but not in their intensities, and can be removed by changing the frequency frame. But, keeping $\theta \neq 0$, these oscillations become nontrivial (they cannot be removed by a frequency frame change) as γ is increased and continues existing till γ reaches a value γ_{B1} where they disappear. The value of γ_{B1} increases with increasing θ .

Keeping θ small (below 0.0225, see below) we see that by increasing γ the stationary solutions are affected by the same bifurcations B2 and B3 we have seen for $\delta = 0$ (although the values of γ at which they appear, let's name them γ_{B2} and γ_{B3} , change) and no new oscillating regimes appear. The increase of θ affects bifurcations B2 and B3 by approaching them to each other, i.e., by decreasing the value of $\gamma_{B2} - \gamma_{B3}$. Regarding the character of bifurcation B1, we have numerically checked that it is a single eigenvalue that becomes null at this bifurcation. This fact, together with the type of pulsations (that reach an infinite period at the bifurcation) identifies this bifurcation as a heteroclinic bifurcation. (We do not give now more details because we describe a similar bifurcation immediately below.)

When θ is further increased, the behaviour for increasing γ changes. The change consists in that now bifurcations B2 and B3 give rise to oscillations. This occurs as follows: as stated, increasing θ makes B2 and B3 approach each other till θ reaches the value $\theta_c = 0.0225$ where they merge ($\gamma_{B2} = \gamma_{B3}$ for $\theta = \theta_c$). For $\theta > \theta_c$, bifurcation B2 occurs at a γ value smaller than that for which bifurcation B3 appears, i.e. $\gamma_{B2} < \gamma_{B3}$, which implies a change in the dynamic behaviour of the system as now these bifurcations give rise to intensity pulsations.

This is well illustrated by Fig. 3, where we have represented the solution intensities as a function of γ for a detuning value $\theta = 0.025 > \theta_c$. In this case the system displays two self-pulsing domains: There is the self-pulsing regime occurring for $0 < \gamma < \gamma_{B1} = 0.035$ (corresponding to the oscillations originating at $\gamma = 0$ that we have already analyzed), and there is a new self-pulsing region, occurring for $\gamma_{B2} \approx 0.083 < \gamma < \gamma_{B3} \approx 0.089$. The existence of this last dynamic domain means that the character of bifurcations B2 and B3 has changed for $\theta > \theta_c$. (In Fig. 3 the maximum and minimum values that the intensities reach during their oscillations correspond to the upper and lower limits of the shadowed areas.)

The origin of the new self-pulsing domain can be easily understood: the change in the order in which B2 and B3 appears when $\theta > \theta_c$ implies that for $\gamma_{B2} < \gamma < \gamma_{B3}$ no stable steady state exists. Hence B2 and B3 are no longer pitchfork bifurcations and become heteroclinic ones as for $\gamma_{B2} < \gamma < \gamma_{B3}$ the system trajectories in phase space have no stable steady state or limit cycles to go to, and they can only move from one unstable steady state to the other, with a period

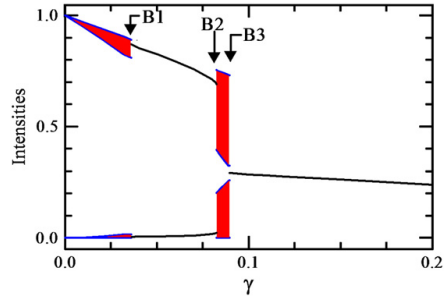


Fig. 3. Intensities of the different solutions found by numerical integration of Eq. (11a) for $\eta = 0.9$, $\Delta = 0$ and $\theta = 0.025$. In the shadowed areas a self-pulsing regime appears, in which intensities oscillate between a maximum and minimum value corresponding to the upper and lower limits of the shadows. B1, B2 and B3 denote the different bifurcations occurring for this parameter set, see text. The symmetric bidirectional solution exists till $\gamma = 0.715$.

that tends to infinity at the bifurcations. We have numerically calculated the system's eigenvalues at bifurcations B2 and B3 and have seen that there is a single eigenvalue that becomes positive when crossing them, i.e., the bifurcations are not Hopf bifurcations: we are in the presence of heteroclinic bifurcations having an infinite period at the bifurcation points.

An example of the type of behaviour found within the self-pulsing regime is shown in Fig. 4 where the phase dynamics of field U_1 is shown in Fig. 4(a), the field intensities are shown in Fig. 4(b), and a phase portrait of field U_1 is shown in Fig. 4(c) for $\gamma = 0.089$ (see caption). The figure confirms that we are in the presence of heteroclinic orbits connecting the unstable steady states (see, in particular, in Fig. 4(c) the dots marking their position in the field phase portrait): Notice in Fig. 4(a) and (b) how the trajectory spends some time in the neighbourhood of the unstable steady states. We notice that this behaviour is very similar to that shown in [16] for a bistably phase locked laser when tuned close but out of the phase locking region. Finally, we notice the antiphase dynamics [17] exhibited by the intensity pulsations.

A comment is in order concerning the phase dynamics. First we notice that the abrupt phase changes visible in Fig. 4(a) are an artifact because we are plotting the phase $mod(2\pi)$ in order to appreciate that the plateaus are located in the proximities of the unstable steady state values. Notice, however, apart from these artificial 2π jumps the phase dynamics is nontrivial exhibiting a sequence of plateaus followed by more abrupt jumps. This phase behaviour was analyzed long ago in the laser-Lorenz model [18,19] and we refer the reader to those papers for details concerning the relation of this phase dynamics with frequency changes in the field spectrum. Notice, however, that the cavity detuning is non-null what implies that the field frequency is no more that of the cavity mode, a fact that is reflected in the phase dynamics in a nontrivial way [18–21]. Another relevant comment is that the existence of amplitude and phase pulsations implies a modulation and a shift of the interference pattern of the bidirectional solution along the ring cavity.

For still larger θ , there is a new qualitative change in the dynamics as bifurcations B1 and B2 approach each other till they merge when $\theta = \theta_{c2} = 0.0313$, which implies that the quasi-unidirectional solution is no longer stable for $\theta > \theta_{c2}$. Now the two dynamical domains described above merge and the symmetric bidirectional solution is the only remaining stable stationary state.

The above results show that detuning is indeed detrimental for phase locking. However for large enough rocking strength γ , phase locking remains and the symmetric bidirectional solution exists and is stable. Hence we can conclude that the results we have described in the previous section for resonant injection are not singular, i.e., there

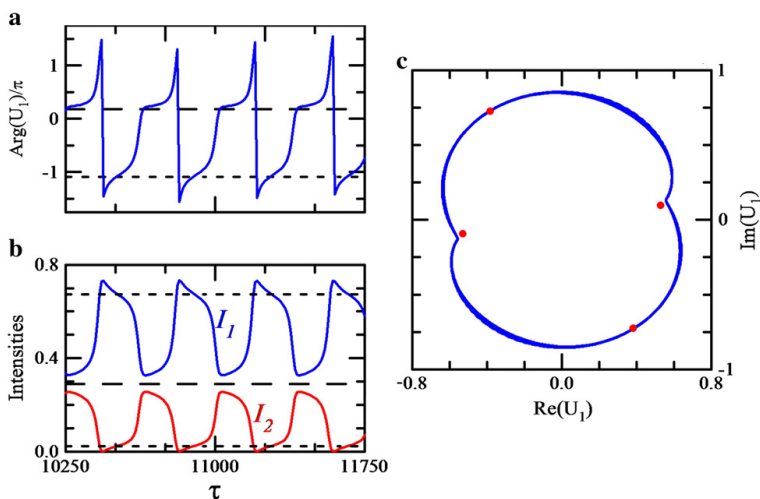


Fig. 4. Phase of field U_1 (a), intensities of the two counterpropagating fields (b), and phase portrait of field U_1 corresponding to $\Delta = 0$, $\theta = 0.025$, $\eta = 0.9$, and $\gamma = 0.089$. The horizontal dashed lines in (a) and (b), as well as the dots in (c), mark the (unstable) steady states, which are the symmetric (short dash) and asymmetric bidirectional (long dash) solutions. Notice in (b) the antiphase dynamics in the intensity pulsations.

exists a certain (small) domain in detuning for which these results remain (qualitatively) valid.

6. Conclusions

In this article we have studied the effect of rocking (i.e., the effect of injecting amplitude modulated signals) on a class A bidirectional laser model. We have derived a simplified model in the limit of large modulation (i.e., large rocking strength and frequency) consisting of a pair of complex Stuart–Landau equations with broken phase invariance, Eq. (11a). We have analyzed these model steady states and found that, apart from the phase symmetry breaking effect of rocking, for symmetric rocking (with a relative dephasing between the rocking fields smaller than $\pi/4$), some bidirectional solutions become stable. Moreover, domains of bistability between unidirectional and bidirectional emission appear in the parameter space. Hence rocking allows for bidirectional cw emission in bidirectional lasers and extends the types of bistabilities that the system displays. We have checked that the results we have derived from the simplified model of Eq. (11a) does reproduce the solutions of the original Eq. (5). Of course the degree of quantitative agreement depends on the choice of the rocking parameters, that must be large enough.

We expect that these results will have relevance for the type of localized structures that this system can develop when a large Fresnel number cavity is considered, as we have commented at the end of Section 4.2.

Acknowledgments

We acknowledge fruitful discussions with K. Staliunas. This work has been supported by the Spanish Government and the European Union FEDER through Project FIS2008-06024-C03-01.

References

- [1] G.J. de Valcárcel, K. Staliunas, Phys. Rev. E 67 (2003) 026604.
- [2] G.J. de Valcárcel, K. Staliunas, Phys. Rev. Lett. 105 (2010) 054101.
- [3] P. Couillet, J. Lega, B. Houchmanzadeh, J. Lajzerowicz, Phys. Rev. Lett. 65 (1990) 1352.
- [4] A. Esteban-Martín, M. Martínez-Quesada, V.B. Taranenko, E. Roldán, G.J. de Valcárcel, Phys. Rev. Lett. 97 (2006) 093903.
- [5] K. Staliunas, G.J. de Valcárcel, M. Martínez-Quesada, S. Gilliland, A. González-Segura, G. Muñoz-Matutano, J. Cascante-Vindas, J. Marqués-Hueso and S. Torres-Peiró, Opt. Commun. 268 (2006) 160.
- [6] K. Staliunas, G.J. de Valcárcel, J.M. Buldú, J. García-Ojalvo, Phys. Rev. Lett. 102 (2009) 010601.
- [7] J.M. Buldú, K. Staliunas, J.A. Casas, J. García-Ojalvo, Chaos 16 (2006) 043126.
- [8] I. Pérez-Arjona, V.J. Sánchez-Morcillo, E. Roldán, Opt. Lett. 32 (2007) 3221.
- [9] L. Colombo, L. Gil, J. Tredecce, Opt. Lett. 33 (2008) 995.
- [10] I. Pérez-Arjona, V.J. Sánchez-Morcillo, J. Redondo, K. Staliunas, E. Roldán, Opt. Express 17 (2009) 4897.
- [11] L. Colombo, L. Gil, J. Tredecce, Eur. Phys. J. D. 58 (2010) 227.
- [12] H. Zeghlache, P. Mandel, N.B. Abraham, L.M. Hoffer, G.L. Lippi, T. Mello, Phys. Rev. A 37 (1988) 470.
- [13] L. Mandel, E. Wolf, Coherence and quantum optics, Cambridge University Press, 1995.
- [14] Let us comment that the factor 2 in front of terms $|F_n|^2 F_m$, $n \neq m$, in Eqs. (1) becomes smaller in inhomogeneously broadened lasers. When this factor is smaller than one, the bidirectional solution becomes stable. See, e.g., [13] or M. Sargent III, M.O. Scully, and W. E. Lamb, Laser Physics (Addison Wesley, Reading, 1974).
- [15] V.J. Sánchez-Morcillo, G.J. de Valcárcel, E. Roldán, and K. Staliunas, Phys. Rev. E 57 (1998) R4911.
- [16] K. Staliunas, G.J. de Valcárcel, E. Roldán, Phys. Rev. A 80 (2009) 025801.
- [17] S. Bielawski, D. Derozier, P. Glorieux, Phys. Rev. A 46 (1992) 2811.
- [18] R. Vilaseca, G.J. de Valcárcel, E. Roldán, Phys. Rev. A 41 (1990) 5269.
- [19] E. Roldán, G.J. de Valcárcel, R. Vilaseca, P. Mandel, Phys. Rev. A 48 (1993) 591.
- [20] E. Roldán, G.J. de Valcárcel, R. Vilaseca, F. Silva, J. Pujol, R. Corbalán, F. Laguarda, Opt. Commun. 73 (1989) 506.
- [21] H. Zeghlache, P. Mandel, N.B. Abraham, C.O. Weiss, Phys. Rev. A 38 (1989) 3128.

Phase-bistable pattern formation in oscillatory systems via rocking: application to nonlinear optical systems.

Germán J. de Valcárcel, Manuel Martínez-Quesada and Kestutis Staliunas.

Philosophical Transactions of the Royal Society A **372**
20140008 (2014).

Research



Cite this article: de Valcárcel GJ, Martínez-Quesada M, Staliunas K. 2014 Phase-bistable pattern formation in oscillatory systems via rocking: application to nonlinear optical systems. *Phil. Trans. R. Soc. A* **372**: 20140008.
<http://dx.doi.org/10.1098/rsta.2014.0008>

One contribution of 19 to a Theme Issue 'Localized structures in dissipative media: from optics to plant ecology'.

Subject Areas:

complexity, mechanics, optics, wave motion

Keywords:

pattern formation, resonant forcing, oscillators, lasers, phase bistability, solitons

Author for correspondence:

Germán J. de Valcárcel
e-mail: german.valcarcel@uv.es

Phase-bistable pattern formation in oscillatory systems via rocking: application to nonlinear optical systems

Germán J. de Valcárcel¹, Manuel Martínez-Quesada¹ and Kestutis Staliunas²

¹Departament d'Òptica, Universitat de València, Dr. Moliner 50, Burjassot 46100, Spain

²ICREA and Departament de Física i Enginyeria Nuclear, Universitat Politècnica de Catalunya, Colom 11, Terrassa 08222, Spain

We present a review, together with new results, of a universal forcing of oscillatory systems, termed 'rocking', which leads to the emergence of a phase bistability and to the kind of pattern formation associated with it, characterized by the presence of phase domains, phase spatial solitons and phase-bistable extended patterns. The effects of rocking are thus similar to those observed in the classic 2:1 resonance (the parametric resonance) of spatially extended systems of oscillators, which occurs under a spatially uniform, time-periodic forcing at twice the oscillations' frequency. The rocking, however, has a frequency close to that of the oscillations (it is a 1:1 resonant forcing) and hence is a good alternative to the parametric forcing when the latter is inefficient (e.g. in optics). The key ingredient is that the rocking amplitude is modulated either in time or in space, such that its sign alternates (exhibits π -phase jumps). We present new results concerning a paradigmatic nonlinear optical system (the two-level laser) and show that phase domains and dark-ring (phase) solitons replace the ubiquitous vortices that characterize the emission of free-running, broad area lasers.

1. Introduction

The phase symmetries of systems of nonlinear oscillators deeply affect the nature of spatial patterns that form therein. For instance, the continuous phase symmetry characterizing the free oscillations is responsible for the spontaneous emergence of vortices and spiral waves in reaction–diffusion, optical and other kinds of oscillatory, spatially extended nonlinear systems [1–8]. In order to control the turbulent-like behaviour associated with the presence of those phase defects different types of forcing have been considered [1,2,4,9–14], the most popular being the classic time-periodic one. Periodic forcing acts as an external clock, which is ‘seen’ by the system oscillations, hence the equivalence of all the oscillation phases disappears, and the original continuous phase symmetry is broken down to a discrete one. The nature of the discrete symmetry depends on the ratio of the forcing frequency, ω_f , to the free oscillations frequency, ω_0 : a simple and elegant symmetry argument [11] allows to conclude that, when ω_f/ω_0 is close to a rational number, say $n:m$, n equivalent phases, given by $\phi_k = \phi_1 + 2\pi(k-1)/n$, $k = 1, \dots, n$ [11], are preferred by the oscillations and the system becomes n -phase multi-stable.¹ Once the continuous phase symmetry is replaced by the discrete one, the vortices are no more stable solutions. They are then substituted by other kind of structures, such as periodic patterns and localized structures (dissipative spatial solitons). Thus periodic forcing of spatially extended systems of oscillators is a powerful tool to control the nonlinear waves existing therein [4,9–28].

According to our previous discussion, when the forcing frequency is approximately twice the system’s natural frequency ($n:m = 2:1$), so-called 2:1 resonance or parametric resonance, two dynamically equivalent oscillation phases exist, which differ by π [9–11]. If the system is large enough, adjacent spatial regions can oscillate with opposite phases thus forming so-called phase domains, which are unstable in the free-running case. Between adjacent domains a π phase jump occurs and the curve containing those jumps is known as a wall or front. When the wall is abrupt, a one-dimensional phase singularity appears and the amplitude of the oscillations becomes null (one speaks then of a non-equilibrium Ising wall [10]), which manifests as a dark line of the light field in the optical case. The wall can also be smoother if the minimum oscillations amplitude is small, not null when crossing the wall (one speaks then of a non-equilibrium Bloch wall [10]), leading to a grey line in the light field in the optical case. As a parameter is varied, Ising walls can bifurcate into Bloch walls through a so-called non-equilibrium Ising–Bloch transition [10,17,29]. These phenomena have been predicted and observed in many different systems [4,10,11,13–18,25–27,29]. Apart from domain walls, pattern formation in a 2:1 resonance includes extended patterns, like rolls or labyrinths, and localized patterns, known as dissipative spatial solitons (cavity solitons in optics for obvious reasons).

Parametric forcing is, however, not always efficient, as it requires that the nonlinearity in the system be strong enough (or the natural resonance be wide enough) so that an excitation at a high frequency (twice the natural one) leads to appreciable response in the system. Optical systems, like lasers, belong to this class (they are insensitive to parametric forcing), and hence a pertinent question arises: is there an alternative to the classic 2:1 resonant forcing leading to similar effects? The positive answer is given by what is known as ‘rocking’ [30,31]. Rocking is a type of forcing in which the external perturbation frequency is close to the system’s natural frequency (it is a kind of 1:1 resonance, to which all systems respond) but, unlike the classic 1:1 periodic forcing, the amplitude of rocking is modulated in time (temporal rocking) or in space (spatial rocking). This modulation must be such that the *sign* of the forcing amplitude alternates in time or in space. As we will show along the rest of this article rocking leads to a behaviour analogous to that of the 2:1 resonant forcing: the oscillatory system is ‘converted’ into a phase-bistable pattern-forming system.

The rest of this article is organized as follows. In §2, we provide a simple explanation of why rocking induces a phase bistability in an otherwise phase invariant oscillatory system. In §3, we

¹The phase ϕ_1 depends on the phase of the external driving and on the (small) mistuning $\omega_f - n\omega_0/m$

give a quantitative description of rocking in terms of universal models. In §4, we review previous work on temporal and spatial rocking in specific systems. In §5, we study the effect of rocking in a particular, very relevant case: the laser. In §6, we consider the case when oscillations are weakly damped (below a Hopf bifurcation) and show that rocking is efficient in that case. Finally, §7 contains the main conclusion.

2. The rationale behind the phase bistability via rocking (and why ‘rocking’?)

According to the discussion in Introduction, the rocking (forcing) field can be written as

$$R(\mathbf{r}, t) = F(\mathbf{r}, t)\exp(-i\omega_R t) + \text{c.c.}, \quad (2.1)$$

where ω_R denotes the carrier frequency of the forcing, which is close to the natural frequency of oscillations ω_0 (we remind that rocking is a generalized 1 : 1 resonant forcing), and $F(\mathbf{r}, t)$ is the rocking amplitude. Importantly, the sign of F must alternate in space or in time (when F is a constant, one gets the classic 1 : 1 resonant forcing, which, in optical terms, can result in injection locking). If the sign alternation occurs on a fast time scale or on a short spatial scale, the system’s oscillations will ‘see’ both phases (differing by π , corresponding to sign changes), but will not be able to accommodate locally to that rapidly varying drive. To which phase of the perturbation will the system lock then? Clearly, if, on average, both phases are equally distributed, the system will tend to lock to any of the driving phases (or to some set of two opposite phases, as explained below) and, as a result, will display phase bistability.

On a more formal basis, rocking can be explained in terms of a mechanical analogy, which historically was the line of reasoning that led to the discovery of rocking and led to its name. A simple way to visualize a (single) nonlinear oscillator is to use a mechanical analogy, in which the real and imaginary parts of the complex oscillation amplitude are interpreted as the two Cartesian coordinates $\mathbf{q} = (q_1, q_2)$ of a fictitious massless particle affected by viscous damping and under the action of a potential V having the form of a Mexican sombrero (see figure 1). The maximum of V at the origin corresponds to the unstable off state (of null oscillation amplitude) and its degenerate minimum (the ‘valley’) to the self-oscillating state of finite amplitude (figure 1). The degeneracy of the minimum signals the phase invariance of the free oscillations, as no angle is preferred. Now, imagine that we rock² that potential in a periodic way around some axis, say q_2 , and that rocking is sufficiently fast. Where would the fictitious particle tend to rest (remind that the particle motion is damped)? It is evident that this would happen at the quietest regions, where the rocking of the potential produces less perturbation, i.e. around any of the ‘poles’ symmetrically located along the q_2 -axis (figure 1). Then, an initially phase invariant oscillator would end up being a phase-bistable one! Note that this phase bistability requires, in this picture, a potential with a maximum (an unstable point) at the origin, as otherwise there are not two separated, quiet regions. The simplest ‘rocked’ potential displaying the above features reads

$$V(\mathbf{q}) = -\frac{\mu}{2}q^2 + \frac{1}{4}q^4 - q_1F_0\cos\Omega t, \quad (2.2)$$

where $q = \sqrt{q_1^2 + q_2^2}$ is the radial coordinate. The parameter μ controls whether the potential has a local maximum at the origin ($\mu > 0$), and then a degenerate circular minimum happens at the radius $q = \sqrt{\mu}$ or the potential single extremum (minimum) occurs at the origin ($\mu < 0$).

²By ‘rock’, we mean ‘to move or cause to move from side to side or backwards and forwards’ (Collins dictionary, first definition of ‘rock’ as a verb: <http://www.collinsdictionary.com/dictionary/english/rock>) or ‘to move back and forth in or as if in a cradle’ (Merriam-Webster dictionary, first definition of ‘rock’ as a transitive verb: <http://www.merriam-webster.com/dictionary/rock>).

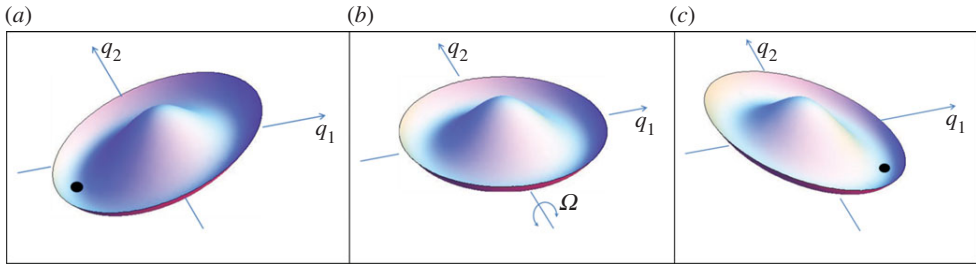


Figure 1. Qualitative three-dimensional plot of the potential V associated with equation (2.1), which describes a rocked system. (b) Without injection ($F = 0$), the potential is radially symmetric in agreement with the phase invariance of the free-running laser. (a,c) With constant injection ($\Omega = 0$), the potential tilts along the direction $\text{Re}(A)$ proportionally to the forcing amplitude F and a single isolated minimum (marked with a black dot) appears, corresponding to the phase-locked state of the usual laser with injected signal. Under rocking ($\Omega \neq 0$), the potential oscillates back and forth between the two cases (a), and (c), through (b) one. Under such forcing, a particle would tend to remain close to the imaginary axis $\text{Re}(A) = 0$, around either of the two regions separated by the local maximum around the origin. (Online version in colour.)

The dynamical equations following from (2.2) read $m\ddot{\mathbf{q}} + \dot{\mathbf{q}} = -\nabla V$, or $dq_i/dt = -\partial V/\partial q_i$ (remind that $m = 0$), and can be written compactly in terms of the complex amplitude of oscillations $A = q_1 + iq_2$ as

$$\frac{dA}{dt} = \mu A - |A|^2 A + F_0 \cos(\Omega t). \quad (2.3)$$

Without its last term, we recognize this equation as the simplest normal form of a Hopf bifurcation. The inhomogeneous, last term accounts for a forcing at the frequency of oscillations (1 : 1 resonant forcing) and amplitude proportional to $F_0 \cos(\Omega t)$ [9]. Hence, physically, rocking of an oscillator is accomplished by an almost periodic forcing at the oscillations frequency, whose amplitude is harmonically modulated in time. As explained in the Introduction, this initial definition became broader as other types of rocking (random versus periodic, and spatial versus temporal) are considered. In all cases, a sign alternation (a π phase jump sequence) is necessary.

We note that equation (2.3) describes a single-mode, two-level laser with injected signal (A is proportional to the complex amplitude of the electric field of the radiation and the signal, injected into the cavity, has amplitude proportional to $F_0 \cos(\Omega t)$, in the limit where the material variables are fast (and can be adiabatically eliminated) and the cavity is perfectly resonant with the atomic line. When $\Omega = 0$ (constant injection), there is no phase symmetry in (2.3) and the oscillations phase locks to that of the injection, corresponding to a tilted, static potential (2.2) displaying a single, isolated minimum (one of the extreme positions in figure 1). Note that the dynamical phase bistability under rocking happens at phases in quadrature with respect to the injection: if the injection amplitude is real, as in figure 1, phase locking occurs at $\pm\pi/2$ (on the q_2 -axis).

3. A universal description of rocking

A lot of physical insight can be gained by studying universal models, which, on the other hand, allow giving a broad applicability to the results. As rocking is a modified 1 : 1 resonant forcing of oscillatory systems, these universal models are complex Ginzburg–Landau (CGL) equations, containing an inhomogeneous term [1,2,10–12,32,33], which are valid close to a spatially uniform Hopf bifurcation. If we express the oscillations field (e.g. the electric field in the optical case) as $\text{Re}[A(\mathbf{r}, t)\exp(-i\omega_R t)]$, where A is a complex field amplitude and ω_R is the angular frequency of rocking (close to the natural frequency of oscillations ω_0), the dynamics of the system is universally governed by the following CGL equation [1,2,10–12,30–33]:

$$\partial_t A(\mathbf{r}, t) = \mu(1 + i\nu)A + i(\omega_R - \omega_0)A + \alpha \nabla^2 A - \beta |A|^2 A + \eta F(\mathbf{r}, t), \quad (3.1)$$

where $r = (x, y)$, $\nabla^2 = (\partial_x^2 + \partial_y^2)$, μ is real and measures the distance from the bifurcation, ν measures the linear variation of the oscillation frequency around the bifurcation, the complex coefficients $\alpha = \alpha_1 + i\alpha_2$ and $\beta = \beta_1 + i\beta_2$ account for diffusion/diffraction and saturation/nonlinear frequency shift, respectively, and η is a parameter that measures how effective forcing is. After a simple rescaling of time, space and amplitudes A and F , equation (3.1) can be made dimensionless and the coefficients α and β and κ can be chosen at will (just the ratios α_2/α_1 and β_2/β_1 are relevant). In particular, we take $|\alpha| = |\beta| = \eta = 1$ without loss of generality.³ As well, if the system is above threshold ($\mu > 0$), which is the situation we consider for most of this work, one can take $\mu = 1$, and the CGL equation becomes

$$\partial_t A(\mathbf{r}, t) = (1 + i\theta)A + \alpha \nabla^2 A - \beta |A|^2 A + F(r, t), \quad (3.2)$$

where we keep the same symbols as in (3.1) and we defined the normalized detuning $\theta = \nu + (\omega_R - \omega_0)/\mu$. Note that, in the following, space, time, the fields A and F , and the three parameters (θ , α and β), in equation (3.2) are dimensionless. Concerning parameters α and β , one can use $\alpha = 1$ ($\alpha = i$) if diffusion (diffraction) dominates, and $\beta = 1$ ($\beta = \pm i$) if saturation (nonlinear dispersion) dominates, without any loss of generality. In the optical context, equation (3.2) represents the simplest description of broad area lasers with injected signal, whose complex amplitude is proportional to $F(\mathbf{r}, t)$.

Equation (3.2) is the one we will consider throughout this section. As for the rocking amplitude, we will consider both

$$\text{the temporal case: } F(\mathbf{r}, t) = F_0 \cos \Omega t \quad (3.3a)$$

$$\text{and the spatial case: } F(\mathbf{r}, t) = F_0 \cos Kx, \quad (3.3b)$$

where F_0 is taken as a real without loss of generality as it just sets the reference phase at $x = 0$.

In order to capture analytically the main effects of rocking, and following our discussion in §2, the limit where the rocking frequency Ω (in the temporal case) or K (in the spatial case) are large, is especially interesting. In this case, the driving term in equation (3.2) is highly oscillating and solutions to the problem should be well approximated by [34,35]

$$A(\mathbf{r}, t) = A_f(\mathbf{r}, t) + A_s(\mathbf{r}, t), \quad (3.4)$$

where the subscripts ‘f’ and ‘s’ refer to fast and slow components, either in time (if rocking is temporal) or in space (if rocking is spatial). Substituting (3.4) and (3.3) into (3.2) and equating like terms with respect to the fast or slow frequencies in the system, and considering only the leading-order terms, we get

$$\partial_t A_f = F_0 \cos \Omega t \quad \text{and} \quad \nabla^2 A_f = -\frac{F_0}{\alpha} \cos Kx, \quad (3.5)$$

in the temporal and in the spatial cases, respectively, yielding

$$A_f = \frac{F_0}{\Omega} \sin \Omega t \quad \text{and} \quad A_f = \frac{F_0}{\alpha K^2} \cos Kx, \quad (3.6)$$

respectively. Concerning the slow components, we obtain the same equation in both cases,

$$\partial_t A_s = (1 + i\theta)A_s + i\alpha \nabla^2 A_s - \beta \left[\langle A_f^2 \rangle A_s^* + 2 \langle |A_f|^2 \rangle A_s + |A_s|^2 A_s + \langle |A_f|^2 A_f \rangle + 2 |A_s|^2 \langle A_f \rangle \right], \quad (3.7)$$

where the angular brackets denote an averaging over the fast scale (temporal or spatial). Using (3.6), we get

$$\partial_t A_s = (1 + i\theta - 2\beta\gamma)A_s - \gamma A_s^* + \alpha \nabla^2 A_s - \beta |A_s|^2 A_s, \quad (3.8)$$

³Equation (3.1) is valid only if $\text{Re } \alpha, \text{Re } \beta \geq 0$, hence $\arg \alpha, \arg \beta \in [-\pi/2, \pi/2]$ in equation (3.4).

where the ‘effective rocking parameter’

$$\gamma = \frac{1}{2} \left(\frac{F_0}{\Omega} \right)^2 \quad \text{and} \quad \gamma = \frac{1}{2} \left(\frac{F_0}{K^2} \right)^2, \quad (3.9)$$

in the temporal and in the spatial cases, respectively.⁴ Equation (3.8) is a central result in rocking theory as it governs the evolution of the ‘slow’ component, which is the one having its own dynamics (the fast component is just ‘slaved’ to the rocking injection; see (3.6)). Alternative derivations of equation (3.8), based on rigorous multiple scale methods [36], can be found in [30–33]. Our derivation has considered the simplest case of harmonic rocking, equation (3.3), but in general any periodic form of rocking, and even certain types of *random rocking*, have been demonstrated to be effective as well [31–33,37]. In these cases, equation (3.8) still holds, the only difference being in the definition of the effective parameter γ , which follows from the averages $\langle A_f^2 \rangle$ and $\langle |A_f|^2 \rangle$ in equation (3.7), and depends on the specific form of forcing.

Equation (3.8) is a so-called parametric CGL equation and captures the main effects rocking. In the absence of forcing ($F_0 = 0$), $\gamma = 0$ and equation (3.8) becomes the classic CGL equation with the continuous phase symmetry $A_s \rightarrow A_s e^{i\phi}$ for arbitrary ϕ , corresponding to free oscillations. Once rocking is on, $\gamma \neq 0$ and the presence of the term proportional to A_s^* breaks the continuous phase symmetry down to the discrete one $A_s \rightarrow -A_s$, so that any two solutions connected by this symmetry are dynamically equivalent. Hence, the system becomes phase bistable and these two phases differ by π . Equation (3.8) also shows that both types of rocking (spatial and temporal) are equivalent, the only difference being in the definition of the effective rocking parameter γ in (3.9). Finally, the effects of rocking are seen not to depend separately on its amplitude (F_0) and frequency (Ω or K), but on the effective rocking parameter γ .

Concerning the conditions for an efficient rocking, we observe that the phase symmetry breaking term, $-\gamma A_s^*$ in equation (3.8), exists only if the average $\langle A_f^2 \rangle \neq 0$ (see equation (3.7)). Note as well that, in passing from equation (3.7) to equation (3.8), the terms proportional to $\langle A_f \rangle$ and $\langle |A_f|^2 A_f \rangle$ have disappeared. This is because of the form of rocking we have considered, leading to (3.6). Should those averages not vanish, no phase symmetry would exist in the end, hence weakening the phase bistability when $\langle A_f \rangle$ is relatively small, or completely destroying phase bistability when $\langle A_f \rangle$ becomes dominant. Hence, the necessary conditions for efficient rocking are $\langle A_f \rangle = \langle |A_f|^2 A_f \rangle = 0$ and $\langle A_f^2 \rangle \neq 0$, which point to a forcing with two opposite phases, equally distributed on average, as we guessed in §2.

Equation (3.8) allows two kinds of spatially homogeneous solutions: the off state $A_s = 0$ (hence $A = A_f$) and the on (or ‘rocked’) state $A_s \neq 0$, the latter of which is phase-bistable. The off state exists always, whereas the rocked states exist in a closed region of the parameter space $\gamma - \theta$ (the ‘rocking balloon’), whose form depends on the structural parameters α and β . Next, we concentrate on the case $\alpha = i$ and $\beta = 1$, which is typical in nonlinear optics. Figure 2 summarizes the bifurcation diagram of both solutions as obtained by a standard linear stability analysis against perturbations with wavenumber k . Increasing γ inside the balloon leads to a decrease of the oscillations amplitude, till A_s becomes null by crossing the balloon upper boundary (continuous line); hence, the bifurcation from the trivial state $A_s = 0$, which exists always, to the rocked states is supercritical by entering the balloon from above. On the contrary, the (V-shaped) lateral boundaries of the balloon correspond to a saddle-node bifurcation. The left one (for negative detuning) gives rise to oscillations of the slow component, meaning a loss of the phase locking. These oscillations have an infinite period at the bifurcation and are the continuation of free-running orbits that exist in the system at $\gamma = 0$: for null injection, equation (3.8) admits the limit cycles $A_s = A_{LC} \exp[-i(\omega_{LC}t + \phi)]$, with $A_{LC} = 1/\sqrt{\text{Re}\beta}$, $\omega_{LC} = -\theta + \text{Im}\beta/\text{Re}\beta$ and arbitrary ϕ , which extend (perturbed) towards non-null values of γ . These orbits can terminate

⁴A phase factor $e^{i2\eta}$ multiplying A_s^* in (3.8) has been removed, as it disappears after the simple rotation $A_s \rightarrow A_s e^{i\eta}$. This phase factor reads $e^{i2\eta} = \beta$ in the temporal case and $e^{i2\eta} = \beta\alpha^{-2}$ in the spatial case (remind that we have chosen $|\alpha| = |\beta| = 1$).

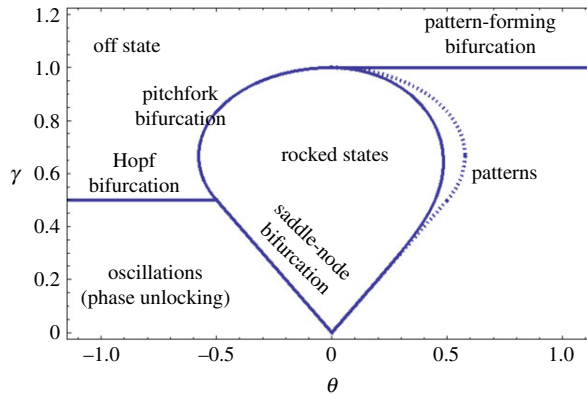


Figure 2. Bifurcation diagram of equation (3.8) corresponding to the case $\alpha = i$, $\beta = 1$. The off solution is stable for large enough γ , whereas the ‘rocked states’ (the homogeneous steady states) are within the balloon. For positive detuning θ patterns form, either from the off state by crossing the horizontal line at $\gamma = 1$ or by leaving the rocking balloon through its right boundary, which is a pattern-forming bifurcation as well. For negative detuning θ oscillations happen, either by leaving the balloon through its left boundary (saddle-node bifurcation) or by crossing the Hopf bifurcation of the off state downwards. The dashed line represents the right boundary of the existing region of the rocked states, which become unstable before reaching it as explained above. (Online version in colour.)

at a saddle-node (with diverging period) or can disappear at a Hopf bifurcation of the off state, similarly to the case of the laser with injected signal [38–40]. For positive detuning, the generic scenario is of pattern formation where the most unstable wavenumber reads $k_c = \sqrt{\theta}$.

4. Rocking in specific systems

The universal description of rocking has been given in [30] (temporal periodic rocking), [31] (spatial rocking, both periodic and random) and [37] (temporal random rocking). Clearly, the predictions from universal nonlinear dynamical models are only quantitative in the very limit where such descriptions hold, which in our case requires operating the system very close to a spatially uniform Hopf bifurcation. Clearly, such predictions must be contrasted with experiments and with theoretical studies of specific models.

So far rocking has been investigated experimentally in photorefractive oscillators (PROs) [41,42], which are a kind of nonlinear optical systems, and in nonlinear electronic circuits [37,43], finding good agreement with the theoretical predictions. Both types of experiments have an oscillatory nature and exhibit phase invariance in the absence of external perturbations. In [41], a PRO was submitted to temporal periodic rocking, and the transmutation of vortices into phase domains and the stable excitation of phase domain walls were demonstrated. A similar set-up, but now with a small aspect ratio (small Fresnel number in the optical terminology) was considered in [42], now under spatial rocking. That experiment could evidence the phase-bistable nature of the rocked emission, but clearly not the pattern formation predicted by the theory; an experiment addressing pattern formation in a spatially rocked PRO is under progress at present. The nonlinear electronic circuits considered in [37,43] were Chua circuits, which are highly versatile and controllable, in particular they can be tuned to a Hopf bifurcation giving rise to self-oscillations. Clearly, these systems are zero-dimensional in space; hence, in those experiments, only the phase-bistable response associated to rocking was demonstrated, both under periodic rocking [43] and under random rocking [37]. The fact rocking shows its effectiveness in systems as diverse as optical and electronic evidences its universality.

From the theoretical side, rocking has been investigated in PRO models under temporal [41] and (small aspect ratio) spatial [42] rocking. Two-level laser models have been studied as

well: temporal rocking in zero-dimensional class B lasers was considered in [44], spatial rocking in small aspect ratio lasers (with just two transverse modes) was studied in [45], and zero-dimensional bidirectional lasers under temporal rocking were investigated in [46]. In all cases, the basic phenomenon, phase bistability, was demonstrated, which in its turn yields new types of solutions, especially in the bidirectional laser case [46]. The spatial rocking has also been numerically investigated in semiconductor-based lasers, namely in broad area semiconductor lasers (so-called BAS lasers), where evidences of rocking patterns were shown [47], also in vertical-cavity surface-emitting lasers (so-called VCSELs), where more rich rocking patterns were demonstrated [48]. Next, we present the first investigation of rocking in a large Fresnel number two-level laser.

5. Pattern formation via rocking in two-level lasers

Lasers are paradigmatic, self-oscillatory nonlinear optical systems. Pattern formation therein is relevant both from the basic science viewpoint and from the applied science one, because of their potential applicability in information storage and processing [49–53]. Here, we investigate pattern formation in two-level lasers submitted to temporal rocking.

The starting point of the study is the classic set of dimensionless Maxwell–Bloch equations for a two-level laser with injected signal

$$\left. \begin{aligned} \partial_t E(\mathbf{r}, t) &= \sigma[-(1 + i\Delta)E + P] + i\nabla^2 E + E_{\text{in}} \\ \partial_t P(\mathbf{r}, t) &= -(1 - i\Delta)P + (r - N)E \\ \text{and} \quad \partial_t N(\mathbf{r}, t) &= b[-N + \text{Re}(EP^*)], \end{aligned} \right\} \quad (5.1)$$

for the complex envelopes of the electric field E , and the medium polarization P , and for the (real) population inversion N . Time t is normalized to the polarization decay rate γ_{\perp} , $\sigma = \kappa/\gamma_{\perp}$ and $b = \gamma_{\parallel}/\gamma_{\perp}$ are normalized decay rates (κ is the one for the cavity and γ_{\parallel} is the one for the population inversion), $\Delta = (\omega_c - \omega_a)/(\gamma_{\perp} + \kappa)$ is the normalized cavity detuning (ω_a is the atomic resonance frequency and ω_c is the closest longitudinal cavity mode frequency), and r is the pump parameter: free-running lasing threshold happens at $r = 1$ for a perfectly tuned cavity ($\Delta = 0$). Finally, E_{in} is the complex envelope of an injected signal, which is the essential element of rocking. Equation (5.1) are written in the frequency frame of the on-axis lasing solution; i.e. the actual light electric field and the injected field are proportional to $Ee^{-i\omega_0\gamma_{\perp}t} + \text{c.c.}$ and $E_{\text{in}}e^{-i\omega_0\gamma_{\perp}t} + \text{c.c.}$, respectively (note that $\gamma_{\perp}t$ is the actual time), where the lasing emission frequency is given by the mode pulling formula $\omega_0 = (\gamma_{\perp}\omega_c + \kappa\omega_a)/(\gamma_{\perp} + \kappa)$. As we are considering temporal rocking, the injected signal has the form

$$E_{\text{in}} = E_0 \cos(\omega t)e^{-i\delta t}, \quad (5.2)$$

which corresponds to the injection of two plane waves into the laser cavity with equal amplitudes ($E_0/2$, which we take as real without loss of generality) and with frequencies $\omega_0 + \gamma_{\perp}\delta \pm \gamma_{\perp}\omega$: the carrier frequency $\omega_0 + \gamma_{\perp}\delta$ plays the role of ω_R in equation (2.1) and the rocking frequency $\gamma_{\perp}\omega$ plays the role of the modulation frequency Ω in equation (2.3). Parameter δ controls the detuning of the rocking mid-frequency from the free-running laser frequency ω_0 . In order that this kind of injection is compatible with the uniform field and single longitudinal mode approximations subjacent to (5.1), both the rocking detuning $\gamma_{\perp}\delta$ and the modulation frequency $\gamma_{\perp}\omega$ must be much smaller than the cavity-free spectral range, which can be expressed as $4\pi\kappa/T$, where T is the (very small) transmission factor of the laser output coupler: $|\delta|, |\omega| \ll 4\pi\sigma/T$. As $0 < T \ll 1$, δ and ω can be large as compared with the normalized cavity damping rate σ without violating the hypothesis leading to (5.1).

In the following, we concentrate on the detuning side $\Delta > 0$ ($\omega_c > \omega_a$), in which, in the absence of injection, the off state $E = 0$ destabilizes to the on-axis (spatially uniform) lasing solution at $r = r_0 \equiv 1 + \Delta^2$.

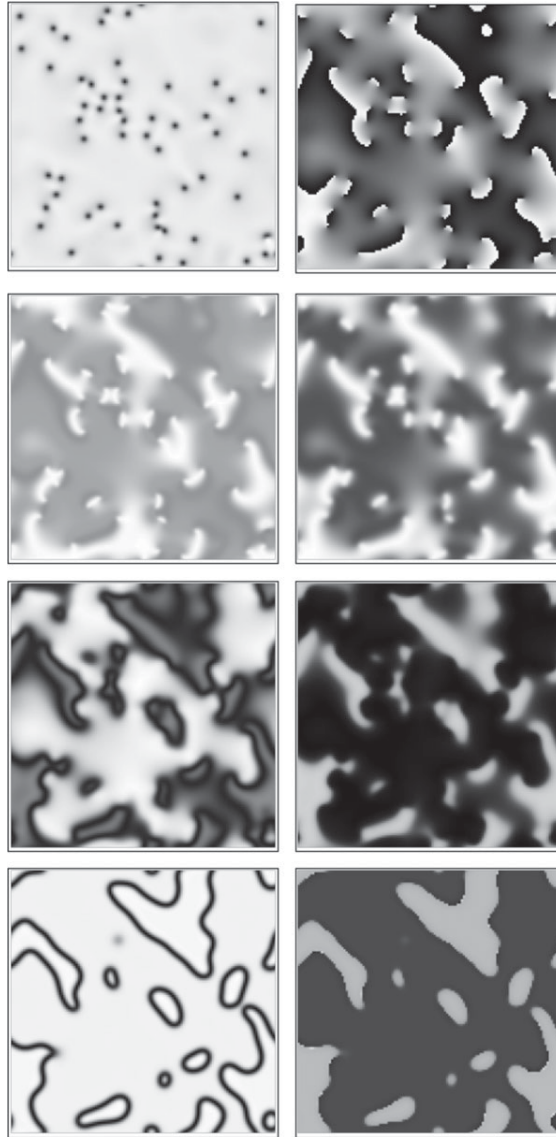


Figure 3. Transformation of vortices into phase domains in a rocked two-level laser as given by a simulation of equations (5.1). The light intensity of the slow component is shown on the left, and its phase is on the right. Rocking is applied from the second frame ($t = 40$) on. Frames are given for $t = 20$, $t = 40$, $t = 50$, and $t = 80$ from top to bottom. The size of the window is 300×300 and the grid of points is 128×128 . Parameters are $\sigma = b = 1$ (class C laser), $r = 6$, $\Delta = 2$, $\delta = 0$, $E_0 = 20$ and $\omega = 2\pi$.

In order to gain analytical insight into the problem, we consider first a limit where an equation isomorphic to (3.8) can be obtained. This occurs close to the free-running lasing threshold, $r - r_0 = O(\varepsilon^2)$, where ε is a smallness parameter, and when injection amplitude and frequencies are small enough: $E_0, \theta = O(\varepsilon^2)$ and $\omega = O(\varepsilon)$. Further introducing slow time scales $T_1 = \varepsilon t$, $T_2 = \varepsilon^2 t, \dots$, and spatial scales $(X, Y) = \varepsilon(x, y)$, motivated by the linear stability analysis of the off solution in the absence of rocking, and making use of standard multiple scale analysis [30–33, 36, 54–62], we are able to express the complex electric field amplitude as the sum of a fast part and of a slow part, as in (3.4), namely $E = (A_f + A_s)e^{-i\delta t}$, where we moved to the reference

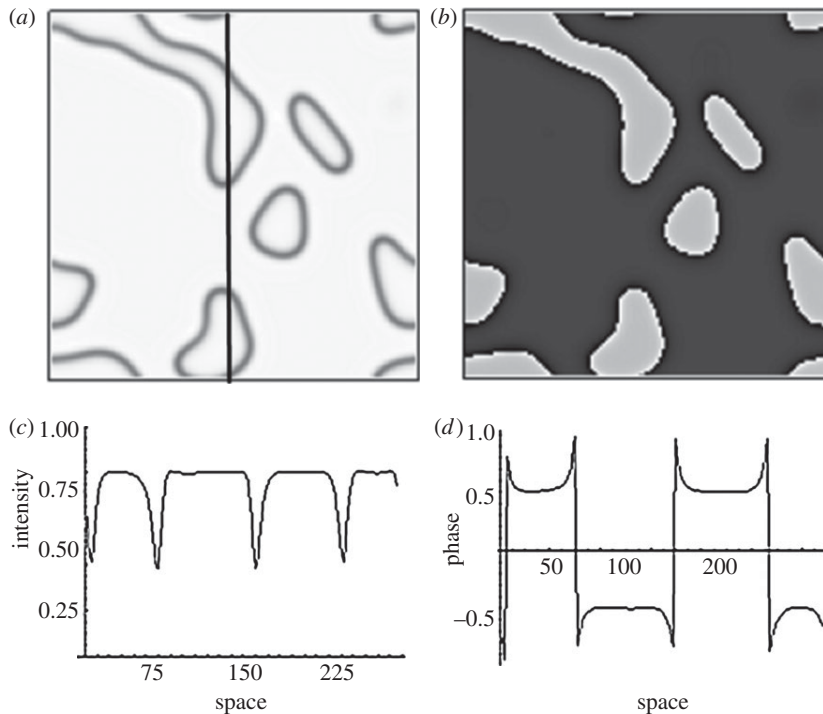


Figure 4. Bloch-type domain walls. Parameters are as in figure 3, but with a smaller rocking amplitude, $E_0 = 13$. (a) Intensity, (b) phase, (c) intensity profile and (d) phase profile (across the vertical line in (a)) are plotted.

frame of the rocking mid-frequency. Here, $A_f = D(E_0/\omega) \sin \omega t$, and the slow envelope verifies the equation

$$\partial_t A_s = \frac{\sigma D}{1 - i\Delta} \left[(r - r_0 - 2\gamma) A_s - \gamma A_s^* - |A_s|^2 A_s \right] + i\delta A_s + iD\nabla^2 A_s, \quad (5.3)$$

where $D = [1 + \sigma(1 + i\Delta)/(1 - i\Delta)]^{-1}$, and $\gamma = 1/2(E_0/\omega)^2$ is the effective rocking parameter, to be compared with (3.9). Equation (5.3) is a CGLE with broken phase invariance, similar to equation (3.8), as expected, which evidences the main effect of rocking: the emergence of a phase bistability. Equation (5.3) has been derived under the assumptions $\Delta > 0$ and $\sigma, b = O(\varepsilon^0)$. (The latter defines so-called class C lasers.) The detuning condition follows from analysing the diffusion coefficient, given by $\text{Re}(iD) = 2\sigma\Delta/[(1 + \sigma)^2 + (1 - \sigma)^2\Delta^2]$, which becomes negative (and then equation (5.3) loses its validity) when $\Delta < 0$ [55,56]. On physical grounds, for $\Delta < 0$, lasing involves off axis emission (tilted waves, having a spatial dependence), which equation (5.3) cannot account for, and a different treatment is necessary. In fact, for small Δ (either positive or negative), a complex Swift–Hohenberg equation, not a CGL equation, governs the dynamics of the free-running laser (and of other nonlinear optical cavities) [41,56,58,59,61–63]. Nevertheless, the specific description (CGL or Swift–Hohenberg) is not essential regarding the effects of rocking, as discussed in [41]. Concerning the size of the normalized decay rates σ and b , equation (5.3) is valid for any value of σ ; in particular, in the usual case $\sigma \ll 1$ (so-called class A laser), $D \rightarrow 1$ simply. However, if $b \ll 1$ (a situation characterizing the so-called class B lasers, like solid-state and semiconductor lasers), not a single equation, but two, are needed to capture the system dynamics: one for E and one for N [44,62,63]. In such case, few analytical insights can be gained; nevertheless, rocking is efficient as well in class B lasers.

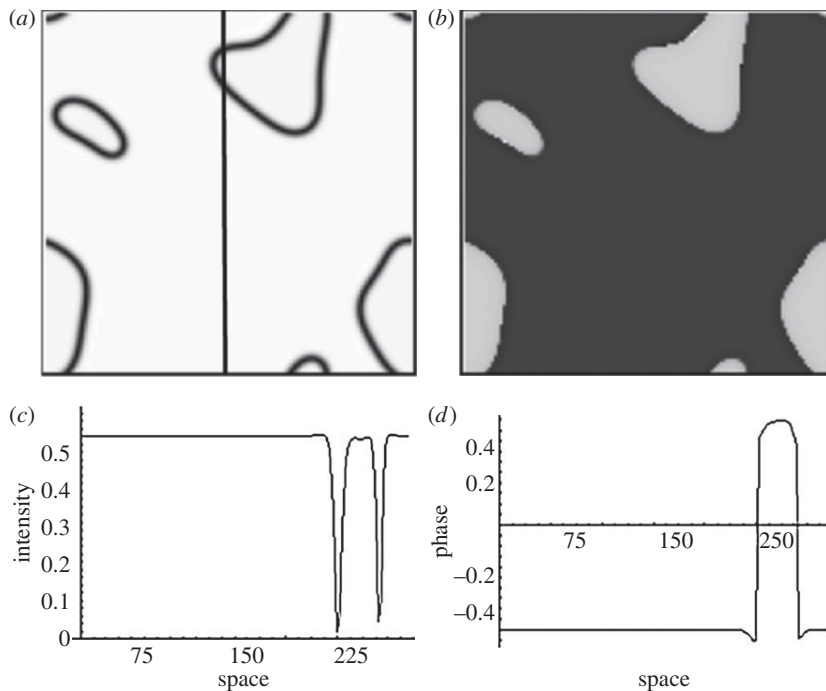


Figure 5. Ising-type domain walls. Parameters are as in figure 3. (a) Intensity, (b) phase, (c) intensity profile and (d) phase profile (across the vertical line in (a)) are plotted.

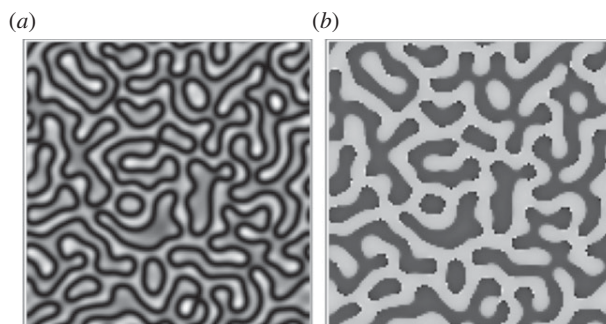


Figure 6. (a,b) Ising-type labyrinths obtained in a rocked two-level laser, for the same parameters as in figures 3–5, but for a slightly positive rocking detuning, $\delta = 0.1$.

We have performed extensive numerical simulations of the original Maxwell–Bloch equations (5.1) under different conditions (class C and class B lasers), finding that the effect of rocking is robust, even extremely far from the conditions used to derive equation (5.3), e.g. for $r - r_0 = 1$. In figure 3, we show an example of the ‘conversion’ of vortices (the basic spatial structures in free-running lasers) into phase domains, which is typical for null or negative detuning δ . These phase domains are of Bloch type for small injection (figure 4), or of Ising type for larger injection (figure 5) [10]. We note that Ising and Bloch walls can coexist in two-dimensional systems because of curvature effects [64,65].

For positive rocking detuning δ , the typical scenario involves pattern formation via labyrinths (figure 6). In a small detuning region close to the labyrinth formation, phase (dark-ring) cavity

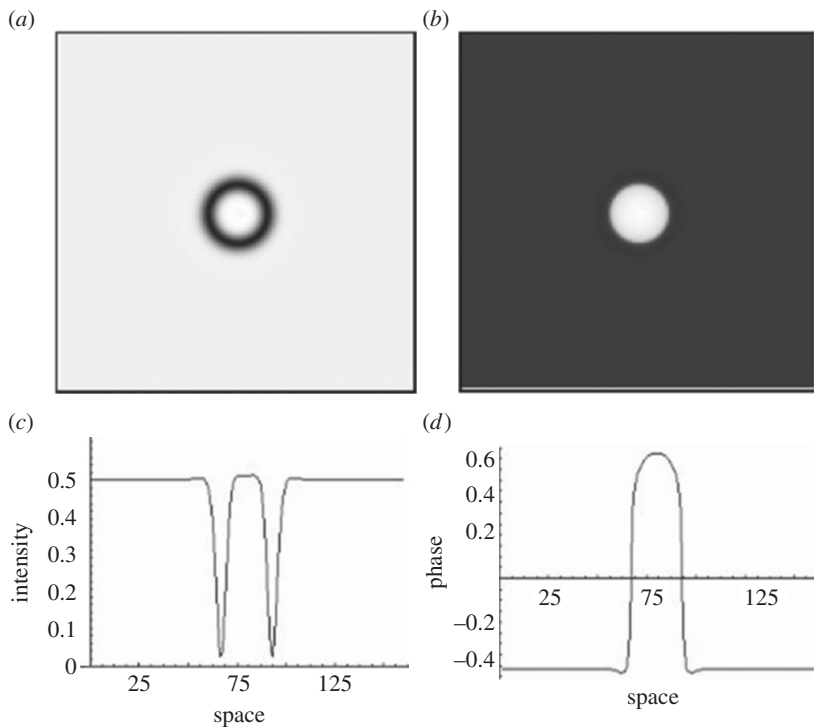


Figure 7. Dark-ring cavity soliton. Parameters are as in figures 5 and 6, but with an intermediate detuning $\delta = 0.055$ and size of the window (150×150). (a) Intensity, (b) phase, (c) intensity profile and (d) phase profile are plotted.

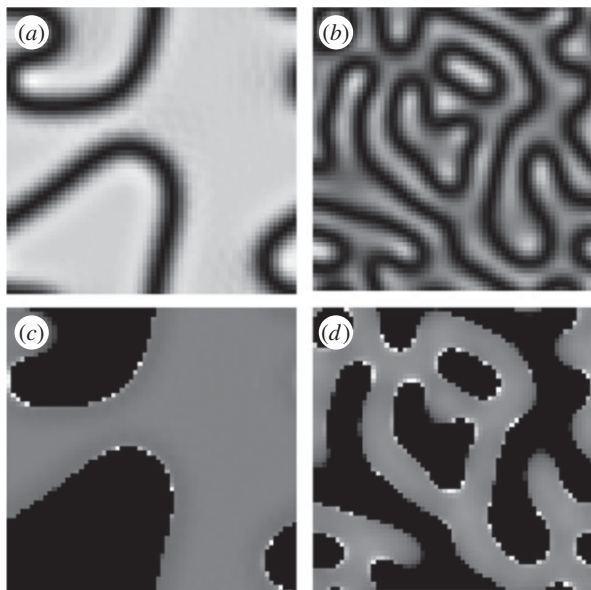


Figure 8. Intensity (a,b) and phase (c,d) of several structures found in class B lasers. From left to right, phase domains ($\delta = 0$) and labyrinths ($\delta = 0.0040$). Rest of parameters: $\Delta = 0$, $r = 1.5$, $b = 0.01$, $\sigma = 0.1$, $F = 0.04$ and $\omega = 0.042$. The size of the integration window is 600×600 . Simulations were performed on a 64×64 grid. Time-step $dt = 0.3$.

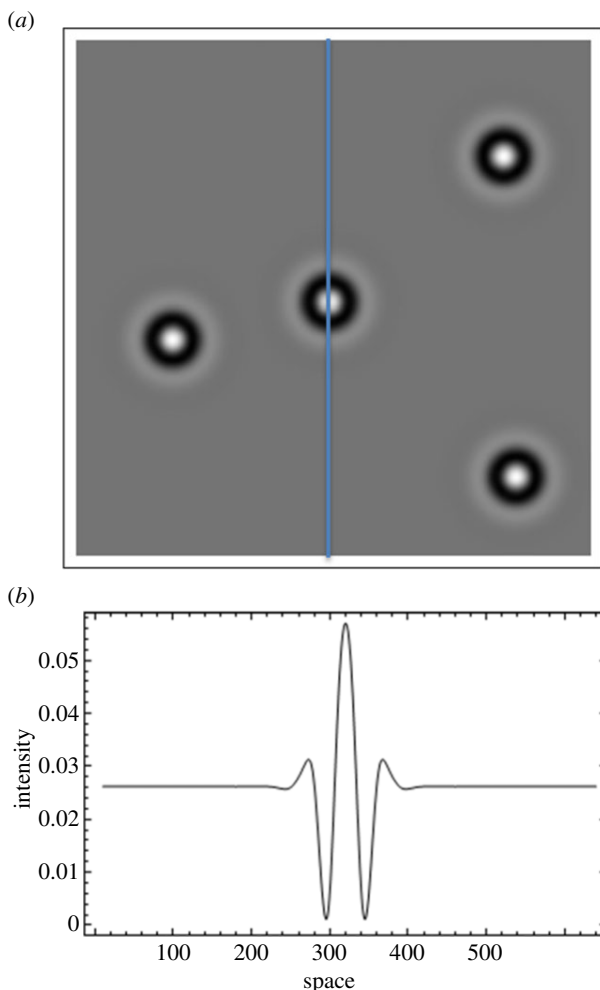


Figure 9. Cavity solitons for class B laser in the case of temporal rocking. Parameters are $\sigma = 0.1$, $b = 0.01$, $r = 1.5$, $\Delta = 0$, $\delta = 0.0026$, $E_0 = 0.04$, $\omega = 0.042$, (a) shows the intensity, and (b) shows the intensity profile across the vertical cut marked in (a). Rest of parameters as in figure 8. (Online version in colour.)

solitons are found (figure 7). The formation of the dark-ring solitons can be interpreted as a stabilization of contracting phase domains to a finite (minimum) size [66–68]. The stabilization is mainly due to the spatial oscillation of the tails of domain boundaries, which trap a segment of domain boundary to the opposite segment of boundary in accordance to [69]. This leads to stable, round, phase solitons, in the form of a dark rings of field intensity, as shown in figure 7.

Similar results are obtained in class B lasers, i.e. lasers in which the population inversion is a very slow variable (small parameter b in equation (5.1)), as shown in figures 8 and 9. The presence of relaxation oscillations in class B lasers deeply affects the performance of rocking as already demonstrated in [44]. In this case for rocking to be effective, its modulation frequency ω (see equation (5.2)) must be on the order of the relaxation oscillations frequency ω_{RO} , whose expression is $\omega_{RO} = \sqrt{2(r - r_0)\sigma b}$. As a marked difference with respect to the class C laser case, we note that phase cavity solitons have a broad dark ring and a large central intensity peak (figure 9).

6. Rocking in weakly damped oscillatory systems

So far, we have considered self-oscillatory systems, i.e. systems in which nonlinear oscillations emerge spontaneously. In other words, we have considered systems above a spatially uniform Hopf bifurcation. As explained in §2, the initial idea leading to rocking led to the conclusion that such above threshold condition was necessary for rocking to be effective. Nevertheless, a recent study [70] has demonstrated that it is not the case: everything depends on the nature of the nonlinearity (real—saturating—or imaginary—dispersive) and on the non-locality (real—diffusive—or imaginary—diffractive). In [70], the effects of rocking in a passive optical cavity containing a Kerr nonlinear medium (the classic Lugiato–Lefever model [71]) were studied. It was demonstrated, analytically and numerically, that the same type of phenomena occurring in lasers (above threshold) happen in such a Kerr cavity. The (dimensionless) model reads

$$\partial_t A = F - (1 + i\eta\theta)A + i\nabla^2 A + i\eta|A|^2 A, \quad (6.1)$$

where A is the intracavity field complex amplitude, F is the amplitude of injected field, $\eta\theta$ is the normalized detuning between the injection frequency and the cavity resonance frequency (the single longitudinal mode case is considered), and η is $+1$ for a self-focusing nonlinearity and -1 for a self-defocusing one. Equation (6.1) is as equation (3.2), with $\alpha = i$, $\beta = -i\eta$, but with damping (the linear term $-A$) instead of gain ($+A$ in (3.2)). As shown in [70], when the injection is of rocking type, as in equation (3.3), the decomposition (3.4), with (3.5) and (3.6), holds and the slow part is governed by the following damped nonlinear Schrödinger equation with parametric gain,

$$\partial_t A_s = -[1 + i\eta(\theta - 2\gamma)]A_s + i\eta\gamma A_s^* + i\nabla^2 A_s + i\eta|A_s|^2 A_s. \quad (6.2)$$

This equation predicts the existence of phase-bistable homogeneous states and patterns, and these predictions hold even far from the conditions leading to (6.2), which are fast rocking.

Note that this result concerning the effectiveness of Rocking below a Hopf bifurcation (i.e. for weakly damped waves) is not at odds with the reasoning in §2 because in the case of the Kerr cavity, equation (6.1), no mechanical analogue (in terms of a potential) can be drawn. In fact, if we consider a variational case (deriving from a potential) below the oscillation threshold ($\mu = -1$), it is easy to check, following the steps in §3, that equation (2.3) for a single oscillator admits solutions of the form ((3.4) and (3.6)), where the slow part verifies

$$\frac{dA_s}{dt} = -(1 + 2\gamma)A_s - \gamma A_s^* - |A_s|^2 A_s, \quad (6.3)$$

and this equation does not hold but the trivial solution $A_s = 0$, i.e. no phase bistability below the Hopf bifurcation if the nonlinearity is real. It is the imaginary character of the Kerr nonlinearity that makes rocking effective below the oscillation threshold.

Figures 10 and 11 illustrate typical results of the numerical integration of a Kerr nonlinear system below the threshold, equation (6.1). We note that both the temporal and the spatial rocking is possible, as already shown in [70]. Here, we concentrate on spatial rocking by injecting a periodic pattern in the form of parallel stripes (figure 10), which can be called one-dimensional rocking, and by injecting a pattern of square symmetry (figure 11)—two-dimensional rocking. In both cases, we show the small-scale pattern, its amplitude (figure 11a) and phase (figure 11b), and also the large-scale patterns (figure 11c,d) corresponding to the slow component. The large-scale patterns were obtained by spatial filtering, i.e. by removing in spatial Fourier domain the field components with sufficiently large transverse wavevector. All variety of patterns (rolls, phase domains and phase solitons) can be obtained, depending mainly on the detuning parameter and on the sign of the nonlinearity: here, in figures 10 and 11, we show patterns occurring at moderate detuning values—the metastable phase domains.

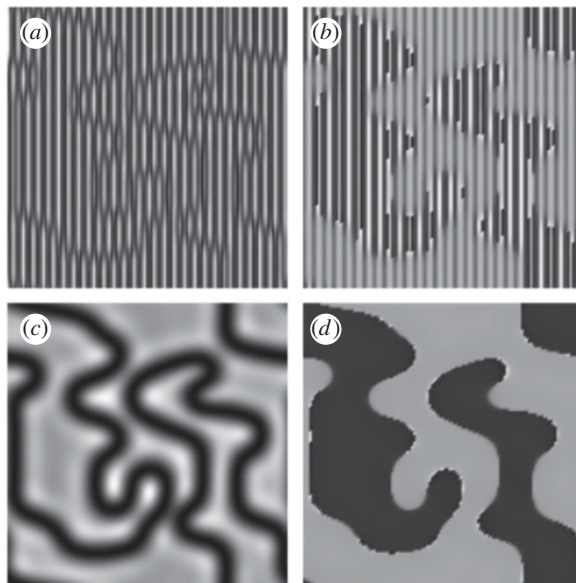


Figure 10. Field domains of opposite phases obtained for the passive resonator with Kerr nonlinearity, for $\eta = -1$ (defocusing nonlinearity) in the cases of spatial rocking, by injecting one-dimensional-periodic function (stripes). (a,b) The amplitude the phase of small-scale pattern, respectively; (c,d) The intensity and the phase of the large-scale pattern (after low- k pass filtering). Parameters: space window (70×70), detuning $\theta = 2.5$, $F_0 = 9.5$ and $k_0^2 = 7$.

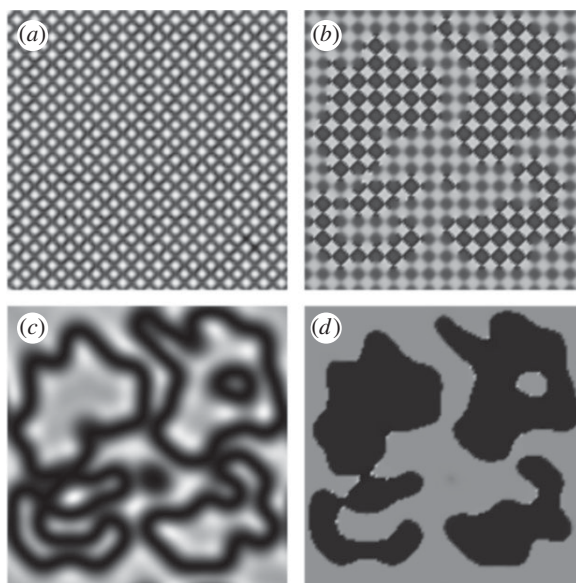


Figure 11. Field domains of opposite phases obtained for the passive resonator with Kerr nonlinearity, for $\eta = -1$ (defocusing nonlinearity), in the cases of spatial rocking, by injecting two-dimensional-periodic function of square symmetry. (a,b) The amplitude and the phase of the small-scale pattern, respectively; (c,d) The intensity and the phase of the large-scale pattern (after low- k pass filtering). Parameters: space window size (70×70), detuning $\theta = 7$, $F_0 = 16$ and $k_0^2 = 2$.

7. Conclusion

We have reviewed, and given new results of, a universal forcing method of self-oscillatory systems known as ‘rocking’. Rocking is a forcing around the oscillators natural frequency (it is a 1:1 resonance), with forcing amplitude whose sign alternates (in time or in space). This alternation creates conditions for phase bistability and for the spatial patterns associated with it as we explained in §§2 and 3 in the context of universal order parameter equations. The method represents an alternative to the classical 2:1 resonant forcing and allows phase-bistable patterns in systems where such forcing is ineffective (e.g. in lasers). The new results presented here demonstrate that rocking is effective for the excitation of phase patterns and phase cavity solitons (dark-ring solitons) in two-level lasers, particularly in class B lasers.

Acknowledgement. We gratefully acknowledge continued and fruitful discussions with Eugenio Roldán, Fernando Silva, Franco Prati and Adolfo Esteban-Martín, and we are grateful to all the colleagues that have collaborated along these years in the study of rocking.

Funding statement. The Spanish Government and the European Union FEDER supported this work through Projects FIS2011–26960 and FIS2011–29734-C02-01.

References

1. Cross MC, Hohenberg PC. 1993 Pattern formation outside of equilibrium. *Rev. Mod. Phys.* **65**, 851. (doi:10.1103/RevModPhys.65.851)
2. Aranson IS, Kramer L. 2002 The world of the complex Ginzburg–Landau equation. *Rev. Mod. Phys.* **74**, 99. (doi:10.1103/RevModPhys.74.99)
3. Winfree AT. 1972 Spiral waves of chemical activity. *Science* **175**, 634–636. (doi:10.1126/science.175.4022.634)
4. Petrov V, Ouyang Q, Swinney HL. 1997 Resonant pattern formation in a chemical system. *Nature* **388**, 655. (doi:10.1038/41732)
5. Ouyang Q, Flesselles J-M. 1996 Transition from spirals to defect turbulence driven by a convective instability. *Nature* **379**, 143. (doi:10.1038/379143a0)
6. Couillet P, Gil L, Rocca F. 1989 Optical vortices. *Opt. Commun.* **73**, 403–408. (doi:10.1016/0030-4018(89)90180-6)
7. Arecchi FT, Giacomelli G, Ramazza P, Residori S. 1991 Vortices and defect statistics in two-dimensional optical chaos. *Phys. Rev. Lett.* **67**, 3749. (doi:10.1103/PhysRevLett.67.3749)
8. Staliunas K, Sánchez-Morcillo VJ. 2003 *Transverse patterns in nonlinear optical resonators*. Berlin, Germany: Springer.
9. Gambaudo JM. 1985 Perturbation of a Hopf bifurcation by an external time-periodic forcing. *J. Diff. Eq.* **57**, 172–199. (doi:10.1016/0022-0396(85)90076-2)
10. Couillet P, Lega J, Houchmanzadeh B, Lajzerowicz J. 1990 Breaking chirality in nonequilibrium systems. *Phys. Rev. Lett.* **65**, 1352. (doi:10.1103/PhysRevLett.65.1352)
11. Couillet P, Emilsson K. 1992 Strong resonances of spatially distributed oscillators: a laboratory to study patterns and defects. *Phys. D* **61**, 119–131. (doi:10.1016/0167-2789(92)90154-F)
12. Walgraef D. 1997 *Spatio-temporal pattern formation*. New York, NY: Springer.
13. Frisch T, Rica S, Couillet P, Gilli J. 1994 Spiral waves in liquid crystal. *Phys. Rev. Lett.* **72**, 1471. (doi:10.1103/PhysRevLett.72.1471)
14. Bertram M, Beta C, Rotermund HH, Ertl G. 2003 Complex patterns in a periodically forced surface reaction. *J. Phys. Chem. B* **107**, 9610–9615. (doi:10.1021/jp0341927)
15. Couillet P. 1986 Commensurate–incommensurate transition in nonequilibrium systems. *Phys. Rev. Lett.* **56**, 724. (doi:10.1103/PhysRevLett.56.724)
16. Lin AL, Bertram M, Martinez K, Swinney H, Ardelea A, Carey G. 2000 Resonant phase patterns in a reaction–diffusion system. *Phys. Rev. Lett.* **84**, 4240. (doi:10.1103/PhysRevLett.84.4240)
17. Vanag VK, Zhabotinsky AM, Epstein IR. 2001 Oscillatory clusters in the periodically illuminated, spatially extended Belousov–Zhabotinsky reaction. *Phys. Rev. Lett.* **86**, 552. (doi:10.1103/PhysRevLett.86.552)

18. de Valcárcel GJ, Pérez-Arjona I, Roldán E. 2002 Domain walls and Ising–Bloch transitions in parametrically driven systems. *Phys. Rev. Lett.* **89**, 164101. (doi:10.1103/PhysRevLett.89.164101)
19. Rüdiger S *et al.* 2003 Dynamics of Turing patterns under spatiotemporal forcing. *Phys. Rev. Lett.* **90**, 128301. (doi:10.1103/PhysRevLett.90.128301)
20. Henriot M, Burguete J, Ribotta R. 2003 Entrainment of a spatially extended nonlinear structure under selective forcing. *Phys. Rev. Lett.* **91**, 104501. (doi:10.1103/PhysRevLett.91.104501)
21. Míguez DG, Nicola E, Munzuri A, Casademunt J, Sagues F, Kramer L. 2004 Traveling-stripe forcing generates hexagonal patterns. *Phys. Rev. Lett.* **93**, 048303. (doi:10.1103/PhysRevLett.93.048303)
22. Lin AL, Aric Hagberg, Ehud Meron, Harry Swinney. 2004 Resonance tongues and patterns in periodically forced reaction–diffusion systems. *Phys. Rev. E* **69**, 066217. (doi:10.1103/PhysRevE.69.066217)
23. Rudzick O, Mikhailov AS. 2006 Front reversals, wave traps, and twisted spirals in periodically forced oscillatory media. *Phys. Rev. Lett.* **96**, 018302. (doi:10.1103/PhysRevLett.96.018302)
24. Rüdiger S, Casademunt J, Kramer L. 2007 Dynamics of domain walls in pattern formation with traveling-wave forcing. *Phys. Rev. Lett.* **99**, 028302. (doi:10.1103/PhysRevLett.99.028302)
25. Bodega PS, Kaira P, Beta C, Krefting D, Bauer D, Mirwald-Schulz B, Punckt C, Rotermund HH. 2007 High frequency periodic forcing of the oscillatory catalytic CO oxidation on Pt (110). *New J. Phys.* **9**, 61. (doi:10.1088/1367-2630/9/3/061)
26. Vanag VK, Epstein IR. 2008 Design and control of patterns in reaction–diffusion systems. *Chaos* **18**, 026107. (doi:10.1063/1.2900555)
27. Manor R, Hagberg A, Meron E. 2009 Wavenumber locking and pattern formation in spatially forced systems. *New J. Phys.* **11**, 063016. (doi:10.1088/1367-2630/11/6/063016)
28. Krefting D, Kaira P, Rotermund HH. 2009 Period doubling and spatiotemporal chaos in periodically forced CO oxidation on Pt(110). *Phys. Rev. Lett.* **102**, 178301. (doi:10.1103/PhysRevLett.102.178301)
29. Esteban-Martín A, Taranenko V, Garcia J, de Valcarcel G, Roldan E. 2005 Controlled Observation of a nonequilibrium Ising–Bloch transition in a nonlinear optical cavity. *Phys. Rev. Lett.* **94**, 223903. (doi:10.1103/PhysRevLett.94.223903)
30. de Valcárcel GJ, Staliunas K. 2003 Excitation of phase patterns and spatial solitons via two-frequency forcing of a 1:1 resonance. *Phys. Rev. E* **67**, 026604. (doi:10.1103/PhysRevE.67.026604)
31. de Valcárcel GJ, Staliunas K. 2010 Pattern formation through phase bistability in oscillatory systems with space-modulated forcing. *Phys. Rev. Lett.* **105**, 054101. (doi:10.1103/PhysRevLett.105.054101)
32. de Valcárcel GJ. 2002 Complex Ginzburg–Landau equation for self-oscillatory systems under amplitude modulated forcing in a 1:1 resonance. (<http://arxiv.org/abs/nlin/0207004>)
33. de Valcárcel GJ. 2010 Phase bistability and phase bistable patterns in self-oscillatory systems under a resonant periodic forcing with spatially modulated amplitude. (<http://arxiv.org/abs/1006.0626>)
34. Kapitza PL. 1951 Dynamic stability of a pendulum when its point of suspension vibrates. *Soviet Phys.* **21**, 588–592.
35. Landau LD, Lifshitz EM. 1976 *Course of theoretical physics*, vol. 1. Oxford, UK: Pergamon Press.
36. Nayfeh AH. 1973 *Perturbation methods*. New York, NY: Wiley.
37. Staliunas K, de Valcarcel G, Buldu J, Garcia-Ojalvo J. 2009 Noise-induced phase bistability via stochastic rocking. *Phys. Rev. Lett.* **102**, 010601. (doi:10.1103/PhysRevLett.102.010601)
38. Zeghlache H, Zehnlé V. 1992 Theoretical study of a laser with injected signal. I. Analytical results on the dynamics. *Phys. Rev. A* **46**, 6015. (doi:10.1103/PhysRevA.46.6015)
39. Solari HG, Oppo G-L. 1994 Laser with injected signal: perturbation of an invariant circle. *Optics Commun.* **111**, 173–190. (doi:10.1016/0030-4018(94)90157-0)
40. Urchueguía JF, Espinosa V, Roldan E, De Valcarcel GJ. 1996 Nonlinear dynamics of a class-A two-photon laser with injected signal. *J. Mod. Opt.* **43**, 2311–2336. (doi:10.1080/09500349608232889)
41. Esteban-Martín A, Martínez-Quesada M, Taranenko V, Roldan E, de Valcarcel G. 2006 Bistable phase locking of a nonlinear optical cavity via rocking: transmuted vortices into phase patterns. *Phys. Rev. Lett.* **97**, 093903. (doi:10.1103/PhysRevLett.97.093903)

42. Kolpakov S, Silva F, de Valcarcel GJ, Roldan E, Staliunas K. 2012 Experimental demonstration of bistable phase locking in a photorefractive oscillator. *Phys. Rev. A* **85**, 025805. (doi:10.1103/PhysRevA.85.025805)
43. Buldú JM, Staliunas K, Casals JA, García-Ojalvo J. 2006 Bistable phase control via rocking in a nonlinear electronic oscillator. *Chaos* **16**, 043126. (doi:10.1063/1.2404776)
44. Staliunas K *et al.* 2006 Bistable phase locking in rocked lasers. *Opt. Commun.* **268**, 160–168. (doi:10.1016/j.optcom.2006.07.007)
45. Staliunas K, de Valcárcel GJ, Roldán E. 2009 Bistable phase locking in a laser with injected signal. *Phys. Rev. A* **80**, 025801. (doi:10.1103/PhysRevA.80.025801)
46. Martínez-Quesada M, Roldán E, de Valcárcel GJ. 2011 Rocking bidirectional lasers. *Opt. Commun.* **284**, 2554–2559. (doi:10.1016/j.optcom.2011.01.028)
47. Radziunas M, Staliunas K. 2011 Spatial ‘rocking’ in broad-area semiconductor lasers. *EPL* **95**, 14002. (doi:10.1209/0295-5075/95/14002)
48. Fernandez-Oto C, de Valcárcel GJ, Tlidi M, Panajotov K, Staliunas K. 2014 Phase-bistable patterns and cavity solitons induced by spatially periodic injection into vertical-cavity surface-emitting lasers. *Phys. Rev. A* **89**, 055802. (doi:10.1103/PhysRevA.89.055802)
49. Esteban-Martín A, Taranenko VB, Roldan E, de Valcarcel G. 2005 Control and steering of phase domain walls. *Opt. Express* **13**, 3631–3636. (doi:10.1364/OPEX.13.003631)
50. Bortolozzo U, Residori S. 2006 Storage of localized structure matrices in nematic liquid crystals. *Phys. Rev. Lett.* **96**, 037801. (doi:10.1103/PhysRevLett.96.037801)
51. Hisaka M, Yoshida K. 2008 Multilayered optical data storage using a spatial soliton. *Appl. Phys. Lett.* **93**, 241103. (doi:10.1063/1.3050454)
52. Pedaci F *et al.* 2008 All-optical delay line using semiconductor cavity solitons. *Appl. Phys. Lett.* **92**, 011101. (doi:10.1063/1.2828458)
53. Leo F, Coen S, Kockaert P, Gorza S-P, Emplit P, Haelterman M. 2010 Temporal cavity solitons in one-dimensional Kerr media as bits in an all-optical buffer. *Nat. Photonics* **4**, 471. (doi:10.1038/nphoton.2010.120)
54. Mandel P, Georgiou M, Erneux T. 1993 Transverse effects in coherently driven nonlinear cavities. *Phys. Rev. A* **47**, 4277. (doi:10.1103/PhysRevA.47.4277)
55. Lega J, Moloney JV, Newell AC. 1995 Universal description of laser dynamics near threshold. *Phys. D* **83**, 478–498. (doi:10.1016/0167-2789(95)00046-7)
56. Moloney JV, Newell AC. 2003 *Nonlinear optics*. Boulder, CO: Westview Press.
57. Mandel P. 1997 *Theoretical problems in cavity nonlinear optics*. Cambridge, UK: Cambridge University Press. *Nonlinear Optics* (Wiley-VCH, 2010).
58. Longhi S, Geraci A. 1996 Swift–Hohenberg equation for optical parametric oscillators. *Phys. Rev. A* **54**, 4581. (doi:10.1103/PhysRevA.54.4581)
59. de Valcárcel GJ, Staliunas K, Roldan E, Sanchez-Morcillo V. 1996 Transverse patterns in degenerate optical parametric oscillation and degenerate four-wave mixing. *Phys. Rev. A* **54**, 1609. (doi:10.1103/PhysRevA.54.1609)
60. Sánchez-Morcillo VJ, de Valcárcel GJ. 1996 Swift–Hohenberg-type equation for nascent two-photon optical bistability in the weakly dispersive limit. *Quantum Semiclass. Opt.* **8**, 919. (doi:10.1088/1355-5111/8/4/013)
61. Sánchez-Morcillo VJ, Roldan E, de Valcarcel G, Staliunas K. 1997 Generalized complex Swift–Hohenberg equation for optical parametric oscillators. *Phys. Rev. A* **56**, 3237. (doi:10.1103/PhysRevA.56.3237)
62. Staliunas K. 1993 Laser Ginzburg–Landau equation and laser hydrodynamics. *Phys. Rev. A* **48**, 1573. (doi:10.1103/PhysRevA.48.1573)
63. Lega J, Moloney JV, Newell AC. 1994 Swift–Hohenberg Equation for Lasers. *Phys. Rev. Lett.* **73**, 2978. (doi:10.1103/PhysRevLett.73.2978)
64. Larionova Y, Peschel U, Esteban-Martin A, Garcia Monreal J, Weiss C. 2004 Ising and Bloch walls of phase domains in two-dimensional parametric wave mixing. *Phys. Rev. A* **69**, 033803. (doi:10.1103/PhysRevA.69.033803)
65. Staliunas K, Sánchez-Morcillo VJ. 2005 Ising–Bloch transition for spatially extended patterns. *Phys. Rev. E* **72**, 016203. (doi:10.1103/PhysRevE.72.016203)
66. Staliunas K, Sánchez-Morcillo VJ. 1998 Dynamics of phase domains in the Swift–Hohenberg equation. *Phys. Lett. A* **241**, 28–34. (doi:10.1016/S0375-9601(98)00084-X)
67. Gomila D, Colet P, Oppo G-L, San Miguel M. 2001 Stable droplets and growth laws close to the modulational instability of a domain wall. *Phys. Rev. Lett.* **87**, 194101. (doi:10.1103/PhysRevLett.87.194101)

68. Tlidi M, Mandel P, Le Berre M, Ressayre E, Tallet A, Di Menza L. 2000 Phase-separation dynamics of circular domain walls in the degenerate optical parametric oscillator. *Opt. Lett.* **25**, 487–489. (doi:10.1364/OL.25.000487)
69. Sanchez-Morcillo VJ, Staliunas K. 1999 Stability of localized structures in the Swift–Hohenberg equation. *Phys. Rev. E* **60**, 6153. (doi:10.1103/PhysRevE.60.6153)
70. de Valcárcel GJ, Staliunas K. 2013 Phase-bistable Kerr cavity solitons and patterns. *Phys. Rev. A* **87**, 043802. (doi:10.1103/PhysRevA.87.043802)
71. Lugiato LA, Lefever R. 1987 Spatial dissipative structures in passive optical systems. *Phys. Rev. Lett.* **58**, 2209. (doi:10.1103/PhysRevLett.58.2209)

Universal description of pattern formation in optical oscillators under bichromatic injection.

Manuel Martínez-Quesada and Germán J. de Valcárcel.

Journal of the Optical Society of America B **35** 1379-1389 (2018).

Universal description of pattern formation in optical oscillators under bichromatic injection

MANUEL MARTÍNEZ-QUESADA* AND GERMÁN J. DE VALCÁRCEL

Departament d'Òptica, Universitat de València, Dr. Moliner 50, 46100 Burjassot, Spain

*Corresponding author: manuel.martinez-quesada@uv.es

Received 21 December 2017; revised 24 April 2018; accepted 26 April 2018; posted 26 April 2018 (Doc. ID 318126); published 24 May 2018

We study pattern formation in a complex Swift–Hohenberg equation with phase-sensitive (parametric) gain. Such an equation serves as a universal order parameter equation describing the onset of spontaneous oscillations in extended systems submitted to a bichromatic injection when the instability is toward long (transverse) wavelengths. Applications include two-level lasers and photorefractive oscillators. Under such an injection, the original continuous phase symmetry of the system is replaced by a discrete one and phase bistability emerges. This leads to the spontaneous formation of phase-locked spatial structures, such as phase domains and dark-ring (phase) cavity solitons. The stability of the homogeneous solutions is studied, and numerical simulations are made covering all the dynamical regimes of the model, which turn out to be very rich. Derivations of the rocked complex Swift–Hohenberg equation, using multiple scale techniques, are given for the two-level laser and the photorefractive oscillator. © 2018 Optical Society of America

OCIS codes: (190.4420) Nonlinear optics, transverse effects in; (270.3100) Instabilities and chaos; (140.3430) Laser theory; (190.5330) Photorefractive optics; (190.6135) Spatial solitons.

<https://doi.org/10.1364/JOSAB.35.001379>

1. INTRODUCTION

The dynamics of nonlinear systems is largely nontrivial in general and numerical simulations, involving sophisticated mathematical techniques, are usually needed to fully understand their temporal evolution. The situation is even more complicated in spatially extended systems, such as in nonlinear optics, in which (multi)dimensional variables are present in the dynamics. In these cases, an analytical (or semi-analytical) approach that allows us to gain physical insight about the system is only possible if we consider universal models [1], which formally capture the dynamics of nonlinear systems close to critical points (such as the threshold of emission in a laser). These models, also known as order parameter equations (OPEs), provide a simplified yet powerful description of the system. Their universal character is due to the fact that very different systems (biological, chemical, physical, etc.) are described by the same OPE, the only difference being the meaning of variables and parameters under this approach.

The symmetries of the system play a central role in the form of the OPE. These OPEs can be real or complex depending on the fundamental variable (electric field, temperature) that is considered or, even better, depending on the phase freedom supported by the system (see below). In nonlinear optics, complex OPEs are commonly used since a complex Ginzburg–Landau for lasers with finite positive detuning was derived

[2] and they have been proven to be very helpful for understanding a variety of systems [3–5]. Another equation, a complex Swift–Hohenberg (CSHE), which is valid for small detunings (positive and negative), was later obtained for lasers [6,7] and optical parametric oscillators [8,9].

The phase symmetry determines the nature of patterns which are possible in the system. In systems with continuous phase symmetry, the dynamics is usually turbulent and the presence of vortices and spiral waves is common. When the systems only allow a finite number of phases (by means of a $n:m$ forcing [10,11], for instance) the dynamics become more ordered and controllable. Furthermore, when a 2:1 (parametric) forcing is applied to a system with continuous phase symmetry, the dynamics of the system allows only two phases in it, which leads to the appearance of novel structures in the system, such as phase domains, domain walls, and localized structures (cavity solitons) [3,10,12,13]. The proper OPE for the system must reflect this change and a generic equation can be derived for systems with $n:m$ forcing [10]. For parametric forcing, a family of OPEs, such as the parametric complex Ginzburg–Landau (PCGLE) [12], is obtained.

Optical systems (like lasers) are usually insensitive to parametric forcing as the nonlinear response of these systems to high frequencies (twice the natural frequency) is negligible. In the last few years a technique involving a new kind of

forcing, known as “rocking,” was introduced [14]. This is a 1:1 forcing (the frequency of the injection is close to the frequency of the system), so it is appropriate for optical systems. The key factor is that the *amplitude* of the injection oscillates in time (temporal rocking) [14] or space (spatial rocking) [15] with a given small frequency unlike the usual 1:1 forcing, which uses purely monochromatic injection. This modulation modifies the dynamics of the system, which becomes phase bistable. It can be shown [16] that a PCGLE describes the universal dynamics of a laser close to threshold under rocking when the undriven system exhibits an homogeneous Hopf bifurcation. Recently, temporal modulation of the pump of a laser in order to excite transverse patterns was considered in [17], where it was found that pattern formation occurs when the modulation frequency is approximately equal to the relaxation frequency, or twice this value, for class B lasers.

Rocking has been successfully applied (theoretically and experimentally) to a wide range of systems [16,18,19]. This has led to the derivation of OPEs describing those systems under certain limits and that provide relevant information of the dynamics. Numerical simulations also prove that the behavior predicted by these OPEs extends (qualitatively) far beyond the conditions imposed in their derivation, which increases the utility of this universal description. A complex Swift–Hohenberg equation with parametric gain, which describes a photorefractive oscillator (PRO) under the injection of rocking, was derived in [20]. Here we show that a similar equation describes lasers with small detuning when rocking forcing is present, as well as we generalize the result of [20] to more general setups.

Therefore, we will consider the spatiotemporal dynamics of extended systems, close to a bifurcation to traveling waves of long wavelength, when the system is forced in time close to its natural frequency (1:1 resonance) and uniformly in space. We will study two paradigmatic examples of optical oscillators, a two-level laser and a two-wave mixing photorefractive oscillator, with continuous phase symmetry (but with different kinds of nonlinearity) and therefore, they have similar nonlinear dynamics close to threshold. The kind of forcing which we refer to can be thus expressed as

$$F(t) = P(t)e^{-i\omega_R t} + c.c., \quad (1)$$

where $P(t + T) = P(t)$ is a T -periodic function of time of period $T \gg \frac{2\pi}{\omega_R}$ and ω_R is a high optical frequency, almost resonant with the natural frequency of the undriven system. A simple realization of $P(t)$ is the function

$$P(t) = F \cos(\omega t), \quad (2)$$

where $\omega \ll \omega_R$ and F is an amplitude. According to Eqs. (1) and (2) the forcing phase (sign) alternates in time.

As we will show below, the state of the system can be expressed as

$$A(\mathbf{r}, t) = A_R(t) + \psi(\mathbf{r}, t), \quad (3)$$

where $A_R(t)$ is a T -periodic, spatially uniform contribution merely following the forcing, plus a spatially two-dimensional field $\psi(\mathbf{r}, t)$, whose dynamics is governed by a parametrically driven Swift–Hohenberg equation.

The structure of the paper is as follows. In Section 2 we derive the equation that is the object of our study for two relevant optical systems. In Section 3 we present the model and their different terms. In Section 4 we obtain their homogeneous solutions and a linear stability analysis is performed, to both trivial and homogeneous solutions, to study instabilities against perturbations of wave vector k . In Section 5 we present some numerical simulations of our model for different values of the parameters and show the patterns that can be found. We conclude in Section 6. In the appendices we present the derivation of the equation for lasers and the PRO.

2. DERIVATION OF THE CSHE

We will consider two optical systems: the two-level laser and a two-wave mixing PRO.

A. Laser

Our starting point is the standard set of Maxwell–Bloch equations for a two-level laser [17,21,22] with injected signal [16,23,24]:

$$\partial_t E = \sigma[-(1 + i\Delta)E + P] + i\nabla^2 E + E_{in}, \quad (4a)$$

$$\partial_t P = -(1 - i\Delta)P + (r - N)E, \quad (4b)$$

$$\partial_t N = b \left[-N + \frac{1}{2}(E^*P + P^*E) \right], \quad (4c)$$

where the injected field is of the form [16]

$$E_{in} = F \cos(\omega t) e^{i\theta t}. \quad (5)$$

The complex fields E and P are the scaled envelopes of the electric field and polarization, $-N$ is proportional to the difference between the population inversion and its steady value in the absence of lasing. $\sigma = \kappa/\gamma_{\perp}$ and $b = \gamma_{\parallel}/\gamma_{\perp}$, where κ , γ_{\perp} , and γ_{\parallel} are, respectively, the decay rates of E , P , and N . The transverse Laplacian $\nabla^2 = \partial_x^2 + \partial_y^2$, where the spatial coordinates (x, y) have been normalized so as to make unity the diffraction coefficient, and t is time in units of γ_{\perp} . Additionally, r is the pump parameter and the detuning $\Delta = (\omega_C - \omega_A)/(\gamma_{\perp} + \kappa)$, with ω_C (ω_A) the cavity (atomic) frequency. We will consider class C lasers so $\sigma \sim b \sim 1$.

Equations (4) have been written in the frequency frame $\omega_L = (\gamma_{\perp}\omega_C + \kappa\omega_A)/(\gamma_{\perp} + \kappa)$ of the on-axis, or plane-wave ($\nabla^2 E = 0$), lasing solution in the absence of injected signal (lasing pulling formula [25]). This means that the actual bichromatically injected field has frequencies given by $\omega_L + \gamma_{\perp}\theta \pm \gamma_{\perp}\omega$.

In the absence of rocking ($F = 0$), the system is phase-invariant: $(E, P, N) \rightarrow (Ee^{i\phi}, Pe^{i\phi}, N)$. The trivial solution ($E = P = N = 0$) is destabilized to a family of traveling-wave solutions $E = E_0 e^{i(\mathbf{k}\cdot\mathbf{r} - \Omega t)}$, $P = P_0 e^{i(\mathbf{k}\cdot\mathbf{r} - \Omega t)}$, and $N = N_0$ [7], where

$$|E_0|^2 = r - 1 - \left(\Delta + \frac{k^2}{\sigma + 1} \right)^2, \quad (6a)$$

$$P_0 = E_0 \left(1 + i \left(\Delta + \frac{k^2}{\sigma + 1} \right) \right), \quad (6b)$$

$$N_0 = |E_0|^2, \quad \Omega = \frac{k^2}{\sigma + 1}. \quad (6c)$$

The threshold for lasing emission under spatial perturbations of wavenumber k is $r_0 = 1 + (\Delta + k^2/(\sigma + 1))^2$. For positive detuning the laser shows patterns with critical wave vector $k_c = 0$ for $r > 1 + \Delta^2$; conversely for negative detuning we have traveling-wave patterns whose threshold is minimum ($r = 1$) for $k_c = \sqrt{-(\sigma + 1)\Delta}$.

Multiple scales expansion is a usual way to derive an order parameter equation [6,9,14]. To do that, we need to know the order of magnitude of the parameters that determine the system dynamics. A linear stability analysis of the trivial solution [7,26] will give insight about the necessary scales: the detuning Δ is chosen $\mathcal{O}(\varepsilon)$ so the Laplacian ∇^2 is also $\mathcal{O}(\varepsilon)$. Additionally, the pump is $r = 1 + \varepsilon^2 r_2$. We will consider two time scales, fast and slow, $T_1 = \varepsilon t$ and $T_2 = \varepsilon^2 t$. We also set

$$(E, P, N) = \varepsilon(E_1, P_1, N_1) + \varepsilon^2(E_2, P_2, N_2) + \dots \quad (7)$$

We will consider two different scales for the parameters of the rocking, “fast” ($\omega \sim \mathcal{O}(\varepsilon)$, $F \sim \mathcal{O}(\varepsilon^2)$) and “slow” ($\omega \sim \mathcal{O}(\varepsilon^2)$, $F \sim \mathcal{O}(\varepsilon^3)$). In both cases, θ is $\mathcal{O}(\varepsilon)$. The consistency of the results will prove the robustness of the method. As is shown in Appendix A, both choices lead to the same final equation. The results, up to the second order, for the slow case (expressions for the fast case can be found in Appendix A) are

$$E = \frac{F e^{i\theta t}}{(1 + \sigma)\omega} \sin(\omega t) + i e^{i\theta t} \psi(\mathbf{r}, t),$$

$$P = E - \frac{i}{(1 + \sigma)} (\nabla^2 E - (1 + \sigma)\Delta E), \quad N = |E|^2. \quad (8)$$

Note that Eq. (8) is consistent with the general case Eq. (3). Lastly, setting $\frac{\nabla^2}{1 + \sigma} \equiv \nabla'^2$, $t' \equiv \frac{\sigma}{\sigma + 1} t$, $\theta' \equiv \frac{\sigma + 1}{\sigma} \theta$, $\alpha \equiv \frac{\sigma + 1}{\sigma}$, defining $\mu = r - 1$, and removing the primed notation for simplicity, the equation for ψ reads

$$\partial_t \psi = (\mu - 2\gamma - i\theta)\psi - |\psi|^2 \psi - (\Delta - \nabla'^2)^2 \psi + i\alpha \nabla'^2 \psi + \gamma \psi^*, \quad (9)$$

where the rocking parameter is

$$\gamma = \frac{1}{2} \frac{F^2}{(1 + \sigma)^2 \omega^2}. \quad (10)$$

This equation is a Swift–Hohenberg equation with parametric gain, which we will analyze later.

B. Two-Wave Mixing Photorefractive Oscillator

Our starting point is the set of equations as in [20,27] in which we consider a bichromatical injection and we make the change $(E', N') \rightarrow (E, N) e^{-i\Delta t}$ for convenience, where $\Delta = (\omega_C - \omega_p)/k$ (ω_p and ω_C are the frequencies of the pump and its nearest longitudinal mode, respectively, whereas k is the cavity linewidth). After removing the commas and considering $\frac{\sigma + 1}{\sigma} \simeq 1$ as $\sigma \gg 1$ as is explained below (we apply this approximation along the further analysis), we get

$$\sigma^{-1} \partial_t E = -(1 + i\Delta)E + i\nabla^2 E + N + E_{in},$$

$$\partial_t N = -(1 - i\Delta)N + g \frac{E}{1 + |E|^2}, \quad (11)$$

where the injected field is as in the previous case, $E(\mathbf{r}, t)$ is the slowly varying envelope of the intracavity field, $N(\mathbf{r}, t)$ is the complex amplitude of the photorefractive nonlinear grating, $\sigma = \kappa\tau$, where τ is the photorefractive response time ($\sigma \gtrsim 10^8$ under typical conditions, and $\tau \sim 1$ s), t is time measured in units of τ , and the detuning, g , is the (real) gain parameter that depends on the crystal parameters and the geometry of the interaction.

In the absence of rocking ($F = 0$), the model [20,27] is, like in the previous case, phase-invariant: $(E, N) \rightarrow (E e^{i\phi}, N e^{i\phi})$. This free-running model has two main solutions: the trivial solution $E = N = 0$ and the family of traveling-wave solutions $F = \sqrt{g/g_0 - 1} e^{i(k \cdot r - \Omega t)}$ and $N = (1 + i\Omega t)E$ with $g_0 = 1 + \Omega^2$ and $\Omega = \Delta + k^2$. From these results we conclude that for $\Delta > 0$ the threshold is minimum for $k = 0$ (homogeneous emission) and occurs at $g = 1 + \Delta^2$ and the frequency of the field is shifted by $\Omega = \Delta$. On the other hand, for $\Delta/a < 0$ the threshold ($g = 1$) is for $k = \sqrt{-\Delta}$ (off-axis emission) and there is no frequency shift ($\Omega = 0$).

As before, a linear stability analysis of the trivial solution [27] provides us the scales for the parameters: we take $\sigma \sim \mathcal{O}(\varepsilon^{-4})$ (results are independent of the specific scale provided that σ is very large) and $\Delta, \theta \sim \mathcal{O}(\varepsilon)$, which implies $\nabla^2 \sim \mathcal{O}(\varepsilon)$. We also assume that g is close to threshold, $g = 1 + g_2 \varepsilon^2$, and that $F \sim \mathcal{O}(\varepsilon)$, $\omega \sim \mathcal{O}(1)$. As in the previous case, we will have “two times,” $T_1 = \varepsilon t$ and $T_2 = \varepsilon^2 t$. We also set

$$(E, N) = \varepsilon(E_1, N_1) + \varepsilon^2(E_2, N_2) + \dots \quad (12)$$

Solving up to the second order, we obtain

$$E = E^\omega(t) - i e^{-i\theta t} \psi(\mathbf{r}, t),$$

$$N = (1 + (-i\Delta + i\nabla^2))E - F \cos(\omega t) e^{i\theta t}, \quad (13)$$

where E^ω is a periodic function (see Appendix B). Note that, as in the previous case, Eq. (13) is consistent with Eq. (3).

We finally obtain (Appendix B), as in the case of the laser, a Swift–Hohenberg equation with parametric gain. Defining $\mu = g - 1$, we can write

$$\partial_t \psi = (\mu - 2\gamma - i\theta)\psi - |\psi|^2 \psi + i\nabla^2 \psi - (\nabla^2 - \Delta)^2 \psi + \gamma \psi^*, \quad (14)$$

where the rocking parameter is

$$\gamma = \frac{1}{2} \frac{F^2}{\omega^2} (\omega^2 + 1). \quad (15)$$

3. CSHE MODEL

Comparing Eqs. (9) and (14), we see that they share the same structure as the only difference is the diffraction term, so we will analyze both of them using an unified model. Therefore, the equation we are going to study is

$$\partial_t \psi(\mathbf{r}, t) = (\mu - |\psi|^2)\psi + i\alpha \nabla^2 \psi - (\Delta - \nabla^2)^2 \psi - i\theta \psi + \gamma(\psi^* - 2\psi). \tag{16}$$

This equation is the usual complex Swift–Hohenberg equation, which models pattern formation arising from a finite wavenumber instability to traveling waves close to threshold [6,8,9,28–30], with additional terms, those multiplied by γ , which appear when rocking is considered [14–16,20]. The term $-2\gamma\psi$ refers to losses whereas the extra term $\gamma\psi^*$ is the actual novelty as it breaks the phase invariance of the system, which becomes phase bistable as the equation only has the discrete symmetry $\psi \rightarrow -\psi$. As for the parameters, μ measures the distance from threshold (it can be removed from the equation by simple scaling but we keep it not to overwhelm the notation) and α controls diffraction/dispersion. Other parameters are Δ , the detuning of the cavity from the natural frequency of the unforced system in the optical case, and θ , which is the detuning of the forcing from the natural frequency of the system. Finally the “rocking parameter” γ is proportional to the squared amplitude of rocking F^2 and also depends on its frequency ω in a way whose exact form depends on the system considered (see Section 2); note that when $\gamma = 0$ the effect of rocking is lost and Eq. (16) becomes a usual complex Swift–Hohenberg equation. In our case, $\alpha = 1$ in the PRO while $\alpha > 1$ for the laser.

Equation (16) with $\gamma = 0$ models class C (and class A) lasers. Class B lasers (such as semiconductor lasers) possess a more complicated dynamics, which cannot be captured by a single equation. Models of two equations for these lasers were considered in [7,31,32]. The interested reader can find in [16,33] theoretical analysis about rocking in class B lasers. As an additional remark, previous studies of rocking considered PCGLE equations for modeling the dynamics of rocked nonlinear systems [16]. In the case of a two-level laser, that equation remains valid only for positive (and large) values of detuning Δ ; however, the CSHE model derived here is suitable (as the original SHE for lasers) for positive and negative values of detuning provided they are small.

4. PHASE-LOCKED SPATIALLY UNIFORM SOLUTIONS: ROCKED STATES AND THEIR STABILITY

The spatially uniform nontrivial solutions of Eq. (16), or “rocked states,” can be expressed as $\psi_{\pm} = |\psi_{\pm}|e^{i\phi_{\pm}}$, where

$$|\psi_{\pm}|^2 = \mu - 2\gamma - \Delta^2 \pm \sqrt{\gamma^2 - \theta^2}, \tag{17a}$$

$$e^{-2i\phi_{\pm}} = -\frac{i\theta \pm \sqrt{\gamma^2 - \theta^2}}{\gamma}. \tag{17b}$$

The state ψ_- is always unstable as follows from a standard linear stability analysis, so we will not consider it in the following. On the other hand, as ϕ_+ can take two values (differing by π), this produces two phase-locked states (with same amplitude) and phase differing by π (bistable phase locking). From now on we rename $\psi_+ \equiv \psi_0$ ($\phi_+ = \phi_0$). The existence of these states requires $\mu - \Delta^2 > 0$ and $\gamma > |\theta|$; see Eq. (17a). Moreover, they exist only if $\gamma_0 < \gamma < \gamma_+$, where

$$\gamma_0 = \begin{cases} |\theta|, & \text{if } |\theta| < (\mu - \Delta^2)/2 \\ \gamma_- & \text{otherwise} \end{cases},$$

$$\gamma_{\pm} = \frac{2(\mu - \theta^2)}{3} \pm \frac{1}{3} \sqrt{(\mu - \theta^2)^2 - 3\Delta^2}. \tag{18}$$

On the plane $\gamma - \theta$ the existence region is a closed domain (“rocking balloon”) as we can see in Fig. 1. Outside that region we have the trivial solution and phase-unlocked solutions (traveling waves or patterns).

We have performed a linear stability analysis of the trivial and uniform solutions against perturbations with wave vector k . The eigenvalue with the largest real part (for the stability of the trivial solution we just set $\psi_0 = 0$) reads

$$\lambda(k) = \mu - 2\gamma - |\psi_0|^2 - (k^2 + \Delta)^2 + \sqrt{|\psi_0|^4 - 2\gamma \cos(2\phi_0)|\psi_0|^2 - [(\alpha k^2 + \theta)^2 - \gamma^2]}. \tag{19}$$

As we have two different nonlocal terms in the Swift–Hohenberg Eq. (16), $\lambda(k)$ will have, in general, two local maxima. One of them (k_s) is associated with a real eigenvalue and it will give rise to static patterns through a pattern-forming bifurcation; the another one (k_n) corresponds to a complex

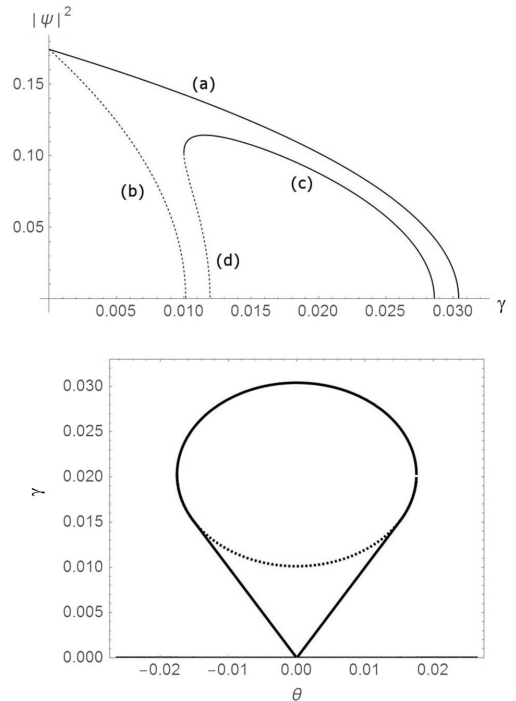


Fig. 1. (Top) Amplitude of the rocking states versus γ for $\theta = 0$, (a) ψ_+ , (b) ψ_- and $\theta = 0.01$, (c) ψ_+ , (d) ψ_- . (Bottom) Domain of existence of ψ_+ (bold line) and ψ_- (dotted line) in the $\theta - \gamma$ plane; the lower bound is the same for both functions. The rest of the parameters are $\mu = 0.05$, $\Delta = 0.14$, and $\alpha = 2$.

eigenvalue and it will produce oscillatory solutions (homogeneous or traveling waves) through a Hopf bifurcation from the trivial solution. We could not obtain an exact analytical expression for k_s , but an approximated one by considering (as is observed numerically) that it is close to $-\theta/\alpha$. Writing $k^2 = -\theta/\alpha + \varepsilon$ in Eq. (19) and expanding λ up to the second order in ε , the resulting quadratic expression can be maximized and solved for ε , leading to

$$k_s^2 = \max\left(-\frac{\alpha\theta + 2\Delta S}{\alpha^2 + 2S}, 0\right), \tag{20}$$

where $S = \gamma$ for the trivial solution and $S = \sqrt{\theta^2 + (2\gamma + \Delta^2 - \mu)^2}$ in the case of the rocked states. The expression for k_o^2 is just

$$k_o^2 = \max(-\Delta, 0),$$

so for $\Delta > 0$ we will have homogenous oscillations, while for $\Delta < 0$ we will obtain traveling waves.

All these results are summarized in Fig. 2 (positive Δ) and Fig. 3 (negative Δ) for $\alpha = 2$ (laser case) and $\mu = 0.05$. For positive Δ , if γ is large, the trivial solution, which always exists, is stable. As we decrease the rocking parameter γ , we see bifurcations to other solutions like static patterns (for the trivial state, $k_s^2 > 0 \Leftrightarrow \theta < -2\gamma\Delta/\alpha$) and homogeneous oscillations (for $\gamma = (\mu - \Delta^2)/2, \theta > \gamma, k_o^2 = 0$). The transition to uniform rocked states is supercritical in the upper bound (the amplitude ψ_0 becomes 0 along that line). Regarding the lower bound (two straight lines, where $\psi_+ = \psi_-$), there is a saddle-node bifurcation which connects with oscillations by means of a complex eigenvalue both for positive and very small negative values of θ (Fig. 2). For negative θ , the rocked states become unstable close to the left edge of the balloon to instabilities (real eigenvalue) of wavenumber k_r^2 for moderate values of γ , whereas oscillations appear for low γ (the line $\gamma = 0$ corresponds to the standard SHE). In Fig. 4 we can see an example of the temporal dynamics of spatially homogenous states close to the bifurcation: as we go closer to this, the period of the oscillations becomes larger and is infinite at the bifurcation.

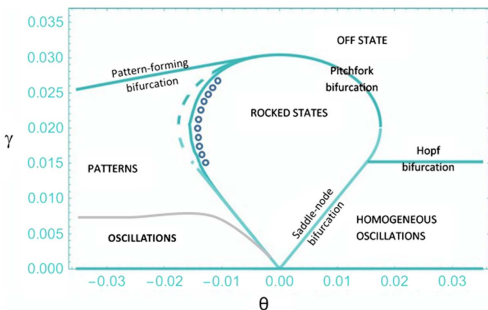


Fig. 2. Bifurcation diagram of Eq. (16) for $\alpha = 2, \mu = 0.05$, and $\Delta = 0.14$. The dashed line indicates the left boundary of existence of the uniform rocked states, which become unstable before reaching it. The circles refer to the existence of dark-ring cavity solitons. The saddle-node bifurcation extends to very small and negative values of θ (lower limit not shown).

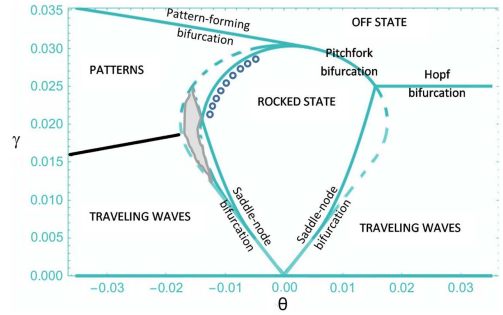


Fig. 3. Bifurcation diagram of Eq. (16) for $\alpha = 2, \mu = 0.05$, and $\Delta = -0.14$. The dashed line indicates the boundary of existence of the uniform rocked states, which become unstable before reaching it. In the shadowed region the two instabilities (with two different spatial frequencies) for the uniform rocked states are present as explained in the text. The circles refer to the existence of dark-ring cavity solitons.

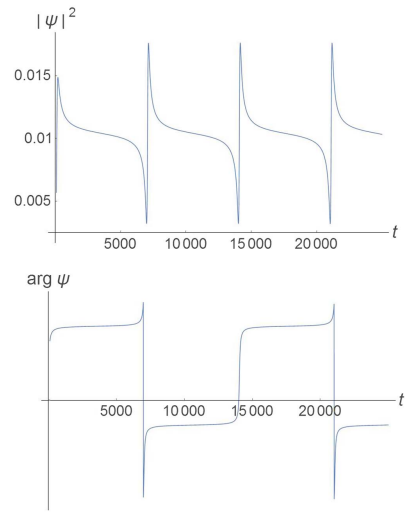


Fig. 4. Temporal evolution of intensity (top) and phase (bottom) of a homogeneous solution close to the saddle-node bifurcation in Fig. 2. Parameters are $\mu = 0.05, \Delta = 0.14, \alpha = 2, \gamma = 0.01$, and $\theta = 0.01001$.

The analysis for negative Δ is richer, as expected, because in this regime the Swift–Hohenberg equation [Eq. (16)] without rocking ($\gamma = 0$) already displays traveling waves of wavenumber $k_{SH} = \sqrt{-\Delta}$. For large positive θ we still have a Hopf bifurcation connecting trivial and traveling-wave solutions (for $\gamma = \mu/2, \theta > \sqrt{\mu^2 - 4\Delta^2}/2, k_o^2 = -\Delta$). For negative and small positive θ ($\theta < -2\gamma\Delta/\alpha$) the trivial solution destabilizes to a pattern with leading wavenumber k_s^2 at a certain $\gamma = \gamma(\theta)$.

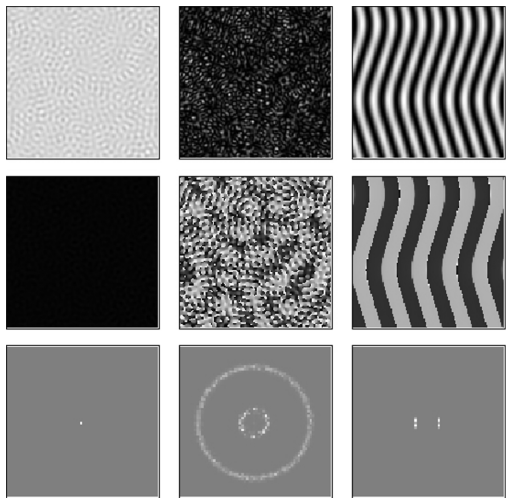


Fig. 5. Competition between two instabilities. Snapshots of intensity (upper row), phase and spatial spectrum (lower row) of the transient dynamics in (left to right) $t = 150$, $t = 1725$, and $t = 120000$. Parameters are $\mu = 0.05$, $\Delta = -0.14$, $\alpha = 2$, $\gamma = 0.0297$, and $\theta = -0.0142$. The size of the windows is 400×400 .

Additionally, for small γ we have traveling waves for both positive and negative θ . Regarding the rocked states, these are destabilized in two ways: (i) through a complex eigenvalue with most unstable wave vector $k_o^2 = -\Delta$, which happens symmetrically around θ (see Fig. 3); and (ii) through a real eigenvalue with most unstable wave vector equal to $k_{s(\text{rocked})}^2$, which happens, as in the case of positive detuning, close to the left side of the balloon (here the unstable region is bigger). The presence of these two unstable wavenumbers can be only seen in the simulations in the transient development of the instabilities (Fig. 5) as only one of the two spatial frequencies eventually survives. Close to the lower bound we find (i) and close to the upper bound we get (ii). In a range of values of Δ (~ -0.14) we find that both instabilities arise simultaneously (the two peaks of $\lambda(k)$ at k_o and $k_{s(\text{rocked})}$ becomes both positive as in Fig. 6: codimension 2 point), this happens for a small region in the $\gamma - \theta$ plane (Fig. 3). This behavior also appears

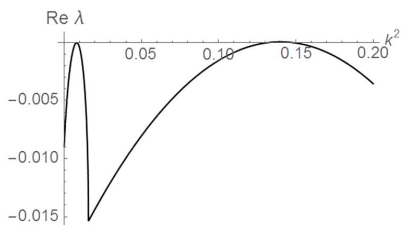


Fig. 6. Real part of the eigenvalue $\lambda(k)$ obtained in the linear stability analysis of the URS solution for parameters: $\mu = 0.05$, $\Delta = -0.14$, $\alpha = 2$, $\gamma = 0.0205$, and $\theta = -0.0139$.

(for negative θ), outside of the region where rocked states exist, along a line that separates static patterns from traveling waves (Fig. 3).

5. SPATIAL STRUCTURES

We studied the spatial patterns that appear outside the tongue, where rocked (phase-bistable) states exist, by means of numerical simulations. They basically confirm the previous analysis as we were able to obtain static spatial patterns that arise from real eigenvalue instabilities, selecting a particular spatial frequency as we have seen in the previous analysis. Then the (slow) dynamics finally leads to a pattern where two spatial modes (of opposite wavenumber) are dominant, leading to roll-like patterns (as in the right column of Fig. 5). Additionally, we observe phase-unlocked patterns as (slightly modulated) traveling waves for negative Δ (Fig. 7), as a result of an instability governed by a complex eigenvalue.

On the other hand, numerical experiments of Eq. (16) confirm the existence of a variety of spatial patterns due to the phase bistability and the instabilities studied in the previous section. In the simulations we fix $\alpha = 2$ (remember that $\alpha = 1$ for photorefractive oscillators and $\alpha > 1$ for lasers) as it can be shown that, after proper rescaling, the parameter α does not affect the dynamics of the system and its value can be set an arbitrarily. Different values of α just change the temporal scale and the spatial scale associated with the real eigenvalue instability, but what is relevant to the dynamics is the

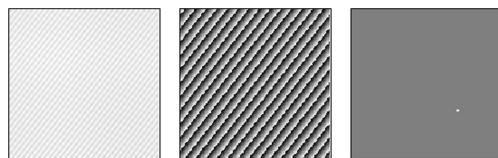


Fig. 7. Intensity (left), phase (middle), and spatial spectrum (right) of a traveling-wave pattern obtained for $\mu = 0.05$, $\Delta = -0.14$, $\alpha = 2$, $\gamma = 0.012$, and $\theta = -0.025$. The size of the windows is 500×500 .

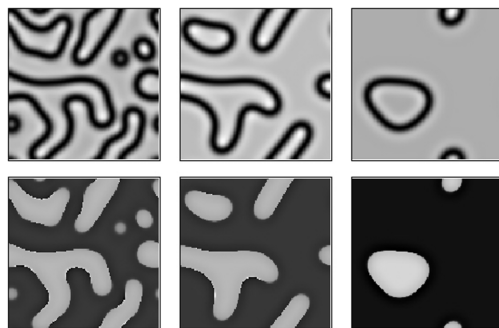


Fig. 8. Contracting phase domains. Snapshots of intensity (upper row) and phase (lower row) of transient dynamics of phase domains starting from noise in (left to right) $t = 1000$, $t = 3000$, and $t = 7500$. Parameters are $\mu = 0.05$, $\Delta = 0.14$, $\alpha = 2$, $\gamma = 0.02$, and $\theta = -0.005$. The rest of the parameters are as in Fig. 7.

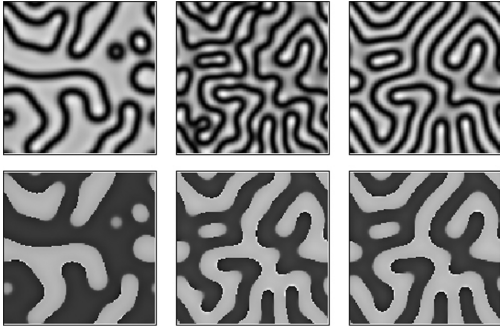


Fig. 9. Labyrinth formation. Snapshots of intensity (upper row) and phase (lower row) of transient dynamics of labyrinths starting from the left picture in Fig. 8 in (left to right) $t = 0$, $t = 500$, and $t = 3000$ for $\theta = -0.012$. The rest of the parameters are as in Fig. 8.

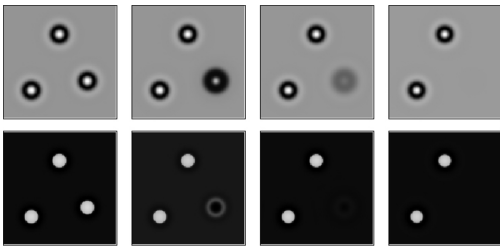


Fig. 10. Writing/erasing phase cavity solitons. Intensity (upper row) and phase (lower row) plots of transient dynamics of the erasing of a dark-ring cavity soliton for $\theta = -0.011$. Times (left to right) are $t = 0$, $t = 150$, $t = 300$, and $t = 450$. The rest of the parameters are as in Fig. 8.

ratio between that scale and the one associated with the complex eigenvalue, which is determined by Δ .

Traveling waves (negative Δ) and homogenous oscillations (positive Δ) are found outside the “rocked” balloon for small values of γ , whereas inside that region two uniform rocked states of opposite phase, connected through domain walls and generating phase domains (Fig. 8), are obtained. In two spatial dimensions, these domains are always a transient state before one phase dominates [34]. Close (but still inside the stability region) to the edge where the uniform rocked states lose their stability with real eigenvalue (see Section 4), the walls become unstable due to curvature effects [34] giving rise to the appearance of labyrinth patterns (Fig. 9). Before reaching the threshold where these labyrinths appear, we find dark-ring cavity solitons [3,20,35–38], which can be written/erased, as is shown in Fig. 10. This happens for both positive and negative Δ .

6. CONCLUSIONS

We have proposed and studied, analytically and numerically, a complex Swift–Hohenberg equation with a parametric term

that breaks the phase invariance, giving rise to phase-bistable patterns. This equation models diverse nonlinear optical cavities and can be thought of as a universal equation for rocked, spatially extended systems close to a homogeneous Hopf bifurcation. In particular we have derived such an equation for two optical oscillators: the two-level laser and the two-wave mixing photorefractive oscillator. The structure of the equation, with two nonlocal terms, produces two kinds of instabilities as revealed by a linear stability analysis of the homogeneous states. These two differ in the character of the eigenvalue governing the instability (real or complex) and in the spatial scale, generating a complex variety of spatial patterns, phase locked and phase unlocked. The existence of extended patterns like Ising domain walls and labyrinths is confirmed with numerical solutions as well as of dark-ring (phase) solitons.

APPENDIX A: LASER

We are considering two types of scales: fast and slow.

1. Fast Scales

As has been explained in the main text, we will consider that the detuning Δ and Laplacian ∇^2 are $\mathcal{O}(\epsilon)$. As we consider class C lasers, σ and b are $\mathcal{O}(\epsilon^0)$. Additionally, $F = \mathcal{O}(\epsilon^2)$ and $\theta = \mathcal{O}(\epsilon)$. We consider two time scales $T_1 = \epsilon t$ and $T_2 = \epsilon^2 t$, and the pump is $r = 1 + \epsilon^2 r_2$ (we are close to the threshold).

$\mathcal{O}(\epsilon^0)$

At this order, $E_0 = P_0 = N_0 = 0$.

$\mathcal{O}(\epsilon)$

This is the first nontrivial order and reads

$$N_1 = 0, \tag{A1}$$

$$\mathcal{L}_0 |v_1\rangle = 0, \tag{A2}$$

where

$$\mathcal{L}_0 = \begin{pmatrix} -\sigma & \sigma \\ 1 & -1 \end{pmatrix},$$

and we have introduced the notation

$$|v_i\rangle = \begin{pmatrix} E_i \\ P_i \end{pmatrix}, \quad i = 1, 2, 3, \dots \tag{A3}$$

Equation (A2) can be easily solved with the help of the left eigenvectors of matrix \mathcal{L}_0 :

$$\langle \zeta_1 | \mathcal{L}_0 = 0 \langle \zeta_1 |, \quad \langle \zeta_2 | \mathcal{L}_0 = \mu \langle \zeta_2 |, \tag{A4}$$

$$\langle \zeta_1 | = (1, \sigma), \tag{A5}$$

$$\langle \zeta_2 | = (1, -1), \quad \mu = -(1 + \sigma). \tag{A6}$$

Projecting Eq. (A2) onto $\langle \zeta_1 |$ we obtain $0 = 0$, and projecting onto $\langle \zeta_2 |$ we obtain

$$P_1 = E_1, \tag{A7}$$

hence

$$|v_1\rangle = E_1 \begin{pmatrix} 1 \\ 1 \end{pmatrix}. \tag{A8}$$

$\mathcal{O}(\varepsilon^2)$

At this order, we obtain

$$N_2 = |E_1|^2, \tag{A9}$$

$$\frac{\partial}{\partial T_1} |v_1\rangle = \mathcal{L}_0 |v_2\rangle + |g_2\rangle, \tag{A10}$$

where

$$|g_2\rangle = \begin{pmatrix} i\nabla^2 E_1 - i\sigma\Delta E_1 + F_1 \cos(\omega T_1) e^{i\theta T_2} \\ i\Delta E_1 \end{pmatrix}. \tag{A11}$$

Projecting Eq. (A10) onto $\langle \zeta_1 |$ and making use of Eq. (A7), we obtain

$$(\sigma + 1) \frac{\partial E_1}{\partial T_1} = i\nabla^2 E_1 + F_1 \cos(\omega T_1) e^{i\theta T_2}. \tag{A12}$$

We solve

$$E_1(\vec{x}, T_1, T_2) = A_1(\vec{x}, T_1, T_2) + F_1(T_1, T_2), \tag{A13}$$

$$F_1(T_1, T_2) \equiv \frac{F}{(1 + \sigma)\omega} \sin(\omega T_1) e^{i\theta T_2}, \tag{A14}$$

$$(\sigma + 1) \frac{\partial A_1}{\partial T_1} = i\nabla^2 A_1. \tag{A15}$$

Projecting onto $\langle \zeta_2 |$ and making use of Eq. (A12), we obtain

$$P_2 = -\left(\frac{\partial}{\partial T_1} - i\Delta\right) E_1 + (1 + \sigma) E_2, \tag{A16}$$

$\mathcal{O}(\varepsilon^3)$

$$\frac{\partial}{\partial T_1} |v_2\rangle + \frac{\partial}{\partial T_2} |v_1\rangle = \mathcal{L}_0 |v_3\rangle + |g_3\rangle, \tag{A17}$$

where

$$|g_3\rangle = \begin{pmatrix} 0 \\ (r_2 - |E_1|^2) E_1 + i\Delta P_2 \end{pmatrix}.$$

Projecting

$$\begin{aligned} \sigma \left(\frac{\partial}{\partial T_1} - i\Delta \right) \left[\left(\frac{\partial}{\partial T_1} - i\Delta \right) E_1 + (1 + \sigma) E_2 \right] \\ = -(1 + \sigma) \frac{\partial E_1}{\partial T_2} + \sigma(r_2 - |E_1|^2) E_1, \end{aligned} \tag{A18}$$

we can rewrite this as follows:

$$\sigma \left(\frac{\partial}{\partial T_1} - i\Delta \right) (1 + \sigma) E_2 = g(T_1, T_2),$$

where

$$\begin{aligned} g(T_1, T_2) = & -\sigma \left(\frac{\partial}{\partial T_1} - i\Delta \right)^2 A_1 - (1 + \sigma) \frac{\partial A_1}{\partial T_2} \\ & + \sigma(r_2 - |A_1|^2) A_1 + -\sigma \left(\frac{\partial}{\partial T_1} - i\Delta \right)^2 F_1 \\ & - (1 + \sigma) \frac{\partial F_1}{\partial T_2} + \sigma(r_2 - |F_1|^2) F_1 \\ & - 2\sigma |A_1|^2 F_1 - 2\sigma |F_1|^2 A_1 - \sigma F_1^2 A_1^* + \sigma F_1^* A_1^2. \end{aligned} \tag{A19}$$

The solution can be written formally as

$$E_2 = \frac{1}{\sigma(1 + \sigma)} \left(e^{i\Delta T_1} + \int_0^{T_1} g(T_1, T_2) dT_1 + A_2(T_2) \right).$$

To ensure convergence it must be true that

$$\lim_{T_1 \rightarrow \infty} \frac{1}{T_1} \int_0^{T_1} g(T_1, T_2) dT_1 = 0. \tag{A20}$$

Taking into account that if A_1 is homogeneous then it does not depend on T_1 , the following condition must be fulfilled [we make use of Eq. (A15)]:

$$\begin{aligned} (1 + \sigma) \frac{\partial A_1}{\partial T_2} = & -\sigma \left(\frac{i\nabla^2}{1 + \sigma} - i\Delta \right)^2 A_1 \\ & + \sigma(r_2 - |A_1|^2) A_1 - \sigma \left(\frac{F}{\omega} \right)^2 A_1 - \frac{\sigma}{2} \left(\frac{F}{\omega} \right)^2 e^{2i\theta T_2} A_1^*, \end{aligned} \tag{A21}$$

in order to avoid divergences (in the case $\nabla^2 A_1 = 0$).

We finally compute the time derivative $\partial_t A_1 = \left(\varepsilon \frac{\partial}{\partial T_1} + \varepsilon^2 \frac{\partial}{\partial T_2} \right) (\varepsilon A_1)$ up to the third order in ε , from which, making use of Eqs. (A21) and (A15), setting $\psi = e^{-i\theta T_2} A_1$, and rescaling to the original variables, we obtain

$$\begin{aligned} (1 + \sigma) \frac{\partial \psi}{\partial t} = & \sigma \left(\frac{i\nabla^2}{1 + \sigma} - i\Delta \right)^2 \psi - (1 + \sigma) i\theta \psi \\ & + i\nabla^2 \psi + \sigma(r - 1 - |\psi|^2) \psi - 2\gamma \psi + \gamma \psi^*, \end{aligned} \tag{A22}$$

where

$$\gamma = \frac{1}{2} \frac{F^2 \sigma}{(1 + \sigma)^2 \omega^2}.$$

2. Slow Scales

The scales in this case will be

$$\begin{aligned} r = 1 + \varepsilon^2 r_2 \Delta, \quad \nabla^2 \sim O(\varepsilon), \\ \omega \sim O(\varepsilon^2) \quad F \sim O(\varepsilon^3), \\ (E, N, P) \sim (E_1, P_1, N_1) \varepsilon + (E_2, P_2, N_2) \varepsilon^2 + \dots \end{aligned} \tag{A23}$$

$O(\varepsilon)$

$$\begin{aligned} N_1 = 0, \\ L_0 |v_1\rangle = 0, \end{aligned} \tag{A24}$$

$$L_0 = \begin{pmatrix} -\sigma & \sigma \\ 1 & -1 \end{pmatrix}. \tag{A25}$$

The left-eigenvectors are $\langle \xi_1 | = (1, \sigma)$ and $\langle \xi_2 | = (1, -1)$, with eigenvalues 0 and $-(1 + \sigma)$, respectively. We can use this to write

$$\begin{aligned} \langle \xi_1 | L_0 | v_1 \rangle &= 0 \langle \xi_1 | v_1 \rangle, \\ \langle \xi_2 | L_0 | v_1 \rangle &= -(1 + \sigma) \langle \xi_2 | v_1 \rangle, \\ v_1 &= \begin{pmatrix} E_1 \\ P_1 \end{pmatrix}. \end{aligned} \tag{A26}$$

We obtain $E_1 = P_1$.
 $O(\epsilon^2)$

$$\begin{aligned} N_2 &= |E_1|^2, \\ \frac{\partial}{\partial T_1} |v_1\rangle &= L_0 |v_2\rangle + |g_2\rangle, \end{aligned} \tag{A27}$$

$$|g_2\rangle = \begin{pmatrix} i\nabla^2 E_1 - i\sigma \Delta E_1 \\ i\Delta E_1 \end{pmatrix}. \tag{A28}$$

Using the same procedure as above, we obtain (we can choose $E_2 = 0$)

$$(1 + \sigma) \frac{\partial E_1}{\partial T_1} = i\nabla^2 E_1, \tag{A29}$$

$$P_2 = -\frac{i}{(1 + \sigma)} (\nabla^2 E_1 - (1 + \sigma) \Delta E_1). \tag{A30}$$

$O(\epsilon^3)$

$$\frac{\partial}{\partial T_1} |v_2\rangle + \frac{\partial}{\partial T_2} |v_1\rangle = L_0 |v_3\rangle + |g_3\rangle, \tag{A31}$$

$$|g_3\rangle = \begin{pmatrix} F \cos(\omega T_1) e^{i\theta T_2} \\ (r_2 - |E_1|^2) E_1 + i\Delta P_2 \end{pmatrix}. \tag{A32}$$

Now we obtain the following equation:

$$\begin{aligned} \sigma \left(\frac{\partial}{\partial T_1} - i\Delta \right) P_2 &= -(1 + \sigma) \frac{\partial E_1}{\partial T_2} + F \cos(\omega T_1) e^{i\theta T_2} \\ &+ \sigma(r_2 - |E_1|^2) E_1. \end{aligned} \tag{A33}$$

Using Eq. (A30) and undoing the scaling,

$$\frac{\partial E}{\partial \tau} = \frac{\partial E_1}{\partial T_1} \epsilon + \frac{\partial E_1}{\partial T_2} \epsilon^2. \tag{A34}$$

We can write

$$\begin{aligned} (1 + \sigma) \frac{\partial E}{\partial \tau} &= \sigma \left(\frac{i\nabla^2}{1 + \sigma} - i\Delta \right)^2 E + i\nabla^2 E \\ &+ \sigma(r - 1 - |E|^2) E + F \cos(\omega t) e^{i\theta t}. \end{aligned} \tag{A35}$$

Setting $E \equiv A e^{i\theta t}$ the previous equation becomes

$$\begin{aligned} (1 + \sigma) \frac{\partial A}{\partial \tau} &= \sigma \left(\frac{i\nabla^2}{1 + \sigma} - i\Delta \right)^2 A - (1 + \sigma) i\theta A \\ &+ i\nabla^2 A + \sigma(r - 1 - |A|^2) A + F \cos(\omega t). \end{aligned} \tag{A36}$$

If the frequency ω is high compared with the dynamics of the system we can set $T = \omega t \rightarrow \epsilon^{-1} t$ with $T \gg t$ and as it is done in [14] separate the slow dynamics from the fast dynamics (we set $F \sim O(\epsilon^{-1})$).

Specifically we consider

$$A(\tau, T) = A_0(\tau, T) + \epsilon A_1(\tau, T), \tag{A37}$$

with $T = \epsilon^{-1} t$ and $\tau = t$.

Now we solve at different orders.
 $O(\epsilon^{-1})$

$$\begin{aligned} (1 + \sigma) \frac{\partial A_0}{\partial T} &= F \cos(T) \rightarrow A_0(T) \\ &= \frac{F}{(1 + \sigma)\omega} \sin(T) + i\psi(\tau). \end{aligned} \tag{A38}$$

$O(\epsilon^0)$

The equation reads at this order

$$\begin{aligned} (1 + \sigma) \frac{\partial A_1}{\partial T} + (1 + \sigma) \frac{\partial \psi}{\partial \tau} \\ = \sigma \left(\frac{i\nabla^2}{1 + \sigma} - i\Delta \right)^2 A_0 + (1 + \sigma) i\theta A_0 + i\nabla^2 A_0 \\ + \sigma(r - 1 - |A_0|^2) A_0 + F \cos(T). \end{aligned} \tag{A39}$$

This can be written as $(1 + \sigma) \frac{\partial A_1(\tau, T)}{\partial T} = g(T, \tau)$, which can be solved: $A_1(\tau, T) = (1 + \sigma)^{-1} \int_0^T dT' g(T', \tau) + B(\tau)$. The boundness of this requires

$$\lim_{T \rightarrow 0} \frac{1}{T} \int_0^T dT' g(T', \tau) = 0. \tag{A40}$$

Therein, we obtain the following solvability condition:

$$\begin{aligned} (1 + \sigma) \frac{\partial \psi}{\partial \tau} &= \sigma \left(\frac{i\nabla^2}{1 + \sigma} - i\Delta \right)^2 \psi - (1 + \sigma) i\theta \psi \\ &+ i\nabla^2 \psi + \sigma(r - 1 - |\psi|^2) \psi - 2\gamma \psi + \gamma \psi^*, \end{aligned} \tag{A41}$$

where

$$\gamma = \frac{1}{2} \frac{F^2 \sigma}{(1 + \sigma)^2 \omega^2}.$$

This condition is exactly the same equation as Eq. (A22), so we recover the result that we obtained considering fast scales by just assuming that F and ω are large. So, independently of the set of scales we consider, the final equation is consistent.

Setting $\frac{\nabla^2}{1 + \sigma} \equiv \nabla'^2$, $\tau' \equiv \frac{\sigma}{\sigma + 1} \tau$, $\theta' \equiv \frac{\sigma + 1}{\sigma} \theta$, $\gamma' \equiv \frac{\gamma}{\sigma}$, $\alpha \equiv \frac{\sigma + 1}{\sigma}$, and defining $\mu = r - 1$, we can write (removing the commas for simplicity)

$$\begin{aligned} \partial_\tau \psi &= (\mu - 2\gamma - i\theta) \psi - |\psi|^2 \psi - (\Delta - \nabla'^2)^2 \psi \\ &+ i\alpha \nabla'^2 \psi + \gamma \psi^*. \end{aligned} \tag{A42}$$

APPENDIX B: PHOTOREFRACTIVE OSCILLATOR

We will solve Eqs. (11) at different orders. We set $F = \epsilon F_1 \cos(\omega T_1) e^{i\theta T_2}$. At order $O(1)$ we trivially have $E_0 = N_0 = 0$.

$O(\epsilon)$

$$\begin{aligned} 0 &= -E_1 + N_1 + F_1 \cos(\omega T_1) e^{i\theta T_2}, \\ \partial_{T_1} N_1 &= -N_1 + E_1. \end{aligned} \tag{B1}$$

The solution is

$$\begin{aligned} N_1 &= E_1 - F_1 \cos(\omega T_1) e^{i\theta T_2}, \\ E_1 &= F_1 \cos(\omega T_1) e^{i\theta T_2} + F_1/\omega \sin(\omega T_1) e^{i\theta T_2} \\ + \varphi_1(\mathbf{r}, T_2) &\equiv E_1^\omega + \varphi_1. \\ O(\varepsilon^2) \\ 0 &= -E_2 + (-i\Delta + i\nabla^2)E_1 + N_2, \\ \partial_{T_1} N_2 + \partial_{T_2} N_1 &= -N_2 + i\Delta N_1 + E_2. \end{aligned} \quad (\text{B2})$$

We solve

$$\begin{aligned} N_2 &= E_2 - (-i\Delta + i\nabla^2)E_1, \\ E_2 &= \int_0^{T_1} G_2(T_1, T_2) dT_2 + \varphi_2(\vec{x}, T_2) \equiv E_2^\omega + \varphi_2, \\ G_2(T_1, T_2) &= (-i\Delta)(-F_1 \omega \cos(\omega T_1) e^{i\theta T_2} \\ + F_1 \cos(\omega T_1) e^{i\theta T_2} + F_1 \cos(\omega T_1) e^{i\theta T_2}) \\ + (i\theta)F_1/\omega \sin(\omega T_1) e^{i\theta T_2} - \partial_{T_2} \varphi_1 + i\nabla^2 \varphi_1. \end{aligned} \quad (\text{B3})$$

Solvability of E_2 requires

$$\lim_{T_1 \rightarrow \infty} \frac{1}{T_1} \int_0^{T_1} G_2(T_1, T_2) dT_2 = 0. \quad (\text{B4})$$

The oscillatory terms in Eq. (B3) vanish so the previous condition remains:

$$\partial_{T_2} \varphi_1 = i\nabla^2 \varphi_1. \quad (\text{B5})$$

$O(\varepsilon^3)$

$$\begin{aligned} 0 &= -E_3 + (-i\Delta + i\nabla^2)E_2 + N_3, \\ \partial_{T_1} N_3 + \partial_{T_2} N_2 &= -N_3 + i\Delta N_2 \\ + E_3 + (g-1)E_1 + |E_1|^2 E_1. \end{aligned} \quad (\text{B6})$$

We already know that

$$\begin{aligned} E_1 &= E_1^\omega(T_1, T_2) + \varphi_1(\mathbf{r}, T_2), \\ E_2 &= E_2^\omega(T_1, T_2) + \varphi_2(\mathbf{r}, T_2). \end{aligned} \quad (\text{B7})$$

We solve

$$N_3 = E_3 - (-i\Delta + i\nabla^2)E_2, \quad (\text{B8})$$

$$E_3 = \int_0^{T_1} G_3(T_1, T_2) dT_2 + \varphi_3(\mathbf{r}, T_2), \quad (\text{B9})$$

$$\begin{aligned} G_3(T_1, T_2) &= [(-i\Delta)(\partial_{T_1} E_2^\omega + \partial_{T_2} E_1^\omega) + (g_2 - 1 - \Delta^2)E_1^\omega - \partial_{T_2} E_2^\omega] \\ + [-\partial_{T_2} \varphi_2 + (g_2 - 1)\varphi_1 - (-i\Delta + i\nabla^2)^2 \varphi_1 + i\nabla^2 \varphi_2 - |\varphi_1|^2 \varphi_1] \\ - [|E_1^\omega|^2 E_1^\omega + 2E_1^\omega |\varphi_1|^2 + (E_1^\omega)^* \varphi_1^2 + 2|E_1^\omega|^2 \varphi_1 + |E_1^\omega|^2 \varphi_1^*]. \end{aligned} \quad (\text{B10})$$

Solvability of E_3 requires

$$\lim_{T_1 \rightarrow \infty} \frac{1}{T_1} \int_0^{T_1} G_3(T_1, T_2) dT_2 = 0. \quad (\text{B11})$$

The oscillatory terms in Eq. (B10) vanish so the previous condition remains:

$$\begin{aligned} \partial_{T_2} \varphi_2 &= -(-i\Delta + i\nabla^2)^2 \varphi_2 + i\nabla^2 \varphi_2 \\ - |\varphi_1|^2 \varphi_1 - 2\gamma \varphi_1 - \gamma \varphi_1^* e^{i2\theta T_2}, \end{aligned} \quad (\text{B12})$$

where $\gamma = \frac{1}{2} \frac{F_2}{\omega^2} (\omega^2 + 1)$.

Finally, developing up to the second order we have

$$\begin{aligned} E &= \varepsilon E_1 + \varepsilon^2 E_2, \\ N &= \varepsilon N_1 + \varepsilon^2 N_2 \\ &= \varepsilon(E_1 - F_1 \cos(\omega T_1) e^{i\theta T_2}) + \varepsilon^2(E_2 - (-i\Delta + i\nabla^2)E_1) \\ &= (1 + (-i\Delta + i\nabla^2))E - F \cos(\omega t) e^{i\theta t}, \\ \varphi &= \varepsilon \varphi_1 + \varepsilon^2 \varphi_2 \quad \partial_t \varphi = \varepsilon \partial_{T_2} \varphi_1 + \varepsilon^2 \partial_{T_2} \varphi_2. \end{aligned} \quad (\text{B13})$$

Undoing the scaling and if we make the change $\psi = i\varphi e^{i\theta T_2}$, we can write (defining $\mu = g - 1$)

$$\partial_t \psi = (\mu - 2\gamma - i\theta)\psi - |\psi|^2 \psi + i\nabla^2 \psi - (\nabla^2 - \Delta)^2 \psi + \gamma \psi^*. \quad (\text{B14})$$

Funding. Ministerio de Economía y Competitividad (MINECO); European Regional Development Fund (ERDF) (FIS2014-60715-P).

Acknowledgment. We acknowledge Eugenio Roldán for fruitful discussions.

REFERENCES

1. M. C. Cross and P. C. Hohenberg, "Pattern formation outside of equilibrium," *Rev. Mod. Phys.* **65**, 851–1112 (1993).
2. P. Couillet, L. Gil, and F. Rocca, "Optical vortices," *Opt. Commun.* **73**, 403–408 (1989).
3. K. Staliunas and V. J. Sánchez-Morcillo, *Transverse Patterns in Nonlinear Optical Resonators* (Springer, 2003).
4. P. Mandel, *Theoretical Problems in Cavity Nonlinear Optics* (Cambridge University, 1997).
5. J. V. Moloney and A. C. Newell, *Nonlinear Optics* (Westview, 2003).
6. J. Lega, J. V. Moloney, and A. C. Newell, "Swift-Hohenberg equation for lasers," *Phys. Rev. Lett.* **73**, 2978–2981 (1994).
7. J. Lega, J. V. Moloney, and A. C. Newell, "Universal description of laser dynamics near threshold," *Phys. D* **83**, 478–498 (1995).
8. S. Longhi and A. Geraci, "Swift-Hohenberg equation for optical parametric oscillators," *Phys. Rev. A* **54**, 4581–4584 (1996).
9. V. J. Sánchez-Morcillo, E. Roldán, G. J. de Valcárcel, and K. Staliunas, "Generalized complex Swift-Hohenberg equation for optical parametric oscillators," *Phys. Rev. A* **56**, 3237–3244 (1997).
10. P. Couillet and K. Emilsson, "Strong resonances of spatially distributed oscillators: a laboratory to study patterns and defects," *Phys. D* **61**, 119–131 (1992).
11. D. Walgraef, *Spatio-Temporal Pattern Formation* (Springer, 1997).
12. P. Couillet, J. Lega, B. Houchmandzadeh, and J. Lajzerowicz, "Breaking chirality in nonequilibrium systems," *Phys. Rev. Lett.* **65**, 1352–1355 (1990).
13. G. J. de Valcárcel, I. Pérez-Arjona, and E. Roldán, "Domain walls and Ising-Bloch transitions in parametrically driven systems," *Phys. Rev. Lett.* **89**, 164101 (2002).
14. G. J. de Valcárcel and K. Staliunas, "Excitation of phase patterns and spatial solitons via two frequency-forcing of a 1:1 resonance," *Phys. Rev. E* **67**, 026604 (2003).
15. G. J. de Valcárcel and K. Staliunas, "Pattern formation through phase bistability in oscillatory systems with space-modulated forcing," *Phys. Rev. Lett.* **105**, 054101 (2010).

16. G. J. de Valcárcel, M. Martínez-Quesada, and K. Staliunas, "Phase-bistable pattern formation in oscillatory systems via rocking: application to nonlinear optical systems," *Philos. Trans. R. Soc. London Ser. A* **372**, 20140008 (2014).
17. A. A. Krents, N. R. Molech, and D. A. Anchikov, "Resonant excitation of transverse patterns in broad-area lasers by periodic temporal pump modulation," *J. Opt. Soc. Am. B* **34**, 1733–1739 (2017).
18. R. Martínez-Lorente, A. Esteban-Martín, E. Roldán, K. Staliunas, G. J. de Valcárcel, and F. Silva, "Experimental demonstration of phase bistability in a broad-area optical oscillator with injected signal," *Phys. Rev. A* **92**, 053858 (2015).
19. M. Radziunas and K. Staliunas, "Spatial "rocking" in broad-area semiconductor lasers," *Europhys. Lett.* **95**, 14002 (2011).
20. A. Esteban-Martín, M. Martínez-Quesada, V. B. Taranenkov, E. Roldán, and G. J. de Valcárcel, "Bistable phase locking of a nonlinear optical cavity via rocking: transmuting vortices into phase patterns," *Phys. Rev. Lett.* **97**, 093903 (2006).
21. A. V. Pakhomov, N. E. Molevich, A. A. Krents, and D. A. Anchikov, "Intrinsic performance-limiting instabilities in two-level class-B broad-area lasers," *Opt. Commun.* **372**, 14–21 (2016).
22. L. A. Lugiato, G. L. Oppo, J. R. Tredicce, L. M. Narducci, and M. A. Pernigo, "Instabilities and spatial complexity in a laser," *J. Opt. Soc. Am. B* **7**, 1019–1033 (1990).
23. P. Mandel, M. Georgiou, and T. Erneux, "Transverse effects in coherently driven nonlinear cavities," *Phys. Rev. A* **47**, 4277–4286 (1993).
24. L. A. Lugiato, M. Brambilla, and A. Gatti, "Nonlinear optical patterns," *Adv. At. Mol. Opt. Phys.* **40**, 229–306 (1998).
25. A. E. Siegman, *Lasers* (University Science Books, 1986).
26. P. K. Jakobsen, J. V. Moloney, A. C. Newell, and R. Indik, "Space-time dynamics of wide-gain-section lasers," *Phys. Rev. A* **45**, 8129–8137 (1992).
27. U. Bortolozzo, V. Villoresi, and P. L. Ramazza, "Experimental evidence for detuning induced pattern selection in nonlinear optics," *Phys. Rev. Lett.* **87**, 274102 (2001).
28. K. Staliunas, "Laser Ginzburg Landau equation and laser hydrodynamics," *Phys. Rev. A* **48**, 1573–1581 (1993).
29. K. Staliunas, M. F. H. Tarroja, G. Slekyš, C. O. Weiss, and L. Dambly, "Analogy between photorefractive oscillators and class-A lasers," *Phys. Rev. A* **51**, 4140–4151 (1995).
30. S. Longhi, "Spatial solitary waves in nondegenerate optical parametric oscillators near an inverted bifurcation," *Opt. Commun.* **149**, 335–340 (1998).
31. L. Spinelli, G. Tissoni, M. Brambilla, F. Prati, and L. A. Lugiato, "Spatial solitons in semiconductor microcavities," *Phys. Rev. A* **58**, 2542–2559 (1998).
32. W. W. Ahmed, S. Kumar, R. Herrero, M. Botey, M. Radziunas, and K. Staliunas, "Stabilization of flat-mirror vertical-external-cavity surface-emitting lasers by spatiotemporal modulation of the pump profile," *Phys. Rev. A* **92**, 043829 (2015).
33. K. Staliunas, G. J. de Valcárcel, M. Martínez-Quesada, S. Gilliland, A. González-Segura, G. Muñoz-Matutano, J. Cascante-Vindas, J. Marqués-Hueso, and S. Torres-Peiró, "Bistable phase locking in rocked lasers," *Opt. Commun.* **268**, 160–168 (2006).
34. R. Gallego, M. San Miguel, and R. Toral, "Self-similar domain growth, localized structures, and labyrinthine patterns in vectorial Kerr resonators," *Phys. Rev. E* **61**, 2241–2244 (2000).
35. K. Staliunas and V. J. Sánchez-Morcillo, "Dynamics of phase domains in the Swift-Hohenberg equation," *Phys. Lett. A* **241**, 28–34 (1998).
36. V. J. Sánchez-Morcillo and K. Staliunas, "Stability of localized structures in the Swift-Hohenberg equation," *Phys. Rev. E* **60**, 6153–6156 (1999).
37. D. Gomila, P. Colet, G.-L. Oppo, and M. San Miguel, "Stable droplets and growth laws close to the modulational instability of a domain wall," *Phys. Rev. Lett.* **87**, 194101 (2001).
38. V. B. Taranenkov, K. Staliunas, and C. O. Weiss, "Pattern formation and localized structures in degenerate optical parametric mixing," *Phys. Rev. Lett.* **81**, 2236–2239 (1998).

Bibliography

- [1] A. Esteban-Martín, M. Martínez-Quesada, V. B. Taranenko, E. Roldán and G. J. de Valcárcel. Bistable phase Locking of a Nonlinear Optical Cavity via Rocking: Transmuting Vortices into Phase Patterns. *Physical Review Letters*, **97**, 093903 (2006).
- [2] K. Staliunas, G. J. de Valcárcel, M. Martínez-Quesada, S. Gilliland, A. González-Segura, G. Muñoz-Matutano, J. Cascante-Vindas, J. Marqués-Hueso and Salvador Torres-Peiró. Bistable phase locking in rocked lasers. *Optics Communications*, **268**, 160-168 (2006).
- [3] M. Martínez-Quesada, E. Roldán and G. J. de Valcárcel. Rocking bidirectional lasers. *Optics Communications*, **284**, 2554-2559 (2011).
- [4] G. J. de Valcárcel, M. Martínez-Quesada and K. Staliunas. Phase-bistable pattern formation in oscillatory systems via rocking: application to nonlinear optical systems. *Philosophical Transactions of the Royal Society A*, **372**, 20140008 (2014).
- [5] M. Martínez-Quesada and G. J. de Valcárcel. Universal description of pattern formation in optical oscillators under bichromatic injection. *Journal of the Optical Society of America B*, **35**, 1379-1389 (2018).
- [6] G. J. de Valcárcel and K. Staliunas. Excitation of phase patterns and spatial solitons via two-frequency forcing of a 1:1 resonance. *Physical Review E*, **67**, 026604 (2003).

- [7] P. Simpson. The stars and stripes of animal bodies: evolution of regulatory elements mediating pigment and bristle patterns in drosophila. *TRENDS in Genetics*, **23**, 350–358 (2007).
- [8] H. Nishimori and N. Ouchi. Formation of ripple patterns and dunes by wind-blown sand. *Physical Review Letters*, **71**, 197 (1993).
- [9] D. Walgraef *Spatio-temporal pattern formation*. Springer New York. (1997).
- [10] Lord Rayleigh. On the dynamics of revolving fluids. *Proceedings Royal Society A*, **93**, 148 (1916).
- [11] A. M. Turing, F. R. S. The chemical basis of morphogenesis. *Philosophical Transactions of the Royal Society B*, **237**, 37-72 (1952).
- [12] V. M. Zaikin and A. M. Zhabotinsky. Concentration Wave Propagation in Two-dimensional Liquid-phase Self-oscillating System. *Nature*, **225**, 535–537 (1970).
- [13] L. A. Lugiato and R. Lefever. Spatial Dissipative Structures in Passive Optical Systems. *Physical Review Letters*, **58**, 2209 (1987).
- [14] M. C. Cross and P. C. Hohenberg. Pattern formation outside of equilibrium. *Review of Modern Physics*, **65** 851 (1993).
- [15] G. Nicolis and I. Prigogine. *Self-organization in nonequilibrium systems*. Wiley, New York (1977).
- [16] G. Nicolis. *Introduction to nonlinear science*. Cambridge University Press. (1995).
- [17] V. K. Vanag and I. R. Epstein. Pattern formation in a tunable medium: The Belousov-Zhabotinsky reaction in an aerosol. *Physical Review Letters*, **87**, 228301 (2001).
- [18] N. Akhmediev and A. Ankiewicz (eds.) *Dissipative solitons: From Optics to Biology*. Springer (2008).
- [19] J. S. Russell. *Report of the fourteenth meeting of the British Association for the Advancement of Science*, pp. 311–390, Plates XLVII-LVII. 2 (1845).
- [20] N. J. Zabusky and M. D. Kruskal, Interaction of ‘solitons’ in a collisionless plasma and the recurrence of initial states. *Physical Review Letters*, **15**, 240 (1965).

- [21] P. B. Umbanhowar, F. Melo and H. L. Swinney. Localised excitations in a vertical vibrated granular layer. *Nature*, **382**, 793 (1986).
- [22] O. Lioubashevski, H. Arbell, and J. Fineberg. Dissipative solitary states in driven surface waves. *Physical Review Letters*, **76**, 3959 (1996).
- [23] J. Dewel, P. Borckmans, A. De Wit, B. Rudovics, J. J. Perraud, E. Dulos, J. Boissonade and P. De Kepper. Pattern selection and localized structures in reaction-diffusion systems. *Physica A*, **213**, 181 (1995).
- [24] F. T. Arecchi, S. Boccaletti, P. Luigi Ramazza. Pattern formation and competition in nonlinear optics. *Physics Reports*, **318**, 1-83 (1999).
- [25] L. A. Lugiato, F. Prati and M. Brambilla. *Nonlinear Optical Systems*. Cambridge University Press (2015).
- [26] N. N. Rosanov. Transverse patterns in wide-aperture nonlinear optical systems. *Progress in Optics*, **35**, 1–60 (1996).
- [27] P. Mandel. *Theoretical Problems in Cavity Nonlinear Optics*. Cambridge University Press (1997).
- [28] P. Mandel and M. Tlidi. Transverse dynamics in cavity nonlinear optics (2000–2003). *Quantum and Semiclassical Optics*, **6**, 60 (2004).
- [29] K. Staliunas and V. J. Sánchez-Morcillo. *Transverse patterns in nonlinear optical resonators*. Springer (2003).
- [30] O. Svelto and D. C. Hanna. *Principles of lasers*. Springer (1998).
- [31] F. Prati, M. Brambilla and L. A. Lugiato. Pattern formation in lasers. *Revista Nuovo Cimento*, **17**, 1 (1994).
- [32] G. J. de Valcárcel, K. Staliunas, E. Roldán, and V. J. Sánchez-Morcillo. Transverse patterns in degenerate optical parametric oscillation and degenerate four-wave mixing. *Physical Review A*, **54**, 1609 (1996).
- [33] V. B. Taranenko, K. Staliunas and C. O. Weiss, Pattern formation and localized structures in degenerate optical parametric mixing, *Physical Review Letters*, **81**, 2236 (1998).
- [34] R. Gallego, M. San Miguel, and R. Toral. Self-similar domain growth, localized structures, and labyrinthine patterns in vectorial Kerr resonators. *Physical Review E*, **61**, 2241 (2000).

- [35] N. Akhmediev and A. Ankiewicz (eds.) *Dissipative solitons*. Springer (2005).
- [36] D. W. Mc Laughlin, J. V. Moloney, and A. C. Newell. Solitary Waves as Fixed Points of Infinite-Dimensional Maps in an Optical Bistable Ring Cavity. *Physical Review Letters*, **51**, 75 (1983).
- [37] N. N. Rosanov and G. V. Khodova. Autosolitons in bistable interferometers. *Optics and Spectroscopy*, **65**, 449 (1988).
- [38] N. N. Rosanov and G. V. Khodova. Diffractive autosolitons in nonlinear interferometers. *Journal of the Optical Society of America B*, **7**, 1057 (1990).
- [39] M. Tlidi, P. Mandel, and R. Lefever. Localized structures and localized patterns in optical bistability. *Physical Review Letters*, **73**, 640 (1994).
- [40] X. Hachair, S. Barland, L. Furfaro, M. Giudici, S. Balle, J. R. Tredicce, M. Brambilla, T. Maggipinto, I. M. Perrini, G. Tissoni, and L. A. Lugiato. Cavity solitons in broad-area vertical-cavity surface-emitting lasers below threshold. *Physical Review A*, **69**, 043817 (2004).
- [41] I. Pérez-Arjona, F. Silva, E. Roldán, and G. J. de Valcárcel. Stabilizing and controlling domain walls and dark-ring cavity solitons. *Optics Express*, **12**, 2130 (2004).
- [42] A. Esteban-Martin, V. B. Taranenko, E. Roldán and G. J. de Valcarcel. Control and steering of phase domain walls. *Optics Express*, **13**, 3631 (2005).
- [43] G. J. de Valcárcel and K. Staliunas. Phase-bistable Kerr cavity solitons and patterns. *Physical Review A*, **87**, 043802 (2013).
- [44] K. Porsezian, V. C. Kuriakose (Eds.). *Optical Solitons: Theoretical and Experimental Challenges*. Springer (2003).
- [45] D. Gomila and G. L. Oppo. Subcritical patterns and dissipative solitons due to intracavity photonic crystals. *Physical Review A*, **76**, 043823 (2007).
- [46] D. Christodoulides and R. Joseph, R. Discrete self-focusing in nonlinear arrays of coupled waveguides. *Optics Letters*, **13**, 794 (1988).
- [47] U. Peschel, O. Egorov, and F. Lederer. Discrete cavity solitons. *Optics Letters*, **29**, 1909 (2004).

- [48] M. Brambilla, T. Maggipinto, G. Patera and L. Columbo, L. Cavity light bullets: Three-dimensional localized structures in a nonlinear optical resonator. *Physical Review Letters*, **93**, 203901 (2004).
- [49] W. J. Firth. Temporal cavity solitons - Buffering optical data. *Nature Photonics*, **4**, 415 (2010).
- [50] L. A. Lugiato, L. M. Narducci, and C. Oldano. Cooperative frequency locking and stationary spatial structures in lasers. *Journal of the Optical Society of America B*, **5**, 879–888 (1988).
- [51] L. A. Lugiato, G. L. Oppo, J. R. Tredicce, L. M. Narducci, and M. A. Pernigo. Instabilities and spatial complexity in a laser. *Journal of the Optical Society of America B*, **7**, 1019–1033 (1990).
- [52] M. Georgiou and P. Mandel. Transverse effects in a laser with an injected signal. *Chaos, Solitons & Fractals*, **4**, 1657–1661 (1994).
- [53] D. Yu, W. Lu, and R. G. Harrison. Origin of spiral wave formation in excitable optical systems. *Physical Review Letters*, **77**, 5051 (1996).
- [54] D. Yu, W. Lu, and R. G. Harrison. Dynamic bistability and spiral waves in a laser. *Journal of Optics B: Quantum and Semiclassical Optics*, **125** (1999).
- [55] M. Brambilla, L. A. Lugiato, V. Penna, F. Prati, C. Tamm, and C. O. Weiss. Transverse laser patterns. II. Variational principle for pattern selection, spatial multistability, and laser hydrodynamics. *Physical Review A* **43**, 5114 (1991).
- [56] K. Staliunas, Laser Ginzburg–Landau equation and laser hydrodynamics. *Physical Review A*, **48**, 1573 (1993).
- [57] K. Staliunas and C.O. Weiss. Tilted and standing waves and vortex lattices in class-A lasers. *Physica D*, **81**, 79 (1995).
- [58] S. Longhi. Transverse patterns in a laser with an injected signal. *Physical Review A*, **56**, 2397 (1997)
- [59] R. Salomaa and S. Stenholm. Gas Laser with Saturable Absorber (I. Single-Mode Characteristics and II. Single mode stability), *Physical Review A*, **8**, 2695 (1973).

- [60] V. B. Taranenko, K. Staliunas and C. O. Weiss. Spatial soliton laser: Localized structures in a laser with a saturable absorber in a self-imaging resonator. *Physical Review A*, **56**, 1582 (1997).
- [61] N. N. Rosanov. *Spatial Hysteresis and Optical Patterns*. Springer (2002).
- [62] R. Vilaseca, M. C. Torrent, J. García-Ojalvo, M. Brambilla and M. San Miguel. Two-Photon Cavity Solitons in Active Optical Media. *Physical Review Letters*, **87**, 083902 (2001).
- [63] V. Ahufinger, J. García-Ojalvo, J. Mompart, M. C. Torrent, R. Corbalán, and R. Vilaseca. Cavity solitons in two-level lasers with dense amplifying medium. *Physical Review Letters*, **91**, 083901 (2003).
- [64] O. Gómez-Calderón, E. Cabrera, M. A. Antón, I. Gonzalo, F. Carreño, and J. M. Guerra. From nearly tilted waves to cavity phase solitons in broad area lasers with squeezed vacuum. *Physical Review Letters*, **92**, 163901 (2004).
- [65] S. Barland, J. R. Tredicce, M. Brambilla, L. A. Lugiato, S. Balle, M. Giudici, T. Maggipinto, L. Spinelli, G. Tissoni, T. Knoedl, M. Miller and R. Jaeger. Cavity solitons as pixels in semiconductor microcavities. *Nature*, **419**, 699 (2002).
- [66] F. Gustave, L. Columbo, G. Tissoni, M. Brambilla, F. Prati, B. Kelleher, B. Tykalewicz, and S. Barland, Dissipative Phase Solitons in Semiconductor Lasers, *Physical Review Letters*, **115**, 043902 (2015).
- [67] B. Garbin, J. Javaloyes, G. Tissoni and S. Barland, Topological solitons as addressable phase bits in a driven laser, *Nature Communications*, **6**, 5915 (2015).
- [68] H. Zeghlache, P. Mandel, N. B. Abraham, L. M. Hoffer, G. L. Lippi, and T. Mello, Bidirectional ring laser: Stability analysis and time-dependent solutions. *Physical Review A*, **37**, 470-497 (1988).
- [69] I. Pérez-Arjona, V. J. Sánchez-Morcillo, and E. Roldán. Bidirectional ring laser cavity solitons, *Optics Letters*, **32**, 3221-3223 (2007).
- [70] L. Columbo, L. Gil and J. Tredicce. Could cavity solitons exist in bidirectional ring lasers? *Optics Letters*, **33**, 995-997 (2008).

- [71] I. Pérez-Arjona, V. J. Sánchez-Morcillo, J. Redondo, K. Staliunas, and E. Roldán. Diffusion stabilizes cavity solitons in bidirectional lasers. *Optics Express*, **17**, 4897 (2009).
- [72] L. Columbo, L. Gil and J. R. Tredicce. Nucleation of wave defects and formation of optical localized structures in bi-directional ring lasers. *European Physical Journal D*, **58**, 227 (2010).
- [73] G. Balzer, C. Denz, O. Knaup and T. Tschudi, Circling vortices and pattern dynamics in a unidirectional photorefractive ring oscillator, *Chaos, Solitons and Fractals*, **10**, 725 (1999).
- [74] C. Denz, M. Schwab and C. Weillnau. *Transverse-Pattern Formation in Photorefractive Optics*. Springer (2003).
- [75] T. Ackemann, W. J. Firth and G. L. Oppo. Fundamentals and applications of spatial dissipative solitons in photonic devices. *Advances in Atomic, Molecular and Optical Physics*, **57**, 323 (2009).
- [76] Y. Tanguy, T. Ackemann, W. J. Firth, and R. Jäger. Realization of a semiconductor-based cavity soliton laser. *Physical Review Letters*, **100**, 013907 (2008).
- [77] P. Genevet, S. Barland, M. Giudici, and J. R. Tredicce. Cavity soliton laser based on mutually coupled semiconductor microresonators. *Physical Review Letters*, **101**, 123905 (2008).
- [78] T. Elsass, K. Gauthron, G. Beaudoin, I. Sagnes, R. Kuszelewicz and S. Barba. Fast manipulation of laser localized structures in a monolithic vertical cavity with saturable absorber. *Applied Physics B*, **98**, 327 (2010).
- [79] F. Prati, G. Tissoni, L. A. Lugiato, K. M. Aghdami, and M. Brambilla. Spontaneously moving solitons in a cavity soliton laser with circular section. *European Physical Journal D*, **59**, 73 (2010).
- [80] F. Prati, L. A. Lugiato, G. Tissoni, and M. Brambilla. Cavity soliton billiards. *Physical Review A*, **84**, 053852 (2011).
- [81] V. L. Ginzburg and L. Landau. On the Theory of superconductivity. *Journal of Experimental and Theoretical Physics*, **20** 1064 (1950).
- [82] I. S. Aranson and L. Kramer. The world of the complex Ginzburg-Landau equation. *Reviews of Modern Physics*, **74** 99 (2002).

- [83] P. Couillet, L. Gil, and F. Rocca. Optical vortices. *Optics Communications*, **73**, 403–408 (1989).
- [84] K. Staliunas. Transverse Pattern Formation in Optical Parametric Oscillators, *Journal of Modern Optics*, **42**, 1261–1269 (1995).
- [85] P. Mandel, M. Georgiou and T. Erneux. Transverse effects in coherently driven nonlinear cavities. *Physical Review A*, **47**, 4277 (1993)
- [86] P. K. Jakobsen, J. V. Moloney, A. C. Newell, and R. Indik. Space-time dynamics of wide-gain-section lasers. *Physical Review A*, **45**, 8129. (1992).
- [87] J. Swift and P. C. Hohenberg. Hydrodynamic fluctuations at the convective instability. *Physical Review A*, **15**, 319 (1977).
- [88] J. Lega, J. V. Moloney, and A. C. Newell. Swift-hohenberg equation for lasers. *Physical Review Letters*, **73**, 2978 (1994).
- [89] J. Lega, J. V. Moloney, A. C. Newell. Universal description of laser dynamics near threshold. *Physica D*, **83**, 478–498 (1995)
- [90] V. J. Sánchez-Morcillo and K. Staliunas. Stability of localized structures in the Swift–Hohenberg equation. *Physical Review E*, **60**, 6153 (1999).
- [91] G. L. Oppo, A. M. Yao, F. Prati, and G. J. de Valcárcel. Long-term spatiotemporal dynamics of solid-state lasers and vertical-cavity surface-emitting lasers *Physical Review A*, **79**, 033824 (2009).
- [92] P. Couillet and K. Emilsson. Strong resonances of spatially distributed oscillators: a laboratory to study patterns and defects. *Physica D*, **61**, 119–131 (1992).
- [93] S. Rudiger, D. G. Míguez, A. P. Muñozuri, F. Sagués, and J. Casademunt. Dynamics of turing patterns under spatiotemporal forcing. *Physical Review Letters*, **90**, 128301 (2003).
- [94] P Couillet, J Lega, B Houchmanzadeh, and J Lajzerowicz. Breaking chirality in nonequilibrium systems. *Physical Review Letters*, **65**, 1352 (1990).
- [95] G. J de Valcárcel and K. Staliunas. Pattern formation through phase bistability in oscillatory systems with space modulated forcing. *Physical Review Letters*, **105**, 054101 (2010).

- [96] J. M. Buldú, K. Staliunas, J. A. Casals, J. García-Ojalvo. Bistable phase control via rocking in a nonlinear electronic oscillator. *Chaos*, **16**, 043126 (2006).
- [97] K. Staliunas, G. J de Valcárcel, J. M. Buldú, and J. Garcia-Ojalvo. Noise-induced phase bistability via stochastic rocking. *Physical Review Letters*, **102**, 010601 (2009).
- [98] K. Staliunas, G. J de Valcárcel and E. Roldán. Bistable phase locking in a laser with injected signal. *Physical Review A*, **80** 025801 (2009).
- [99] S. Kolpakov, F. Silva, G. J. de Valcárcel, E. Roldán and K. Staliunas. Experimental demonstration of bistable phase locking in a photorefractive oscillator. *Physical Review A*, **85**, 025805 (2012).
- [100] C. Fernandez-Oto, G. J. de Valcárcel, M. Tlidi, K. Panajotov, and K. Staliunas. Phase-bistable patterns and cavity solitons induced by spatially periodic injection into vertical cavity surface-emitting lasers. *Physical Review A*, **89**, 055802 (2014).
- [101] R. Martínez-Lorente, A. Esteban-Martín, E. Roldán, K. Staliunas, G. J. de Valcárcel and F. Silva. Experimental demonstration of phase bistability in a broad-area optical oscillator with injected signal. *Physical Review A*, **92**, 053858 (2015).
- [102] R. Martínez-Lorente, F. Silva, and G. J. de Valcárcel. Phase tetrastability in parametric oscillation. arXiv:1804.09125 (2018).
- [103] I. Pérez-Arjona. Tesi doctoral. Universitat de València (2004).
- [104] A. C. Newell and J. V. Moloney. *Nonlinear Optics*. Addison-Wesley (1992).
- [105] A. Gatti, H. Wiedemann, L. A. Lugiato, I. Marzoli, G. L. Oppo, and S. M. Barnett. Langevin treatment of quantum fluctuations and optical patterns in optical parametric oscillators below threshold. *Physical Review A*, **56**, 877 (1997).
- [106] U. Bortolozzo, V. Villoresi, and P. L. Ramazza. Experimental evidence for detuning induced pattern selection in nonlinear optics. *Physical Review Letters*, **87**, 274102 (2001).